Design, Synthesis and Study of Redox and Optoelectronic Properties of Aromatic Oxidants and Polycyclic Aromatic Hydrocarbons

Mohammad Mosharraf Hossain
Marquette University

DESIGN, SYNTHESIS AND STUDY OF REDOX AND OPTOELECTRONIC PROPERTIES OF AROMATIC OXIDANTS AND POLYCYCLIC AROMATIC HYDROCARBONS

By

Mohammad Mosharraf Hossain, B.Sc., M.S.

A Dissertation submitted to the Faculty of the Graduate School,
Marquette University,
in Partial Fulfillment of the Requirements for the Degree of Doctor of Philosophy

Milwaukee, Wisconsin
August, 2018

ABSTRACT

DESIGN, SYNTHESIS AND STUDY OF REDOX AND OPTOELECTRONIC PROPERTIES OF AROMATIC OXIDANTS AND POLYCYCLIC AROMATIC HYDROCARBONS

Mohammad Mosharraf Hossain, B.Sc., M.S.
Marquette University, 2018

Organic materials play a significant role for the next generation photovoltaic devices that convert solar energy into usable forms of energy. In this regard, polycyclic aromatic hydrocarbons (PAHs) are fundamental tools in the developing area of molecular electronics and photovoltaics as they show excellent optical/electronic properties and are well-suited for applications in such developing areas as flexible display devices, field effect transistors and solar cell panels. Design and synthesis of novel materials for photovoltaics applications would require the proper understanding the mechanism of charge transport and identification of the structural features necessary in a particular molecular wire or PAH.

To understand the charge transport mechanism and the hole delocalization one needs to generate the cation radical of a given electron donor in solution by using robust aromatic oxidants. Among these oxidants, magic blue has been widely used as an aromatic oxidant for the one electron oxidation due to its commercial availability and a reasonable oxidizing power. However, a modest stability of the magic blue salt leads to a slow decomposition to produce unknown impurities, which have been named “blues brothers”. Importantly, these impurities produce a noticeable band in the near-IR region—that is the same region where one usually expects to see an intervalence band of the cation radical with extensive hole delocalization. In this work a rational approach to synthesis of novel analogue of the magic blue that does not undergo degradation has been demonstrated.

Furthermore, in the course of the rational design of novel molecular wires with enhanced redox and optical properties, one usually considers various geometrical factors in order to control the mechanism of charge delocalization. For example, a relatively small interplanar dihedral angle between adjacent units in poly-p-phenylene wire leads to a significant interchromophoric electronic coupling and thereby to extensive hole delocalization. However, it remains unclear how change in the interplanar angle would impact the redox and optical properties of the wire as well the mechanism of the hole delocalization in its cation radical. Accordingly, in this work it has been described the syntheses and study of the electrochemical and optoelectronic properties of a number of different series of biaryls connected by different numbers of methylene group to vary the dihedral angle in order to probe the mechanism and extent of hole delocalization in biaryls.

Although significant progress has been made in understanding the charge transport mechanisms in various polycyclic aromatic hydrocarbons (PAHs), the usefulness of such materials in functional devices remains limited; hence design and synthesis of new PAHs to better understand the charge transport mechanisms remains an active area of research. An oxidative cyclodehydrogenation strategy was used for synthesizing a highly soluble, fluorene based larger derivative of hexa-*peri*-hexabenzocoronene (FHBC), where twelve carbon-carbon bonds are formed in a single step. Deployment of fluorenes at the periphery of the HBC core not only imparts solubility to the structure, but also allows the new PAHs to be functionalized further to make bigger PAHs to tune its desirable electronic properties.

ACKNOWLEDGEMENT

Mohammad Mosharraf Hossain, B.Sc., M.S.

I would like to express my acknowledgements and gratitude to my supervisor Prof. Rajendra Rathore for his continuous encouragement, criticism, assistance, guidance and giving me an opportunity to work in his research group as a synthetic organic chemist. He was extremely helpful and supportive to build up my foundation in organic chemistry throughout my graduate studies. I also wholeheartedly thank Prof. Scott Reid for his kind assistance, suggestions and guidance on my research works and continuous efforts to help writing my thesis.

I would also like to thank my committee members Prof. James Gardinier, Prof. Adam Fiedler and Prof. Qadir Timerghazin for their continuous constructive criticism from the beginning of my PhD journey by giving suggestions and advices during my research meeting and my annual review meetings which helped me to attain the endpoint of the PhD journey successfully. I would like to express my gratitude to all faculty members in the chemistry department who directly or indirectly contributed to my academic progress at Marquette University. I sincerely thank O'Brien fellowship for providing me a unique opportunity to focus on my research work during the last year of my graduate studies.

I would like to acknowledge Dr. Maxim V. Ivanov and Dr. Elena Ivanova for their continuous feedback on my different projects by corelating experimental results with the theoretical results as well as continuous suggestions and corrections of my thesis. I am thankful to Dr. Marat Talipov for the computational studies for some of my projects and developing the new software program which can be applied to redox titrations. I am thankful to Dr. Khushabu Thakur and Dr. Anitha Boddeda for helping me to learn the synthetic skills, analytical techniques and valuable suggestions during my research. Also thanks to Dr. Denan Wang for the help and suggestions during my research work. I am also thankful to Dr. Ruchi Shukla and Dr. Tushar Navale for the synthesis of biaryls and FHBC compounds mentioned in chapter 2 and chapter 3. I would like to thank my current group members Saber Mirzaei, Ainur Abzhanova for their support and help. I would like to acknowledge the funding sources from Marquette University, Department of Chemistry. I also thank Dr. Sergey V. Lindeman for single crystal X-ray crystallography and helpful discussions and Dr. Sheng Cai for the help with NMR instruments, Mark Bartelt for his prompt help for the instrumental troubleshooting, extremely helpful office assistant Linda and Lori and business manager Paul Dion. I would also like to extend my thanks to the Marquette University staff that was always hands on for help.

Finally, I wish to thank all my family and friends whose continuous support and inspiration constantly motivated me to undertake and finish this wonderful journey for doctoral program. I would specially like to thank my mother, father, wife and my three kids (Margia, Anisha and Saifan) for their patience and sacrifice during all these years of my doctoral research.

DEDICATION

To the memory of my Late advisor Prof. Rajendra (Raj) Rathore

I miss and always will miss his excitement about a new molecule he wanted synthesize as quick as possible. A great mentor who always had softness inside his mind for his students.

TABLE OF CONTENTS

LIST OF TABLES

CHAPTER 1:

CHAPTER 2:

CHAPTER 4:

LIST OF FIGURES

GENERAL INTRODUCTION:

CHAPTER 2:

LIST OF CHARTS

GENERAL INTRODUCTION:

CHAPTER 1:

CHAPTER 2:

CHAPTER 4:

LIST OF SCHEMES

CHAPTER 1:

CHAPTER 2:

CHAPTER 3:

CHAPTER 4:

GENERAL INTRODUCTION

Availability of the readily functionalized polycyclic aromatic hydrocarbons (PAHs) plays a significant role in the developing area of molecular electronics and photovoltaics. These materials often display outstanding optical and electronic properties and are well-suited for applications in such emerging areas as flexible display devices, field effect transistors and solar cell panels.[1-3] It is thus crucial to develop efficient organic synthesis techniques that could afford novel organic molecules with desired redox and optoelectronic properties.

In the context of molecular electronics and photovoltaics, it is critical to develop an intuitive understanding of the mechanism of the charge transfer in electroactive organic molecules. For example, in order to study the charge transfer across a long π-conjugated molecular wire one usually considers a donor-wire-acceptor triad. It has been shown that depending on the interchromophoric electronic coupling and length of the wire, the charge mechanism across the donor-wire-acceptor triad can be either tunneling, where charge transfer from donor to acceptor occurs without involvement of the wire (**Figure 1 A**), or incoherent hopping, where charge transfer occurs by a sequential hop between the chromophores in the wire (**Figure 1 B**) or by a combination of these two mechanisms (**Figure 1 C**). [4-11]

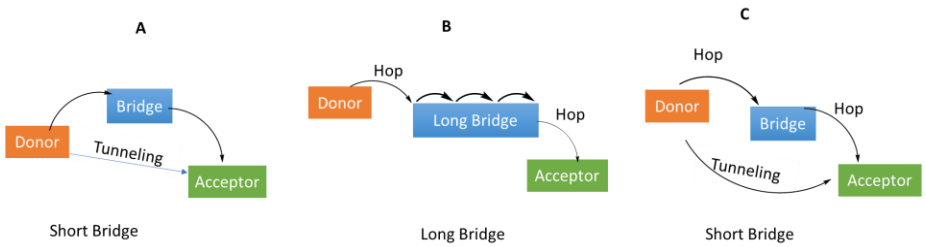

Figure 1 Schematic diagram showing the charge-transfer mechanisms in donor-bridge-acceptor triads (hopping vs. tunneling).

For photovoltaic applications, materials should have certain characteristics, such as high molar absorption coefficients, relatively broader absorption bands, customizable HOMO and LUMO energies for efficient charge transfer, molecular stability and self-assembling ability. The color of the compounds determines the first two characteristic, which can be controlled by tuning the energy gap between the ground and excited state energy. For example, the energy gap for a given chromophore can be reduced by adopting various approaches, including via greater delocalization of the π systems, inclusion of donor-acceptor substituents, and polymerization.

The design and synthesis of novel functional materials for long-range charge transport necessitates the development of the fundamental understanding of the mechanisms of charge (i.e., electron or hole) transfer in a π-conjugated molecule. In fact, electron transfer (ET) process was first explained in 1940s by Rudolph A. Marcus with the aid of the transition state theory, that is an empirical concept for understanding the dependence of the ET rate constants on the electronic coupling (H_{ab}) and structural reorganization (λ) parameters.[12-14] Based on these ideas, Robin and Day first introduced a classification of mechanism of charge delocalization for the mixed valence species, i.e.,

compounds that contain an element which is present in more than one oxidation state.[15] For example, well-known mixed valence compounds include the Creutz-Taube complex[16], Prussian blue[12] and Molybdenum blue[17]. Later, Allen and Hush modified Marcus theory in order to explain the electronic transitions that are unique to mixed valence species, i.e., the near-IR intervalence band often observed in their UV-vis spectra.[18]

Following the Robin-Day classification and Marcus-Hush theory, there are three classes of the mixed valence species that give rise to different mechanism of charge delocalization and nature of the intervalence transitions (**Figure 2**). [12, 15, 19-20] In Class I, there is no electronic coupling between redox centers leading to the charge localization on a single redox center and absence of the intervalence band. In Class II, due to the sizable electronic coupling, the charge is delocalized over both redox centers with the maximum of the charge density at one of the redox centers. This results in the presence of two minima separated by the activation barrier and the charge is distributed via 'dynamic hopping' mechanism. In such scenario, the intervalence band corresponds to charge-transfer transition and the excitation energy equals the structural reorganization parameter λ. In Class III, the charge is 'statically' delocalized over both redox centers due to the large electronic coupling and the excitation energy of the intervalence band is twice the electronic coupling ($2H_{ab}$).

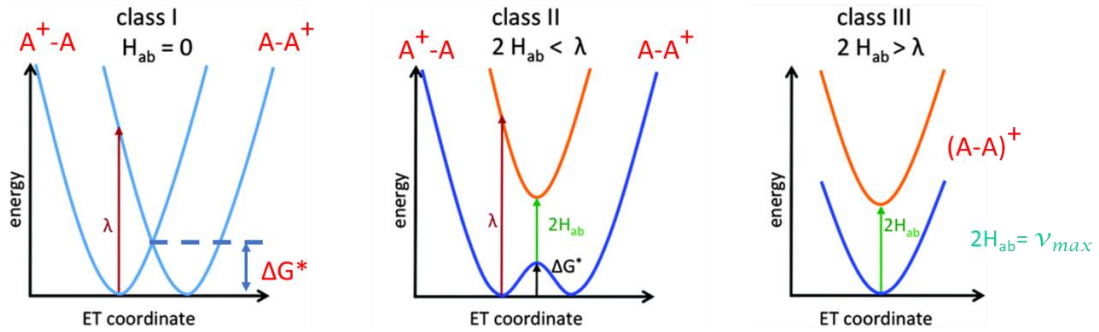

Figure 2 Potential curves for the three primary Robin–Day classes: **class I** (left), **class II** (middle) and **class III** (right)[19].

Because poly-p-phenylene-based materials can be easily functionalized, they have versatile applications in organic electronics. Their multi-dimensional structural features can be customized to produce materials with varied colors. This important property makes poly-p-phenylene wires very suitable for photovoltaic uses.

Incorporation of the solubilizing groups into the poly-p-phenylene wires may increase the solubility, and also increase steric interaction between the individual polymer chain as opposed to the unsubstituted poly-p-phenylene spacers.[21] Furthermore, it is also well known that the optical and electronic properties of these conjugated molecules are directly related to the intramolecular delocalization of the π-orbitals and extent of the orbital overlap, the torsional motion between phenylene.[21-24] A further tuning of the desired properties in polyphenylene based materials is based on the frequency of bridging of adjacent moieties: a ladder type polyphenylene (LPPP)[25] where all the individual phenyl units are linked by a methylene bridge or a step-ladder[26] where the continuous array of phenyl units is interrupted resulting in either randomly distributed bridged and unbridged units or regular polymers like polyfluorene [21], poly(2,7-silafluorene)[27],

polycarbazole[28], poly(ladder type tetraphenylene and pentaphenylene), polyindenofluorenes etc [29-30](**Chart 1**).

Chart 1. Different kinds of polyphenylenes

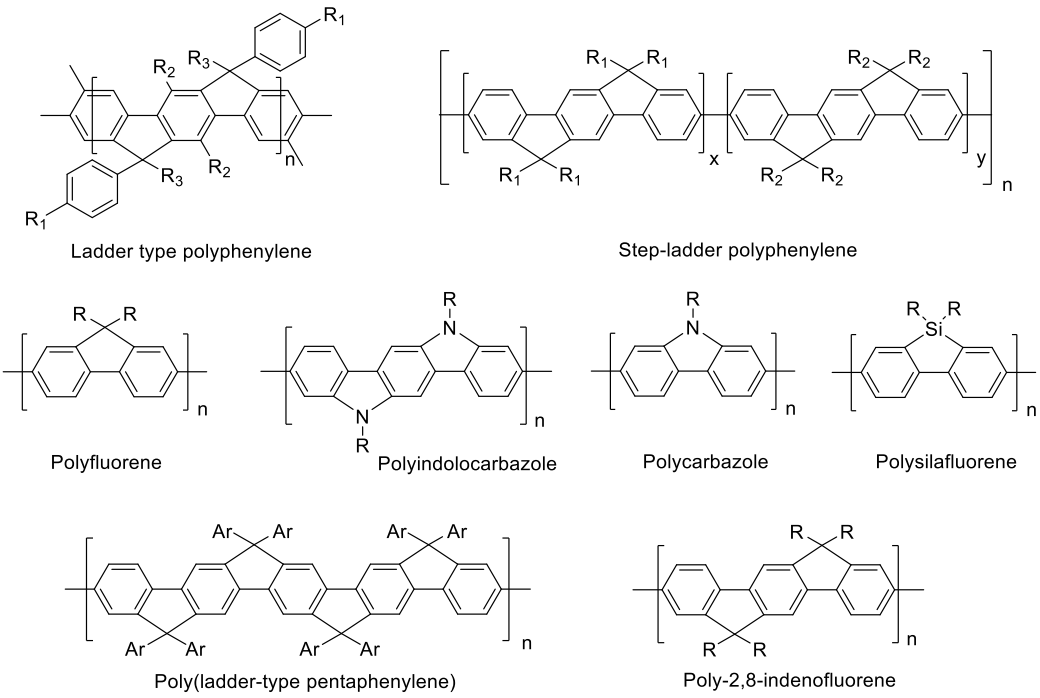

It is to this effect that Rathore *et. al*[21-24] have undertaken a systematic study to understand the structure-property relationship of such planar (Ladder) type polyfluorene oligomers by substituting solubilizing groups (hexyl) along the conjugated backbone. Also in this oligomeric series the first oxidation potentials decreases exponentially with the number of phenyl units. Same trend we saw in case of poly-p-phenylenes with isoalkyl end-capping groups. However, in case of planar polyfluorenes the first oxidation potentials were being less when compare with the poly-p-phenylenes with isoalkyl end-capping groups which indicates better stabilization of the resulting hole on

electrochemical oxidation resulting from a planar π-system or a more extended effective conjugation length.

Our interest in various polyphenylene based molecules arises from the fact that such materials have the potential to be used as functional molecular wires to transport energy or an electron (or hole) from a donor to an acceptor moiety acting as a bridging spacer.[21-24] The most important criterion for designing such materials is a proper understanding as to how the charge is stabilized or transported through multiple aryl moieties that constitute the spacer. Towards this goal, we have already synthesized and studied a homologous series of p-phenylene oligomers with different end-capping groups and also studied the polyfluorenes, planar type polyfluorenes, the results of which have already been communicated. These studies of the distance dependent behavior of π-conjugated polymers, are realized by establishing a structure-property relationship over a homologous series of oligomers as models for the related infinite chain. Since π-conjugated polymers reach a convergence limit for certain physical properties such as redox and optical, this approach provides on extrapolation the value of the effective conjugation length (ECL) i.e. a measure of the size of the polymer that is required for size-independent physical properties. With these ideas now we undertake the systematic study of angular dependent polyfluorenes.

Recently, Rathore group has shown that the experimental redox potentials (E_{ox}) of poly-p-phenylene wires (^{R}PPn: R = H, iA, iAO, and iA_2N, where n is the number of phenylene units) and the optical properties (ν_{max}) of the resulting cation radicals (i.e., $^{R}PPn^{\bullet+}$) saturate with $n \leq 8$.[21-24] With the increasing electron-donor strength of endcapping group, the saturation point moves to smaller n; i.e., saturation occurs at n = 5

for ^{iAO}PPn and n = 3 for ^{iA2N}PPn. Density Functional Theory (DFT) calculations and theoretical modeling showed that migration of the hole toward one end of the molecule for continuous engagement of the end-capped p-phenylene unit in hole stabilization causes the saturation of the redox and optical properties.[21-24]

Unlike the simple poly-p-phenylene wires (^{R}PPn), in FPPn wires the dihedral angle between p-phenylenes within one fluorene (~0.08 ± 0.05°) and adjacent fluorenes (~37.15 ± 0.11°) are different, and therefore, the values of the coupling (β) will alternate for each pair of the adjacent p-phenylenes as depicted in **Figure 3**.

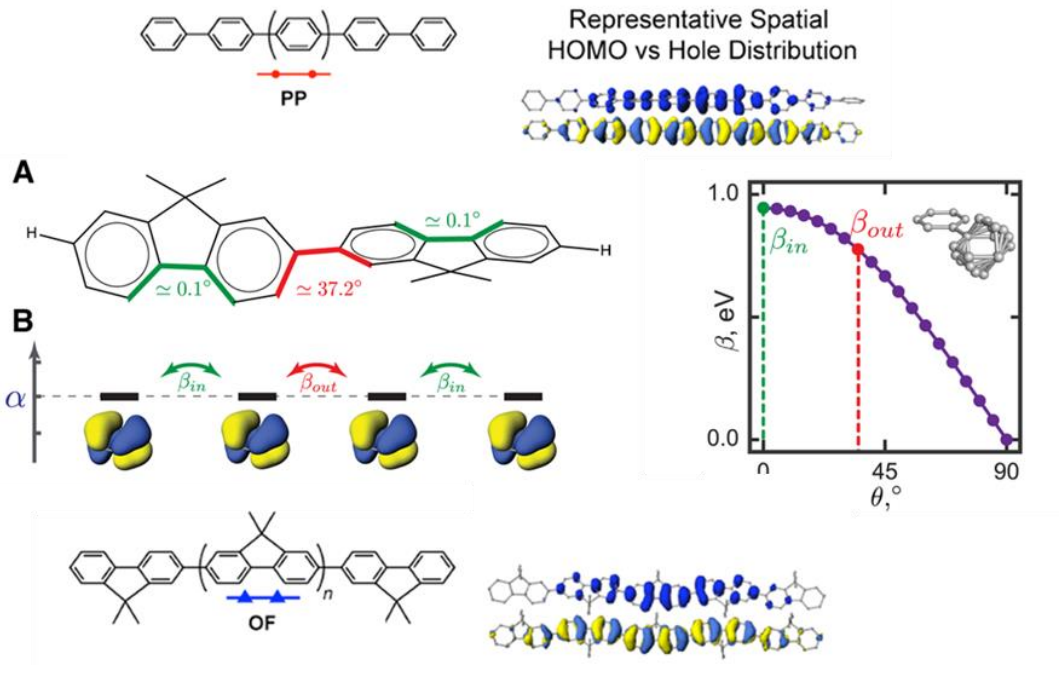

Figure 3. (A) Structure of FPP4 with the highlighted alternation in the dihedral angles. (B) Isosurface (0.02 au) of "bisallylic" HOMO of benzene and its HOMO energies (α) used to model the monomeric units in FPPn. The alternating couplings between the monomeric units are shown as β_{in} and β_{out}. [24]

Importantly, the generality of the Marcus-Hush theory makes it applicable not only to the mixed-valence systems, but also to the cation radicals of various PAHs, including molecular wires. Extension of the two-state Marcus-Hush theory to treat multiple units in a molecular wire has shown that the mechanism of hole delocalization depends on interplay between the energetic gain from the delocalization and the concomitant energetic penalty from the structural reorganization. In case of poly-p-phenylene wires, the interplay between these two factors leads to the hole delocalization up to 8 p-phenylene units.[24]

In the course of the rational design of novel poly-p-phenylene-based wires with enhanced redox and optical properties, one usually considers various geometrical factors in order to control the mechanism of charge delocalization. For example, a relatively small (~30o) interplanar dihedral angle (φ) between adjacent units in poly-p-phenylene wire leads to a significant interchromophoric electronic coupling and thereby to extensive hole delocalization. However, it remains unclear how change in the interplanar angle would impact the redox and optical properties of the wire as well the mechanism of the hole delocalization in its cation radical.[24]

In this respect, biaryl compounds represent the smallest building blocks for exploration of the fundamental properties of the charge transfer in pi-conjugated molecular wires. For example, the angular dependence of the charge transfer in biaryls has been probed by conductance measurements using break-junction techniques that showed that under the tunneling charge transfer mechanism the charge-transfer rates scale as the square of the electronic coupling in biaryl compounds. Because the electronic coupling varies with the interplanar dihedral angle between the aryl groups, the

charge-transfer rates follow a squared cosine trend with φ. On the other hand, in the case of non-coherent charge transfer mechanism it is not clear how the interplanar angle controls the mechanism of hole delocalization. In order to probe this effect, one has to design a set of the biaryls where the interplanar angle is varied with the aid of polymethylene chain or bulky groups and generate their cation radicals. Availability of the set of cation radicals with varied interplanar angle would allow probing the mechanism of their hole delocalization via electrochemical and electronic absorption (i.e., UV-vis) spectroscopy techniques.

Poly-*p*-phenylene-based wires are prototypical systems for charge-transfer studies with potential applications in photovoltaic and molecular electronics devices.[31-35] Electronic coupling between a pair of phenylenes in a poly-*p*-phenylene-based wire is a crucial parameter that controls its redox and optical properties, as well as the rates of electron transfer in corresponding donor-wire-acceptor systems.[36-39] For example, unsubstituted poly-*p*-phenylene wires are characterized by strong interchromophoric electronic coupling due to the favorable nodal arrangement of the HOMO lobes and relatively small interplanar dihedral angles, which promote effective orbital overlap between adjacent phenylenes.[24, 40] This strong electronic coupling is reflected in the sensitivity of redox/optical properties to the wire length, as can be judged by large slopes in their $1/n$ or $\cos[\pi/(n+1)]$ dependences,[23-24] where n is number of chromophoric units in a wire.

In this context, an interesting question concerns how many phenylenes should be included in a single chromophore. For example, a poly-*p*-phenylene-based wire shown in **Figure 4** can be either considered as a poly-fluorene (i.e., **PF**$_n$) or poly-*p*-phenylene (i.e.,

PP$_n$). Irrespective of how the chromophore is defined, the absorption band of **PF**$_n$ or **PP**$_n$ shifts red with increasing wire length, indicating that interchromophoric electronic coupling is significant (**Figure 4**).[24] But can the value of the electronic coupling depend on how one defines the chromophore?

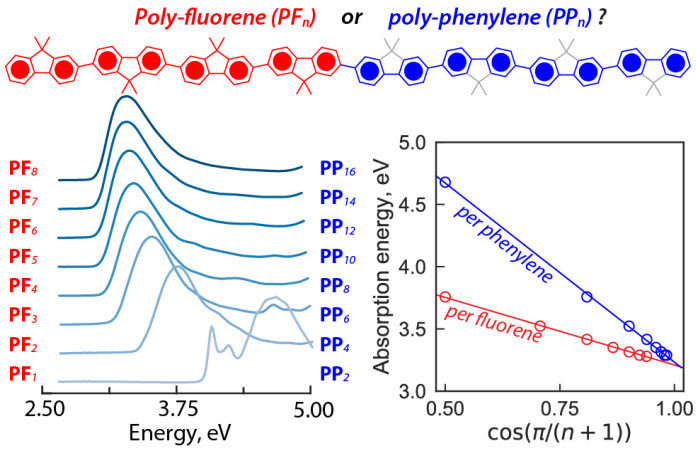

Figure 4. Depending on the choice of the monomeric unit, a molecular wire on the top can be either considered as poly-fluorene (**PFn**) or poly-phenylene (**PPn**). Left. Absorption spectra of **PFn** (or **PPn**). Right: Energies of maximum absorption plotted against cos[π/(n+1)], where n is number of phenylenes (blue) or fluorenes (red).

According to the Hückel molecular orbital theory, the energy of the HOMO to LUMO transition scales linearly with cos[π/(*n*+1)] and the scaling factor depends on the electronic coupling.[24,41] Remarkably, the slope of the linear ν-vs-cos[π/(*n*+1)] plot is smaller by nearly a factor of two when *n* is number of fluorenes as compared to the plot where *n* is number of phenylenes (**Figure 4**), suggesting that the electronic coupling between fluorenes is by a factor of two smaller than between a pair of phenylenes for the same wire.

As the magnitude of the electronic coupling directly impacts the redox/optical properties of the wire and the extent of hole (i.e., polaron) delocalization in the corresponding cation radicals, a choice of the chromophore size either by length (e.g molecular wire) or two dimensionally extended π systems (e.g Polycylic Aromatic Hydrocarbons, PAHs) seems to be an important additional parameter.

Polycyclic aromatic hydrocarbons (PAHs) consist of multiple aromatic ring having sp^2 carbon centers, which together are considered as a graphitic core. PAHs with expanded graphitic core have received tremendous attention as potential candidates for their application in thin film electronic devices, field effect transistors, and photovoltaic applications.[42-47] Most often, these PAHs show strong tendency to form π-stacked dimers in solution and form face-to-face contacts with some extent of face-to-edge configurations in the solid state. The enhanced charge mobility and attractive photo physical properties arising from the expanded graphitic core and strong inter-molecular π–π interactions make PAHs good candidates as charge-transfer materials for applications in opto-electronic devices.

In the 1960s, Clar and coworkers [48] suggested that the "fully benzenoid" hexa-peri-hexabenzocoronene (HBC) should possess exceptional thermal and photochemical stability, although its insolubility in most organic solvents has made it challenging to study.

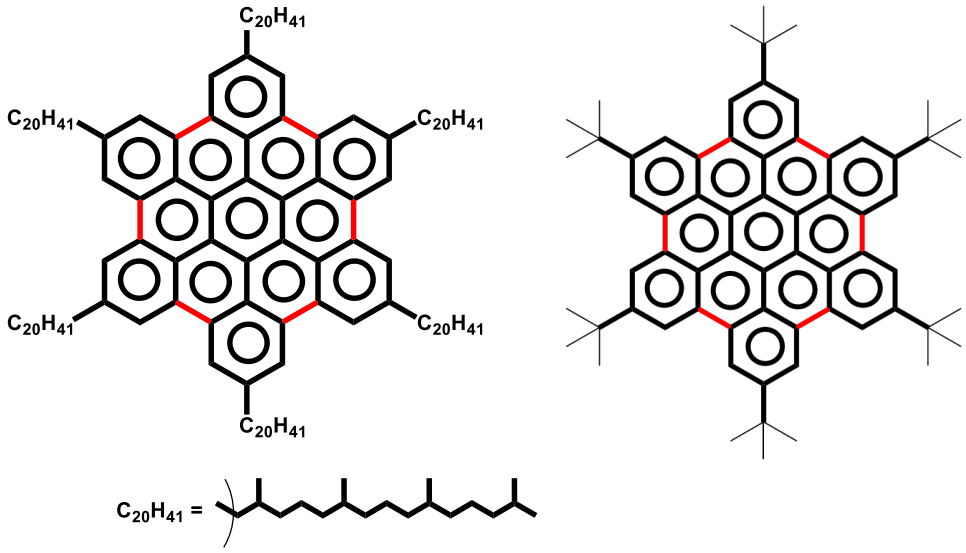

Figure 5. Hexa-perihexabenzocoronene substituted with long alkyl chains [50] (left) and hexa-perihexabenzocoronene substituted with tert-butyl groups.[51]

To address the solubility issue, Mùllen and co-workers[49] prepared a variety of soluble derivatives of hexa-perihexabenzocoronene (and its higher homologues) by substitution of its free para positions with either long alkyl chains [50] or with bulky tert-butyl groups[51] to prevent aggregation in solution. In the solid state the disc-shaped HBCs self-assemble into columnar stacks through strong intermolecular π–π interactions. Synthetic versatility also allows for a large variation in functional groups on the HBC molecule. This has led to potential applications as nano-structured materials in biology, energy storage, and organic electronics. By functionalizing the HBC molecule with different substituents, the properties of the molecule can be modulated dramatically to afford improved solubility, altered solid packing, liquid crystallinity and improved charge carrier mobility.[52-55]

The promising potential applications of HBC prompted Rathore and co-workers to seek a cost-effective and facile synthesis of a soluble derivative of hexa-peri-hexabenzocoronene (HBC) from readily available hexaphenylbenzene (HPB). The design of a facile procedure in which the substitution of the free para positions of the propeller-shaped hexaphenylbenzene with tert-butyl groups and the oxidative cyclodehydrogenation to planar HBC was achieved in a one-pot reaction using ferric chloride both as a Lewis acid catalyst and as an oxidant in excellent yields. [51,56-57] Although PAH materials based on **HBC**s are promising for variety of photovoltaic applications, it is still required to develop a soluble, versatile **HBC**-based platform, which can be easily modified to include electro-active groups or groups that can arranged by self-assembly. However, a successful synthesis of such **HBC**-based hybrids with extended graphitic core that can resists aggregation, highly soluble and readily functionalizable at its vertices remains a great challenge.

The requirements described above put forward a requirement on the stability of the oxidants used to generate the cation radical of a given electron donor in solution. Rathore and coworkers have shown that cation radicals of numerous PAHs, e.g. substituted benzenes, naphthalenes, anthracenes, pyrenes, poly-phenylenes, hexa-peri-hexabenzocoronenes (HBCs) and many others,[58-61] can be generated using stable aromatic cation radical salts (**Chart 2**) such as **NAP**$^{\bullet+}$ $SbCl_6^-$ (1,2,3,4,7,8,9,10-octahydro-1,1,4,4,7,7,10,10-octamethylnaphtacene, E_{red} = 1.34 V vs. SCE, λmax = 673 nm, log ε673 = 3.97),[62] **THE**$^{+\bullet}$$SbCl_6^-$ (1,2,3,4,5,6,7,8-octa-hydro-9,10-dime-thoxy-1,4:5,8-dimethanoanthracene, E_{red} = 1.11 V vs. SCE, λmax = 518 nm, log ε518 = 3.86) [63]

and **MB**$^{\bullet+}$$SbCl_6^-$ **(**tris-4-bromophenylamminium or magic blue, E_{red} = 1.15 V vs. SCE, λmax = 728 nm, log ε728 = 4.45).[62,64]

Chart 2. Cation-Radical salts as 1 -Electron Oxidants

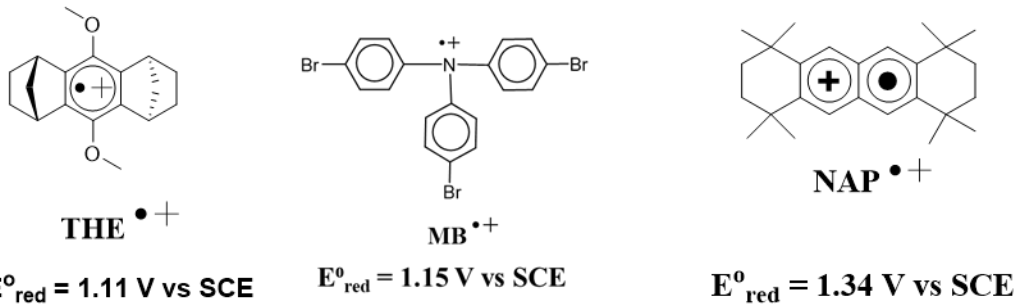

Among these oxidants, magic blue (**MB**$^{+\bullet}$ $SbCl_6^-$ salt) has been widely used as an aromatic oxidant for the one electron oxidation of organic, inorganic, and organometallic donors due to its commercial availability and a reasonable oxidizing power.[65-75] With an intense and uncluttered visible absorption (λ_{max} = 728 nm, ε_{max} = 28 200 cm^{-1} M^{-1}) magic blue has also found extensive application for (quantitative) spectroscopic characterization of cation radicals and dications of organic electron donors and oxidized inorganic metal complexes and organometallic species.

However, a modest stability of the **MB**$^{+\bullet}$ $SbCl_6^-$ salt leads to a slow decomposition to produce unknown impurities, which have been named "blues brothers".[76] Importantly, these impurities produce a noticeable band in the near-IR region—that is the same region where one usually expects to see an intervalence band of the cation radical with extensive hole delocalization (**Figure 6**).[77]

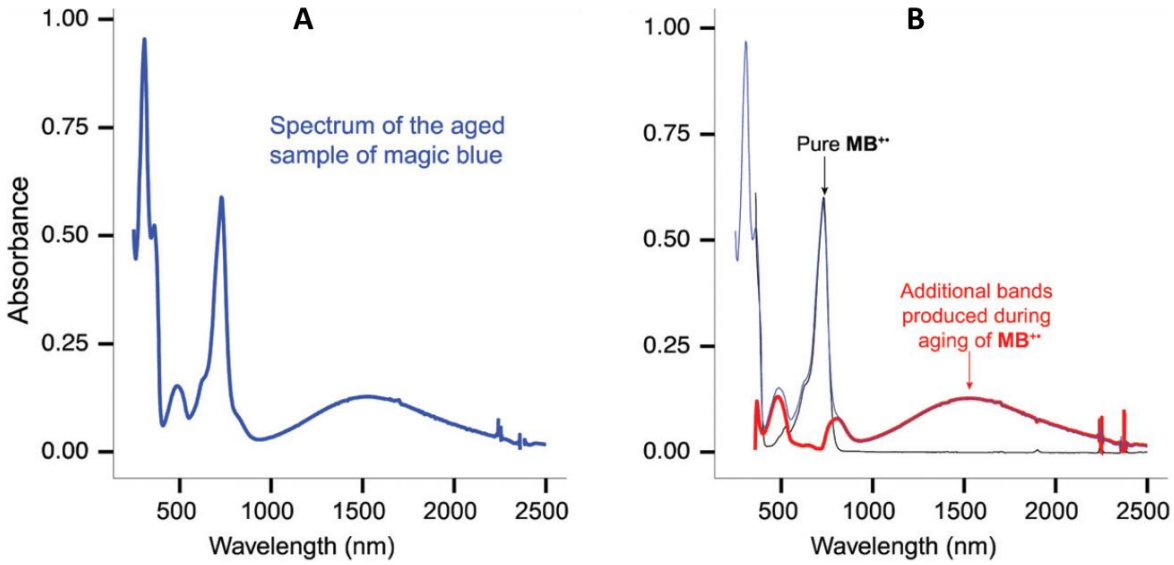

Figure 6 (**A**) Absorption spectrum of the aged **MB**$^{+\bullet}$ **SbCl6**$^{-}$ salt at 22 °C in CH_2Cl_2; (**B**) spectrum obtained by the subtraction of aged **MB**$^{+\bullet}$ (shown in panel **A**) and freshly prepared **MB**$^{+\bullet}$.

Thus, presence of these impurities presents a significant issue in accurate characterization of the mechanism of hole delocalization in the cation radicals. While in practice in order to generate a cation radical of a PAH one can use other oxidants such as **THE**$^{+\bullet}$ or **NAP**$^{+\bullet}$, a relatively low reduction potential of **MB**$^{+\bullet}$ makes it especially useful when generation of the cation radicals of the PAH with low oxidation potentials is required. Examples of the PAH with low oxidation potential include long poly-p-phenylene wires or PAHs with expanded graphitic core, e.g. HBC. Thus, a rational approach in the development of the **MB** analogues with similar optoelectronic properties and improved stability is of significant importance.

RESEARCH OBJECTIVES

Given the diversity of the challenges that exists in the area of the design and synthesis of novel charge-transfer materials this research work aims to address the issue outlined above as follows:

1. We will develop a fundamental understanding of the structure-function relationship of the poly-p-phenylene wires in the context of their application as charge-transfer medium. In particular, this work will address how the interplanar dihedral angle between two aryl groups impacts the redox/optoelectronic properties and hole delocalization of a biaryl cation radicals. With the aid of Marcus-Hush theory these results will allow to develop an intuitive understanding on how the interplay between electronic coupling and structural reorganization controls the hole delocalization.

2. Motivated by the need to develop various robust aromatic oxidants we aim to investigate the content of the impurities that are generated during the aging of the magic blue oxidant. Based on these findings we will propose and synthesis a novel MB-analogue that could effectively resist degradation, while remaining or somewhat improving its redox and optoelectronic properties.

3. As there remains the need for a soluble HBC-based platform, which can include electro-active groups or groups that can prompt self-assembly, we aim to synthesize a new HBC-fluorene hybrid (FHBC) with expanded graphitic core that is highly soluble, resists aggregation, and can be readily functionalized at its vertices. We will show that this new HBC platform can be tailored to incorporate

six electro-active groups at its vertices, as will be exemplified by a facile synthesis of a representative hexaaryl derivative of FHB

4. During the course of the rational design of polychromophoric assemblies it is often unclear how the interchromophoric electronic coupling varies with chromophore size in linearly connected molecular wires. We will demonstrate that as the number of aromatic moieties in a single chromophore increases, the interchromophoric electronic coupling decreases and may reach negligible values if the chromophore is sufficiently large.

CHAPTER 1

A search for blues brothers: X-ray crystallographic/ spectroscopic characterization of the tetraarylbenzidine cation radical as a product of aging of solid magic blue.

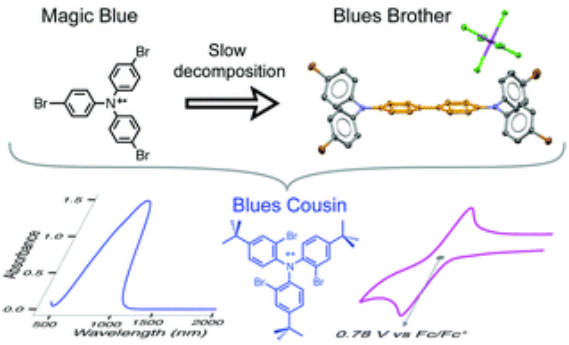

Abstract: Magic blue ($MB^{+\bullet}$ $SbCl_6^-$), *i.e.* tris-4-bromophenylamminium cation radical, is a routinely employed one-electron oxidant that slowly decomposes in the solid state upon storage to form so called 'blues brothers', which can complicate the quantitative analyses of the oxidation processes. Herein, we indentify the primary 'blues brother' as the cation radical and dication of tetrakis-(4-bromophenyl) benzidine (**TAB**), using a combined Density Functional Theory (DFT) and experimental approach, including isolation of $\mathbf{TAB}^{+\bullet}$ $SbCl_6^-$ and its characterization by X-ray crystallography. The formation of **TAB** in aged magic blue samples occurs by a Scholl-type coupling of a pair of **MB**, followed by the loss of molecular bromine. The recognition of this fact led us to the rational design and synthesis of *tris*(2-bromo-4-*tert*-butylphenyl)amine, referred to as 'blues cousin' (**C**: E_{ox1} = 0.78 V *vs.* Fc/Fc^+, λ_{max} ($\mathbf{BC}^{+\bullet}$) = 805 nm, ε_{max} = 9930 cm^{-1} M^{-1}), whose oxidative dimerization is significantly hampered by positioning the sterically demanding *tert*-butyl groups at the *para*-positions of the aryl rings. A ready two-step synthesis of **BC** from triphenylamine and the high stability of its cation radical ($\mathbf{BC}^{+\bullet}$) promise that **BC** will serve as a ready replacement for **MB** and an oxidant of choice for mechanistic investigations of one-electron transfer processes in organic, inorganic, and organometallic transformations.

Disclaimer: The results discussed in this chapters were further supplemented by DFT calculations and relevant computational works by my coworker Dr. Marat R Talipov. The presence of an impurity in Magic blue was first observed by my coworker Dr. Anitha Boddeda. My contribution to this chapter includes synthesis and spectroscopic studies. Blues Cousin was synthesized and studied by another coworker, Dr. Khushabu Thakur

INTRODUCTION

Magic blue ($MB^{+\bullet}$ $SbCl_6^-$), i.e. tris-4-bromophenylamminium cation radical,[1] is widely utilized as an aromatic oxidant for the one electron ($1e^-$) oxidation of organic, inorganic, and organometallic donors.[2–10] The popularity of the magic blue cation radical as an oxidant in part arises due to its perceived high stability, commercial availability, and reasonable oxidizing power (E_{red} = 0.70 V vs. Fc/Fc^+). With an intense and uncluttered visible absorption (λ_{max} = 728 nm, ε_{max} = 28 200 cm^{-1} M^{-1}) magic blue has also found extensive application for (quantitative) spectroscopic characterization of cation radicals and dications of organic electron donors and oxidized inorganic metal complexes and organometallic species.[11,12] Although $MB^{+\bullet}$ $SbCl_6^-$ is reasonably stable, it has been long known that $MB^{+\bullet}$ undergoes slow decomposition to produce impurities which have been dubbed 'blues brothers'.[2,13] During the course of our studies of organic cation radicals and dications, we observed that the presence of additional bands in the spectrum of $MB^{+\bullet}$ not only interfered with spectroscopic characterization of oxidized species, but also prevented accurate quantification of redox processes.[14] Here, we identify the major impurity responsible for the presence of additional absorption bands in the old samples of $MB^{+\bullet}$ $SbCl_6^-$ salt as a tetraarylbenzidine cation radical/dication with the aid of electronic absorption spectroscopy, X-ray crystallography, and detailed computational studies.

Chart 1. 1. Structures and Naming schemes of various possible candidates of 'blues brother'

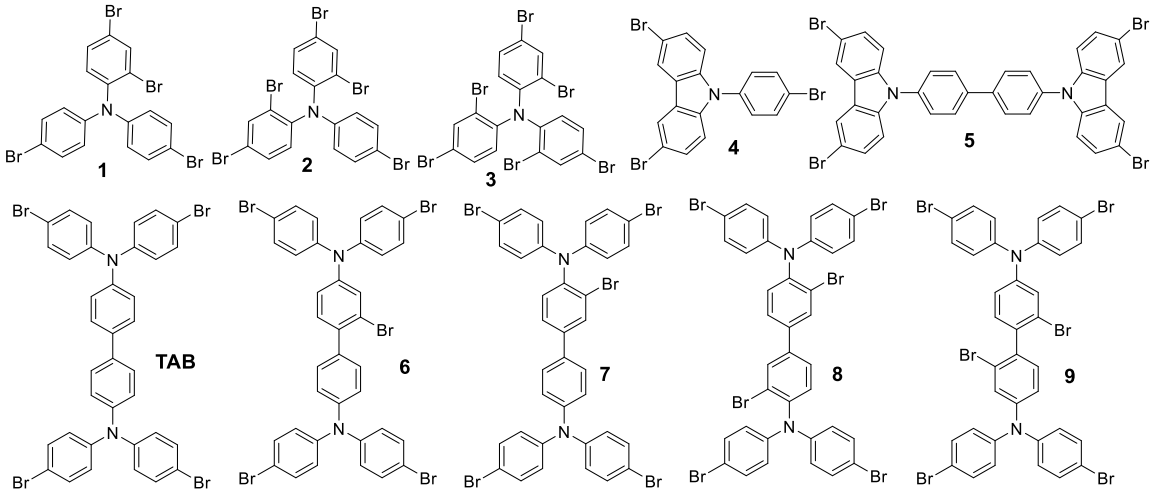

Finding that the 'blues brother' in the aged $MB^{+\bullet}$ sample is produced by a dimerization reaction led us to the rational synthesis of a new triarylamine derivative which prevents the dimerization reaction. This triarylamine derivative forms a stable cation radical with similar spectral properties and somewhat improved oxidizing power, and it is referred to as blues cousin, which should serve as a ready replacement for MB as an oxidant of choice for mechanistic investigations of one-electron transfer processes in a variety of organic, inorganic, and organometallic transformations.

RESULTS AND DISCUSSION

The initial attempt to identify the species responsible for additional absorption bands in aged samples of $MB^{+\bullet}$ was carried out by its reduction using zinc dust or ferrocene, followed by ^1H NMR analysis of the resulting neutral residue. The ^1H NMR analysis suggested that the sample largely contained MB^0 together with a significant amount of a new, unidentified species,

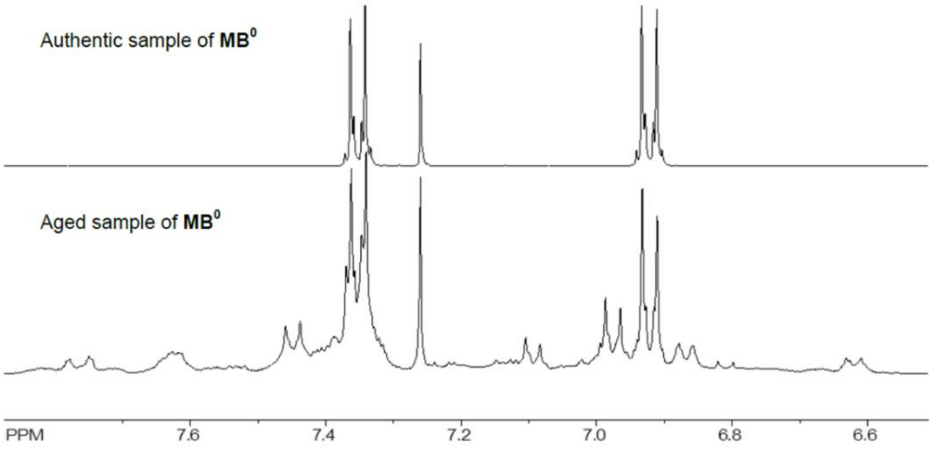

Figure 1. 1 Comparison of the ^{1}H NMR spectra of aged sample of **MB**$^{+\bullet}$ reduced by Zn dust or ferrocene (bottom) and the authentic sample of neutral **MB**^{0} (top).

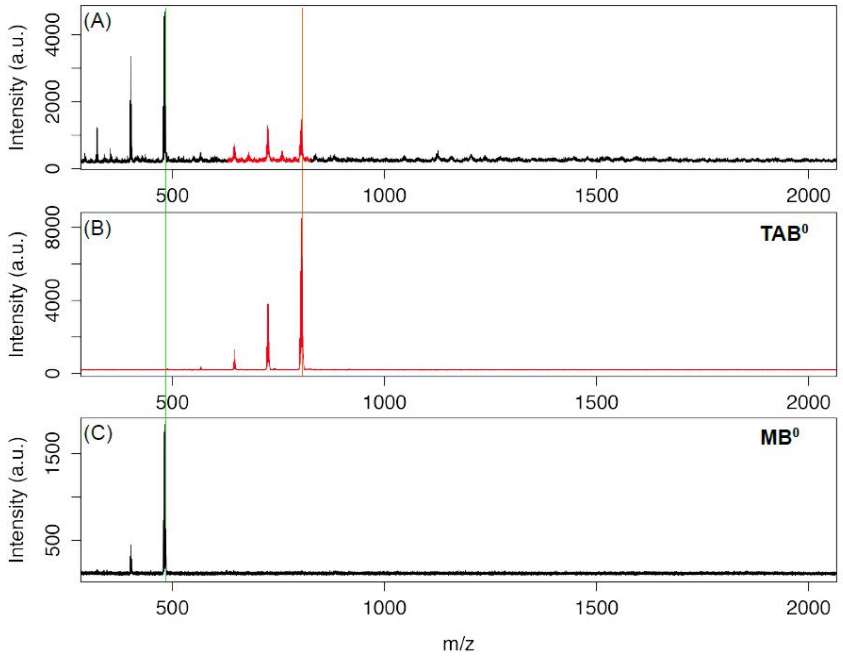

Figure 1. 2 MALDI-TOF mass spectra of the aged sample of **MB**$^{+\bullet}$, reduced to **MB**^{0} using ferrocene in dichloromethane [The NMR spectrum of the same sample is shown above in **Figure 1.1**] (A), and authentic samples of **TAB**^{0} (B) and **MB**^{0} (C).

and multiple other compounds in minor quantities (**Figure 1.1**). The new species was tentatively identified by MALDI mass spectrometry to be a dimer of MB, which had lost a molecule of bromine, and was hypothesized to be a tetrakis-(4 bromophenyl) benzidine (**Figure 1.2**). Unfortunately, full identification of this dimer and other minor species could not be achieved by chromatographic separation, despite several attempts. In order to establish that additional absorption bands in the aged samples of $MB^{+\bullet}$ (**Figure 1. 3. A**) arise from its decomposition, we obtained an authentic spectrum of $MB^{+\bullet}$ via redox titration of neutral MB using a bicyclo[2.2.1]heptane-annulated hydroquinone ether cation radical $THEO^{+\bullet}\ SbCl_6^-$ (E_{red1} = 0.67 V vs. Fc/Fc^+, λ_{max} = 518 nm, ε_{max} = 7300 $cm^{-1}\ M^{-1}$)[15–17] as an oxidant. The spectrum of $MB^{+\bullet}$ obtained via redox titration according to **Figure 1.3** was found to be identical to the spectrum of the freshly prepared sample of $MB^{+\bullet}$ using MB^0 and $SbCl_5$ or $NO^+\ SbCl_6^-$ as oxidants (**Figure 1.3. B**). A subtraction of the authentic spectrum of $MB^{+\bullet}$ with that of the aged sample (∼14 months old, Aldrich Chemical Co.) produced a spectrum containing bands at 480, 805, and 1550 nm (**Figure 1.3 C**). Moreover, the intensities of these bands increase with aging of the sample. The fact that these absorption bands are not attributable to pure $MB^{+\bullet}\ SbCl_6^-$ together with the presence of a low-energy transition at 1550 nm, suggested that the new absorption bands most likely arise from a cation radical and/or dication of a tetraarylbenzidine derivative.[18]

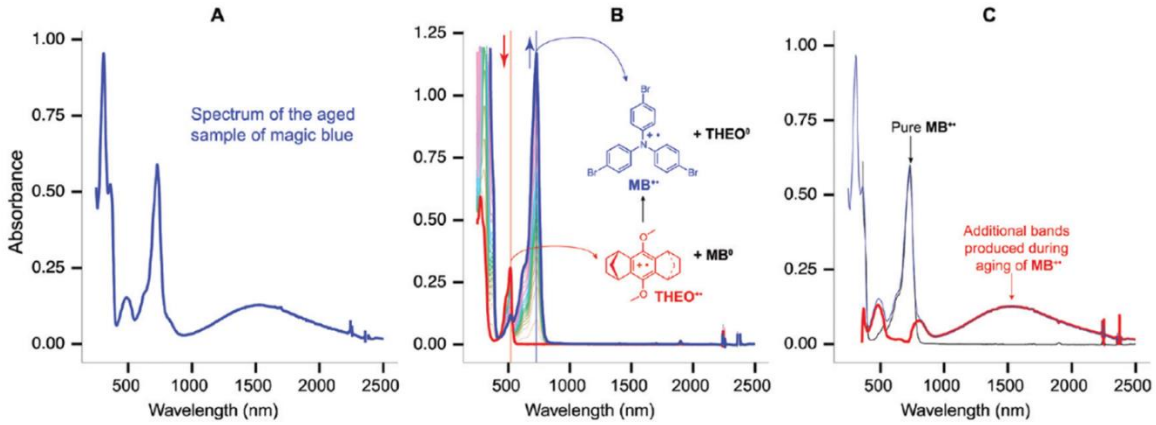

Figure 1. 3 (**A**) Absorption spectrum of the aged $\mathbf{MB^{+\bullet}\ SbCl6^{-}}$ salt at 22 °C in CH_2Cl_2; (**B**) spectral changes observed upon the redox titration of 42 μM $\mathbf{THEO^{+\bullet}\ SbCl6^{-}}$ with an incremental addition of 3.2 mM $\mathbf{MB^{0}}$ in CH_2Cl_2 at 22 °C; (**C**) spectrum obtained by the subtraction of aged $\mathbf{MB^{+\bullet}}$ (shown in panel **A**) and freshly prepared $\mathbf{MB^{+\bullet}}$ (shown in panel **B**).

Before undertaking the synthesis of authentic samples of tetrakis(4-bromophenyl)benzidine (TAB) and other products arising from bromination of either MB or TAB or by intramolecular oxidative cyclization of MB to carbazole derivatives (see **Chart 1.1**), we first carried out (TD)DFT calculations of all compounds in **Chart 1.1** to obtain both redox potentials and electronic absorption spectra of their cation radicals. For this purpose, we utilized the B1LYP-40 functional [i.e. B1LYP-40/6 31G(d)+PCM(CH2Cl2)][19,20], because as recent careful benchmarking studies from our research group on a number of polyaromatic systems[17,20–22] showed that this functional allows an accurate description of the spin/charge (hole) distribution in their cation radicals, and, in turn, the prediction of the corresponding redox/optical properties (E_{ox1}, $\upsilon_{D0\rightarrow D1}$) in good agreement with experimental data. The excellent performance of the B1LYP-40 functional owes to the fact that 40% contribution of the exact (i.e. Hartree–

Fock) exchange term alleviates the self-interaction error[23,24] that causes artificial charge delocalization.

The calculated equilibrium geometries of the neutral and cation radical forms of all compounds listed in **Chart 1.1** produced their free energies of oxidation ΔG_{ox1} by a simple subtraction of the free energies of cation radicals and the corresponding neutral molecules. A plot of the computed oxidation energies (ΔG_{ox1}) against electrochemical oxidation potentials (E_{ox1}) of compounds MB, 1, 2, and 3, available from the literature[25] (see blue diamonds and correlation line in **Figure 1.4.**), showed an excellent linear correlation, instilling confidence in our use of the B1LYP-40 functional and allowed the prediction of the oxidation potentials of various compounds in **Chart 1.1** which are yet to be synthesized, see **Table 1.1**. The additional bands in the $MB^{+\bullet}$ spectrum are expected to arise from the oxidized (i.e. cation radical or dication) forms of the blues brothers, and thus the oxidation potentials of these molecules should be lower or comparable to that of MB^0 (i.e. 0.70 V vs. Fc/Fc^+). Accordingly, the predicted values of E'_{ox1} of various compounds in **Chart 1.1** (**Table 1.1**) allow one to easily rule out the possibility of brominated MB analogues (i.e. 1–3) and carbazole derivatives 4 and 5 as blues brothers in the spectrum of aged $MB^{+\bullet}$.

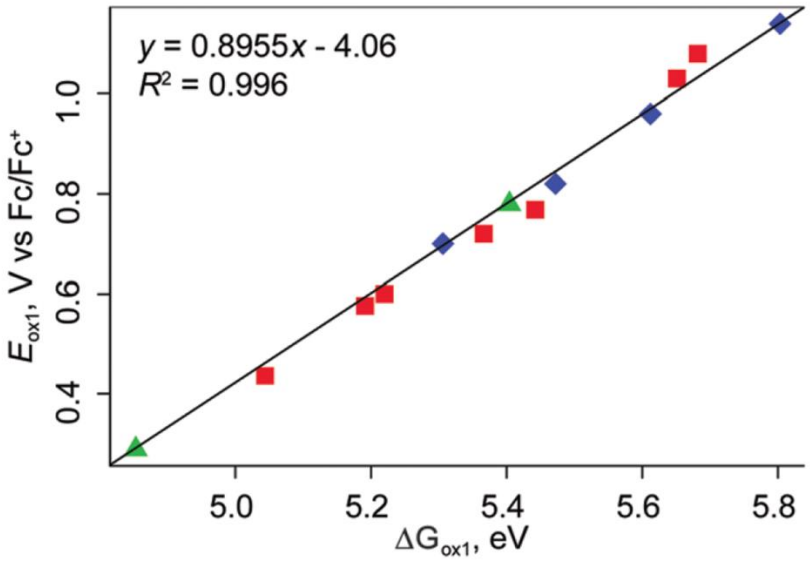

Figure 1. 4 A plot of experimental $\mathbf{E_{ox1}}$ of compounds in **Chart 1** against computed $\mathbf{\Delta G_{ox1}}$. Note that the correlation line was generated using only **MB** and **1–3** (shown by blue diamonds) for which the electrochemical oxidation potentials were available from the literature. The red squares represent the remaining compounds in **Chart 1**, while the green triangles are for '**blues cousins**' **10** and **BC** discussed later in the text.

In contrast, the E'_{ox1} values of TAB^0 and its brominated analogues 6–9 were predicted to have lower or comparable oxidation potentials to that of MB^0, and thus constitute plausible candidates for the blues brothers. In addition, TD-DFT calculations (**Tables 1.1** and **Figure 1.5**) predict the existence of low-energy bands in the spectra of $TAB^{+\bullet}$ and $6^{+\bullet}$–$9^{+\bullet}$, which are absent in the cation radicals of brominated MB analogues 1–3 and carbazole derivatives 4.[25]

Table 1. 1. Calculated [B1LYP-40/6–31G(d) + PCM(CH_2Cl_2)] free energies of oxidation (ΔG_{ox1} and E'_{ox1} [a]) and electrochemical (E_{ox1} and E_{ox2} vs. Fc/Fc^+) oxidation potentials of various compounds in **Chart 1.1**, as well as the optical properties of their cation radicals (CRs) obtained by TD-DFT calculations ($\lambda_{D0\rightarrow D1}$ and f_{osc}) and by spectroscopic redox titration (λ_{max}(CR) and ε_{max}(CR))

Compound	**ΔG_{ox1}, eV**	**E_{ox1} [a], V**	**E_{ox1}, V**	**E_{ox2}, V**	**$\lambda_{D_o\rightarrow D1}$, nm**	**f_{osc}**	**λ_{max}(CR), nm**	**ε (CR), $M^{-1}cm^{-1}$**
MB	5.306	0.69	0.70 [25,b]	–	604	0.30	728	28200
1	5.472	0.84	0.82 [25]	–	686	0.35	757 [25]	–
2	5.612	0.97	0.96 [25]	–	721	0.24	805 [25]	–
3	5.803	1.14	1.14 [25]	–	823	0.14	880 [25]	–
4	5.682	1.03	1.080 [25]	–	1291	0.03	820 [25]	–
5	5.651	1.00	1.030 [b]	–	1526	0.27	854, 2500	–
TAB	5.044	0.46	0.436 [b]	0.636 [b]	1353	1.00	1490	38100
6	5.191	0.59	0.576 [b]	0.760 [b]	1420	0.73	1735	24000
7	5.220	0.61	0.600 [b]	0.780 [b]	1304	0.56	1750	24500
8	5.442	0.81	0.768 [b]	0.856 [b]	1339	0.21	2150	15000
9	5.366	0.75	0.720 [b]	0.823 [b]	1428	0.30	2128	15000
10 [c]	4.853	0.29	0.290 [b]	–	575	0.23	681	31500
BC[c]	5.404	0.78	0.780 [b]	–	785	0.09	805	9930

[a] $E_{ox1} = 0.8955\ \Delta G_{ox1} - 4.06$ (Fig. 1.4). [b] Obtained in this work by cyclic voltammetry. [c] See the experimental section.

Based on the predictions from the (TD) DFT calculations we undertook the synthesis of TAB and its brominated derivatives 6–9 as well as carbazole derivatives 4 and 5 using standard literature procedures,[26–36] and all synthetic details are included in the experimental section. All compounds were characterized by $^1H/^{13}C$ NMR spectroscopy as well as by MALDI spectrometry. These compounds were then subjected to the cyclic voltammetric analysis at 22 °C in CH_2Cl_2 containing 0.2 M tetra-n-butylammonium hexafluorophosphate at a platinum electrode. The reversible voltammograms of TAB and 6–9 showed two oxidation waves (**Figure 1.5**) corresponding to the formation of the

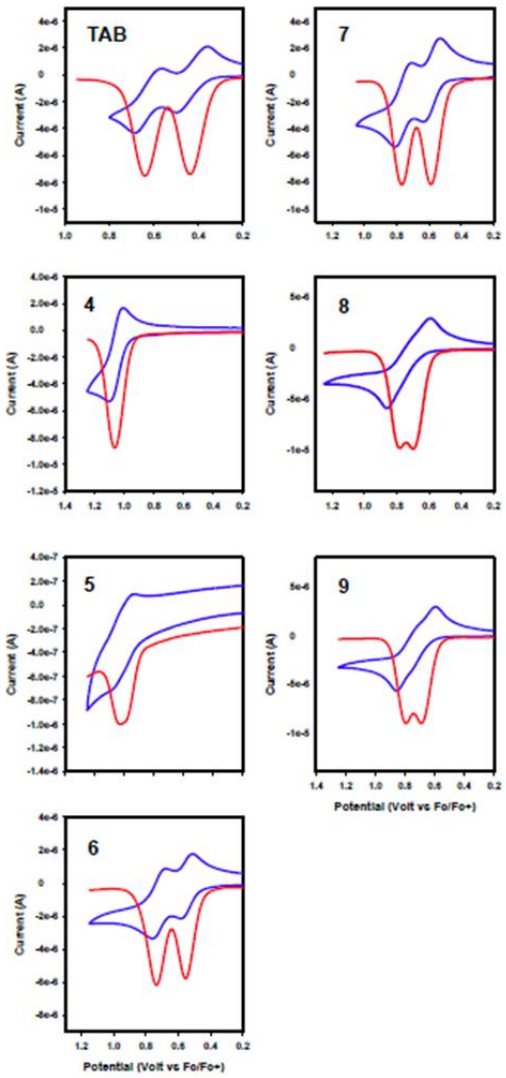

Figure 1. 5. Cyclic and square-wave voltammograms of **TAB** and **4-9** (**Chart 1.1**). Poor CV quality of **5** was due to its poor solubility in CH_2Cl_2.

cation radical and dication. The electrochemical oxidation potentials of various molecules in **Chart 1.1** are compiled in **Table 1.1** (columns 4 and 5), and they were in excellent agreement with the predicted oxidation potentials using DFT calculations (**Table 1.1**, column 3). Having obtained the oxidation potentials of all compounds in **Chart 1.1**, they

were included in **Figure 1. 4**, and all the new points (shown as red squares) fell on the original correlation line.

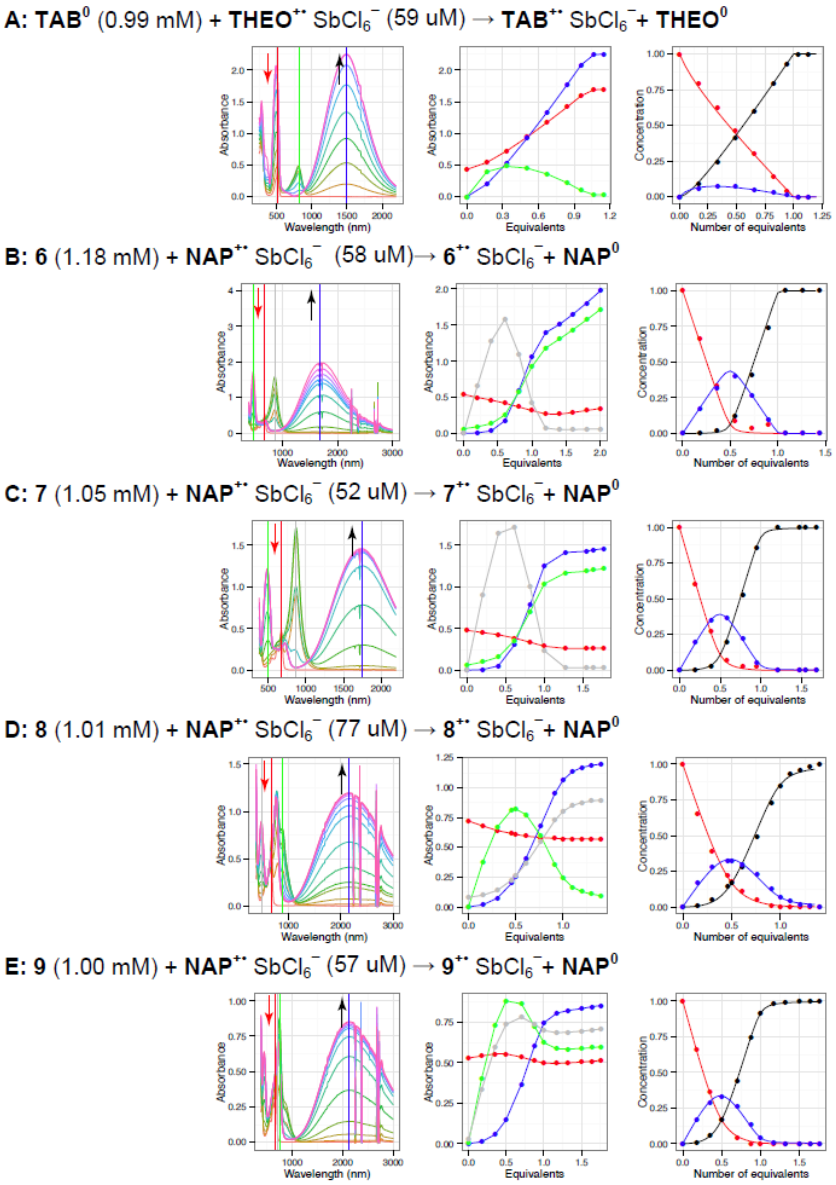

Figure 1. 6 Spectral changes attendant upon the reduction of **TAB** and **6-9** (**A-E**, as denoted) by **THEO$^{+\bullet}$ SbCl$_6^-$** and **NAP$^{+\bullet}$ SbCl$_6^-$** in CH_2Cl_2 at 22 ºC as well as the corresponding molar fraction plots against the number of added equivalents of neutral electron donor (i.e. **TAB** and **6-9**). See also **Table 1.2**.

We next generated the cation radicals/dications of TAB and 6–9 using a hindered naphthalene (i.e. 1,2,3,4,7,8,9,10-octahydro-1,1,4,4,7,7,10,10-octamethylnaphtacene) cation radical (E_{red} = 0.94 V vs. Fc/Fc_+, λ_{max} = 672 nm, ε_{max} = 9300 cm^{-1} M^{-1})[37,38] via redox titration under careful exclusion of moisture; see, e.g. **Figure 1. 6**.

Table 1. 2. Wavelengths and oscillator strengths corresponding to the lowest-energy transition in the cation radicals of compounds in **Chart 1.1**, obtained from the TD-DFT calculations [B1LYP-40/6-31G(d)+PCM(CH_2Cl_2)] ($\lambda_{D0\rightarrow D1}$ and f_{osc}) as well as the lowest-energy transition of cation radicals (λ_{max}(CR) and ε_{max}(CR)) and dications (λ_{max}(DC) and ε_{max}(DC)) of these compounds obtained by spectroscopic redox titration

Compound	$\lambda_{D0\rightarrow D1}$, nm	f_{osc}	λ_{max}(CR), nm	ε_{max}(CR), M^{-1} cm^{-1}	λ_{max}(DC), nm	ε_{max}(DC), M^{-1} cm^{-1}
MB	604	0.30	728	28200	-	-
1	686	0.35	757[18]	-	-	-
2	721	0.24	805[18]	-	-	-
3	823	0.14	880[18]	-	-	-
4	1291	0.03	820[18]	-	-	-
5	1526	0.27	854, 2500	-	-	-
TAB	1353	1.00	1490	38100	807	112600
6	1420	0.73	1735	24000	860	66500
7	1304	0.56	1750	24500	869	87700
8	1339	0.21	2150	15000	883	25590
9	1428	0.30	2128	15000	752	41750

The resulting absorption spectra of the cation radicals and dications of TAB and 6–9 are compared in **Figure 1.7**. Interestingly, the bands contained in the absorption spectra of the cation radical and dication of TAB (i.e. $TAB^{+\bullet}$: λ_{max} = 1490 nm, ε_{max} = 38 100 cm^{-1} M^{-1}, and λ_{max} = 489 nm, ε_{max} = 35 000 cm^{-1} M^{-1}; TAB^{2+}: λ_{max} = 807 nm, ε_{max} = 112 600 cm^{-1} M^{-1}) closely matched the additional absorption bands in the spectrum of

the aged sample of $MB^{+\bullet}$, i.e. compare **Figure 1.7** and **Figure 1. 3 (C)**. In order to further confirm the presence of both $TAB^{+\bullet}$ and TAB^{2+} in the spectrum of the aged $MB^{+\bullet}$ sample, we carried out a redox titration by an incremental addition of sub-stoichiometric amounts of TAB^{0} to a solution of freshly prepared $MB^{+\bullet}$ in CH_2Cl_2 at 22 °C (**Figure 1.8**).

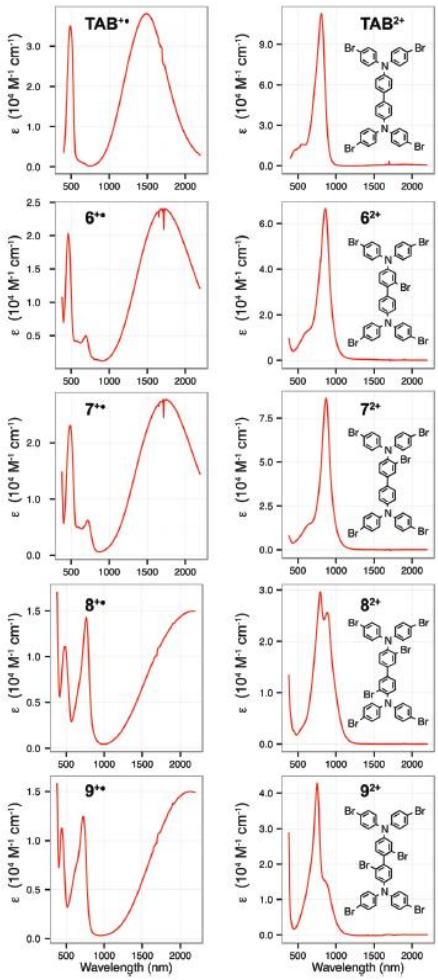

Figure 1. 7. Absorption spectra of cation radicals (left) and dications (right) of **TAB**, **6–9** in CH_2Cl_2 at 22 °C obtained via spectroscopic redox titrations using **THEO**$^{+\bullet}$ or **NAP**$^{+\bullet}$ (see **Figure 1.6** for the corresponding titration figures).

Interestingly, the spectrum obtained after addition of ~0.15 equivalents of TAB^0 to a solution of $MB^{+\bullet}$ produced a spectrum which closely resembled the spectrum of the aged $MB^{+\bullet}$ sample (shown as thick blue line). The relative amounts of $TAB^{+\bullet}$ and TAB^{2+} at various titration points in **Figure 1.8** were evaluated by a deconvolution of the individual spectra using the clean absorption spectra of $MB^{+\bullet}$, $TAB^{+\bullet}$, and TAB^{2+}, which resulted in the concentrations of each species for a given titration point. This spectral deconvolution procedure allowed accurate determination of the concentrations of $MB^{+\bullet}$, $TAB^{+\bullet}$, and TAB^{2+} at every titration point in **Figure 1.8**, and these are plotted as molar fractions against the added equivalents of TAB^0 in **Figure 1.8 (B)**.

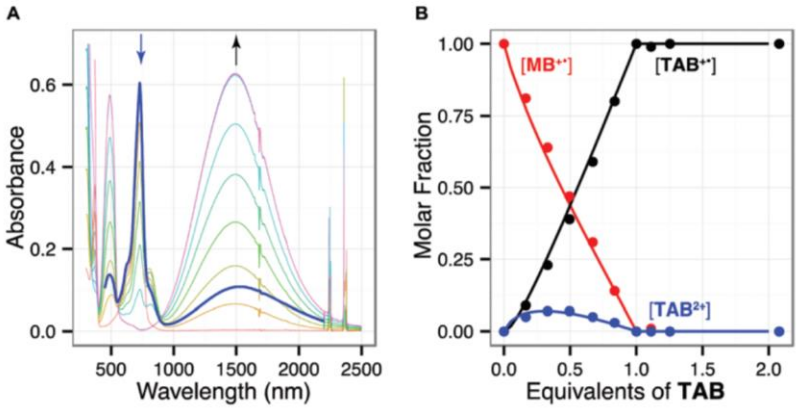

Figure 1. 8. (A) Spectral changes observed upon the incremental addition of 1.52 mM **TAB** to a freshly prepared solution of $\mathbf{MB^{+\bullet}\ SbCl_6^-}$ (20 μM) in CH_2Cl_2 at 22 °C. Thick blue line shows the absorption spectrum of the aged sample of $\mathbf{MB^{+\bullet}\ SbCl_6^-}$. (B) Molar fractions of $\mathbf{MB^{+\bullet}}$ (red circles), $\mathbf{TAB^{+\bullet}}$ (black circles), $\mathbf{TAB^{2+}}$ (blue circles) plotted against the number of added equivalents of neutral **TAB** at each addition. The data points in panel B were fitted by accounting multiple equilibria amongst various oxidized and neutral species which showed that the second oxidation potential of **TAB** is somewhat higher (E_{ox2} = 0.71 V) as compared to the electrochemical potentials (0.64 V) owing to the fact that redox titrations are carried out in the absence of an electrolyte.

The molar fraction vs. the added TAB^0 plot clearly shows that oxidation of TAB^0 by $MB^{+\bullet}$, up to the equimolar concentration of $MB^{+\bullet}$ and TAB^0, produces both the cation radical and dication of TAB. Indeed, this analysis confirmed the presence of ~0.11 equivalents of $TAB^{+\bullet}$ and ~0.04 equivalents of TAB^{2+}, i.e. it amounts to the presence of ~0.15 equivalents of TAB in the sample of $MB^{+\bullet}$ used in this study.

The presence of TAB in the aged samples of $MB^{+\bullet}$ was further validated by comparison of the ^1H NMR spectrum of the reduced MB^0 with the spectrum of authentic TAB^0 (**Figure 1.1** and **Figure 1.9**).

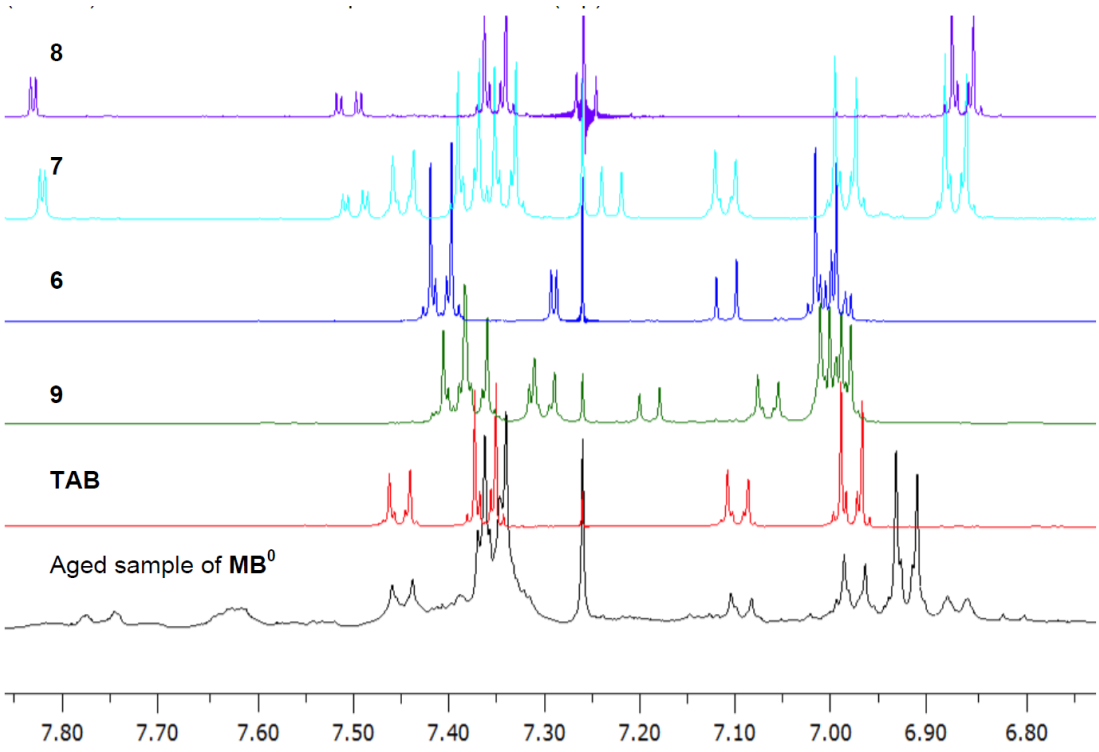

Figure 1. 9. Comparison of the ^1H NMR spectra of the aged sample of **$MB^{+\bullet}$**, reduced to **MB^0** by using ferrocene (identical to that in **Figure 1.1**), and NMR spectra of authentic **TAB** and **6**-**9**.

At the same time, the ^{1}H NMR spectral analysis showed the absence of 6–9 in the aged (reduced) sample of MB^{0} (**Figure 1.9**). Beyond its role as an impurity in the aged sample of $MB^{+\bullet}$, $TAB^{+\bullet}$ represents an interesting example of a mixed-valence compound, where the DFT calculations predict that the hole was largely (88%) localized on the benzidine fragment and spread only slightly onto the p-bromophenyl rings (i.e. 3% per aryl group), as shown by the spin/charge distribution in **Figure 1.10** (see also **Figure 1.11**) Importantly, the $1-e^{-}$ oxidation induced bond length in TAB → $TAB^{+\bullet}$ transformation were in accordance with the disposition of the bonding/antibonding lobes of HOMO, i.e. bonds with bonding HOMO lobes undergo elongations, whereas the bonds with antibonding lobes undergo contraction, see **Table 1.3**. [12,39–43]

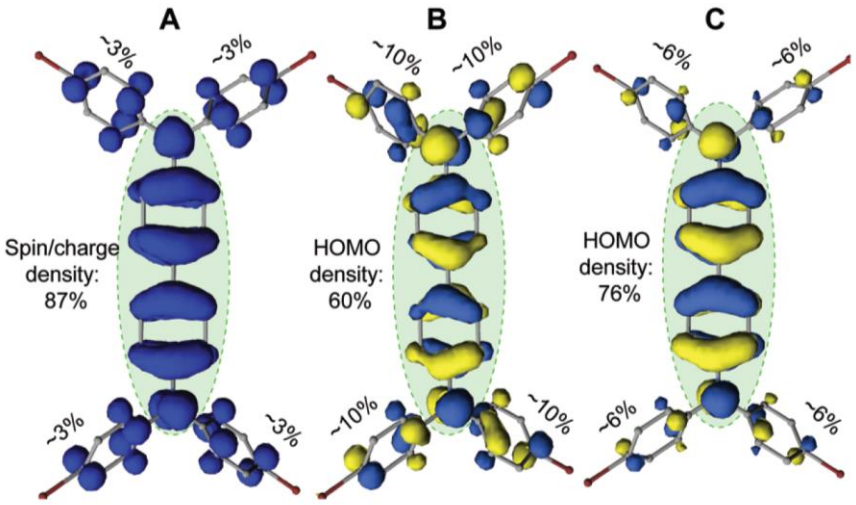

Figure 1. 10. (A) Spin density (0.001 au) distribution plot of **$TAB^{+\bullet}$** [B1LYP-40/ 6–31G(d) + PCM(CH_2Cl_2)] showing, with the aid of green ellipsoid, that 88% of spin/charge density (evaluated by the Natural Population Analysis) [44] is localized onto the benzidine fragment while the remaining 12% is evenly distributed over the four p-bromophenyl groups. (B, C) Showing the spatial distribution of HOMO of **TAB^{0}** and the

distribution of the HOMO density [evaluated as $q_m = \Sigma_n c_{mn}^{\ 2}$ where c_{mn} is the coefficient of the atomic orbital χ_{mn} in HOMO ($\varphi HOMO = \Sigma_k c_k \chi_k$), m is the atomic index, and n is the index of the atomic orbital in atom m] calculated at the equilibrium geometry of neutral **TAB^0** (B) and at the equilibrium geometry of its cation radical, i.e. **TAB$^{+\bullet}$** (C).

However, it is noted that HOMO density distribution in TAB^0 is more delocalized as compared with the spin/charge distribution in $TAB^{+\bullet}$ due to the oxidation-induced structural reorganization that involves planarization of the benzidine fragment (i.e. dihedral angle between central phenylene rings θ reduces from 35 to 19°).[17] Indeed, the HOMO density of TAB^0 at the $TAB^{+\bullet}$ geometry is much closer to the spin/charge density distribution in $TAB^{+\bullet}$ (i.e. 76% on the benzidine fragment and 6% per each aryl group) than the HOMO density at the neutral TAB geometry (i.e. 60% on the benzidine fragment and 10% per each aryl group), see **Figure 1.10**.

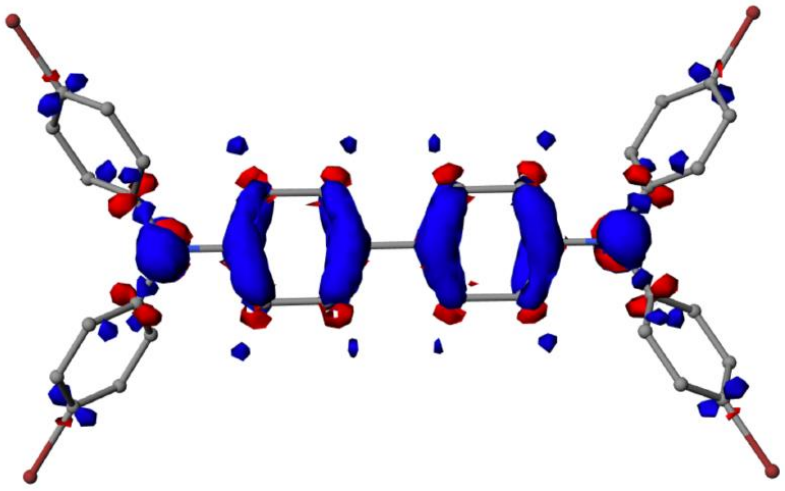

Figure 1. 11. Difference between the spatial electron density distributions in the **TAB** and **TAB$^{+\bullet}$**, with the geometries corresponding to **TAB$^{+\bullet}$** [B1LYP-40/6 31G(d)+PCM(CH_2Cl_2)].

In order to confirm this DFT prediction, we obtained single crystals of $TAB^{+\bullet}$ $SbCl_6^-$ for crystallographic analysis. In a typical experiment, a chilled (~0 °C) Schlenk tube was charged with TAB (30 mg, 0.037 mmol), anhydrous CH_2Cl_2 (5 mL), and triethyloxonium hexachloroantimonate (Et_3O^+ $SbCl_6^-$)[45] (32 mg, 0.074 mmol) under an argon atmosphere, and the resulting mixture was stirred for 30 minutes. The resulting dark-orange solution was carefully layered with dry toluene (10 mL) and placed in a refrigerator for 12 hours at −10 °C. After this time, a well-formed array of single crystals of $TAB^{+\bullet}SbCl_6^-$ was obtained and subsequently analysed by X-ray crystallography (**see Figure 1.18 –1.20 and Tables 1.4-1.6 in the experimental part**). The ORTEP diagrams of TAB and $TAB^{+\bullet}$ as well as the crystal packing diagram of $TAB^{+\bullet}$ are presented in **Figure 1.12**. The $TAB^{+\bullet}$ and $SbCl_6^-$ counter ions form mixed layers along the ab plane, and within these layers, the $SbCl_6^-$ counter ions gravitate toward nitrogen atoms.

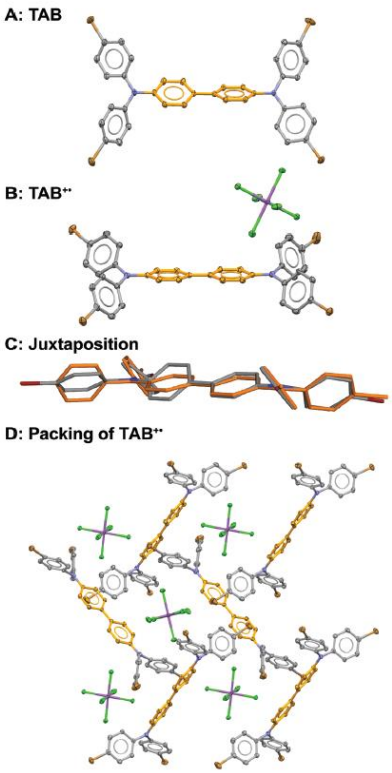

Figure 1. 12. The ORTEP diagrams (50% probability) of **TAB^{0}** (A) and **TAB$^{+\bullet}$ SbCl$_6^-$** (B) as well as the juxtaposition of **TAB^{0}** (grey color) and **TAB$^{+\bullet}$** (orange color) showing planarization of the benzidine fragment and enhanced propeller arrangement of the p-bromophenyl groups around the nitrogen atoms (C). The packing arrangement of **TAB$^{+\bullet}$SbCl$_6^-$** showing the layers of **TAB** units with no close contact between the benzidine fragments, which are separated by the **SbCl$_6^-$** counter anions (D). Note that the co crystallized CH_2Cl_2 molecules and hydrogens were omitted for clarity. Also see **Figure 1.18 –1.20 and Tables 1.4-1.6 in the experimental part** in the experimental part.

The benzidine moieties are positioned in the clefts formed by the brominated aryl rings without any parallel overlap between the benzene rings, see **Figure 1.12. D**. An overlap of TAB and TAB$^{+\bullet}$ structures clearly show that the benzidine fragment of TAB is significantly planarized (i.e., the value of θ decreased from 22° to 3°) while the p-bromophenyl rings become much more propeller shaped (i.e. reduced conjugation with nitrogen lone pairs as judged by change in the average dihedral angle from ~45° to ~35°)

upon 1e$^-$ oxidation. The availability of precise X-ray structures of $TAB^{+\bullet}$ $SbCl_6^-$ as well as of neutral TAB allowed a comparison of the bond length changes in the TAB → $TAB^{+\bullet}$ transformation. Expectedly, the bond contractions and elongations were mostly confined to the benzidine fragment of TAB, which was significantly planarized (i.e., the value of θ decreased from 22° to 3°) upon 1e− oxidation, while the four p-bromophenyl rings did not undergo significant bond length changes (**Figure 1.13**). Moreover, a comparison of the bond length changes in TAB → $TAB^{+\bullet}$ transformation by DFT calculations and X-ray structural analysis clearly shows a linear correspondence (**Figure 1.13**), and thus confirming the validity of the usage of B1LYP-40 functional for DFT calculations. These results clearly suggest that spectral contamination in the aged sample of $MB^{+\bullet}$ is largely due to the formation of $TAB^{+\bullet}$ and TAB^{2+}, which most likely are produced by the oxidative Scholl-type reaction,[46] where an eventual loss of a molecular bromine produces TAB, which undergoes oxidation with $MB^{+\bullet}$.[47]

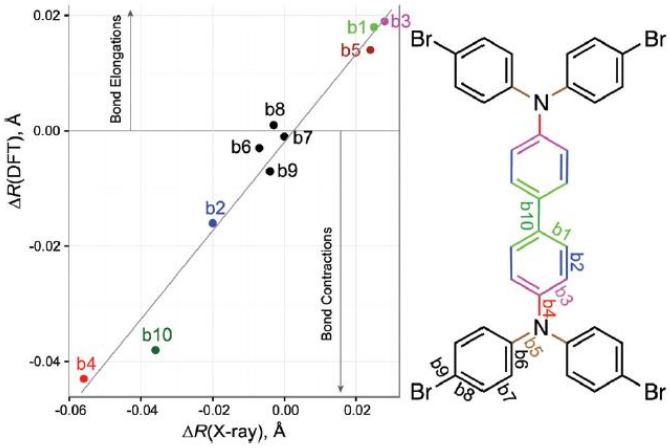

Figure 1. 13. Comparison of the oxidation-induced bond length changes (in Å) in **TAB** obtained by X-ray crystallography (abscissa) and DFT calculations (ordinate). Note that

the bond length changes (i.e. b1–b10) depicted in the structure are based on the averages of equivalent bonds. See also **Figure 1.21** and **Table 1.3**

To prevent degradation of $MB^{+\bullet}$, we propose to substitute bromine atoms in the para-positions of MB by the sterically demanding tertiary-butyl groups, and place bromine atoms at ortho-positions of the aromatic ring (see **Scheme 1.8** in experimental part). The synthesis of the proposed tris(2-bromo-4-tbutylphenyl) amine (BC) was easily accomplished from readily available triphenylamine by a facile t-butylation[48] using t-butanol and trifluoroacetic acid followed by bromination using NBS in DMF (see **Scheme 1. 8** in the experimental part for details). Cyclic voltammetric analysis of tris(4-tbutylphenyl) amine (**10**) and its brominated analogue BC (**Figure 1.14.A** and **Figure 1.16 in the experimental part**) showed that they undergo reversible one-electron oxidation at varying scan rates (v = 50 to 300 mV s^{-1}). Interestingly, a placement of bromine atoms at the ortho-positions in 10 increases its oxidation potential from 0.29 to 0.78 V vs. Fc/ Fc^{+}, which suggests that 'blues cousin' has slightly higher oxidizing power [i.e. $E_{red}(BC^{+\bullet})$ = 0.78 V] as compared to 'magic blue' [i.e. $E_{red}(MB^{+\bullet})$ = 0.70 V].

Table 1. 3. Comparison of the bond lengths (in Å) of **TAB^{0}** (N) and **TAB$^{+\bullet}$** (CR), obtained by X-ray crystallography and by DFT calculations

		X-ray			DFT		
Atom1	Atom2	N	CR	Δ	N	CR	Δ
C1	C2	1.391	1.410	0.019	1.399	1.417	0.018
C2	C3	1.385	1.374	-0.011	1.385	1.369	-0.016
C1	C6	1.394	1.424	0.030	1.399	1.417	0.018
C3	C4	1.385	1.416	0.031	1.396	1.415	0.019
C4	C5	1.384	1.418	0.034	1.396	1.415	0.019
C5	C6	1.392	1.365	-0.027	1.385	1.369	-0.016
N1	C4	1.428	1.367	-0.061	1.417	1.374	-0.043
N1	C13	1.416	1.442	0.026	1.413	1.427	0.014
N1	C19	1.408	1.443	0.035	1.413	1.427	0.014
C13	C14	1.402	1.392	-0.010	1.397	1.394	-0.003
C13	C18	1.392	1.382	-0.010	1.397	1.394	-0.003
C14	C15	1.386	1.389	0.003	1.387	1.386	-0.001
C15	C16	1.377	1.376	-0.001	1.387	1.388	0.001
C16	C17	1.391	1.378	-0.013	1.387	1.388	0.001
C17	C18	1.386	1.387	0.001	1.387	1.386	-0.001
Br1	C16	1.903	1.907	0.004	1.906	1.899	-0.007
C19	C20	1.402	1.390	-0.012	1.397	1.394	-0.003
C19	C24	1.394	1.384	-0.010	1.397	1.394	-0.003
C20	C21	1.383	1.387	0.004	1.387	1.386	-0.001
C21	C22	1.383	1.385	0.002	1.387	1.388	0.001
C22	C23	1.385	1.387	0.002	1.387	1.388	0.001
C23	C24	1.390	1.386	-0.004	1.387	1.386	-0.001
Br2	C22	1.904	1.894	-0.010	1.906	1.899	-0.007
C1	C7	1.484	1.448	-0.036	1.479	1.441	-0.038
C7	C12	1.396	1.421	0.025	1.399	1.417	0.018
C7	C8	1.397	1.422	0.025	1.399	1.417	0.018
C8	C9	1.389	1.365	-0.024	1.385	1.369	-0.016
C9	C10	1.390	1.412	0.022	1.396	1.415	0.019
C10	C11	1.393	1.417	0.024	1.396	1.415	0.019
C11	C12	1.389	1.370	-0.019	1.385	1.369	-0.016
N2	C10	1.423	1.372	-0.051	1.417	1.374	-0.043
N2	C25	1.418	1.434	0.016	1.413	1.427	0.014
N2	C31	1.414	1.434	0.020	1.413	1.427	0.014
C25	C26	1.400	1.391	-0.009	1.397	1.394	-0.003
C25	C30	1.391	1.392	0.001	1.397	1.394	-0.003
C26	C27	1.385	1.383	-0.002	1.387	1.386	-0.001
C27	C28	1.382	1.383	0.001	1.387	1.388	0.001
C28	C29	1.388	1.384	-0.004	1.387	1.388	0.001
C29	C30	1.389	1.394	0.005	1.387	1.386	-0.001
Br3	C28	1.904	1.900	-0.004	1.906	1.899	-0.007
C31	C32	1.396	1.392	-0.004	1.397	1.394	-0.003
C31	C36	1.397	1.393	-0.004	1.397	1.394	-0.003
C32	C33	1.387	1.386	-0.001	1.387	1.386	-0.001
C33	C34	1.390	1.384	-0.006	1.387	1.388	0.001
C34	C35	1.378	1.376	-0.002	1.387	1.388	0.001
C35	C36	1.386	1.384	-0.002	1.387	1.386	-0.001
Br4	C34	1.902	1.898	-0.004	1.906	1.899	-0.007

The cation radical of BC was first generated by the spectroscopic redox titration, where sub-stoichiometric amounts of BC^{0} were incrementally added to a solution of $NAP^{+\bullet}$ (**Figure 1.14**). The absorption spectrum of $BC^{+\bullet}$ showed a low-energy band at λ_{max}

= 805 nm (ε_{max} = 9930 cm^{-1} M^{-1}) which is slightly redshifted as compared to the absorption band of $MB^{+\bullet}$ (λ_{max} = 728 nm, ε_{max} = 28200 cm^{-1} M^{-1}). Note that $BC^{+\bullet}$ $SbCl_6^-$ can be prepared as a crystalline solid either by reaction with $SbCl_5$ or NO^+ $SbCl_6^-$ similar to the preparation of $MB^{+\bullet}$ $SbCl_6^-$ (see Experimental part), and the spectrum of the resulting $BC^{+\bullet}$ was identical to the spectrum presented in **Figure 1.14. B.** The high stability of $BC^{+\bullet}$ $SbCl_6^-$ will allow it to serve as a convenient replacement of $MB^{+\bullet}$ $SbCl_6^-$, and we believe that it will find widespread use for the spectroscopic characterization of various oxidized species and will become a useful chemical oxidant for various oxidative transformations.

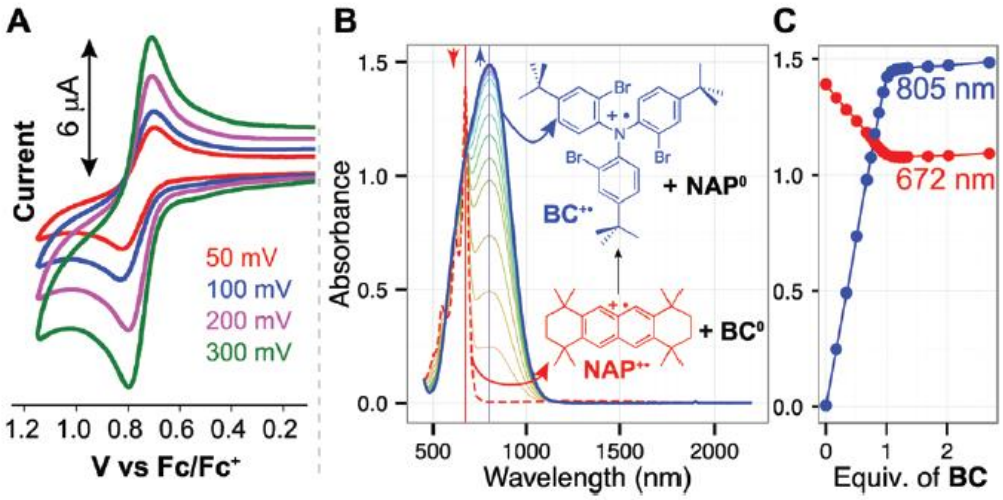

Figure 1. 14. (A) Cyclic voltammograms of 5 mM **BC** in CH_2Cl_2 (22 °C) containing 0.2 M tetra-n-butylammonium hexafluorophosphate at different scan rates (as denoted). (B) Spectral changes attendant upon incremental addition of 3.0 mM $\mathbf{BC^0}$ to a solution of $\mathbf{NAP^{+\bullet}}$ $\mathbf{SbCl_6^-}$ (0.15 mM) in CH_2Cl_2 at 22 °C (see also **Figure 1.15** in the Experimental), and (C) plot of decrease of absorbance at 672 nm (due to the disappearance of $\mathbf{NAP^{+\bullet}}$) and increase of absorbance at 805 nm (due to the formation of $\mathbf{BC^{+\bullet}}$) against the equivalents of added neutral $\mathbf{BC^0}$.

CONCLUSION

In summary, we have demonstrated that 'magic blue' ($MB^{+\bullet}$) undergoes slow decomposition in the solid state upon aging thus giving rise to the additional absorption bands at 480 nm, 805 nm, and 1550 nm. A combined DFT and experimental (NMR, electrochemistry, optical spectroscopy, and X-ray crystallography) study led to the identification of the main decomposition product, or blues brother, as tetrakis-(4 bromophenyl)benzidine whose cation radical (λ_{max} = 489, 1490 nm) and dication (807 nm) are responsible for the additional absorption bands. This study allowed us to further demonstrate the excellent performance of the B1LYP-40 functional for accurately predicting the electrochemical oxidation potentials of a variety of triarylamine derivatives and the optical properties of their cation radicals by (TD-)DFT calculations which aided in identification of the blues brother. Moreover, the excellent performance of the B1LYP-40 functional[17,19–22] was further demonstrated by close correspondence of the calculated structures of TAB and $TAB^{+\bullet}$ with those obtained by X-ray crystallography.

The fact that TAB is formed by dimerization of MB led us to design and synthesize its close analogue tris(2-bromo-4-tertbutylphenyl) amine referred to as 'blues cousin' (BC: E_{ox1} = 0.78 V vs. Fc/Fc^{+}, λ_{max} ($BC^{+\bullet}$) = 805 nm, ε_{max} = 9930 cm^{-1} M^{-1}), in which oxidative dimerization is hampered by positioning the sterically demanding tert-butyl groups at the para-positions of the aryl rings. The ease of preparation of BC^{0} and high stability of its cation radical ($BC^{+\bullet}$) suggest that it will become a useful one-electron oxidant for widespread use in organic, organometallic, and inorganic chemistry.

GENERAL EXPERIMENTAL METHODS AND MATERIALS

All reactions were performed under an argon atmosphere unless otherwise noted. All commercial reagents were used without further purification unless otherwise noted. Dichloromethane (Aldrich) was repeatedly stirred with fresh aliquots of concentrated sulfuric acid (~10 % by volume) until the acid layer remained colorless. After separation, the CH_2Cl_2 layer was washed successively with water, 5% aqueous sodium bicarbonate, water, and saturated aqueous sodium chloride and dried over anhydrous calcium chloride. The CH_2Cl_2 was distilled twice from P_2O_5 under an argon atmosphere and stored in a Schlenk flask equipped with a Teflon valve fitted with Viton O-rings. Acetonitrile was stirred with molecular sieves overnight, filtered, and again stirred with $CaCl_2$ overnight. After that it was filtered and distilled twice from P_2O_5 under an argon atmosphere and stored in a Schlenk flask equipped with a Teflon valve fitted with Viton O-rings. The hexanes and toluene were distilled over P_2O_5 under an argon atmosphere and then refluxed over calcium hydride (~12 h). After distillation from CaH_2, the solvents were stored in Schlenk flasks under an argon atmosphere. Tetrahydrofuran (THF) was dried initially by distilling over lithium aluminum hydride under an argon atmosphere and stored in a Schlenk flask equipped with a Teflon valve fitted with Viton O-rings. NMR spectra were recorded on a Varian 400 MHz NMR spectrometer

Method of Cyclic Voltammetry of TAB and 4-9

The CV cell was of an air-tight design with high vacuum Teflon valves and Viton O-ring seals to allow an inert atmosphere to be maintained without contamination by grease. The working electrode consisted of an adjustable platinum disk embedded in a glass seal to allow periodic polishing (with a fine emery cloth) without changing the surface area (~1 mm^2) significantly. The reference SCE electrode (saturated calomel electrode) and its salt bridge were separated from the catholyte by a sintered glass frit. The counter electrode consisted of a platinum gauze that was separated from the working electrode by ~3 mm. The CV measurements were carried out in a solution of 0.1 M supporting electrolyte (tetra-*n* butylammonium hexafluorophosphate) and the substrate in dry CH_2Cl_2 under an argon atmosphere at 22 ºC. All cyclic voltammograms were recorded at a sweep rate of 50 mV sec^{-1} and were IR compensated (**Figure 1.5**). The oxidation potentials (E_{ox}, calculated by taking the average of anodic and cathodic peaks) were referenced to the added (equimolar) ferrocene.

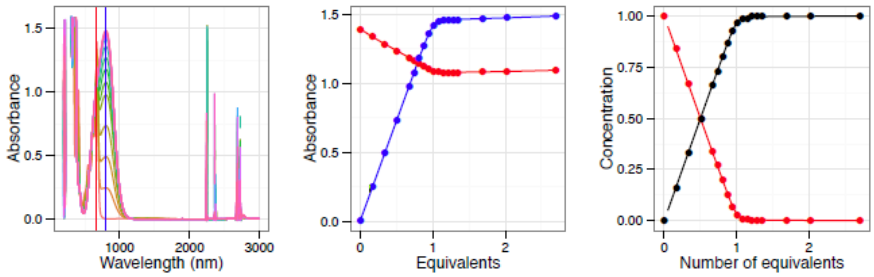

Figure 1. 15. Spectral changes attendant upon the reduction of 3.03 mM **BC** by 0.15 mM **$NAP^{+\bullet}$ $SbCl_6^-$** in CH_2Cl_2 at 22 ºC as well as the corresponding molar fraction plot against the number of added equivalents of neutral **BC**.

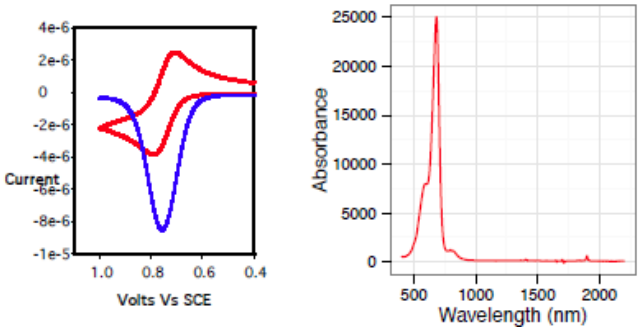

Figure 1. 16. (Left) Cyclic and square-wave voltammograms of 5 mM 10 in CH_2Cl_2 (22 ºC) containing 0.2 M tetra-n-butylammonium hexafluorophosphate at v = 200 mV s^{-1}. (Right) The molar absorptivity spectrum of cation radical **10** in CH_2Cl_2 (22 ºC).

Synthesis of compounds in Chart 1.1.

Synthetic schemes for the preparation of compounds in **Chart 1.1** are presented below in individual schemes S1-S8 together with the detailed experimental procedures for each step of synthesis and their characterization data (i.e. numerical spectroscopic data) as well as $^{1}H/^{13}C$ NMR spectra are given below. Note that identity of each molecule was further confirmed by MALDI mass spectrometry.

Scheme 1. 1: Synthesis of 3, 6-dibromo-9-(4′-bromophenyl)-9*H*-carbazole (S1-2 or 4).

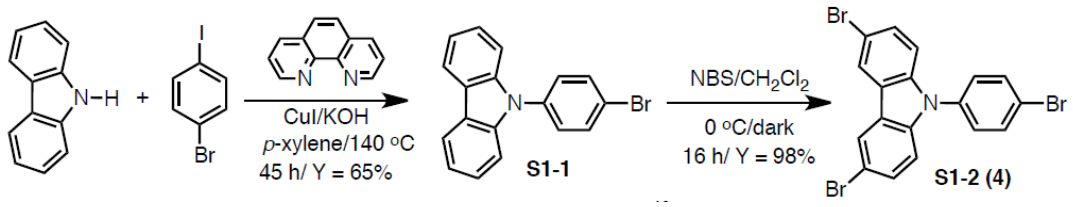

Preparation of 9-**(4-bromophenyl)-9*H*-carbazole (S1-1).**[49] A mixture of carbazole (1.0 g, 5.98 mmol), 4-bromoiodobenzene (1.86 g, 6.58 mmol), CuI (1.13 g,

5.98 mmol), 1,10 phenanthroline (1.05 g, 5.86 mmol) and KOH (1.50 g, 26.8 mmol) in *p*-xylene (50 mL) was stirred at ~140 °C for 45 hours. The reaction mixture was cooled to room temperature and the resulting suspension was filtered and residue was washed with *p* xylene (3x 10mL). To the resulting filtrate was added dichloromethane (160 mL) and water, and the mixture was dried over anhydrous $MgSO_4$. After removal of the solvent in vacuo, the crude product was purified on a silica gel chromatography with hexanes as eluent to afford compound **S1-1** as a solid. Yield: 1.26 g (65%). m.p. 146-147 ºC (lit.[49] m.p. 149-150 ºC). ^{1}H NMR (400 MHz, $CDCl_3$) δ ppm 7.3 (t, 2H, *J* = 7.24 Hz), 7.41 (m, 6H), 7.73 (d, 2H, *J* = 7.70 Hz), 8.14 (d, 2H, *J* = 7.70 Hz); ^{13}C NMR (400 MHz, $CDCl_3$) δ ppm 109.71, 120.37, 120.56, 121.03, 123.62, 126.25, 128.88, 133.27, 136.95, 140.73.

Preparation of 3,6-dibromo-9-(4-bromophenyl)-9*H*-carbazole (S1-2 or 4).[50]

Compound **S1-1** (1.0 g, 3.10 mmol) was dissolved in dichloromethane (17 mL) in a Schlenk flask wrapped with aluminum foil. NBS (1.36 g, 7.69 mmol) was added as solid at 0 °C in the dark and the reaction mixture was stirred overnight (~16 h), quenched with water and extracted with dichloromethane (3 x 40 mL). The combined organic extracts were dried over anhydrous $MgSO_4$ and filtered. The organic layer was evaporated under reduced pressure. The residue was purified by silica gel chromatography with hexanes as the eluent to afford **S1-2** (**4**) as a crystalline solid. Yield: 1.46 g (98%). m.p. 208-210 ºC. ^{1}H NMR (400 MHz, $CDCl_3$) δ ppm 7.21 (d, 2H, *J* = 8.75 Hz), 7.38 (d, 2H, *J* = 8.76 Hz), 7.50 (dd, 2H, *J* = 8.75 Hz, 1.9 Hz), 7.74 (d, 2H, *J* = 8.76 Hz), 8.18 (d, 2H, *J* = 1.9 Hz); ^{13}C NMR (400 MHz, $CDCl_3$) δ ppm 111.46, 113.54, 121.90, 123.51, 124.21, 128.72, 129.74, 133.57, 136.00, 139.77.

Scheme 1. 2: Synthesis of 4,4'-*bis*(3,6-dibromo-9H-carbazol-9-yl)-1,1'-biphenyl (S2-2 or 5)

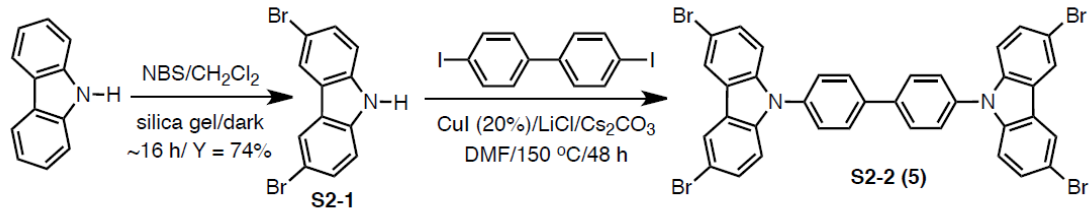

Preparation of 3,6-dibromo-9H-carbazole (S2-1).[51] Carbazole (0.5 g, 3.0 mmol) was dissolved in CH_2Cl_2 (100 mL) and SiO_2 (10 g, dried beforehand at 120 °C) and NBS (1.07 g, 6.0 mmol) was added slowly. The reaction mixture was stirred overnight (~16 h) at 22 °C in the dark under an argon atmosphere. The mixture was filtered and the silica gel was washed with CH_2Cl_2 (3 x 30 mL). The combined organic layers were washed with brine (3 x 20 mL), dried over anhydrous $MgSO_4$, filtered, and evaporated to give **S2-1** as a greenish solid, which was further purified by crystallization from a mixture of ethanol and water (70:30). Yield: 0.724 g (74%). m.p. 203-205 ºC (lit.[52] m.p. 204-206 ºC). ^{1}H NMR (400 MHz, $CDCl_3$) δ ppm 7.31 (d, 2H, *J* = 8.4 Hz), 7.52 (dd, 2H, *J* = 8.59 Hz, 2.0 Hz), 8.09 (br s, 1H), 8.12 (d, 2H, *J* = 2.0 Hz); ^{13}C NMR (400 MHz, $CDCl_3$) δ ppm 112.43, 112.82, 123.45, 124.28, 129.50, 138.52.

Preparation of 4,4'-*bis*(3,6-dibromo-9H-carbazol-9-yl)-1,1'-biphenyl (S2-2 or 5)[53] Compound **S2-1** (0.59 g, 1.83 mmol), Cs_2CO_3 (0.59 g, 1.83 mmol), 4,4′-diiodobiphenyl (0.41 g, 1.01 mmol), CuI (0.035 g, 0.183 mmol), LiCl (0.077 g, 1.83 mmol) and DMF (6 mL) were added in a sealed tube with screw cap and stirred in a ~150 °C oil bath. After 48 h, the reaction mixture was cooled to room temperature and diluted

with saturated aqueous ammonium chloride. The product was extracted, first with ethyl acetate and then with chloroform. The combined organic extracts were dried over anhydrous $MgSO_4$, filtered and the solvent was evaporated under reduced pressure. The compound **S2-2 (or 5)** is partially soluble in most common organic solvents and therefore the accurate yield was determined. Measured m.p. > 400 ºC. ^{1}H NMR (400 MHz, $CDCl_3$) δ ppm 7.36 (d, 2H, *J* = 8.70 Hz), 7.55 (dd, 2H, *J* = 8.89 Hz, 1.88 Hz), 7.65 (d, 2H, *J* = 8.33 Hz), 7.91 (d, 2H, *J* = 8.28 Hz), 8.23 (d, 2H, *J* = 1.88 Hz). ^{13}C NMR was not taken due to poor solubility in $CDCl_3$.

Scheme 1. 3:Synthesis of *tetrakis*-(4-bromophenyl)benzidine (S3-2 or TAB).

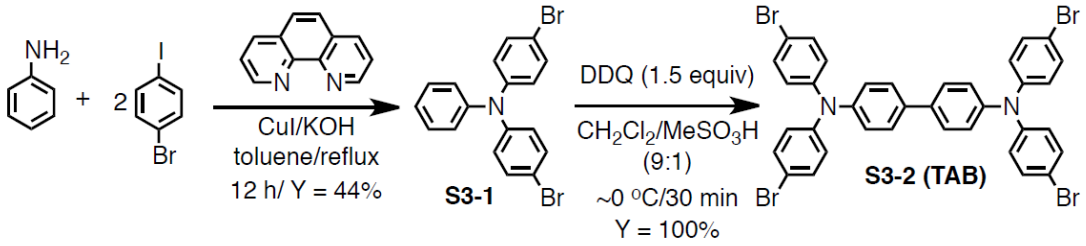

Preparation of 4-bromo-*N*-(4-bromophenyl)-*N*-phenylaniline (S3-1).[54] In a dry Schlenk flask a mixture of aniline (1.1 g, 12 mmol), 1-bromo-4-iodobenzene (8.5 g, 30 mmol), CuI (0.07 g, 0.36 mmol), 1,10-phenanthroline (0.065 g, 0.36 mmol), potassium hydroxide (5.2 g, 92 mmol) and toluene (60 mL) was stirred under an argon atmosphere at reflux overnight (~16 h). The resulting mixture was then cooled to room temperature and poured into distilled water. The products were extracted with dichloromethane (4 × 50 mL), and the organic layers were dried over anhydrous $MgSO_4$. The solvent was evaporated under reduced pressure, and the resulting crude product was purified by silica gel column chromatography using hexanes as an eluent to obtain **S1-1** as a colorless viscous liquid. Yield: 2.14 g (44%). ^{1}H NMR (400 MHz, $CDCl_3$) δ ppm

6.94 (d, 4H, *J* = 8.9 Hz), 7.06 (m, 3H), 7.27 (m, 2H), 7.34 (d, 4H, *J* = 8.9 Hz); ^{13}C NMR (400 MHz, $CDCl_3$) δ ppm 115.60, 123.88, 124.74, 125.55, 129.70, 132.48, 146.66, 147.04.

Preparation of S3-2 (TAB).[55,56] In a dry Schlenk flask compound **S1-1** (0.32 g, 0.79 mmol) was dissolved in dry dichloromethane (27 mL) and cooled to 0°C. After 5 minutes, methanesulfonic acid (3 mL) was added under an argon atmosphere. Solid DDQ (2,3-dichloro 5,6-dicyanobenzoquinone) (0.27 g, 1.2 mmol) was added, and the resulting mixture was stirred for 30 minutes. The reaction was quenched with saturated aqueous $NaHCO_3$ solution (50 mL) and extracted with dichloromethane (3 x 25 mL). The organic extracts were washed with water and dried over anhydrous $MgSO_4$. Solvent was removed under reduced pressure and the resulting crude solid was crystallized from acetonitrile to afford **TAB** as a colorless crystalline solid in nearly quantitative yield. m.p. 226-227 ºC. ^{1}H NMR (400 MHz, $CDCl_3$) δ ppm 6.97, (d, 4H, *J* = 8.93 Hz), 7.09 (d, 2H, *J* = 8.64 Hz), 7.36 (d, 4H, *J* = 8.93 Hz), 7.45 (d, 2H, *J* = 8.7 Hz$^{);}$ ^{13}C NMR (400 MHz, $CDCl_3$) δ ppm 115.88, 124.68, 125.78, 127.85, 132.60, 135.63, 146.16, 146.53.

Scheme 1. 4: Synthesis of 2-bromo-*N4,N4,N4',N4'-tetrakis*(4-bromophenyl)-[1,1'-biphenyl]-4,4'-diamine (S4-4 or 6)

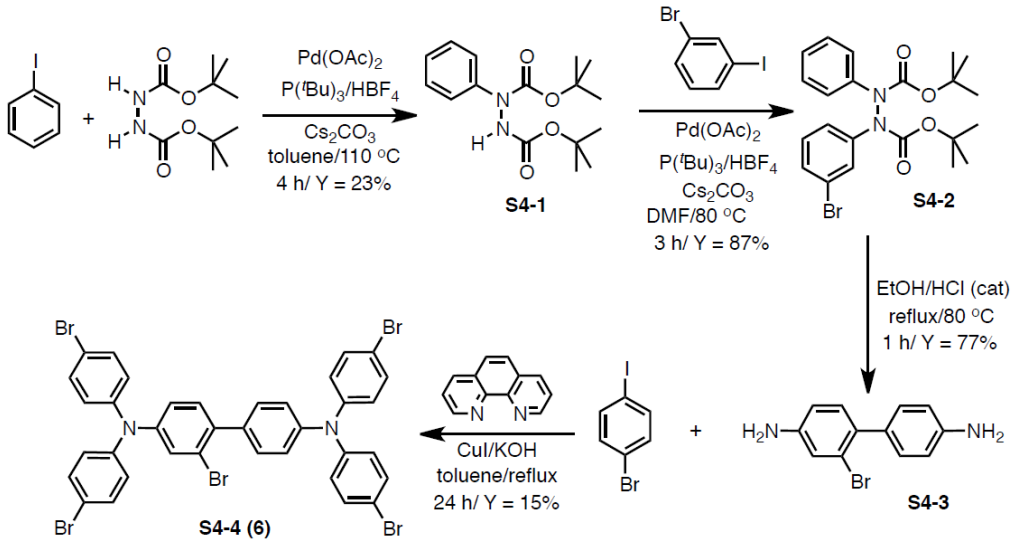

Preparation of di-*tert*-butyl-1-phenylhydrazine-1,2-dicarboxylate (S4-1).[57] A sealed tube was charged with iodobenzene (1.83 g , 8.97 mmol), di-*tert*-butylhydrazine-1,2 dicarboxylate (2.5 g, 10.76 mmol), $Pd(OAc)_2$ (0.1 g, 0.45 mmol), $P(t\text{-}Bu)_3 \cdot HBF_4$ (0.26 g, 0.89 mmol), Cs_2CO_3 (4.09 g, 12.55 mmol) and dry toluene (20 mL) at room temperature. The reaction mixture was degassed, and tube was filled with argon, sealed with a screw cap and heated at 110 °C for 4h. The reaction mixture was then cooled to room temperature and filtered through a short pad of silica gel using ethyl acetate as the eluent. The organic solution was concentrated and purified by flash column chromatography on silica gel (hexanes: ethyl acetate = 10:1) to afford hydrazide **S4-1** as a pale yellow solid. Yield = 0.75 g (23%). m.p. 78-80 ºC. ^{1}H NMR (400 MHz, $CDCl_3$) δ ppm 1.49 (s, 18H), 6.81/6.60 (rotamers, 2 x br s, 1H, NHBoc), 7.13 –7.17 (m, 1H), 7.33 – 7.29 (m, 2H), 7.40 (m, 2H); ^{13}C NMR (400 MHz, $CDCl_3$) δ ppm 28.26, 28.31, 81.6, 82.3, 123.8, 125.6, 128.5, 142.3, 153.7, 155.5.

Preparation of di-*tert*-butyl-1-(3-bromophenyl)-2-phenylhydrazine-1,2 dicarboxylate (S4-2).[58] A sealed tube was charged with 1-bromo-3-iodobenzene (0.41 g, 1.46 mmol), **S4-1** (0.41 g, 1.32 mmol), CuI (0.28 g, 1.46 mmol), 1,10-phenanthroline (0.26 g, 1.46 mmol), Cs_2CO_3 (0.47 g, 1.46 mmol) and DMF (3.0 mL) at room temperature. The reaction mixture was degassed, the tube was filled with argon, sealed with a screw cap and heated at 80 °C for 3 h. The reaction mixture was then cooled to room temperature and filtered through a short pad of silica gel using ethyl acetate as the eluent. The organic solution was concentrated and purified by flash column chromatography on silica gel using hexanes as the eluent to afford compound **S4-2**. Yield: 0.54 g, 87%. ^{1}H NMR (400 MHz, $CDCl_3$) δ ppm 7.14-7.18 (t, 2H, *J* = 7.9 Hz), 7.26-7.40 (m, 6H), 7.66 (bs, 1H); ^{13}C NMR (400 MHz, $CDCl_3$) δ ppm 28.26, 28.29, 83.3, 83.5, 121.1 (bs), 122.7, 122.9 (bs), 126.4, 129.0, 129.3, 130.5, 135.0, 141.5, 143.1, 153.4, 153.6.

Preparation of 2-bromo-[1,1'-biphenyl]-4,4'-diamine (S4-3).[58] A Schlenk flask was charged with **S4-2** (0.47 g, 1.01 mmol), 10 mL of ethanol and 0.5 mL of conc. HCl at room temperature. The reaction mixture was heated to reflux for 1 h, then cooled to 0 °C, neutralized with aqueous $NaHCO_3$, extracted with dichloromethane and dried over anhydrous $MgSO_4$. The resulting mixture was filtered and the solvent evaporated under reduced pressure. The crude product was purified by silica gel chromatography to afford **S4-3,** which was rather unstable and thus was used in the next step without further purification. Yield: ~77%. ^{1}H NMR (400 MHz, $CDCl_3$) δ ppm 3.71 (bs, 4H), 6.63 (dd, 1H, *J* = 8.23 Hz, 2.4 Hz), 6.70 (d, 2H, *J* = 8.63 Hz), 6.97 (d, 1H, *J* = 2.38 Hz), 7.08 (d,

1H, *J* = 8.23 Hz), 7.18 (d, 2H, *J* = 8.63 Hz); ^{13}C NMR (400 MHz, $CDCl_3$) δ ppm 114.35, 114.56, 119.07, 123.33, 130.65, 131.57, 131.86, 132.70, 145.51, 146.33.

2-bromo-*N4,N4,N4',N4'-tetrakis*(4-bromophenyl)-[1,1'-biphenyl]-4,4'-diamine (S4-4 or 6).[54] In a dry Schlenk flask, a mixture of **S4-3** (0.28 g, 1.06 mmol), 1-bromo-4-iodobenzene (1.23 g, 4.36 mmol), CuI (0.08 g, 0.42 mmol), 1,10-phenanthroline (0.076 g, 0.42 mmol), potassium hydroxide (0.45 g, 8.15 mmol) and toluene (20 mL) was stirred and refluxed under argon atmosphere for 24h. The mixture was then cooled to room temperature and poured into distilled water. The products were extracted with dichloromethane (4 x 50 mL) and the organic layers were dried over anhydrous $MgSO_4$, filtered and evaporated under reduced pressure. The resulting crude product was purified by silica gel column chromatography using hexanes as the eluent. The brown solid was further purified by multiple treatment with charcoal (20 mg) in dichloromethane (100 mL). The resulting solid was crystallized from a mixture of acetonitrile and dichloromethane to afford **S4-4** (or **6**) as pale yellow solid. Yield: 0.14 g, (15%). m.p. 244-246 ºC. ^{1}H NMR (400 MHz, $CDCl_3$) δ ppm 6.99 (m, 9H), 7.06 (d, 2H, *J* = 8.68 Hz), 7.19 (d, 1H, *J* = 8.40 Hz), 7.30 (m, 3H), 7.38 (m, 8H); ^{13}C NMR (400 MHz, $CDCl_3$) δ ppm 116.03, 116.64, 122.54, 123.12, 123.17, 126.04, 126.16, 127.73, 130.68, 131.86, 132.61, 132.79, 135.40, 136.53, 145.97, 146.30, 146.44, 147.09.

Scheme 1. 5: Synthesis of 3-bromo-*N4,N4,N4',N4'-tetrakis*(4-bromophenyl)-[1,1' biphenyl]-4,4'-diamine (S5-5 or 7).

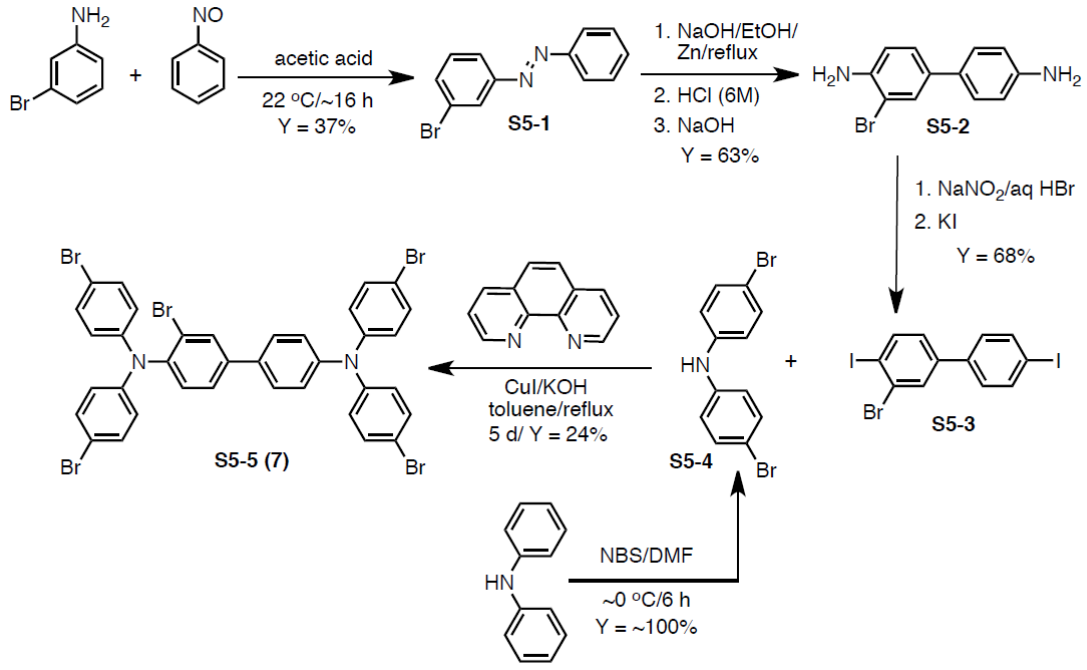

Preparation of (*E*)-1-(3-bromophenyl)-2-phenyldiazene (S5-1)[59] To a solution of nitrosobenzene (5.25 g, 49.01 mmol) in glacial acetic acid (40 mL), 2-bromoaniline (10.11 g, 58.81 mmol) was added, resulting immediately in the formation of a green solution. The mixture was stirred overnight (~16 h) at 22°C, after which time it turned deep red. This mixture was poured into 700 mL of water. Aqueous NaOH (50 g in 300 mL water) was added slowly until the solution was almost neutralized (tested by pH paper). **[Caution: Addition of alkali to this reaction mixture is highly exothermic!]** The resulting solution was extracted with diethyl ether (3 x 100 mL) and the combined ether extracts were washed with aqueous Na_2CO_3 solution (2 x 100 mL). The ethereal solution was then treated with a mixture of diethyl ether and HCl (30 mL HCl in 50 mL diethyl ether). The precipitated 2-bromoaniline hydrochloride was filtered off, and the

filtrate evaporated to about 100 mL. The red solution containing bromoazobenzene **S5-1** was subjected to column chromatography on basic alumina using diethyl ether as the eluent. The resulting red oil from chromatographic separation solidified upon treating with ethanol-solid carbon dioxide (dry ice). The red solid mass was allowed to warm to 0 °C and was filtered. Yield: 4.84 g (37%). m.p. 35-36 ºC (lit.[52] m.p. 36 ºC). ^{1}H NMR (400 MHz, $CDCl_3$) δ ppm 7.32 (td, 1H, *J* = 7.61 Hz, 1.67 Hz, 0.65 Hz), 7.40 (td, 1H, 7.7 Hz, 1.67 Hz, 0.70 Hz), 7.53 (m, 3H), 7.68 (dd, 1H, *J* = 7.96 Hz, 1.75 Hz), 7.76 (dd, 1H, *J* = 7.88 Hz, 1.33 Hz), 7.98 (m, 2H); ^{13}C NMR (400 MHz, $CDCl_3$) δ ppm 117.95, 123.58, 125.89, 128.14, 129.33, 131.75, 132.04, 133.89, 149.76, 152.76.

Preparation of 3-bromo-[1,1'-biphenyl]-4,4'-diamine (S5-2).[59] To a solution of bromoazobenzene **S5-1** (3.26 g) in ethanol (40 mL) zinc dust (1.70 g, 26.20 mmol) was added and the mixture was stirred. An aqueous ethanolic solution of NaOH (2 g NaOH dissolved in 5.0 mL water + 35 mL ethanol) was added to the above reaction mixture and it was refluxed until the red color disappeared (~2 h). It was then cooled to ambient temperature and filtered into an excess of concentrated hydrochloric acid. The solid Zn residue was washed with warm ethanol and the washings were added to the main filtrate. The resulting precipitate of 3-bromobenzidine hydrochloride was filtered and the precipitate was added to an aqueous NaOH solution (20 g NaOH in 300 mL H_2O) and stirred for 20 min, and then extracted with dichloromethane (3 x 30 mL) and dried over anhydrous $MgSO_4$. The solvent was removed under reduced pressure and crude product was crystallized from dilute aqueous HCl solution to afford pure **S5-2**. Yield: 2.08 g (63%). m.p. 79-81 ºC (lit.[52] m.p. 81 ºC). ^{1}H NMR (400 MHz, $CDCl_3$) δ ppm 3.69 (bs, 2H), 4.06 (bs, 2H), 6.72 (d, 2H, *J* = 8.71 Hz), 6.79 (d, 1H, *J* = 8.31 Hz), 7.31 (m, 3H),

7.60 (d, 1H, *J* = 2.17 Hz); ^{13}C NMR (400 MHz, $CDCl_3$) δ ppm 109.94, 115.55, 116.11, 126.46, 127.41, 130.30, 130.39, 133.11, 142.57, 145.54.

Preparation of 3-bromo-4,4'-diiodo-1,1'-biphenyl (S5-3).[60] To a stirred solution of **S5-2** (0.5 g, 1.90 mmol) in 48% HBr (3.0 mL) and water (10.0 mL) at 0 °C was added slowly an aqueous solution of $NaNO_2$ (0.393 g, 5.70 mmol in 5 mL H_2O). The resulting mixture was stirred vigorously for 1h at ~0 °C. A cold aqueous solution of KI (6.30 g, 38 mmol in 10.0 mL H_2O) was added in above reaction mixture dropwise and it was allowed to stir and warm to room temperature stir during the course of overnight (~16 h). The reaction mixture was then diluted with dichloromethane (100 mL) and washed with 10% aqueous NaOH solution (100 mL) and Na2S2O3 solution (100 mL) and dried over anhydrous $MgSO_4$, filtered, and the solvent was removed under reduced pressure. The resulting crude product was purified through flash column chromatography using hexanes as the eluent to afford pure **S5-3**. Yield: 0.63 g (68%). m.p. 81-83 ºC. ^{1}H NMR (400 MHz, $CDCl_3$) δ ppm 7.16 (dd, 1H, *J* = 8.23 Hz, 2.14 Hz), 7.26 (d, 2H, *J* = 8.04 Hz), 7.77 (d, 2H, *J* = 8.60 Hz), 7.80 (d, 1H, *J* = 2.14 Hz), 7.90 (d, 1H, *J* = 8.23 Hz); ^{13}C NMR (400 MHz, $CDCl_3$) δ ppm 94.37, 100.29, 126.99, 128.78, 130.55, 131.03, 138.28, 138.32, 140.78, 141.85.

Preparation of *bis*(4-bromophenyl)amine (S5-4).[61] A solution of *N*-bromosuccinimide (5.27 g, 29.6 mmol) in DMF (25 mL) was added dropwise during the course of 30 min to a stirred solution of diphenylamine (2.5 g, 14.8 mmol) in DMF (25 mL) at ~0 °C. The resulting mixture was stirred at ~0 °C for 6 h. Water was added and the precipitate was filtered, washed with water and dried in vacuo to afford **S5- 4** as a colorless solid. Yield: 4.83 g (~100%). m.p. 104-106 ºC (lit.[32,33] m.p. 105-107 ºC). ^{1}H

NMR (400 MHz, $CDCl_3$) δ ppm 5.65 (bs, 1H), 6.91 (d, 4H, *J* = 8.75 Hz), 7.36 (d, 4H, *J* = 8.75 Hz); ^{13}C NMR (400 MHz, $CDCl_3$) δ ppm 113.56, 119.65, 132.55, 141.86.

Preparation of 3-bromo-*N4,N4,N4',N4'-tetrakis*(4-bromophenyl)-[1,1'-biphenyl] 4,4'-diamine (S5-5 or 7).[54] In a dry Schlenk flask, a mixture of **S5-3** (0.40 g, 0.82 mmol), *bis*(4-bromophenyl)amine (**S5-4**, 0.56 g, 1.73 mmol), CuI (0.033 g, 0.173 mmol), 1,10 phenanthroline (0.031 g, 0.173 mmol), potassium hydroxide (0.77 g, 13.84 mmol) and toluene (30 mL) was refluxed under an argon atmosphere for 5 d. It was then cooled to room temperature, poured into distilled water and extracted with dichloromethane (4 x 20 mL). The organic layers were dried over anhydrous $MgSO_4$, filtered, and the solvent evaporated under reduced pressure. The resulting crude product was purified by silica gel column chromatography using hexanes as the eluent to afford **S5-5 (or 7)**. Yield: 0.18 g (24%). m.p. 213- 215 ºC. ^1H NMR (400 MHz, $CDCl_3$) δ ppm 6.87 (d, 4H, *J* = 8.95 Hz), 6.98 (d, 4H, *J* = 8.95 Hz), 7.11 (d, 2H, *J* = 8.74 Hz) 7.23 (d, 1H, *J* = 8.25 Hz), 7.34 (d, 4H, *J* = 8.95 Hz), 7.38 (d, 4H, *J* = 8.95 Hz), 7.44 (d, 2H, *J* = 8.75 Hz), 7.49 (dd, 1H, *J* = 8.28 Hz, 2.17 Hz), 7.82 (d, 1H, *J* = 2.09 Hz); ^{13}C NMR (400 MHz, $CDCl_3$) δ ppm 115.18, 116.27, 123.72, 123.81, 124.23, 126.03, 127.37, 128.14, 131.46, 132.39, 132.69, 132.78, 133.64, 140.38, 143.35, 145.75, 146.31, 147.05.

Scheme 1. 6:Synthesis 3,3'-dibromo-*N4,N4,N4',N4'-tetrakis*(4-bromophenyl)-[1,1' biphenyl]-4,4'-diamine (S6-3 or 8).

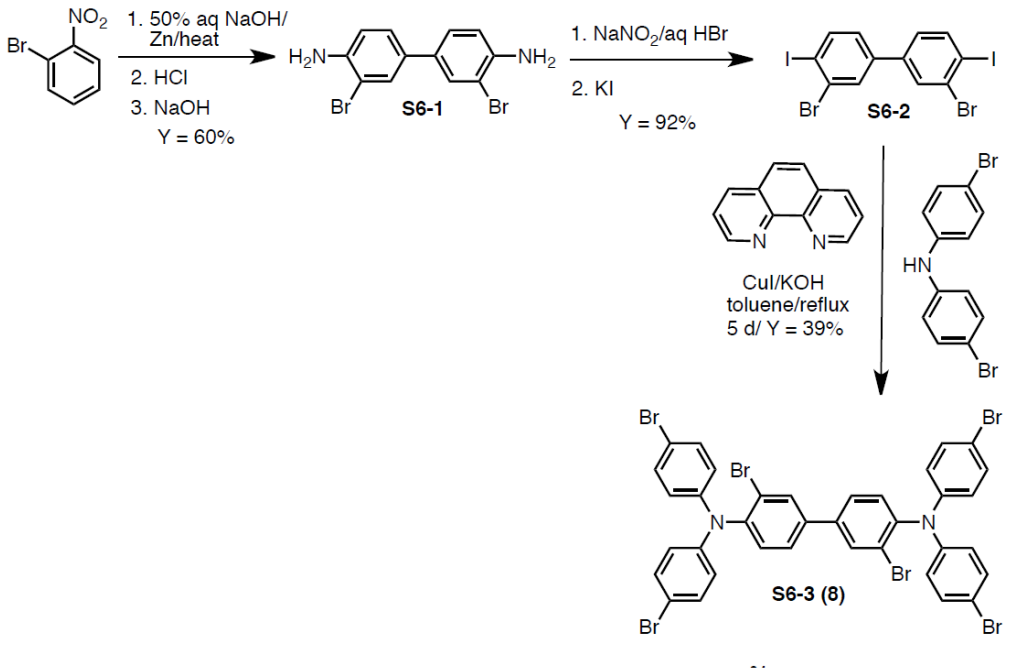

Preparation of 3,3'-dibromo-[1,1'-biphenyl]-4,4'-diamine (S6-1).[62] A mixture of *o*–nitrobromobenzene (5.5 g) and 50% aqueous sodium hydroxide (1.5 mL) was stirred at 60 °C, and zinc dust was added intermittently in small portions such that the temperature did not exceed 70-80 °C. After a total of 3.5 g of zinc had been added, the resulting sludge was diluted with water (12.5 mL) and 20% aqueous sodium hydroxide (7.5 mL). Another portion of zinc (5 g) was added all at once, and the mixture was stirred at 70-80 °C until it was nearly colorless. The mixture was then cooled to room temperature, poured slowly into 25% sulfuric acid (50 mL) cooled to ~10 °C and then filtered. The black-ash colored solid was triturated with diethyl ether (2 x 100 mL). Combined ether extracts were dried over anhydrous $MgSO_4$, filtered, and evaporated

under reduced pressure. The crude solid was dissolved in 50 mL ether and slowly poured into a stirred concentrated HCl (20 mL) cooled in an ice bath (0 °C). After stirring for 1 hour, the precipitated salt was filtered and washed with ether. The hydrochloride salt was suspended in excess 10% aqueous sodium hydroxide and heated on a steam bath for 1h. The free base was extracted from the cooled mixture with ether and the ether extracts were dried over anhydrous $MgSO_4$ and evaporated. The crude product was crystallized from a mixture of ethanol and water to afford pure **S6-1**. Yield: 2.79 g (60%). m.p. 128-129 ºC (lit.[62] m.p. 127-129 ºC). ^{1}H NMR (400 MHz, $CDCl_3$) δ ppm 4.09 (bs, 4H), 6.79 (d, 2H, *J* = 8.28 Hz), 7.25 (dd, 2H, *J* = 8.28 Hz, 2.10 Hz), 7.56 (d, 2H, *J* = 2.10 Hz); ^{13}C NMR (400 MHz, $CDCl_3$) δ ppm 109.90, 116.13, 126.54, 130.44, 131.71, 143.04.

Preparation of 3,3'-dibromo-4,4'-diiodo-1,1'-biphenyl (S6-2).[61] Using a slightly modified literature procedure, a stirred solution of **S6-1** (0.5 g, 1.46 mmol) in a mixture of 48% HBr (3.0 mL) and water (10.0 mL) at ~0 ºC was added dropwise an aqueous solution of $NaNO_2$ (0.302 g, 4.38 mmol in 5 mL H_2O). The reaction mixture was stirred vigorously for 1h at ~ -5 ºC. A cold aqueous solution of KI (4.84 g, 29.2 mmol in 10 mL H_2O) was slowly added to the reaction mixture, and it was stirred overnight (~16 h) and then allowed to warm to room temperature. The mixture was diluted with dichloromethane (100 mL) and washed with aqueous 10% NaOH solution (100 mL) and aqueous $Na_2S_2O_3$ solution (100 mL). Combined organic extracts were dried over anhydrous $MgSO_4$, filtered, and evaporated under reduced pressure. The crude product was purified by silica get column chromatography using hexanes as the eluent to afford pure **S6-2**. Yield: 0.76 g (92%). m.p. 179-181 ºC. ^{1}H NMR (400 MHz, $CDCl_3$) δ ppm 7.15 (dd, 2H, *J* = 8.27 Hz, 2.18 Hz), 7.78 (d, 2H, *J* = 2.18 Hz), 7.91 (d, 2H, *J* = 8.27

Hz); ^{13}C NMR (400 MHz, $CDCl_3$) δ ppm 101.14, 126.98, 130.73, 131.02, 140.53, 140.93.

Preparation of 3,3'-dibromo-*N4,N4,N4',N4'-tetrakis*(4-bromophenyl)-[1,1' biphenyl] 4,4'-diamine (S6-3 or 8).[54] In a dry Schlenk flask, a mixture of compound **S6-2** (0.40 g, 0.71 mmol), *bis*(4- bromophenyl)amine **S5-4** (0.48 g, 1.48 mmol), CuI (0.28 g, 0.148 mmol), 1,10-phenanthroline (0.26 g, 0.148 mmol), potassium hydroxide (0.66 g, 11.90 mmol) and toluene (30 mL) was refluxed under an argon atmosphere for 5 d. The mixture was then cooled to room temperature and poured into distilled water and extracted with dichloromethane (4 x 50 mL). The organic layer was dried over anhydrous $MgSO_4$, filtered, evaporated. The crude product was purified by silica gel column chromatography using hexanes as the eluent to afford pure **S6-3** (**8**). Yield: 0.27 g (39%). m.p. 228-230 ºC ^{1}H NMR (400 MHz, CD_2Cl_2) δ ppm 6.87 (d, 8H, *J* = 8.95 Hz), 7.27 (d, 2H, *J* = 8.25 Hz), 7.35 (d, 8H, *J* = 8.95 Hz), 7.55 (dd, 2H, *J* = 8.25 Hz, 2.20 Hz), 7.87 (d, 2H, *J* = 2.20 Hz); ^{13}C NMR (400 MHz, CD_2Cl_2) δ ppm 115.52, 124.13, 124.24, 128.16, 132.00, 132.71, 133.50, 139.06, 144.68, 146.12.

Scheme 1. 7: Synthesis of 2,2'-dibromo-*N4,N4,N4',N4'-tetrakis*(4-bromophenyl)-[1,1'-biphenyl]-4,4'-diamine (S7-2 or 9).

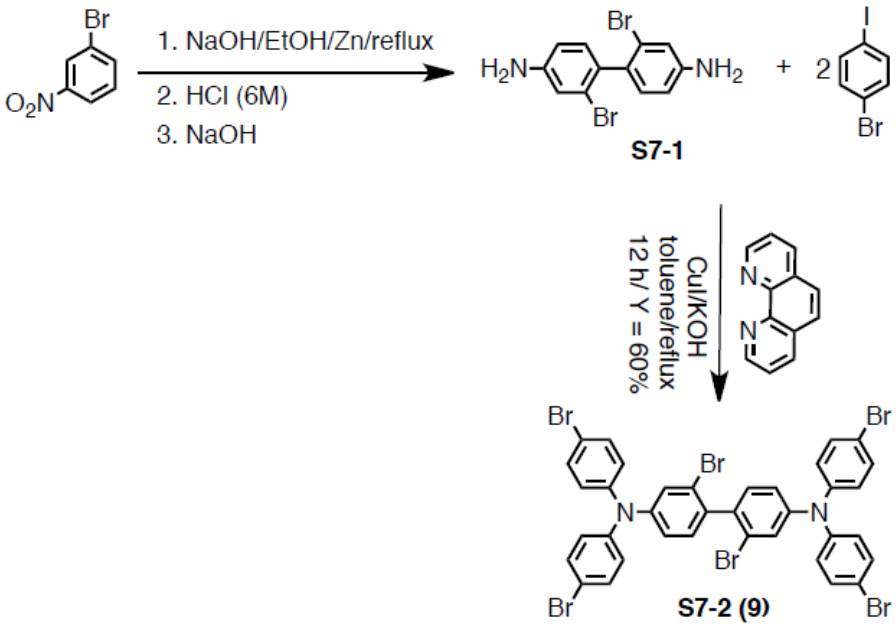

Preparation of 2,2'-dibromo-[1,1'-biphenyl]-4,4'-diamine (S7-1).[63] To a stirred solution of 3-bromonitrobenzene (5.5 g, 27.2 mmol) in ethanol (60 mL) were added in portions a solution of sodium hydroxide (2.5 g in 15 mL water) and zinc powder (10 g). The mixture was brought to 70 °C and after 15 minutes, more zinc (6 g) was added. After an additional 15 min, the mixture became pale yellow. It was then brought to a boil and filtered under an argon atmosphere. The zinc residue was washed with ethanol (2 x 10 mL). The combined filtrate was mixed with water (50 mL), and cooled in an ice bath, which resulted in the formation of a pale yellow precipitate. The filtered precipitate was added to hydrochloric acid (6 M, 50 mL) and stirred at 60 °C for 15 minutes, then cooled rapidly. The solid benzidine hydrochloride was collected, washed with 6M hydrochloric acid and diethyl ether, and suspended in warm water containing excess sodium

hydroxide. This mixture was extracted with diethyl ether (3 x 50 mL) and the extracts were dried over anhydrous $MgSO_4$, filtered, and evaporated. The crude benzidine **S7-1** was crystallized from an ethanol-water mixture. Yield: 0.85 g (18%). m.p. 150-152 ºC (lit.[63] m.p. 151-153ºC). ^{1}H NMR (400 MHz, $CDCl_3$) δ ppm 3.74 (br s. 4 H for NH_2), 6.64 (dd, 2H, *J* = 8.18 Hz, 2.36 Hz), 6.97 (d, 2H, *J* = 2.33 Hz), 7.00 (d, 2H, *J* = 8.18 Hz); ^{13}C NMR (400 MHz, $CDCl_3$) δ 113.95, 118.44, 124.95, 132.17, 132.24, 146.99.

Preparation of 2,2'-dibromo-*N4,N4,N4',N4'-tetrakis*(4-bromophenyl)-[1,1'-biphenyl]-4,4' -diamine (S7-2 or 9).[54] In a dry Schlenk flask, a mixture of **S7-1** (0.4 g, 1.17 mmol), 1-bromo-4-iodobenzene (1.35 g, 4.8 mmol), CuI (0.013 g, 0.07 mmol), 1,10-phenanthroline (0.012 g, 0.07 mmol), potassium hydroxide (0.502 g, 8.96 mmol), and toluene (35 mL) was refluxed under an argon atmosphere for 24 h. The mixture was then cooled to room temperature and poured into distilled water. The crude product was extracted with dichloromethane (4 x 50 mL) and the combined organic layers were dried over anhydrous $MgSO_4$, filtered, and evaporated. The crude product was purified by silica gel column chromatography using hexanes as the eluent to afford **S7-2 (or 9)** as a brown-colored solid. The colored impurities were removed by repeated treatments (3 times) with charcoal (20 mg) in refluxing dichloromethane (25 mL) followed by crystallization from a mixture of acetonitrile and chloroform to afford shiny crystals of **S7-2 (or 9)**. Yield: 0.67 g (60%). m.p. 278-280 ºC. ^{1}H NMR (400 MHz, $CDCl_3$) δ ppm 7.00 (m, 10H), 7.11 (d, 2H, *J* = 8.32 Hz), 7.29 (d, 2H, *J* = 2.37 Hz), 7.40 (d, 8H, *J* = 8.80 Hz); ^{13}C NMR (400 MHz, $CDCl_3$) δ ppm 116.89, 121.56, 124.53, 126.38, 126.45, 131.95, 132.87, 135.93, 145.91, 147.67.

Scheme 1. 8: Synthesis of *tris*(2-bromo-4-(*tert*-butyl)phenyl)amine (S8-2 or BC)

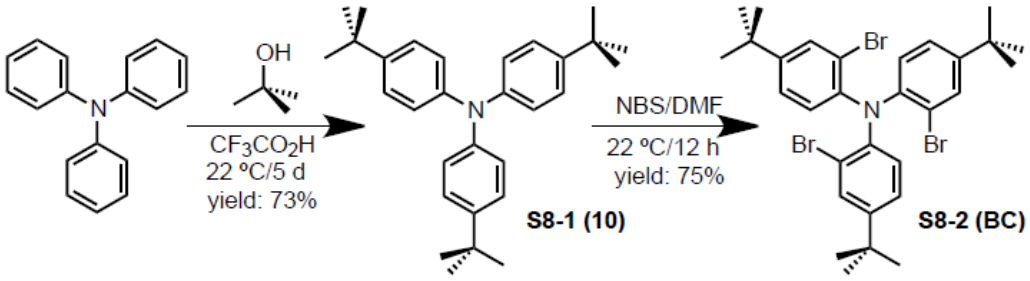

Preparation of *tris*(4-(*tert*-butyl)phenyl)amine (S8-1 or 10). A mixture of triphenylamine (1.23 g, 5 mmol), 2-methylpropane-2-ol (5 ml), and trifluoroacetic acid (20 mL) was stirred at 22^{o}C for 5 days. The formed precipitate was filtered, dried and recrystallized from a mixture of dichloromethane and hexanes to afford pure **S8-1** (**or 10**). Yield: 1.5 g (73%), m.p. 286-288 ^{o}C (lit.[64] m.p. 276-278 ^{o}C). ^{1}H NMR ($CDCl_3$) δ ppm 1.30 (s, 27H), 7.01 (d, *J* = 8.3Hz, 6H), 7.23 (d, *J* = 8.3Hz, 6H); ^{13}C NMR ($CDCl_3$) δ ppm 31.37, 34.14, 123.42, 125.93, 145.09, 145.44.

Preparation of *tris*(2-bromo-4-(*tert*-butylphenyl)amine (S8-2 or BC). To a solution of 4-(*tert*butylphenyl)amine (0.35 g, 0.85 mmol) in dichloromethane (15 mL) was added a solution of NBS (0.53 g, 2.96 mmol) in DMF (5 mL) dropwise under an argon atmosphere, and stirred overnight (~16 h) at 22 ^{o}C. The reaction mixture was quenched with water and extracted with dichloromethane (3 x 25 mL). The combined organic extracts were dried over anhydrous $MgSO_4$, filtered, and evaporated. The crude product was filtered through a short pad of silica gel using dichloromethane as the elutant followed by recrystallization from a mixture of dichloromethane and hexanes to afford pure **S8-2** (or **BC**). Yield: 0.42 g (75%), m.p. 238-240 ^{o}C. ^{1}H NMR ($CDCl_3$) δ 1.30 (s, 27H), 6.74 (d, *J* = 8.36Hz, 3H), 7.19 (d, *J* = 8.36Hz, 2.23Hz, 3H), 7.56 (d, *J* = 2.23Hz,

3H); ^{13}C NMR ($CDCl_3$) δ ppm 31.48, 34.60, 121.23, 125.07, 126.70, 131.60, 143.51, 148.87.

General procedures for preparative isolation of cation-radical hexachloroantimonate salts.

Preparation of $MB^{+\bullet}SbCl_6^-$ using $NO^+SbCl_6^-$. To a 50-mL flask fitted with a Schlenk adaptor and charged with nitrosonium hexachloroantimonate (44 mg, 0.12 mmol) was added a cold solution (~0 °C) of **MB⁰** (58 mg, 0.12 mmol) in anhydrous dichloromethane (5 mL) under an argon atmosphere at -10 °C. The solution immediately turned blue and was stirred (while slowly bubbling argon through the solution to entrain gaseous NO) for 10 min to yield a solution of $MB^{+\bullet}SbCl_6^-$. To this solution was then added dry ether (15 mL) to precipitate the dissolved $MB^{+\bullet}SbCl_6^-$ salt. The microcrystalline precipitate was filtered using a medium-grade sintered-glass funnel under dry nitrogen and washed with dry diethyl ether (2 x 5 mL) using the apparatus described below. The resulting salt was dried *in vacuo* at room temperature to afford $MB^{+\bullet}SbCl_6^-$ in essentially quantitative yield (0.89 g, 91%).

Preparation of $MB^{+\bullet}SbCl_6^-$ using $SbCl_5$. A solution of **MB^0** (0.96 g, 2 mmol) in anhydrous dichloromethane (20 mL) was added to a flask equipped with a dropping funnel and argon inlet and outlet adapters. The dropping funnel was charged with a solution of $SbCl_5$ in dichloromethane (2 mL, 1 M) and the flask was cooled in a dry ice-acetone bath (approximately –78 °C). The $SbCl_5$ solution was slowly added (3-5 min) under a flow of argon. The reaction mixture immediately turned blue and a large amount of material precipitated. The resultant mixture was warmed to ~0 °C during 5-10 min, and anhydrous diethyl ether (30 mL) was added to precipitate the dissolved $MB^{+\bullet}SbCl_6^-$ salt.

The dark-blue microcrystalline precipitate was suction filtered using a medium-grade sintered-glass funnel under a blanket of dry argon and washed with dry diethyl ether (2 x 20 mL) using the apparatus shown below. The resulting salt was dried *in vacuo* at room temperature to afford **$MB^{+\bullet}SbCl_6^-$** (1.43 g, 88%).

An apparatus for filtration of cation-radical salts under argon atmosphere. A large inverted funnel, connected to an argon outlet, positioned above the sintered glass funnel is generally sufficient for maintaining an inert atmosphere during filtration of the cation radical salt (see sketch of the apparatus below).

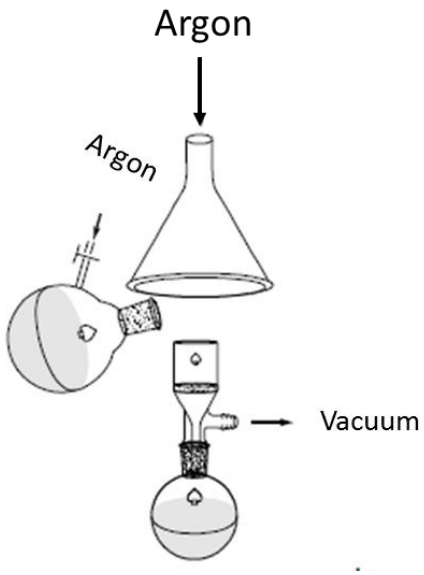

Figure1. 17. A basic apparatus for filtration of cation-radical salts under argon atmosphere Similar procedures were used for preparative isolation of **$BC^{+\bullet}SbCl_6^-$**.

Preparation of $TAB^{+\bullet}SbCl_6^-$ salt.

A 25 mL schlenk tube equipped with a magnetic stir bar was charged with a solution of the tetrakis (4bromophenyl) benzidine **TAB** (30 mg, 0.037 mmol) in

anhydrous dichloromethane (5 mL) under an argon atmosphere. Then triethyloxonium hexachloroantimonate **$Et_3O^+SbCl_6^-$** (32 mg, 0.074 mmol) was added under an argon atmosphere at ~0 °C and stirred for 30 minutes. The mixture immediately took on a yellowish-orange coloration which intensified with time. The mixture was layered with dry toluene (10 mL) and kept in a refrigerator overnight, which resulted in the formation of orange colored crystals of **$TAB^{+\bullet}SbCl_6^-$**.

$^{1}H/^{13}C$ NMR spectroscopy of Compounds

^{1}H NMR spectrum of S1-1 in $CDCl_3$

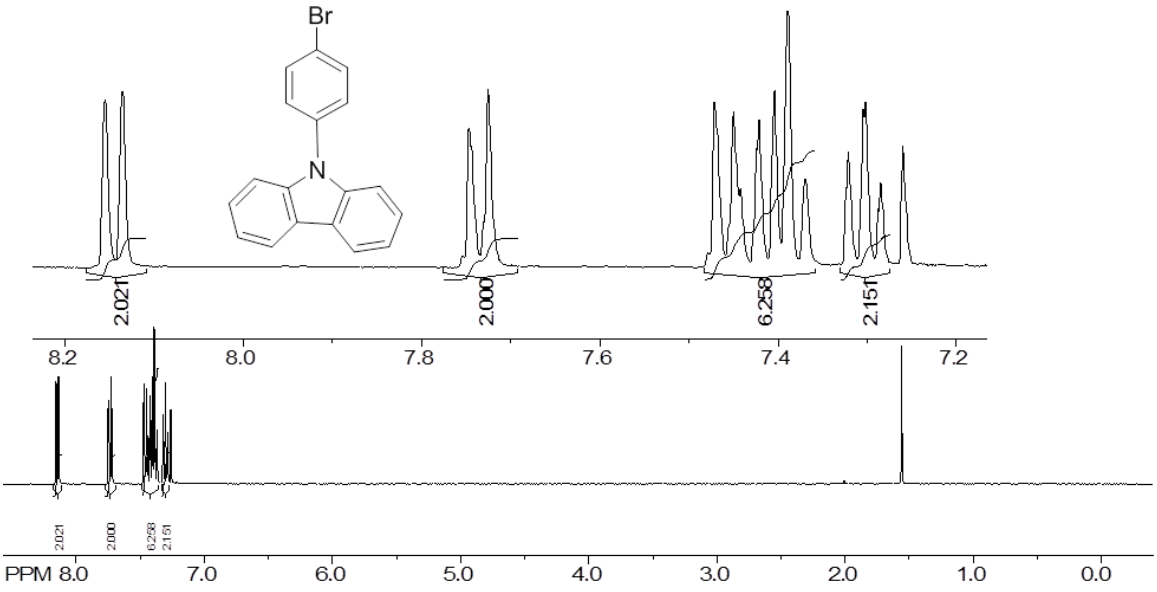

^{13}C NMR spectrum of S1-1 in $CDCl_3$

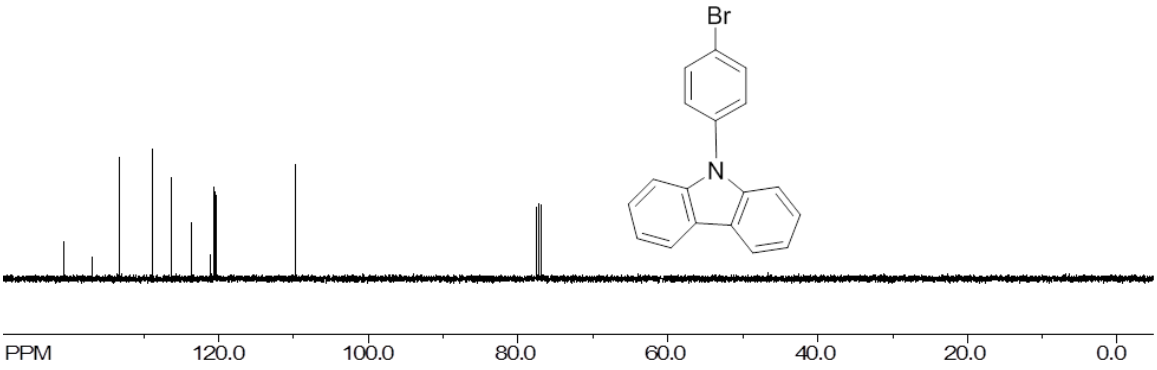

^{1}H NMR spectrum of S1-2 (4) in $CDCl_3$

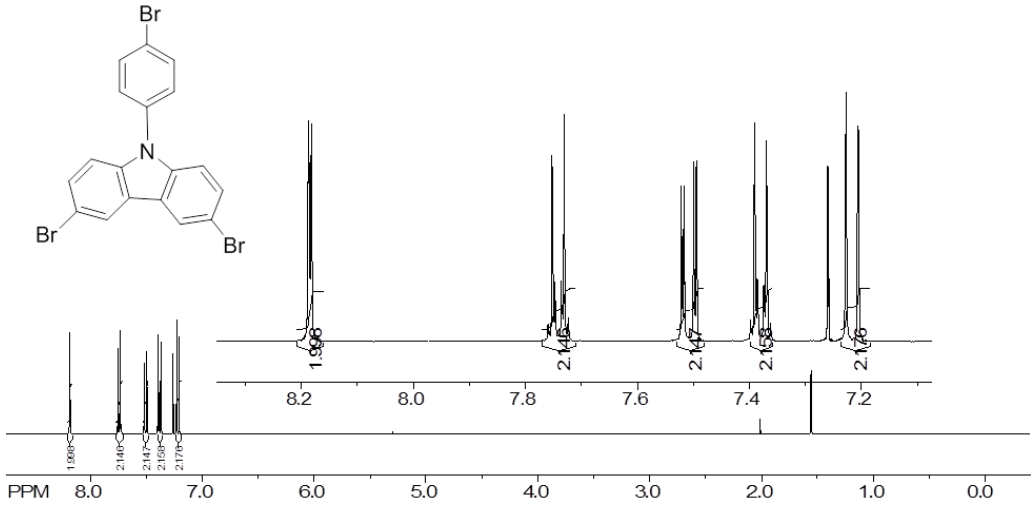

^{13}C NMR spectrum of S1-2 (4) in $CDCl_3$

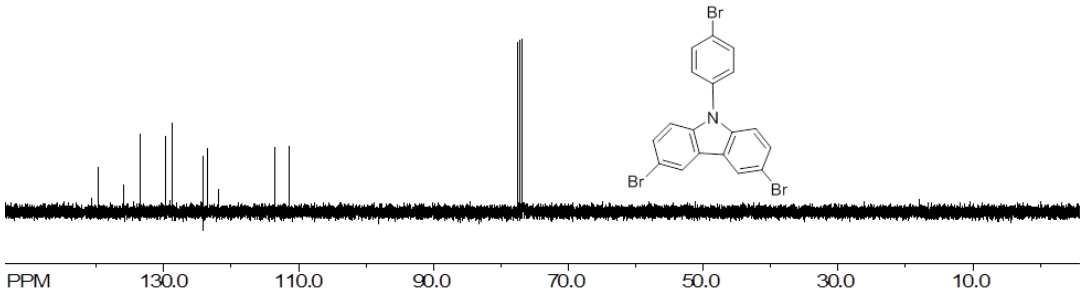

^{1}H NMR spectrum of S2-1in $CDCl_3$

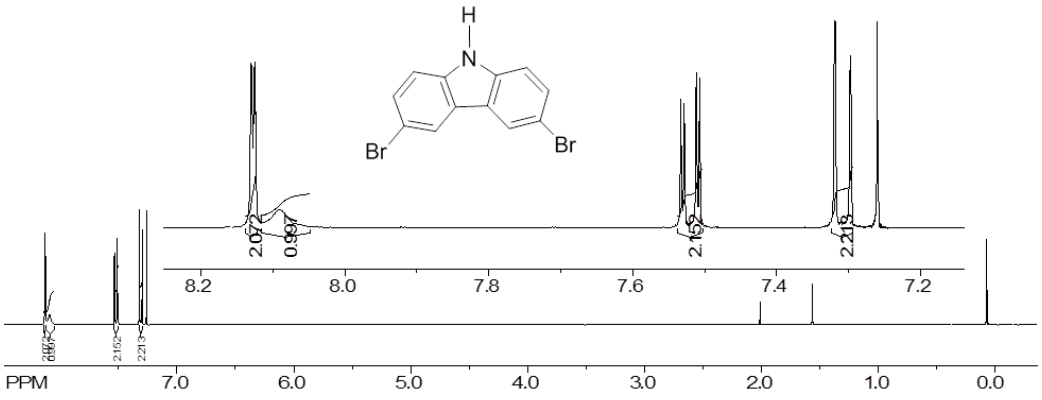

^{13}C NMR spectrum of S2-1 in $CDCl_3$

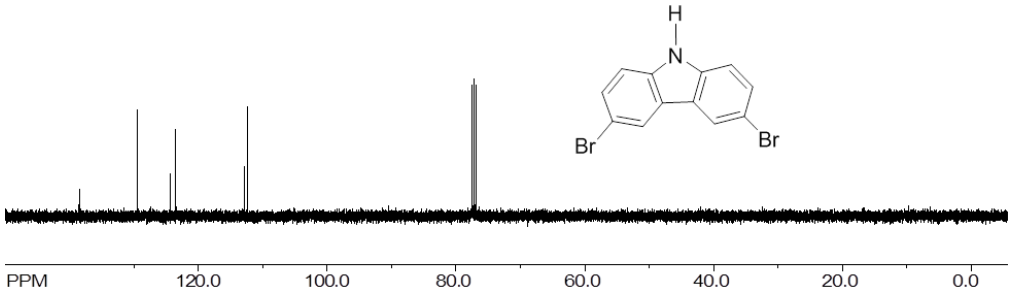

^{1}H NMR spectrum of S2-2 (5) in $CDCl_3$

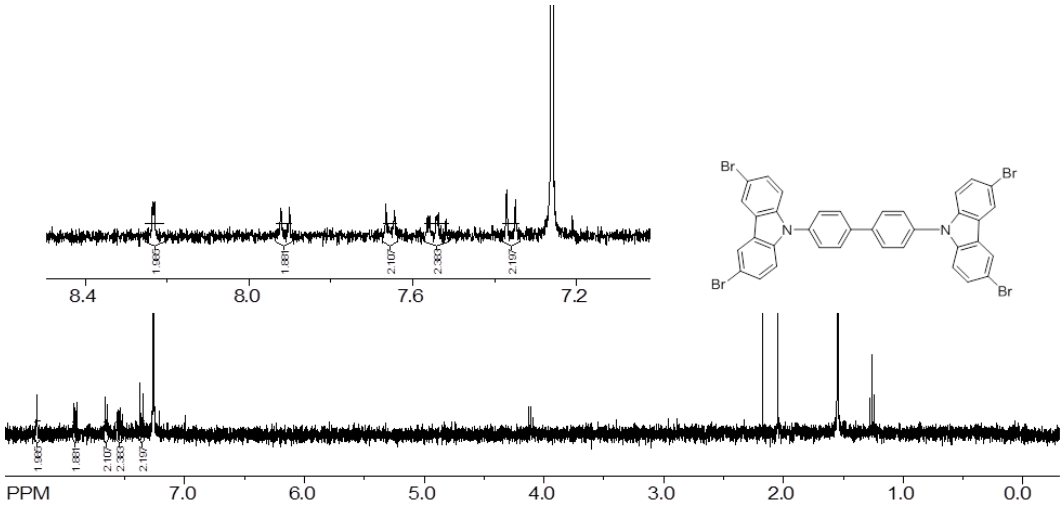

^{1}H NMR spectrum of compound S3-1 in $CDCl_3$

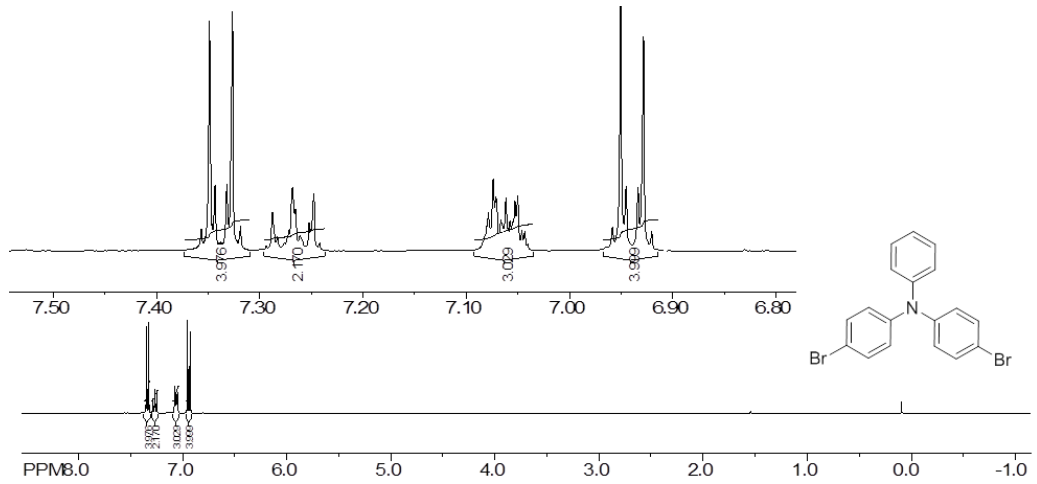

^{13}C NMR spectrum of S3-1 in $CDCl_3$

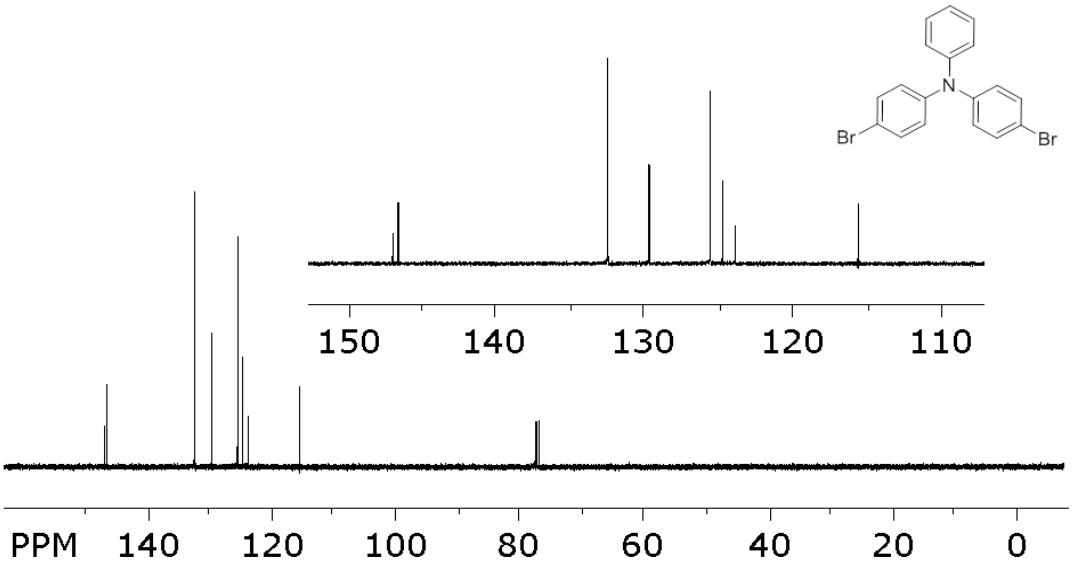

^{1}H NMR spectrum of S3-2 (TAB) in $CDCl_3$

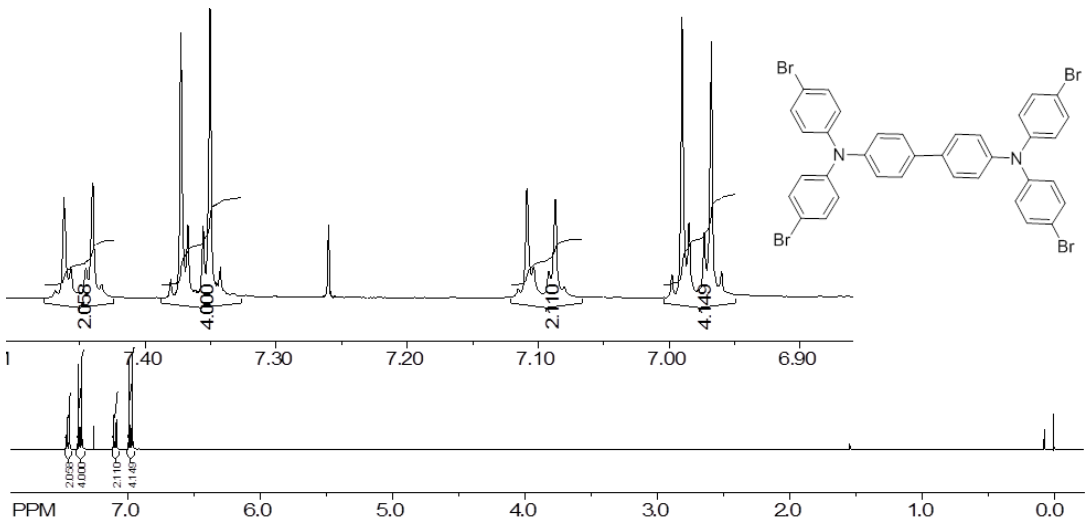

^{13}C NMR spectrum of S3-2 (TAB) in $CDCl_3$

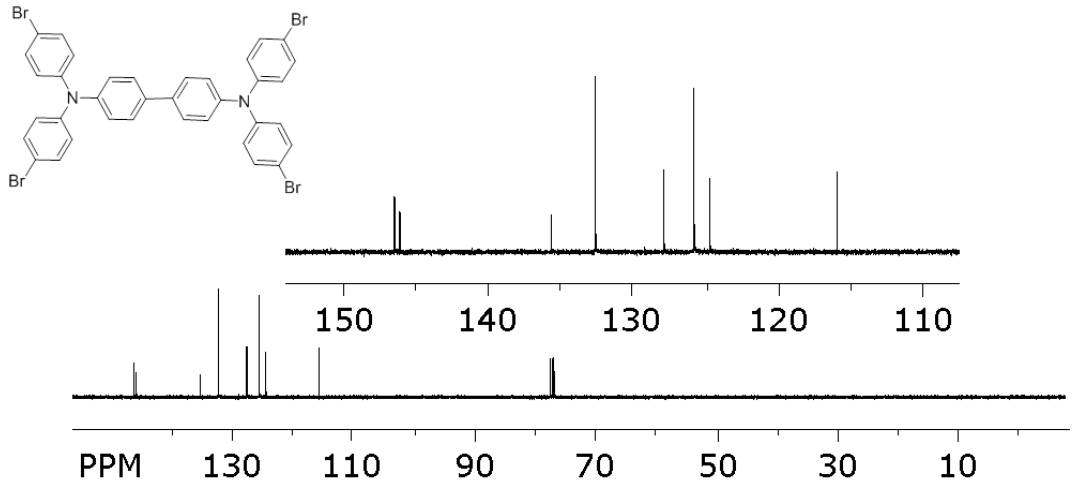

^{1}H NMR spectrum of S4-1 in $CDCl_3$

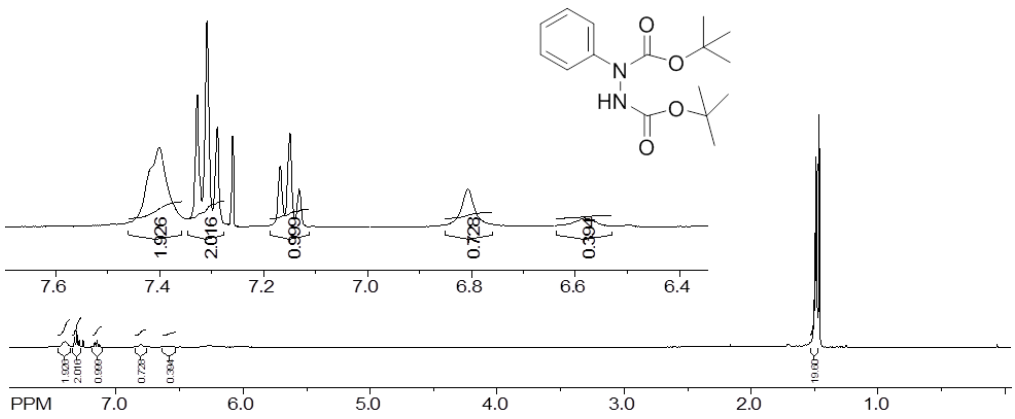

^{13}C NMR spectrum of S4-1 in $CDCl_3$

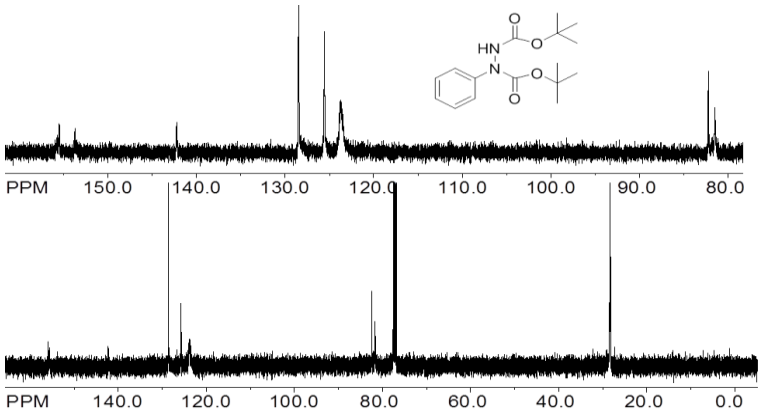

^{1}H NMR spectrum of S4-2 in $CDCl_3$

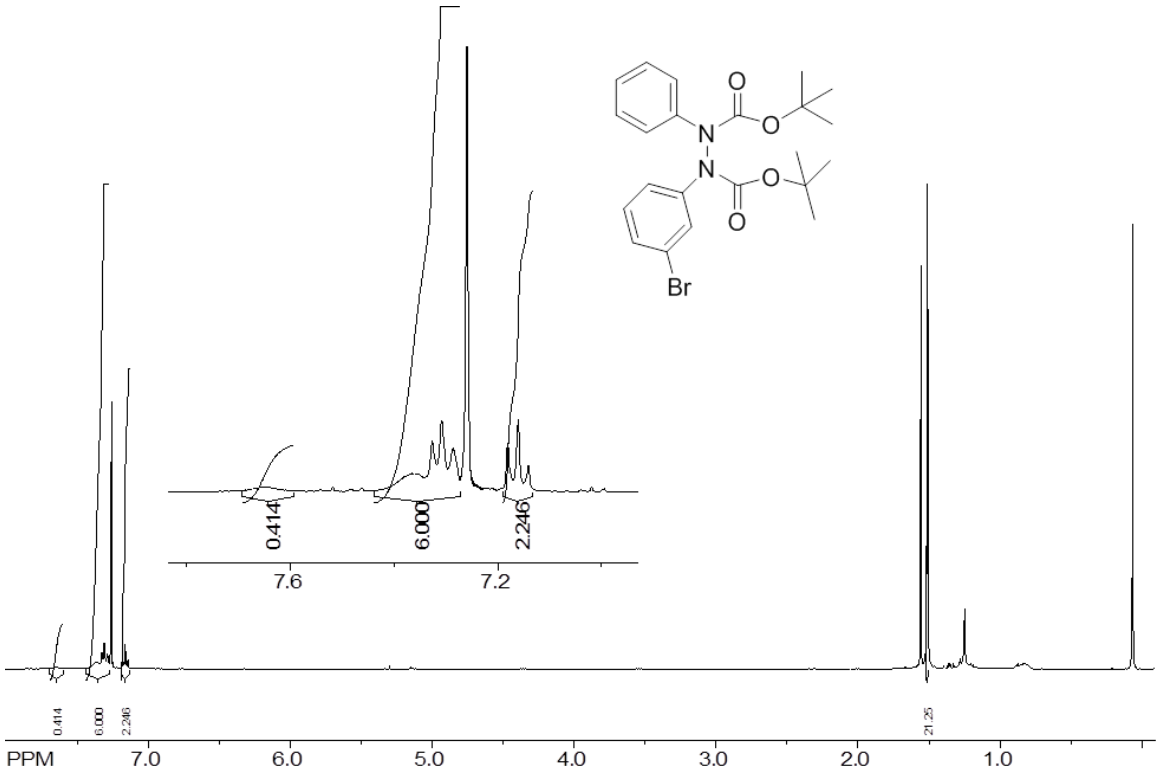

^{13}C NMR spectrum of S4-2 in $CDCl_3$

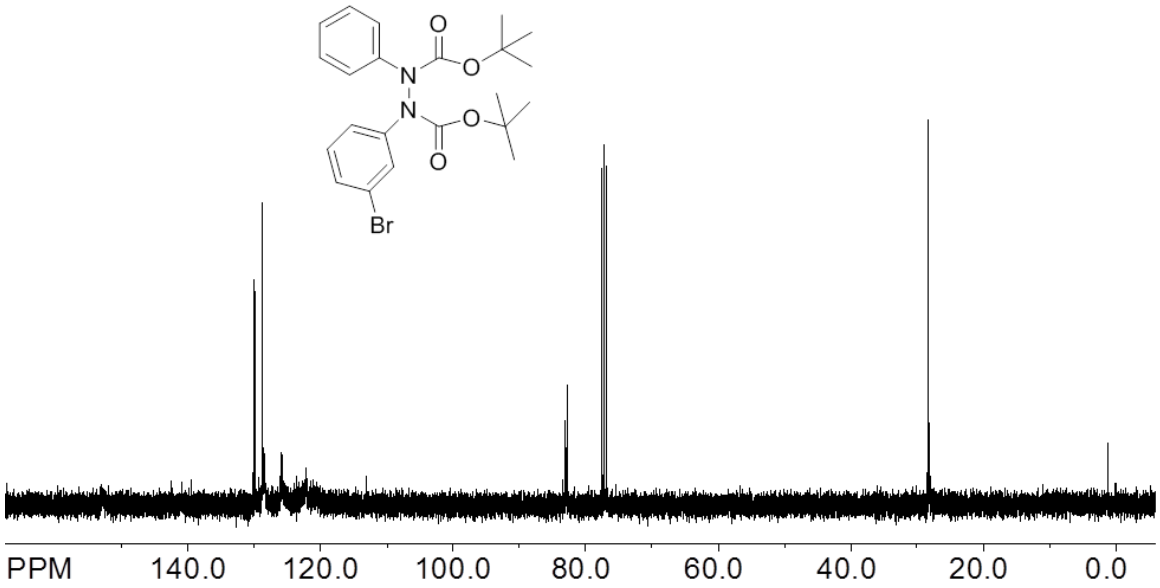

^{1}H NMR spectrum of S4-3 in $CDCl_3$

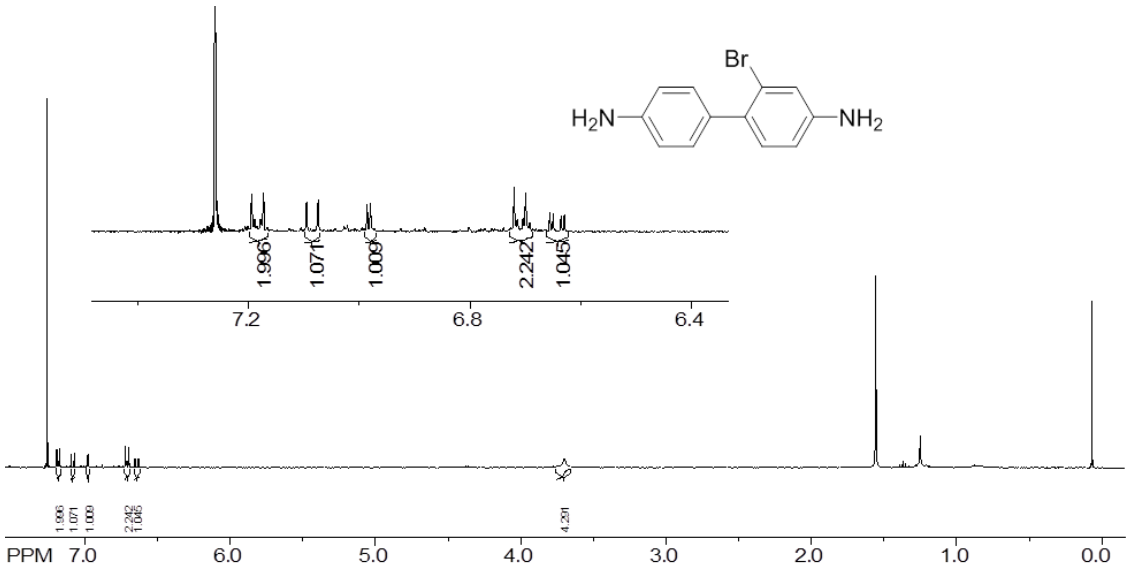

^{13}C NMR spectrum of S4-3 in $CDCl_3$

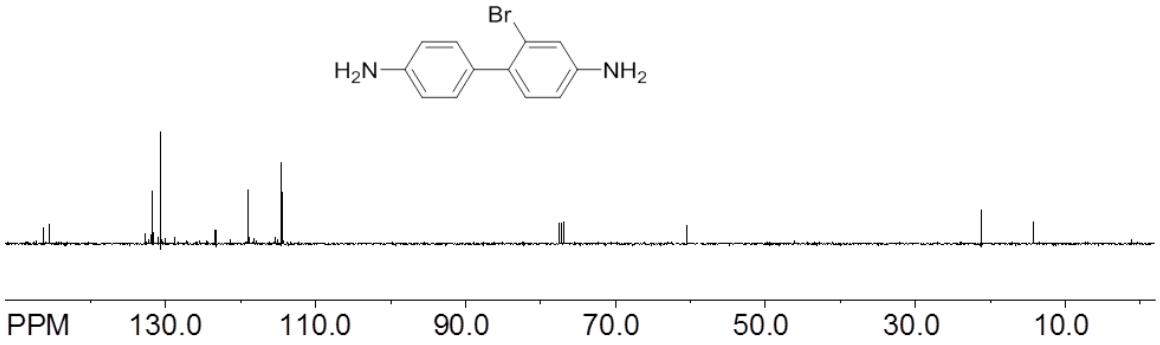

^{1}H NMR spectrum of S4-4 (or 6) in $CDCl_3$

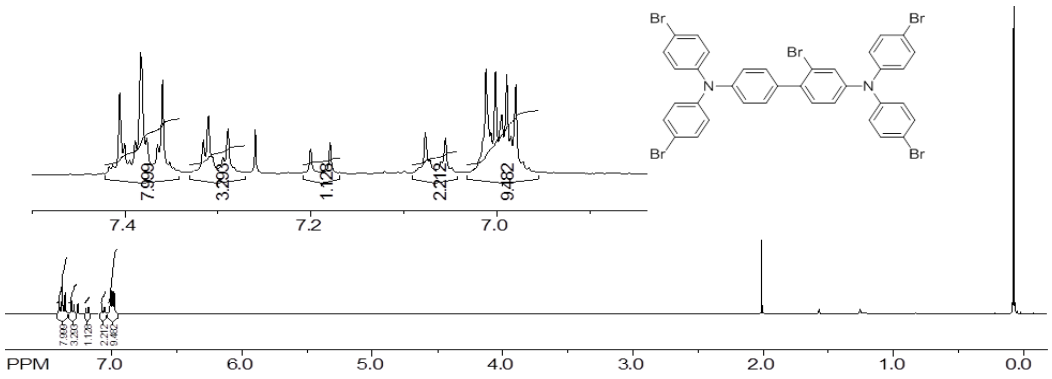

^{13}C NMR spectrum of S4-4 (or 6) in $CDCl_3$

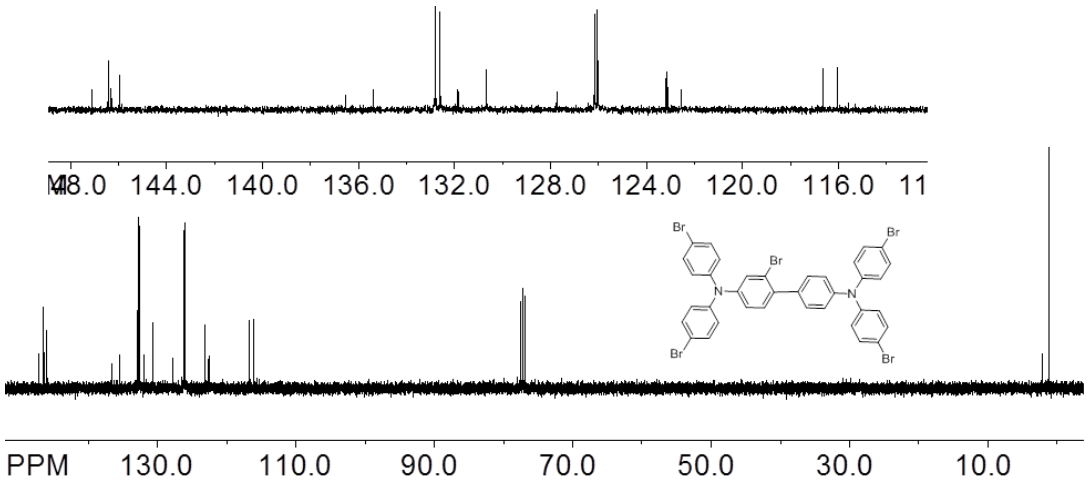

^{1}H NMR spectrum of S5-1 in in $CDCl_3$

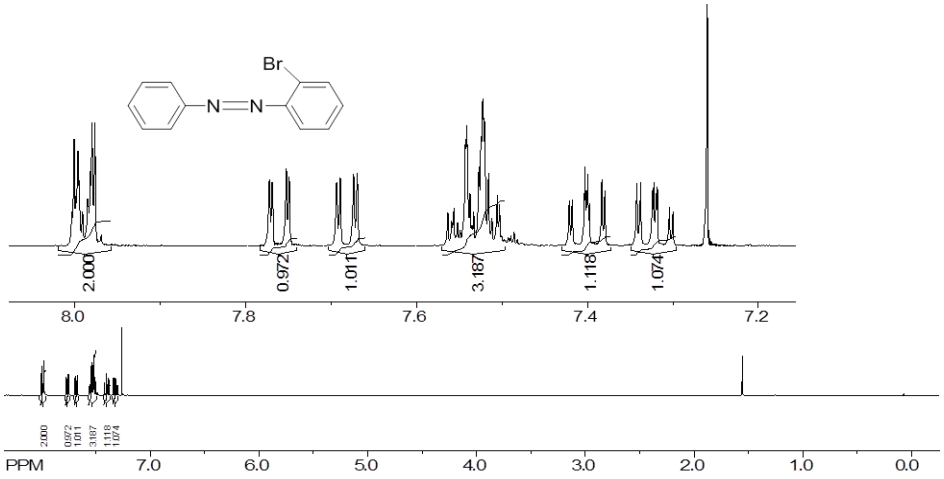

^{13}C NMR spectrum of S5-1 in $CDCl_3$

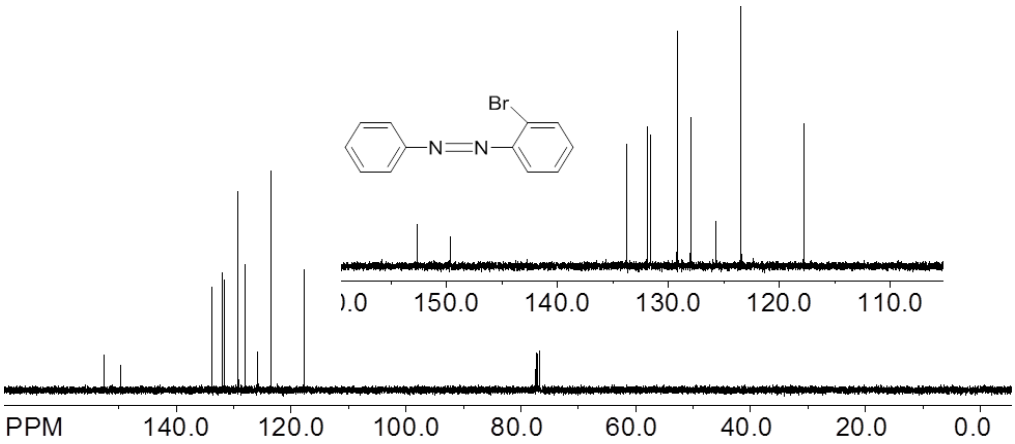

^{1}H NMR spectrum of S5-2 in in $CDCl_3$

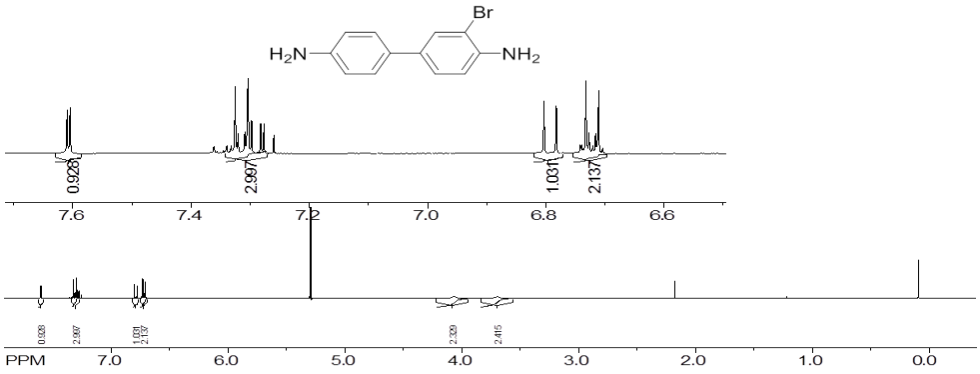

^{13}C NMR spectrum of S5-2 in $CDCl_3$

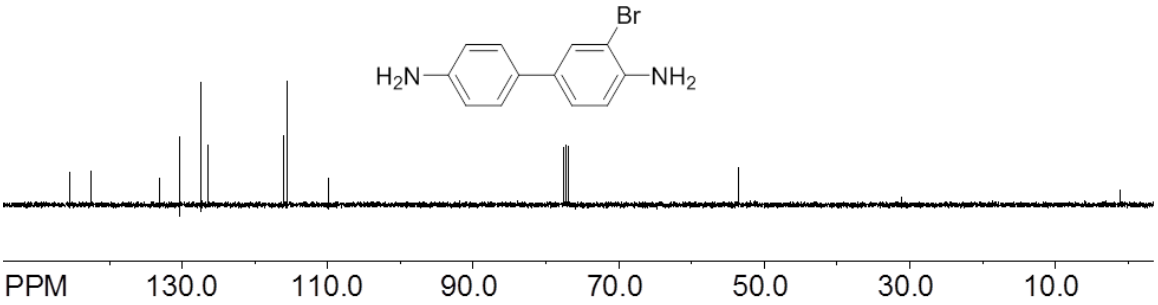

^{1}H NMR spectrum of S5-3 in $CDCl_3$

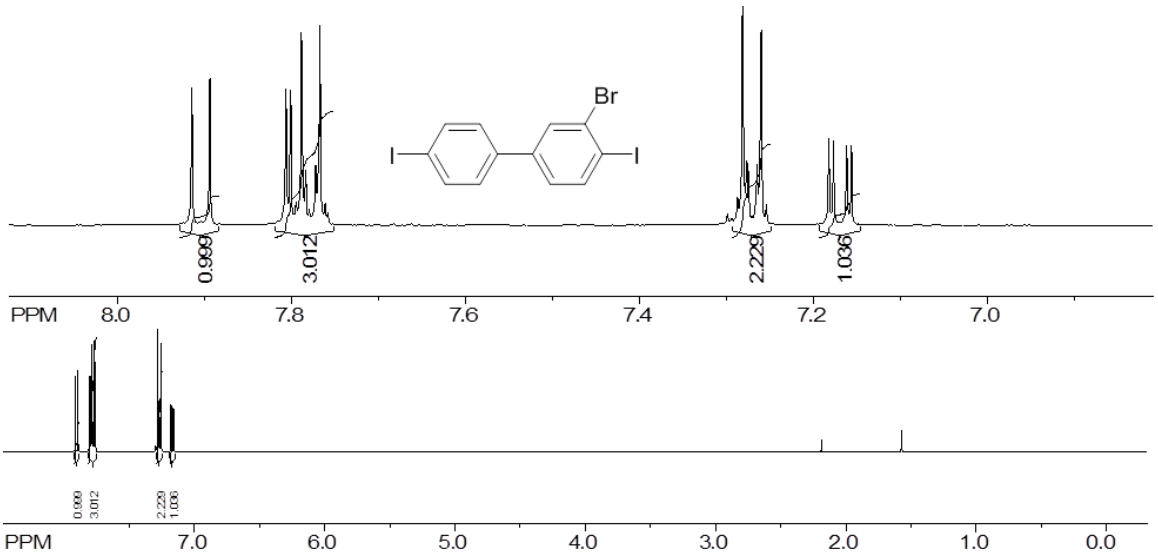

^{13}C NMR spectrum S5-3 in $CDCl_3$

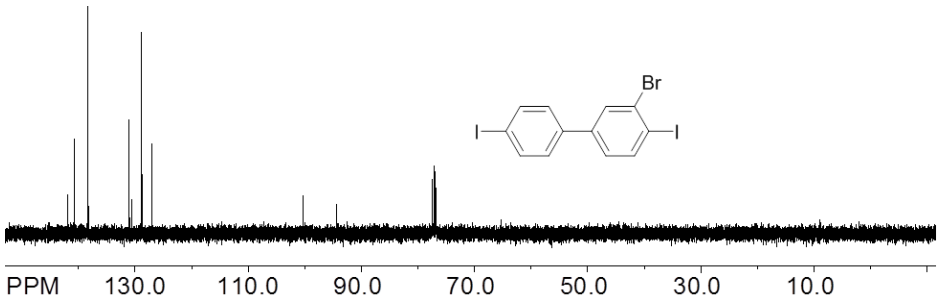

^{1}H NMR spectrum of S5-4 in $CDCl_3$

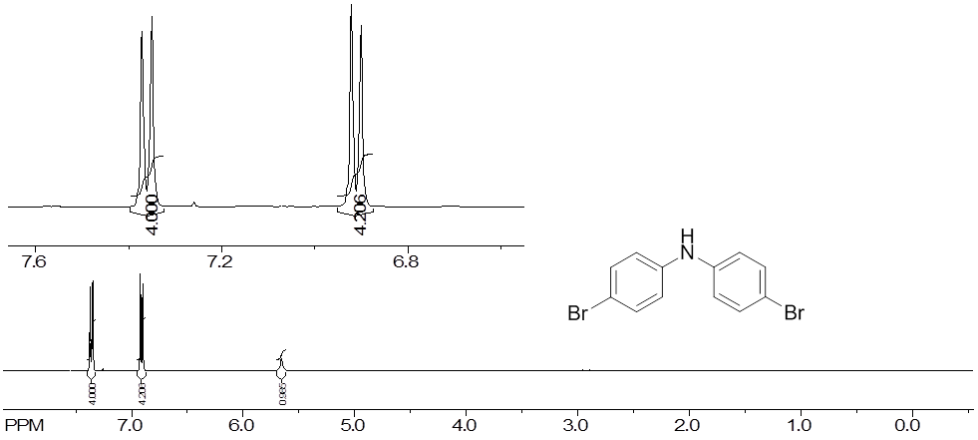

^{13}C NMR spectrum of S5-4 in $CDCl_3$

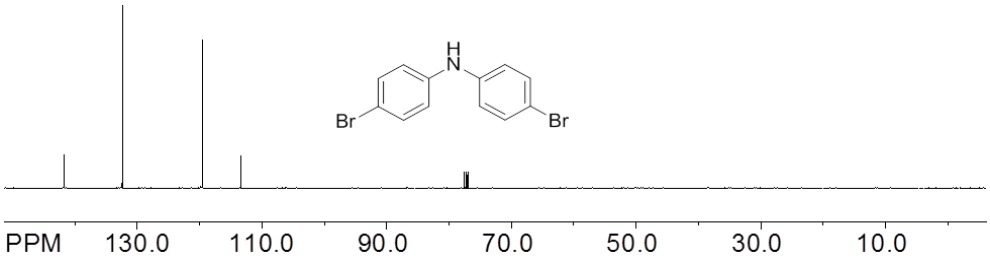

^{1}H NMR spectrum of S5-5 (or 7) in $CDCl_3$

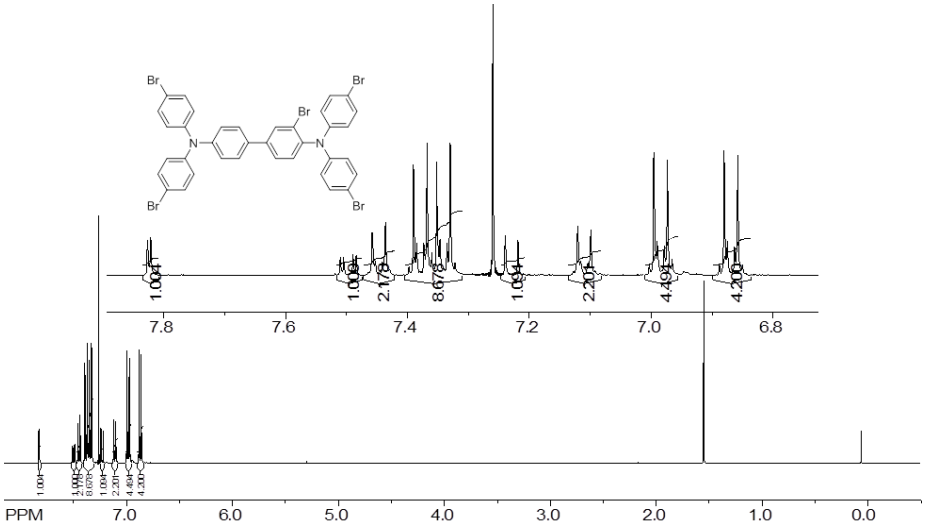

^{13}C NMR spectrum of S5-5 (or 7) in $CDCl_3$

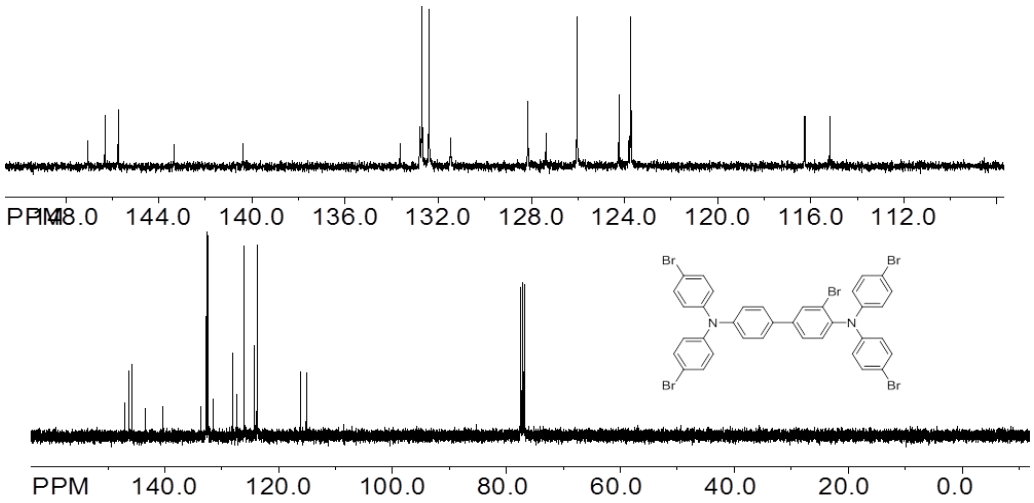

^{1}H NMR spectrum of S6-1 in $CDCl_3$

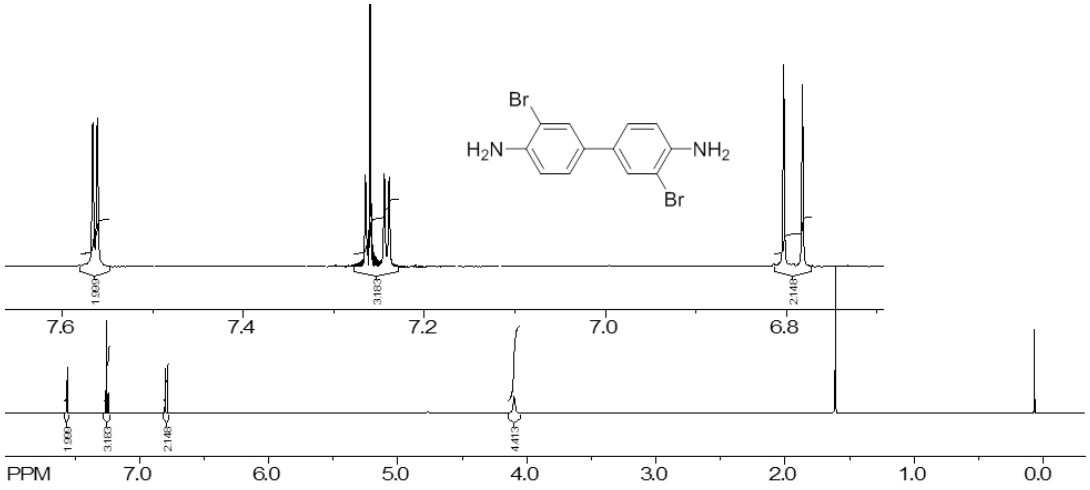

^{13}C NMR spectrum of S6-1 in $CDCl_3$

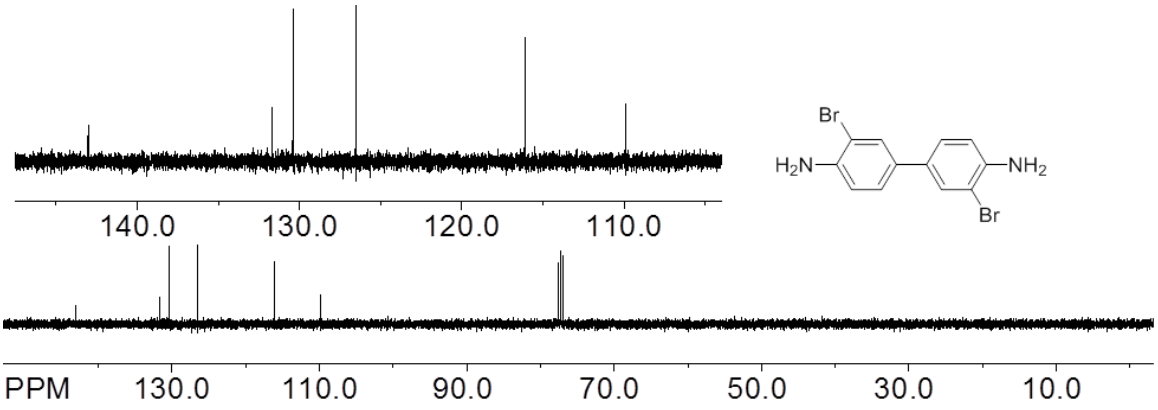

^{1}H NMR spectrum of S6-2 in $CDCl_3$

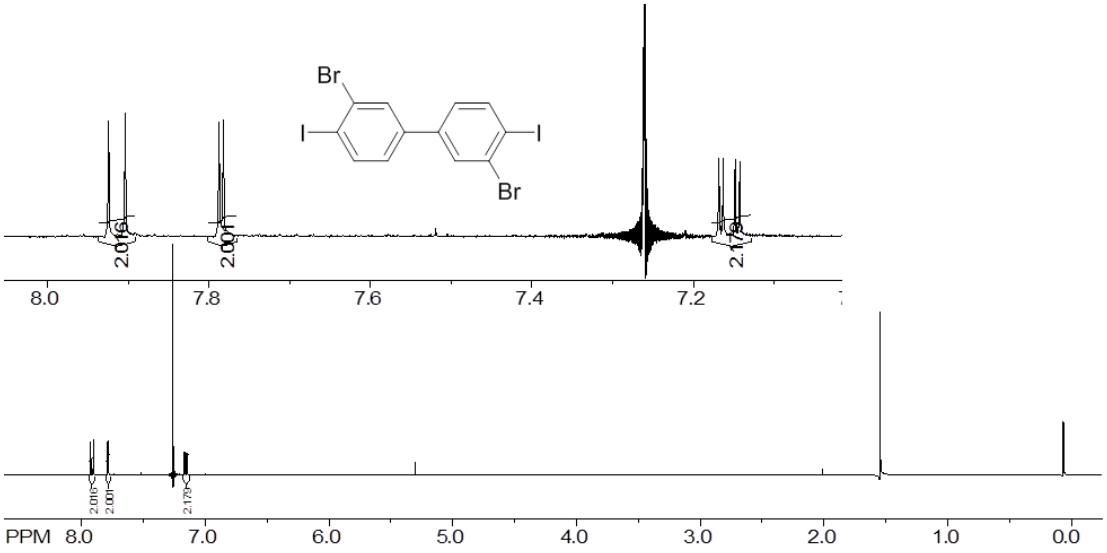

^{13}C NMR spectrum of S6-2 in $CDCl_3$

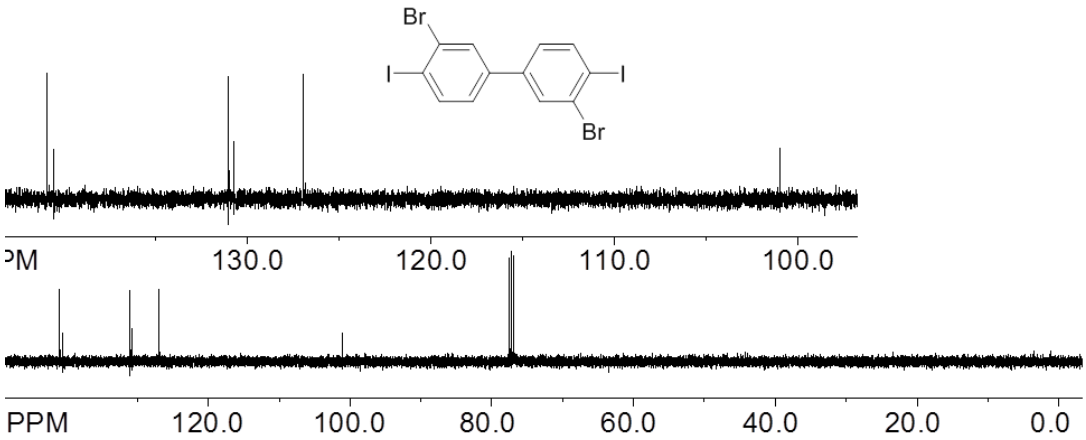

^{1}H NMR spectrum of S6-3 (8) in CD_2Cl_2

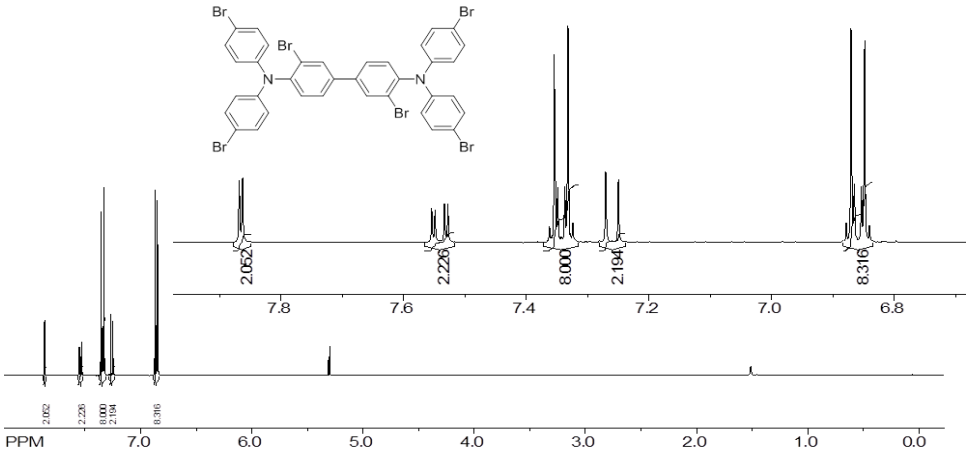

^{13}C NMR spectrum of S6-3 (8) in CD_2Cl_2

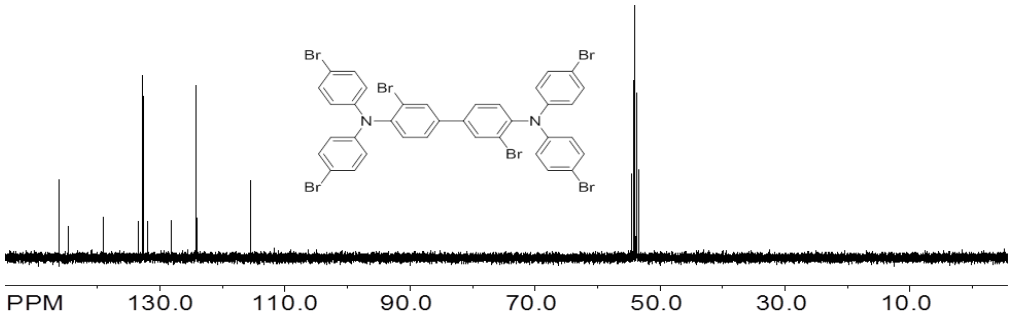

^{1}H NMR spectrum of S7-1 in $CDCl_3$

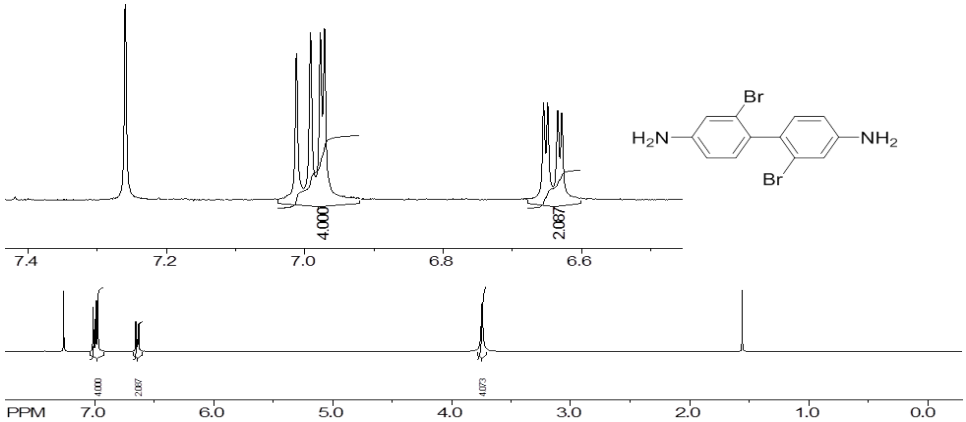

^{13}C NMR spectrum of S7-1 in $CDCl_3$

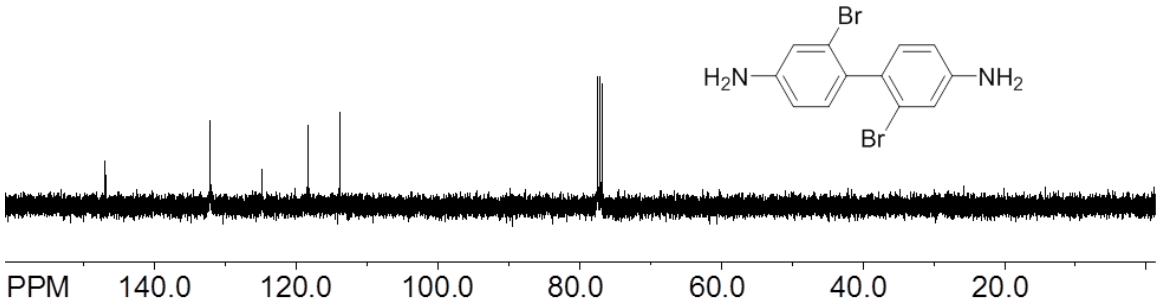

^{1}H NMR spectrum of S7-2 (or 9) in $CDCl_3$

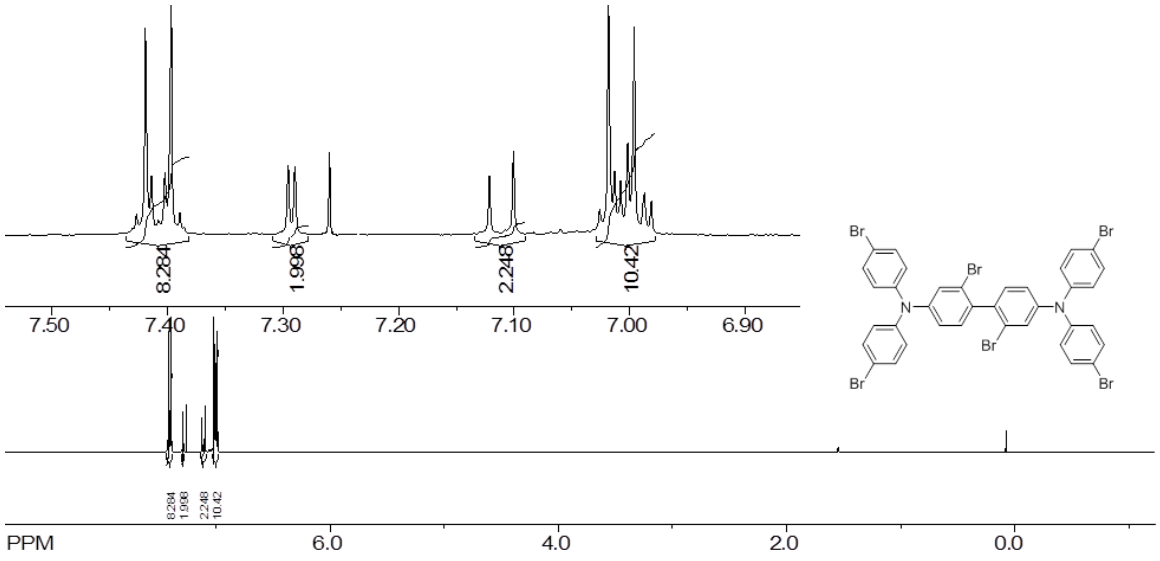

^{13}C NMR spectrum of S7-2 (or 9) in $CDCl_3$

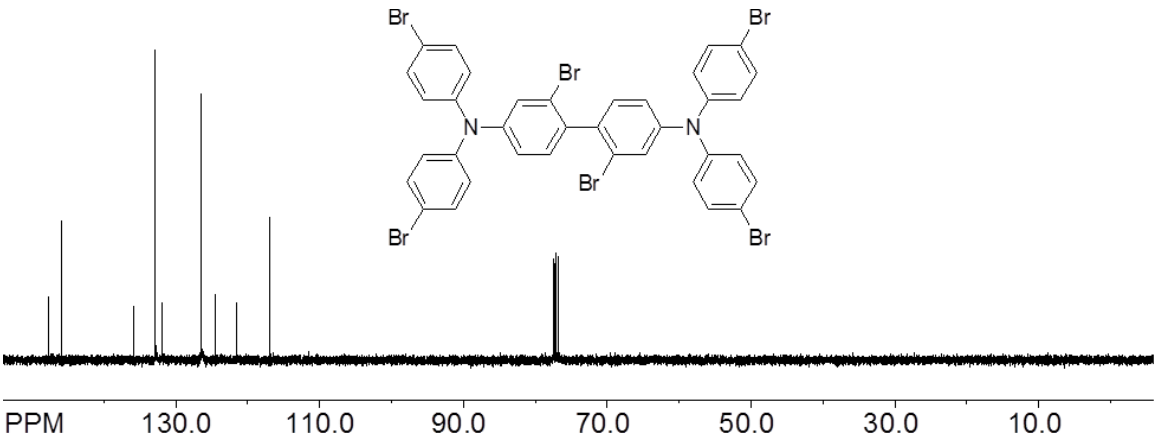

^{1}H NMR spectrum of S8-1 (or 10) in $CDCl_3$

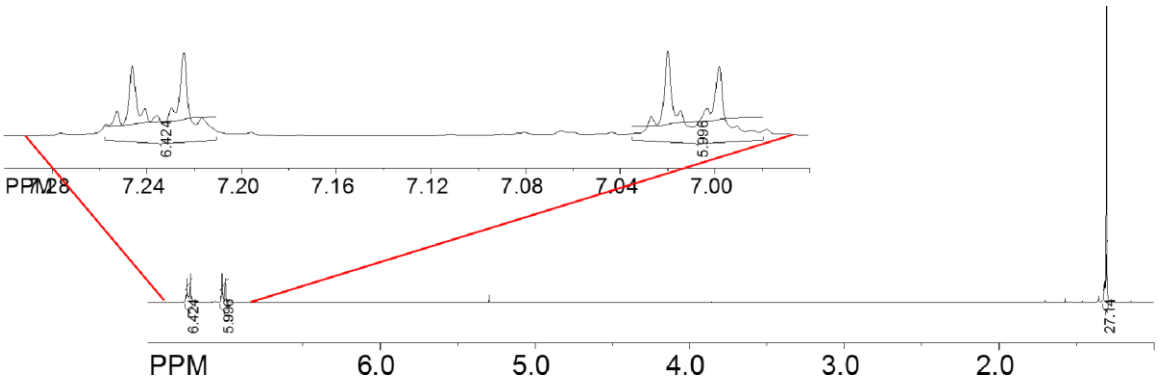

^{13}C NMR spectrum of S8-1 (or 10) in $CDCl_3$

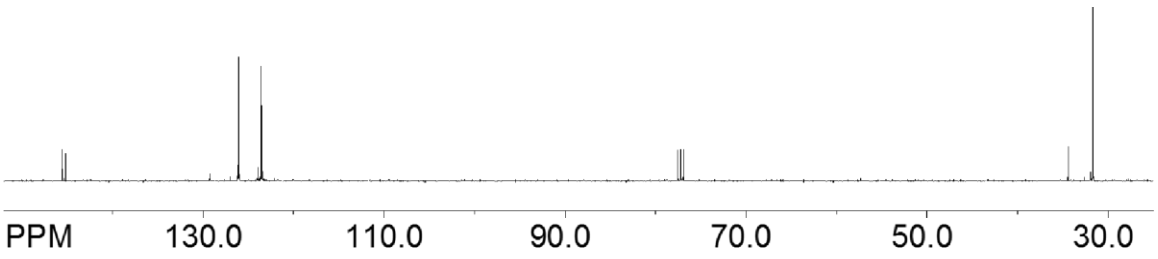

^{1}H NMR spectrum of S8-2 (or BC) in $CDCl_3$

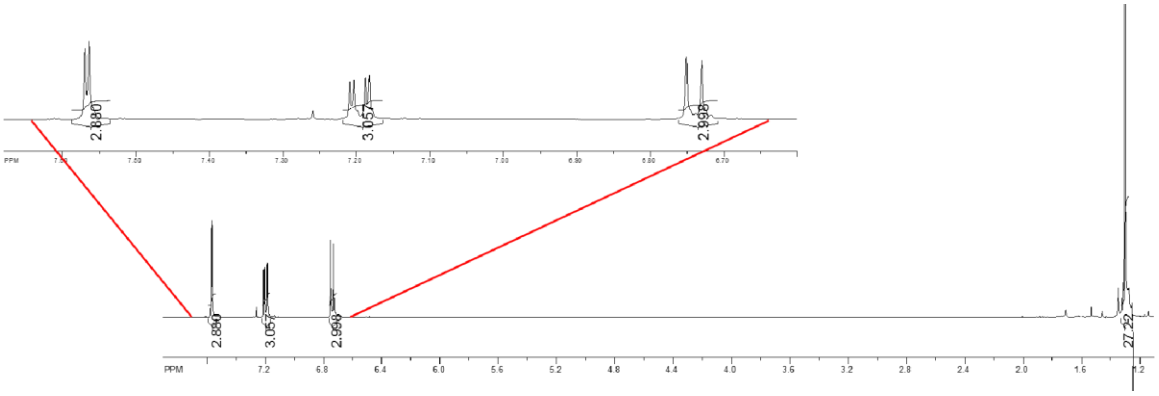

^{13}C NMR spectrum of S8-2 (or BC) in $CDCl_3$

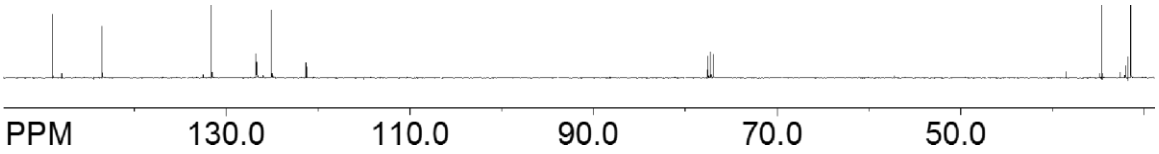

Crystal data and structure refinement:

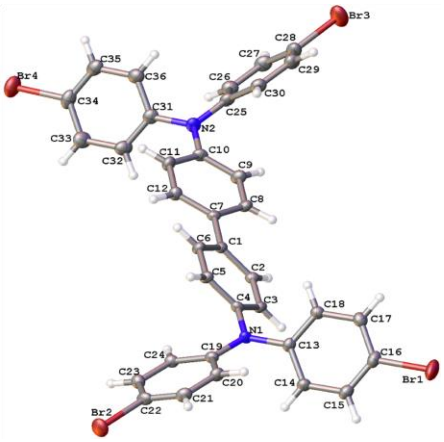

Figure1. 18. ORTEP diagram of TAB.

Table1. 4. Crystal data and structure refinement for TAB

Identification code	raj25b
Empirical formula	$C_{36}H_{24}Br_4N_2$
Formula weight	803.95
Temperature/K	100.00(10)
Crystal system	triclinic
Space group	P-1
a/Å	15.3203(2)
b/Å	15.5925(2)
c/Å	19.8315(3)
α/°	87.2838(12)
β/°	81.2554(13)
γ/°	82.7604(12)
Volume/Å^3	4643.06(12)
Z	6
ρ_{calc}g/cm^3	1.725
μ/mm^{-1}	6.559
F(000)	2363.0
Crystal size/mm^3	0.4519 × 0.2202 × 0.0592
Radiation	CuKα (λ = 1.54184)
2Θ range for data collection/°	5.72 to 148.1
Index ranges	$-19 \leq h \leq 19$, $-19 \leq k \leq 19$, $-24 \leq l \leq 21$
Reflections collected	88456
Independent reflections	18598 [R_{int} = 0.0359, R_{sigma} = 0.0223]
Data/restraints/parameters	18598/0/1135
Goodness-of-fit on F^2	1.014
Final R indexes [I>=2σ (I)]	R_1 = 0.0369, wR_2 = 0.0957
Final R indexes [all data]	R_1 = 0.0425, wR_2 = 0.1009
Largest diff. peak/hole / e Å^{-3}	2.42/-1.52

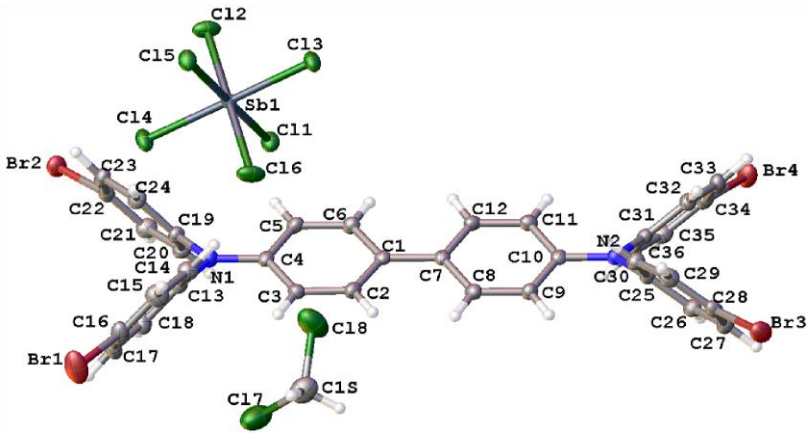

Figure1. 19. ORTEP diagram of **TAB$^{+\bullet}$.**

Table1. 5. Crystal data and structure refinement for **$TAB^{+\bullet}$**

Identification code	raj25f
Empirical formula	$C_{37}H_{26}N_2Cl_8Br_4Sb$
Formula weight	1223.59
Temperature/K	100.00(10)
Crystal system	monoclinic
Space group	$P2_1/n$
a/Å	15.37545(18)
b/Å	14.15367(14)
c/Å	19.4760(2)
α/°	90.00
β/°	91.4952(10)
γ/°	90.00
Volume/Å^3	4236.90(8)
Z	4
ρ_{calc}g/cm^3	1.918
μ/mm^{-1}	14.474
F(000)	2356.0
Crystal size/mm^3	0.2391 × 0.105 × 0.0323
Radiation	CuKα (λ = 1.54184)
2Θ range for data collection/°	7.24 to 148.2
Index ranges	$-18 \le h \le 19$, $-17 \le k \le 17$, $-19 \le l \le 23$
Reflections collected	41012
Independent reflections	8456 [R_{int} = 0.0366, R_{sigma} = 0.0238]
Data/restraints/parameters	8456/0/469
Goodness-of-fit on F^2	1.023
Final R indexes [I>=2σ (I)]	R_1 = 0.0266, wR_2 = 0.0628
Final R indexes [all data]	R_1 = 0.0310, wR_2 = 0.0659
Largest diff. peak/hole / e Å^{-3}	1.36/-1.10

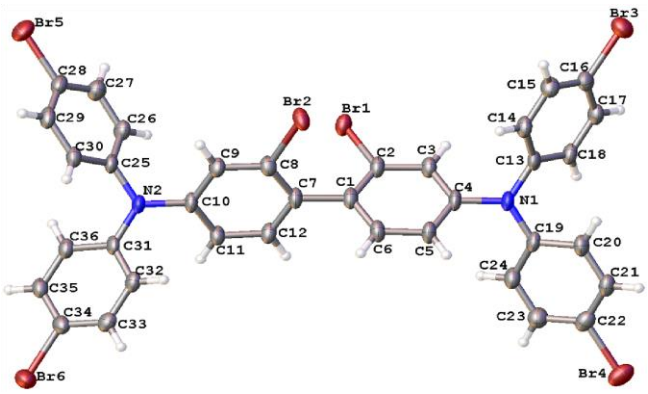

Figure1. 20. ORTEP diagram of **9**.

Table1. 6. Crystal data and structure refinement for **9**

Identification code	raj25j
Empirical formula	$C_{36}H_{22}N_2Br_6$
Formula weight	962.02
Temperature/K	100.00(10)
Crystal system	triclinic
Space group	P-1
a/Å	10.1188(2)
b/Å	13.8839(3)
c/Å	16.4081(5)
α/°	107.983(2)
β/°	106.750(2)
γ/°	96.924(2)
Volume/Å^3	2043.19(9)
Z	2
ρ_{calc}g/cm^3	1.564
μ/mm^{-1}	7.282
F(000)	924.0
Crystal size/mm^3	0.3829 × 0.1448 × 0.0709
Radiation	CuKα (λ = 1.54184)
2Θ range for data collection/°	6.04 to 147.4
Index ranges	$-12 \le h \le 12$, $-14 \le k \le 17$, $-20 \le l \le 20$
Reflections collected	38897
Independent reflections	8166 [R_{int} = 0.0378, R_{sigma} = 0.0219]
Data/restraints/parameters	8166/0/397
Goodness-of-fit on F^2	1.052
Final R indexes [I>=2σ (I)]	R_1 = 0.0334, wR_2 = 0.0931
Final R indexes [all data]	R_1 = 0.0371, wR_2 = 0.0955
Largest diff. peak/hole / e Å^{-3}	1.42/-1.10

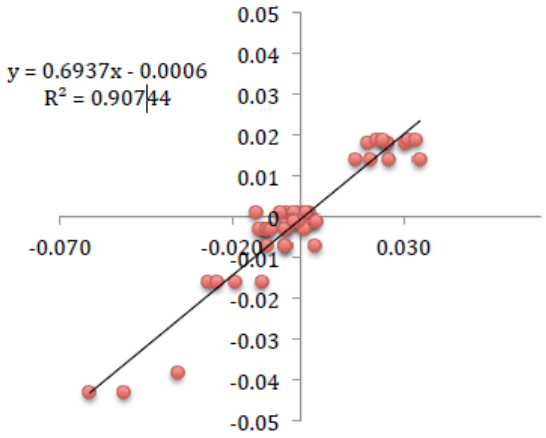

Figure1. 21. Comparison of the oxidation-induced bond length changes (in Å) in **TAB** obtained by means of X-ray crystallography (abscissa) and DFT calculations (ordinate

CHAPTER 2

Dihedral Angle-Controlled Crossover from Static Hole Delocalization to Dynamic Hopping in Biaryl Cation Radicals

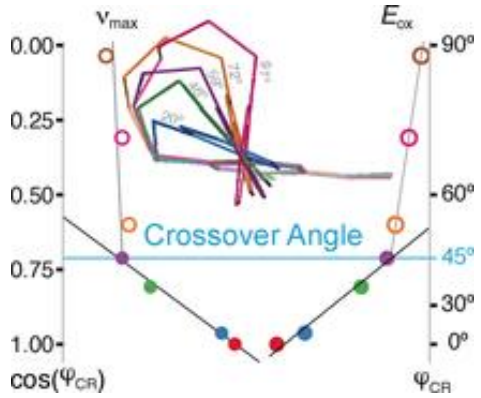

Abstract: Biaryls have been extensively used to understand fundamental properties of charge transfer in multichromophoric systems. It is known that in cases of coherent charge-transfer mechanism in biaryls, the rates follow a squared cosine trend with varying dihedral angle. Herein we demonstrate with a well-designed series of biaryl cation radicals with varying dihedral angles that the hole stabilization shows two different regimes where the mechanism of the hole stabilization switches over from (static) delocalization over both aryl rings to (dynamic) hopping between rings. The experimental data and DFT calculations unequivocally support that a crossover from delocalization to hopping occurs at a unique dihedral angle where the reorganization energy is exactly one half of the electronic coupling, i.e. $H_{ab} = \lambda/2$. The implication of this finding for non-coherent charge transfer rates is being investigated.

Disclaimer: The results discussed in this chapters were further supplemented by DFT calculations and relevant computational works by my coworkers Drs. Marat R Talipov and Maxim V. Ivanov. My contribution to this chapter is limited to synthesis of various molecules and spectroscopic studies of all molecules, with my coworkers Drs. Tushar S Navale and Ruchi Shukla.

INTRODUCTION

Biaryls represent the smallest building blocks for exploration of the fundamental properties of the charge transfer in π-conjugated molecular wires, and have thus been extensively studied. For example, the angular dependence of the charge transfer in biaryls has been probed by conductance measurements using break junction techniques.[1-4] These measurements have shown that under a coherent transport mechanism the charge-transfer rates scale as the square of the electronic coupling in biaryls, and since the electronic coupling varies with the interplanar dihedral angle (φ) between the aryl groups, the charge transfer rates are expected to follow a squared cosine trend with varying φ (from 0^{o} to ~90^{o}).[5-9] Importantly, it is noted that charge transfer using break junction techniques involves static molecules,[1,3] i.e. the residence time for the charge onto biaryls is negligible.

Unlike the break junction technique, the charge transfer in a biaryl linkage under non-coherent conditions would involve a finite residence time onto the biaryl, and would depend on the interplay between the electronic coupling and the structural reorganization. In such a charge transfer scenario, it is unclear how the interplanar dihedral angle between aryl groups controls the mechanism of charge stabilization. In order to address this question, we undertake synthesis and study of a series of biaryls where φ was varied through a polymethylene chain or *tert*-butyl groups linked at the 2 and 2' positions (**Chart 2.1**).

Chart 2. 1. The structures and naming scheme for biaryls

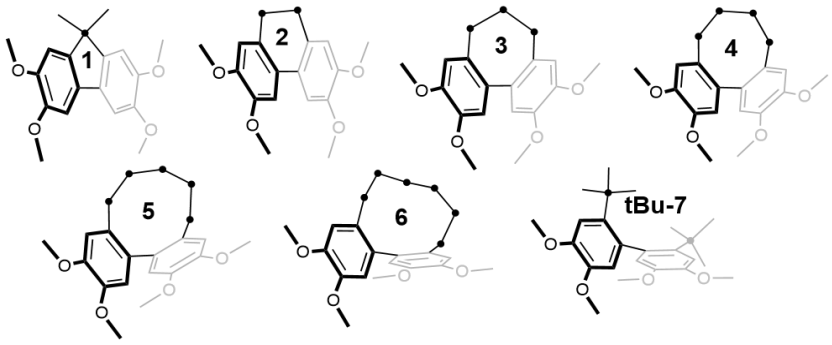

RESULTS AND DISCUSSION

Electrochemical analysis, followed by the generation of stable cation radicals of **1**-**7** and their electronic spectroscopy together with X-ray crystallography and DFT calculations allow us to demonstrate for the first time that the stabilization of cationic charge (or hole) in biaryls follow a linear cos φ trend only for small angles (φ = 0º - 45º). At larger angles (φ > 45º) the breakdown of the linear trend is observed, due to a crossover of the hole stabilization mechanism from (static) delocalization to (dynamic) hopping. We will demonstrate that the crossover occurs due to the interplay between electronic coupling, which varies with φ, and the structural/solvent reorganization. Biaryls **1**-**6** and **^{t}Bu-7** (**7**) were synthesized by adopting literature procedures,[10-12] and the experimental details including X-ray crystal structure data of **1**-**4** are compiled in the experimental section below. The X-ray structures of **1**-**4** were accurately reproduced by DFT calculations [B1LYP-40/631G(d)+ PCM(CH_2Cl_2)][13-17] (**Figure 2.1**). However, a thorough conformational search revealed multiple possible conformers for higher homologues **4**-**6** (**Tables 2.1, 2.2**). In order to establish the actual identity of the conformations of **2**-**7** in solution, we resorted to ^{1}H NMR spectroscopy.

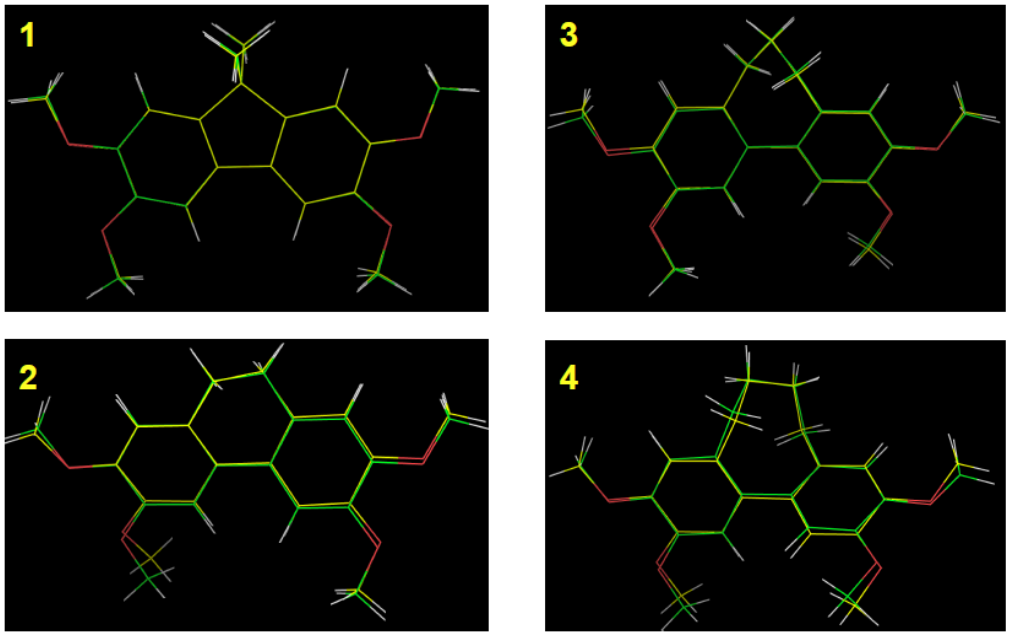

Figure 2. 1. Juxtaposition of the structures of **1-4** obtained by X-ray crystallography (green color) vs DFT calculations (yellow color).

It has been shown that ^{1}H NMR chemical shifts of aromatic protons are highly sensitive to the dihedral angle φ between aryl moieties.[18] The chemical shieldings of the 2,2'-aryl protons for all possible conformations of **1-7** were determined using a gauche-independent atomic orbital (GIAO) approach (see the experimental section for details). The linear relationship between computed chemical shieldings of 2,2'-protons of the lowest-energy conformer against the experimental chemical shifts (**Figure 2.2.A**) establishes the conformational identity of **1-7** in solution, as depicted in **Figure 2.2.B**.

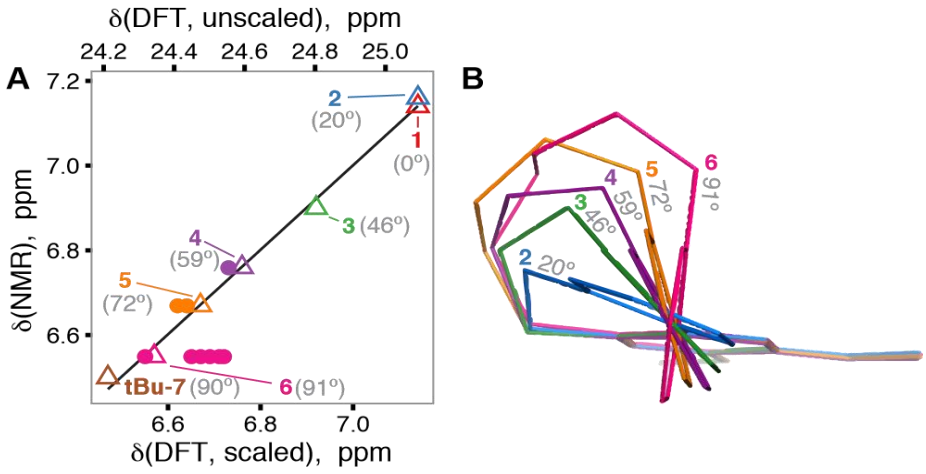

Figure 2. 2. (A) ^{1}H NMR chemical shift of 2,2'-protons of **1**-**7** plotted against the calculated/scaled (top/bottom axis) chemical shifts. The lowest energy conformers of **4**-**6** are shown by empty triangles, while higher energy conformers are depicted with filled circles. **(B)** Superposition of the structures of **2**-**6** showing the variation in dihedral angles with increasing number of methylenes. Note that the methoxy groups on one of aryl rings are omitted for clarity.

Fully reversible cyclic voltammograms in CH_2Cl_2 at 22 ºC (**Figure 2.3.A**) provided the oxidation potentials (E_{ox1}) of **1**-**7** (**Table 2.3**), which showed an increase of ~0.5 V going from a planarized biaryl (i.e. φ = 0º in **1**) to a nearly perpendicularly oriented (i.e. φ ~ 90º in **6** and **7**) biaryl. Interestingly, the E_{ox1} of biaryls with largest φ of ~90º (**6**: 0.83 V, **7**: 0.87 V) were found to be similar to the E_{ox1} of corresponding model arenes, i.e. 3,4-dimethoxytoluene (E_{ox1} = 0.87 V)[12] or 3,4-dimethoxy-1-*tert*butylbenzene (E_{ox1} = 0.90 V), respectively.[19]

Table 2. 1. Compilation of the dihedral angles around the C-C bonds in the polymethylene linker in neutral 1-7.

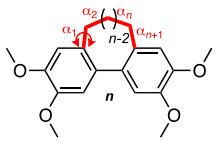

Name	Conformer #	α1	α2	α3	α4	α5	α6	α7
1	1	0	0	-	-	-	-	
2	1	36	-53	36	-	-	-	
3	1	71	-42	-42	71	-	-	
4	1	-92	83	-54	83	-92	-	-
4	2	19	65	-63	-45	87	-	-
5	1	114	-52	-58	94	-98	96	-
5	2	56	43	-120	69	-71	97	-
5	3	-48	-52	61	61	-52	-48	-
6	1	110	-57	-66	145	-66	-57	110
6	2	96	-68	87	-150	87	-68	96
6	3	127	-53	-80	57	59	-144	106
6	4	-93	84	-107	62	77	-58	-61
6	5	118	-148	84	-63	84	-148	118
6	6	58	56	-112	77	-112	56	58
6	7	-120	32	74	-68	85	-146	48
6	8	12	-79	-15	65	57	-54	-57

Table 2. 2. Compilation of the computed properties of neutral **1-7** and their cation radicals.

Name	Conformer #	ΔE(N), kcal/mol	ΔE(CR), kcal/mol	φ, º	φ_{CR}, º	λ_{max}(CR), nm	f_{osc}(CR)	ΔG_{ox}, eV	Class
1	1	0.0	0.0	0	0	909	0.232	4.813	III
2	1	0.0	0.0	20	16	972	0.242	4.899	III
3	1	0.0	0.0	46	36	1366	0.195	5.062	III
4	1	0.0	0.0	59	45	1696	0.171	5.175	III
4	2	4.1	3.3	77	43	1457	0.176	-	II-III
5	1	0.1	0.0	72	53	1521	0.117	5.234	II
5	2	1.6	2.6	86	85	1341	0.000	-	I
5	3	3.9	4.3	84	73	1415	0.029	-	I-II
6	1	0.0	0.0	91	106	1417	0.047	5.307	I-II
6	2	2.7	1.1	105	117	1550	0.121	-	II
6	3	2.9	0.0	66	48	1622	0.179	-	II-III
6	4	4.1	3.7	101	110	1492	0.060	-	II
6	5	5.2	1.8	55	44	1518	0.192	-	III
6	6	6.7	6.4	105	111	1452	0.045	-	I-II
6	7	10.4	7.4	53	43	1568	0.174	-	II-III
6	8	13.8	13.4	81	79	1310	0.005	-	I
tBu-7	-	0.0	0.0	91	88	1321	0.000	5.351	I

Table 2. 3. Redox and optical properties of biaryls **1-7** in CH_2Cl_2.

Name	E_{ox1}, V[a]	E_{ox2}, V[a]	λ_{max}(CR), nm	ε_{max}(CR), $M^{-1}cm^{-1}$
1	0.40	0.87	1098	11 100
2	0.49	0.85	1153	8 200
3	0.67	1.06	1580	7 700
4	0.76	1.07	1850	4 000
5	0.78	1.03	1777	1 600
6	0.83	1.06	1850	1 200
7	0.87	1.13	2050	900

The high electrochemical reversibility of **1-7** allowed the generation of their cation radicals via quantitative redox titrations using well-characterized aromatic

oxidants, i.e. **THE**$^{+\bullet}$$SbCl_6^-$ (**THE** = 1,2,3,4,5,6,7,8-octahydro-9,10-dimethoxy-1,4,5,8-dimethanoanthracene, E_{red1} = 0.67 V, λ_{max} = 518 nm, ε_{max} = 7300 cm^{-1} M^{-1})[20] and **NAP**$^{+\bullet}$$SbCl_6^-$ (**NAP** = 1,2,3,4,7,8,9,10-octahydro-1,1,4,4,7,7,10,10-octamethylnaphtacene, E_{red} = 0.94 V vs Fc/Fc^+, λ_{max} = 672 nm, ε_{max} = 9300 cm^{-1} M^{-1}).[21,22] The redox titrations were performed by an incremental addition of the neutral biaryl to a solution of **THE**$^{+\bullet}$ (or **NAP**$^{+\bullet}$) in CH_2Cl_2 at 22 ºC under argon atmosphere, and the resulting absorption spectra were quantitatively analyzed (see **Generation of cation radicals of 1-7** in Experimental section) to obtain reproducible absorption spectra of **1**$^{+\bullet}$-**7**$^{+\bullet}$ (**Figure 2.3.B**). The spectra of **1**$^{+\bullet}$-**4**$^{+\bullet}$ showed a red shift of the characteristic near-IR band from 1098 to 1850 nm, while **5**$^{+\bullet}$-**7**$^{+\bullet}$ showed little variance in the position of the low-energy band, but rather a dramatically reduced molar absorptivity for the near infrared band decreasing from **4**$^{+\bullet}$ to **7**$^{+\bullet}$ (**Figure 2.3.B**).

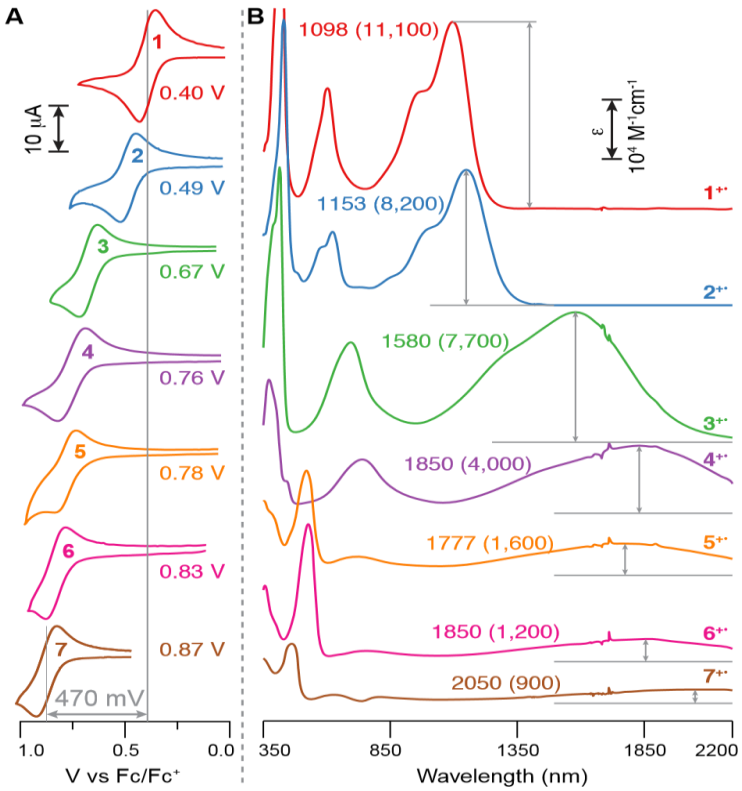

Figure 2. 3. (A) Cyclic voltammograms (CVs) of 2 mM **1-7** in CH_2Cl_2 (0.1 M *n*-Bu_4NPF_6) at a scan rate of 200 mV s^{-1} and 22 ºC. The value of E_{ox1} is indicated in each CV. **(B)** Compilation of the absorption spectra of $\mathbf{1}^{+\bullet}$-$\mathbf{7}^{+\bullet}$ in CH_2Cl_2 at 22 ºC. The position of lowest-energy band (in nm) and molar absorptivity (in parenthesis, in $M^{-1}cm^{-1}$) are shown on each spectrum.

The X-ray crystallographic analysis of representative cation-radical salts ($\mathbf{1}^{+\bullet}SbCl_6^-$ and $\mathbf{3}^{+\bullet}SbCl_6^-$) shows considerable oxidation-induced bond length changes in the biaryl moieties, especially in the central aryl-aryl C–C bond (contracted by 0.036 Å and 0.022 Å, respectively), see the Experimental section for detailed analysis of the X-ray structures and ORTEP diagrams. It is noted that dihedral angle between aryl moieties in $\mathbf{3}^{+\bullet}$ (φ_{CR} = 36º) showed an oxidation-induced decrease of ~10º. Unfortunately, repeated

attempts to obtain the X-ray quality single crystals of other biaryl cation radicals have thus far been unsuccessful.

Our DFT calculations [B1LYP-40/6-31G(d)+PCM(CH_2Cl_2)] accurately reproduced the available X-ray structures and dihedral angles for neutral (i.e. φ) and cation radical (i.e. φ_{CR}) of biaryls (**Tables 2.4, 2.5** and **Figures 2.4, 2.5**). The (TD-)DFT calculations of the structures of neutrals and cation radicals of **1**-**7** reproduced the experimental E_{ox1} values and the excitation energies for the lowest-energy transition in $\mathbf{1}^{+\bullet}$-$\mathbf{7}^{+\bullet}$ (**Figure 2.6**). The calculated dihedral angles between the aryl moieties in biaryl cation radicals show an oxidation-induced decrease of 4º-19º (**Table 2.2**), and the most pronounced changes in the dihedral angle were observed with $\mathbf{4}^{+\bullet}$- $\mathbf{6}^{+\bullet}$ owing to the flexibility of the polymethylene linker (**Figure 2.2**).

A comparison of the structures of neutral **1**-**7** and their cation radicals shows that the central arylaryl C–C bond in $\mathbf{1}^{+\bullet}$-$\mathbf{7}^{+\bullet}$ experiences the most notable shortening and variation with the dihedral angle φ_{CR} (i.e. $\mathbf{2}^{+\bullet}$: 16º, $\mathbf{3}^{+\bullet}$: 36º, $\mathbf{4}^{+\bullet}$: 45º, $\mathbf{5}^{+\bullet}$: 53º, $\mathbf{6}^{+\bullet}$: 74º, $\mathbf{7}^{+\bullet}$: 88º) as depicted in **Figure 2.7**.

Table 2. 4. The experimental (X-ray) and calculated [B1LYP-40/6 31G(d)+PCM(CH_2Cl_2)] bond lengths of the neutral and cation radicals of **1** (in Å).

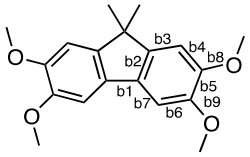

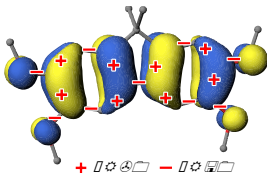

	X-ray crystallography			DFT calculations		
bond[a]	**1**	**1**$^{+\bullet}$	Δ	**1**	**1**$^{+\bullet}$	Δ
b1	1.464	1.428	**-0.036**	1.465	1.423	**-0.042**
b2	1.394	1.411	**0.017**	1.391	1.419	**0.028**
b3	1.395	1.367	**-0.028**	1.39	1.376	**-0.014**
b4	1.392	1.399	**0.007**	1.39	1.399	**0.009**
b5	1.416	1.440	**0.024**	1.415	1.445	**0.030**
b6	1.385	1.373	**-0.012**	1.387	1.374	**-0.013**
b7	1.399	1.404	**0.005**	1.396	1.404	**0.008**
b8	1.366	1.334	**-0.032**	1.358	1.322	**-0.036**
b9	1.371	1.336	**-0.035**	1.358	1.334	**-0.024**

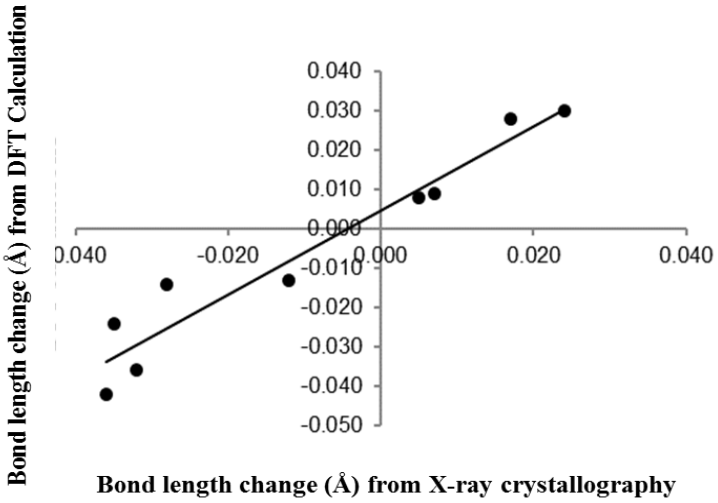

Figure 2. 4. Comparison of the oxidation-induced bond length changes (in Å) of $1/1^{+\bullet}$, obtained by X-ray crystallography and DFT calculations.

Table 2. 5. The experimental (X-ray) and calculated [B1LYP-40/6-31G(d)+PCM(CH_2Cl_2)] bond lengths of the neutral and cation radicals of **3** (in Å).

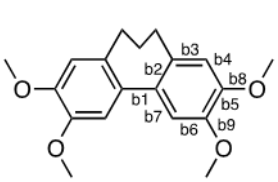

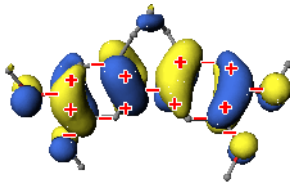

	X-ray crystallography			DFT calculations		
bond[a]	**3**	**3**$^{+\bullet}$	Δ	**3**	**3**$^{+\bullet}$	Δ
b1	1.478	1.456	**-0.022**	1.485	1.446	**-0.039**
b2	1.404	1.434	**0.030**	1.398	1.43	**0.032**
b3	1.403	1.378	**-0.025**	1.399	1.383	**-0.016**
b4	1.389	1.395	**0.006**	1.386	1.396	**0.010**
b5	1.410	1.429	**0.019**	1.409	1.433	**0.024**
b6	1.391	1.374	**-0.017**	1.384	1.373	**-0.011**
b7	1.406	1.416	**0.010**	1.403	1.413	**0.010**
b8	1.368	1.333	**-0.035**	1.357	1.322	**-0.035**
b9	1.363	1.349	**-0.014**	1.358	1.335	**-0.023**

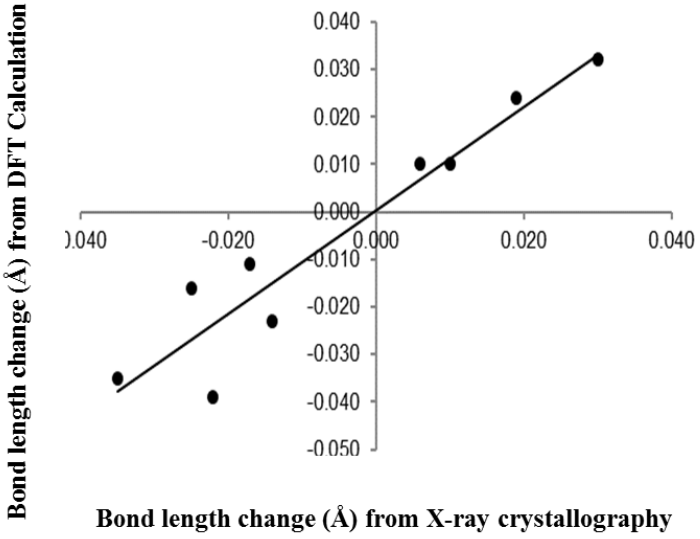

Figure 2. 5. Comparison of the oxidation-induced bond length changes (in Å) of **3**/**3**$^{+\bullet}$, obtained by X-ray crystallography and DFT calculations.

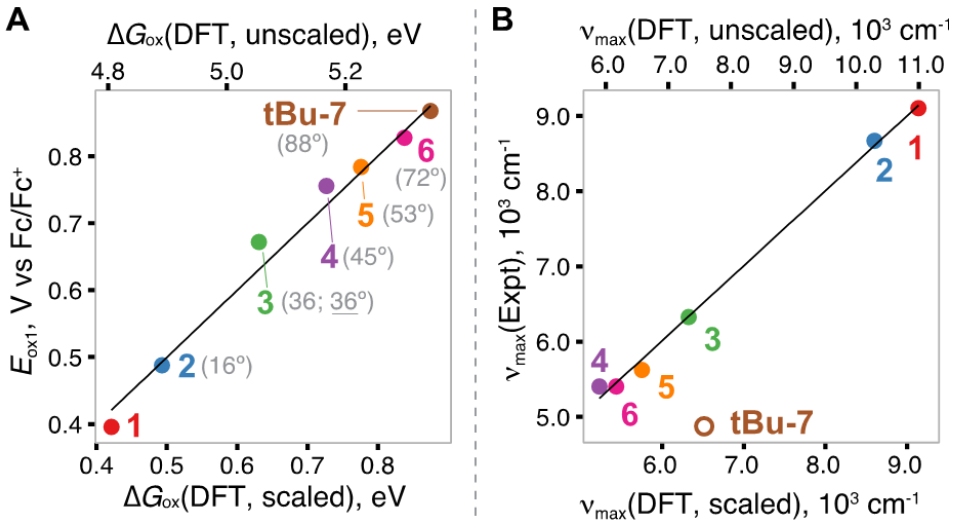

Figure 2. 6. Comparison of the experimental oxidation potentials of **1**-**7** (A) and lowest-energy absorption maxima of **1**$^{+\bullet}$-**7**$^{+\bullet}$ (B) with the corresponding calculated values [(TD-)B1LYP-40/6-31G(d)+PCM (CH_2Cl_2)] (top axes). The bottom axes show scaled values, obtained from the linear correlations shown in the corresponding panels. Note that the data point excitation energy for **tBu-7**$^{+\bullet}$ was not used in linear correlation in Panel B, because small intensity of the intervalence band in the spectrum of **tBu-7**$^{+\bullet}$ prevented accurate determination of its position. The experimental observation of relatively red-shifted and weak transition for **tBu-7**$^{+\bullet}$ likely originates from the non-equilibrium conformations of **tBu-7**$^{+\bullet}$ with lower dihedral angle, i.e. $\varphi_{CR} < 90°$.

Most importantly, **Figure 2.7** shows that the biaryls with dihedral angles $\varphi_{CR} = 0°– 45°$ (*i.e.* **1**$^{+\bullet}$-**4**$^{+\bullet}$) exhibit (almost) identical oxidation-induced central C–C bond contraction (0.04 ± 0.002 Å) and a complete delocalization of the hole over both aryl moieties (**Figure 2.7**). In contrast, biaryls with a larger dihedral angle $\varphi_{CR} > 45°$ show a systematic decrease in the C–C bond shortening with increasing φ_{CR}, i.e. 0.028 Å in **5**$^{+\bullet}$, 0.014 Å in **6**$^{+\bullet}$, and 0.004 Å in **7**$^{+\bullet}$ and a concomitant increase in the localization of the spin/charge on a single aryl moiety (**Figure 2.7**). This surprising observation of two different regimes based on dihedral angle,

i.e. complete vs partial charge delocalization on two aryl moieties in biaryl cation radicals, suggests that a change occurs in the mechanism of charge delocalization/stabilization.

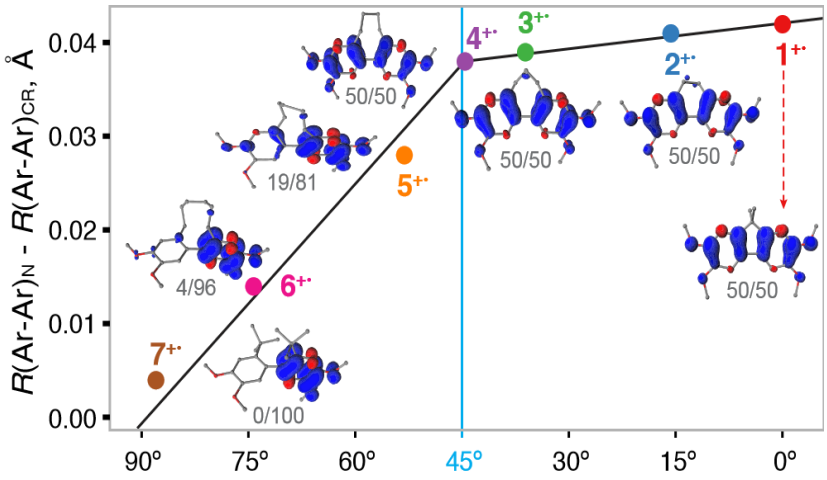

Figure 2. 7. Changes in the oxidation-induced central aryl-aryl C–C bonds in various biaryls cation radicals against φ_{CR} and the corresponding isovalue plots of spin/charge distribution. The fraction of spin/charge distribution per aryl moiety, obtained by the natural population analysis,[23,24] is indicated below the structures. A vertical line at 45º separates biaryls with completely delocalized (**1**$^{+\bullet}$- **4**$^{+\bullet}$) vs partially /fully localized charge (**5**$^{+\bullet}$-**7**$^{+\bullet}$).

Supporting this view, plots of experimental oxidation potentials E_{ox1} and excitation energies ν_{max} of **1**$^{+\bullet}$-**7**$^{+\bullet}$, shown in **Figure 2.8**, also reveal two different trends in the range of 0º–45º and 45º–90º, where the biaryl with φ_{CR} ~ 45º represents a crossover point (see **Figure 2.8**). Excitation energies for the $D_0 \rightarrow D_1$ transition in biaryls **1**$^{+\bullet}$-**4**$^{+\bullet}$ in the '0º–45º regime' show a linear red shift against cos(φ_{CR}), and the nature of this electronic transition is consistent with completely delocalized ground and excited states (**Figure 2.9**). The position of the $D_0 \rightarrow D_1$ transition in **5**$^{+\bullet}$-**7**$^{+\bullet}$ in the '45º–90º regime' remains largely unchanged except reduced molar absorptivity with increasing φ_{CR}, and

the corresponding electronic transition was shown to have a charge transfer character (**Figure 2.9**). Note that the cation radical **^{t}Bu-7**$^{+\bullet}$ with $\varphi_{CR} \approx 90^o$ shows that the charge is fully localized onto one unit with extremely weak $D_0 \rightarrow D_1$ transition of charge transfer character (**Figure 2.9**). The observed angular dependence of redox and optical properties of **1**$^{+\bullet}$-**7**$^{+\bullet}$ in **Figure 2.8** and the nature of the $D_0 \rightarrow D_1$ transitions clearly suggests that there is crossover from delocalization to hopping mechanism that depends on dihedral angle.

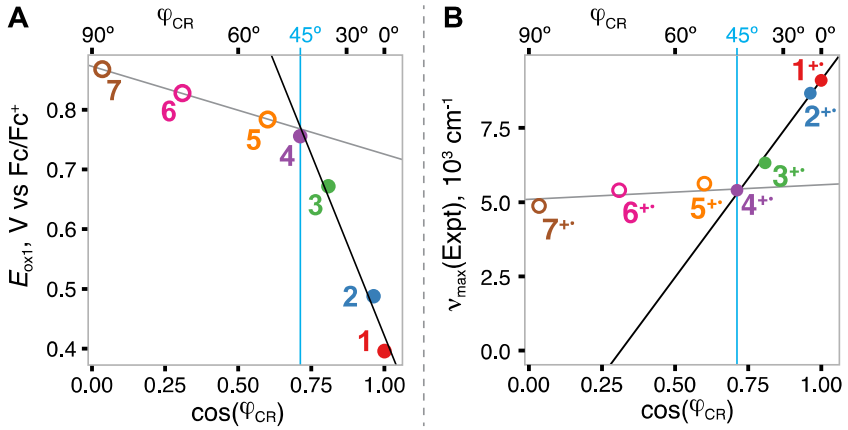

Figure 2. 8. Plots of E_{ox1} of **1**-**7** against cos(φ_{CR}) (A) and ν_{max} of **1**$^{+\bullet}$-**7**$^{+\bullet}$ against cos(φ_{CR}) (B). A vertical line at 45º separates biaryls with different linear trends, i.e. **1**$^{+\bullet}$-**4**$^{+\bullet}$ (filled circles) vs **5**$^{+\bullet}$-**7**$^{+\bullet}$ (empty circles).

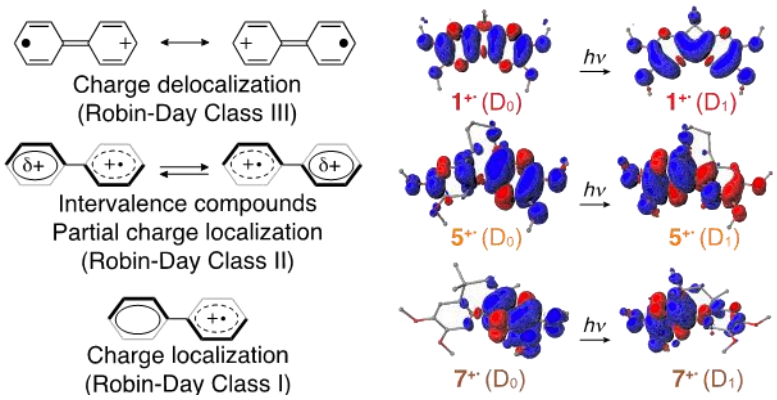

Figure 2. 9. Typical examples of complete delocalization to partial or full localization and nature of the accompanying electronic transition.

Because the biaryls **1**-**7** do not probe the entire continuum of dihedral angles, we carried out a systematic computational scan on a model biaryl cation radical (**Figure 2.10**), where a series of constrained optimizations with fixed φ_{CR} and subsequent TD-DFT calculations allowed us to construct a plot of the excitation energies (ν_{max}) with the evolution of dihedral angle φ, **Figure 2.10**.[25]

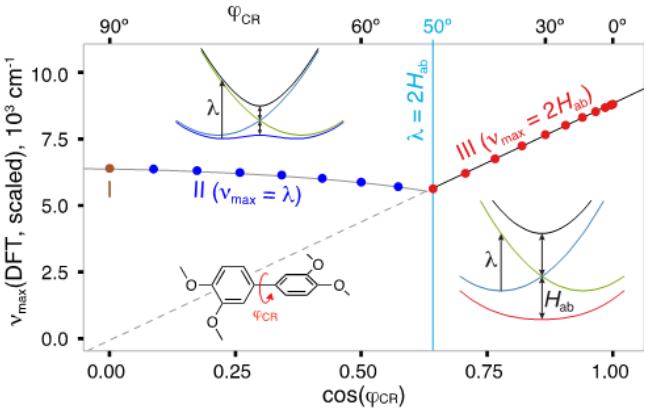

Figure 2. 10. A plot of ν_{max} against cos(φ_{CR}), obtained from the scan on a model biaryl (structure shown) with the φ_{CR} step size of 5º [TD-B1LYP-40/6-31G(d)+PCM(CH_2Cl_2)]. The ν_{max} were scaled according to linear trend with experiment (**Figure 2.6**). The two distinct regions, separated by a blue line, are identified using Marcus two-state model where H_{ab} is the electronic coupling between (charge-localized) diabatic states and λ is the structural/solvent reorganization parameter.[17,26]

As the electronic coupling H_{ab} scales linearly with cos(φ_{CR}),[27,28] the computed ν_{max} in the model biaryl also follow a linear dependence with cos(φ_{CR}) in 0º–50º range (**Figure 2.10**, red symbols) in accordance with Marcus two-state model for fully delocalized systems (**Figure 2.10**, bottom right). In contrast, the crossover from the linear ν_{max}/cos(φ_{CR}) trend in model biaryl with φ > 50º is surprising considering that the electronic coupling H_{ab} continues to decrease linearly with cos(φ_{CR}). The invariance of ν_{max} with the increasing φ_{CR} (**Figure 2.10**, blue symbols) signifies, based on the Marcus model (**Figure 2.10**, top left), that the charge transfer occurs by the hole hopping and thereby ν_{max} directly provides the value of reorganization energy, i.e. $\nu_{max} = \lambda$.[26] Thus, the interplay between the invariant λ and decreasing H_{ab} in model biaryl with φ > 50º represents the cases where $2H_{ab} < \lambda$, i.e. hole distribution switches over from complete delocalization over both aryl units (i.e. $2H_{ab} \geq \lambda$) to partial and then full hole localization

onto a single aryl unit. The crossover point in such a system is thus expected to occur when $2H_{ab} = \lambda$ (**Figure 2.8 B**). Interestingly, the crossover point of 50º obtained by computational scan of a model biaryl is similar to the experimental crossover point of ~ 45º observed for biaryls **1-7** (compare Figures **2.8.B** and **2.10**).

CONCLUSION

In summary, we have demonstrated for the first time using a well-defined series of biaryl cation radicals with varied interplanar dihedral angles that a crossover occurs from a fully delocalized regime to a mixed-valence regime due to the interplay between the electronic coupling and reorganization energy. The observation of a crossover point between two regimes is expected because it represents a unique point where the reorganization energy is exactly one half of the electronic coupling, i.e. $H_{ab} = \lambda /2$. Thus, the linear dependence of charge transfer rates against $\cos^2\varphi$ trend[29] over the entire range of dihedral angles under a coherent tunneling mechanism should be contrasted with non-coherent mechanism, where the hole stabilization mechanism changes from (static) delocalization to (dynamic) hopping at a unique dihedral angle. Note that such crossover dihedral angle must satisfy the condition of $H_{ab} = \lambda /2$, and therefore the crossover angles will be different for different molecules owing to the varied reorganization energies and electronic couplings. The studies of non-coherent charge-transfer rates will be undertaken using donor-biaryl-acceptor triads with varied dihedral angles in order to demonstrate the implication of the crossover of the hole stabilization mechanism from delocalization to hopping.

GENERAL EXPERIMENTAL METHODS

Biaryls **1**-**6** and **^{t}Bu-7** (**7**) were synthesized using literature procedures and were characterized by NMR spectroscopy, mass spectrometry, and X-ray crystallography. The reversible cyclic and square-wave voltammograms of **1-7** and the corresponding model compounds were recorded by the electrochemical oxidation at a platinum electrode in CH_2Cl_2 containing 0.1 M *n*-Bu_4NPF_6 at 22 ºC at scan rate of 200 mV s^{-1} and were referenced to ferrocene as an added internal standard. The $\mathbf{1}^{+\bullet}$-$\mathbf{7}^{+\bullet}$ cation radicals compounds were quantitatively generated via the redox titrations with robust aromatic oxidants $\mathbf{THE}^{+\bullet}$ $SbCl_6^-$ and $\mathbf{NAP}^{+\bullet}SbCl_6^-$.

Materials. All reactions were performed under argon atmosphere unless otherwise stated. Veratrole, 3,4-dimethoxybenzaldehyde, 3,4-dimethoxyacetophenone, adipoyl chloride, sodium iodide, triethylamine, chlorotrimethylsilane, iodine, red mercuric oxide, anhydrous ferric chloride, anhydrous aluminium chloride, mercuric chloride, 10% Pd/C, Zn dust, mossy zinc metal, $TiCl_4$, Ag_2O, *tetrakis*(triphenylphosphine)-nickel(0), analytical grade acetone, and anhydrous acetonitrile were commercially available and were used without further purification. Anhydrous tetrahydrofuran (THF) was prepared by refluxing commercial tetrahydrofuran over lithium aluminum hydride under an argon atmosphere for 24 hours followed by distillation under an argon atmosphere. It was stored in a Schlenk flask equipped with a Teflon valve fitted with Viton O-rings. Dichloromethane was repeatedly stirred with fresh aliquots of conc. sulfuric acid (~10 % by volume) until the acid layer remained colorless. After separation, it was washed successively with water, aqueous sodium bicarbonate, water, and aqueous sodium chloride, and dried over anhydrous calcium

chloride. The dichloromethane was distilled twice from P_2O_5 under an argon atmosphere and stored in a Schlenk flask equipped with a Teflon valve fitted with Viton O-rings. The hexanes and toluene were distilled from P_2O_5 under an argon atmosphere and then refluxed over calcium hydride (~12 h). After distillation from CaH_2, the solvents were stored in Schlenk flasks under an argon atmosphere. NMR spectra were recorded on 300 and 400 MHz NMR spectrometers.

Preparation of 2,3,6,7-tetramethoxy-9,9-dimethylfluorene (1)

Scheme 2. 1: Synthetic scheme for 2,3,6,7-tetramethoxy-9,9-dimethylfluorene (1)

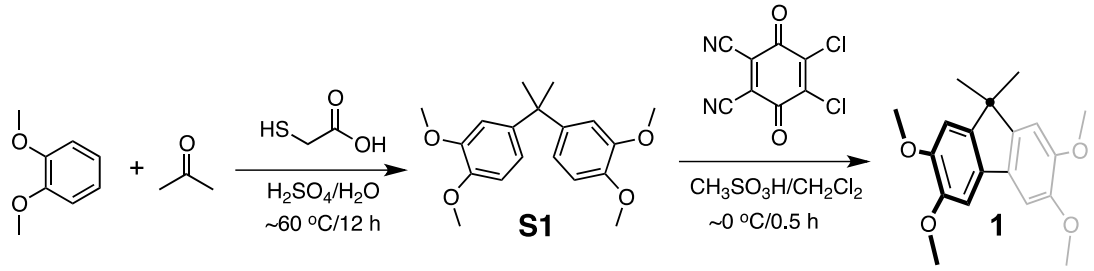

2,2-Bis(3,4-dimethoxyphenyl)propane (S1). 1,2-Dimethoxybenzene (9.5 mL), acetone (2.0 mL), and mercaptoacetic acid (0.4 mL) were added to a solution of conc. H_2SO_4 (*d* 1.84, 8.0 mL) and water (8.0 mL). Theresulting mixture was stirred overnight (~12 h) at ~60 °C, cooled to room temperature and poured in ice water (200 mL) and extracted with CH_2Cl_2 (3 x 50 mL). The combined organic extracts were dried over anhydrous $MgSO_4$, filtered and evaporated. The crude solid was crystallized from methanol to afford 2,2-*bis*(3,4-dimethoxyphenyl)propane (**S1**) as a colorless crystalline solid. Yield: 3.1 g, 72%, mp 91-92 °C; ^{1}H NMR ($CDCl_3$) δ ppm 1.65 (s, 6H), 3.77 (s,

6H), 3.86 (s, 6H), 6.69 (d, 2H, *J* = 2 Hz), 6.76-6.84 (m, 4H); ^{13}C NMR ($CDCl_3$) δ ppm 31.2, 42.4, 55.8, 55.9, 110.4, 110.8, 118.5, 143.5, 147.0, 148.4.

2,3,6,7-tetramethoxy-9,9-dimethylfluorene (1). Under argon atmosphere, CH_3SO_3H (1 mL) was added to a solution of 2,2-bis(3,4-dimethoxyphenyl)propane (316 mg, 1.0 mmol) in dichloromethane (9 mL) at ~0 ^{o}C. To this mixture, solide DDQ (227 mg, 1.0 mmol) was added and the resulting mixture was stirred under an argon atmosphere for 30 min. The reaction mixture was poured into a saturated aqueous $NaHCO_3$ solution (25 mL), the organic layer was separated, and the aqueous layer was extracted with CH_2Cl_2 (2 x 10 mL). The combined organic layer was washed with aqueous sodium carbonate solution, dried over anhydrous MgSO4, filtered and evaporated. Crystallization from a mixture of CH_2Cl_2/CH_3OH afforded **1** as a white crystalline solid, yield: 312 mg, 99 %; mp 178-180 ^{o}C; ^{1}H NMR ($CDCl_3$) δ ppm 1.65 (s, 6H), 3.77 (s, 6H), 3.86 (s, 6H), 6.69 (d, 2H, *J* = 2 Hz), 6.76-6.84 (m, 4H); ^{13}C NMR ($CDCl_3$) δ ppm 27.4, 46.7, 56.2, 56.3, 102.5, 106.1, 131.8, 146.1, 148.2, 148.7.

Preparation of 2,3,6,7-tetramethoxy-9,10-dihydrophenanthrene (2).

Scheme 2. 2: Synthetic scheme for 2,3,6,7-tetramethoxy-9,10-dihydrophenanthrene (2)

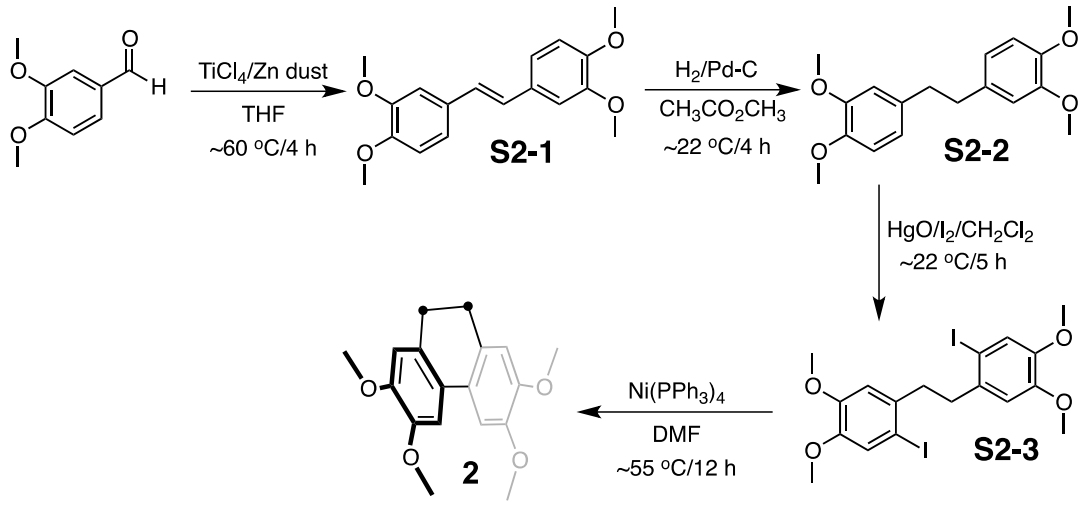

3,3',4,4'-Tetramethoxystilbene (S2-1). To chilled (~10 ºC) anhydrous tetrahydrofuran (240 mL) containing Zn dust (10 g, 154 mmol) was added $TiCl_4$ (8.2 mL, 74 mmol) dropwise with the aid of a dropping funnel under an argon atmosphere. The resulting mixture was warmed to room temperature. The black suspension thus obtained was refluxed for two hours. A solution of 3,4-dimethoxybenzaldehyde (6.7 g, 40 mmol) in anhydrous tetrahydrofuran (50 mL) was then added drop wise to this black reaction mixture during a course of 4 h while refluxing. The resulting mixture was cooled to room temperature and quenched with 10% aqueous Na_2CO_3 (300 mL). The organic layer was separated and the aqueous suspension was extracted with dichloromethane (3 x 50 mL) followed by diethyl ether (3 x 50 mL). The combined organic layers were dried over anhydrous $MgSO_4$ and filtered. Evaporation of the solvent in vacuo afforded 3,4,3',4'-tetramethoxystilbene **S2-1** in excellent yield as a pale yellow solid. Yield: 5.9 g, 98%; mp

152-153 °C (lit [1] mp 152-154 °C); ^{1}H NMR ($CDCl_3$) δppm 3.88 (s, 6H), 3.93 (s, 6H), 6.84 (d, *J* = 8 Hz, 2H), 6.91 (s, 2H), 7.01-7.05 (m, 4H); ^{13}C NMR ($CDCl_3$) δ ppm 75.832, 75.838, 79.2, 79.4, 80.0, 80.4, 80.7, 81.93, 81.96.

3,3',4,4'-Tetramethoxybibenzyl (S2-2). A yellow solution of **S2-1** (4.5 g, 15 mmol) and 10% Pd/C (0.2 g) in ethyl acetate (180 mL) was hydrogenated in a Parr apparatus (45 psi) at room temperature for 4 h. After which time, the reaction mixture was filtered through a short pad of silica gel. Evaporation of the solvent in vacuo afforded 3,3',4,4'-tetramethoxybibenzyl **S2-2** as a white solid. Yield: 4.4 g, 97%; mp 109-110 °C (lit[2] mp 109-110 °C); ^{1}H NMR ($CDCl_3$) δ ppm 2.82 (s, 4H), 3.81 (s, 6H), 3.83 (s, 6H),6.64 (d, 2H, *J* = 1.7 Hz), 6.68 (dd, 2H, *J* = 8, 1.7 Hz), 6.76 (d, 2H, *J* = 1.7 Hz); ^{13}C NMR ($CDCl_3$) δ ppm 37.7, 55.8, 55.9, 111.1, 111.8, 120.3, 134.4, 147.2, 148.6.

3,3',4,4'-Tetramethoxy-6,6'-diiodobibenzyl (S2-3). To a solution of **S2-2** (4.2 g, 14 mmol) in dichloromethane (30 mL) was added in small portions, a mixture of iodine (7.1 g, 28 mmol) and red mercuric oxide (6.1 g, 28 mmol), and the reaction mixture was allowed to stir at room temperature for 5 h. After which time, the solid was removed by filtration through a short pad of silica gel. The filtrate was washed with 5% aqueous sodium thiosulphate solution (3 x 100 mL) and then brine (1 x 50 mL). The organic layer was dried over anhydrous $MgSO_4$ and filtered. Evaporation of the solvent in vacuo afforded 3,3',4,4'-tetramethoxy-6,6'-diiodobibenzyl **S2-3** as a white solid. Yield: 7.0 g, 90%; mp 152-153 °C (lit [2] mp 152-153 °C); ^{1}H NMR ($CDCl_3$) δ ppm 2.90 (s, 4H), 3.78 (s, 6H), 3.84 (s, 6H), 6.64 (s, 2H), 7.21 (s, 2H); ^{13}C NMR ($CDCl_3$) δ ppm 41.1, 56.0, 56.3, 88.3, 112.7, 121.6, 136.1, 148.0, 149.3.

2,3,6,7-Tetramethoxy-9,10-dihydrophenanthrene (2). Following a literature procedure,[3] a solution of **3** (0.28 g, 0.5 mmol) in DMF (52 mL) was thoroughly degassed and *tetrakis*(triphenylphosphine)nickel(0) (0.83 g, 0.75 mmol) was added. The reaction mixture was then stirred at 25 °C for 20 min and at 55 °C for 12 h, during which time the color of the reaction mixture changed from dark red to yellow. The resulting mixture was cooled to room temperature and quenched with 5% hydrochloric acid (50 mL). The organic layer was repeatedly washed with water (3 x 100 mL) and the aqueous suspension extracted with dichloromethane (5 x 20 mL). The combined organic extract were dried over anhydrous $MgSO_4$ and filtered. After removal of the solvent, the residue was purified by column chromatography using a 1:4 mixture of ethylacetate/hexanes as eluent to afford pure **4** as white solid. Yield: 0.1 g, 67%; mp 174-175 °C (lit[2] mp 174-175.5 °C); ^{1}H NMR ($CDCl_3$) δ ppm 2.78 (s, 4H), 3.90 (s, 6H), 3.96 (s, 6H), 6.75 (s, 2H), 7.14 (s, 2H); ^{13}C NMR ($CDCl_3$) δ ppm 28.8, 55.8, 56.3, 106.9, 111.4, 126.9, 129.3, 147.9.

Preparation of 3.

Scheme 2. 3: Synthetic scheme for 3

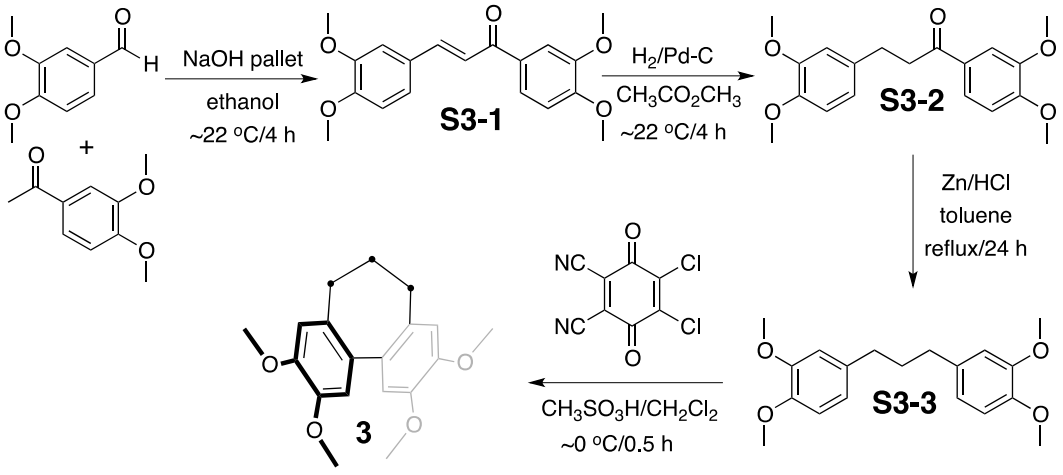

1,3-Bis(3,4-dimethoxyphenyl)-2-propen-1-one (S3-1). To a stirred solution of 3,4-dimethoxyacetophenone (15.5 g, 86 mmol) and 3,4-dimethoxybenzaldehyde (14.3 g, 86 mmol) in ethanol (100 mL) was added 2 pellets of solid NaOH and the resulting mixture was stirred at 22 ^{o}C for 4 h. The resulting yellow solid was isolated by filtering in vacuo and washed with cold water (until the washings were neutral to litmus and then with ice-cold ethanol (2 x 20 mL). Recrystallization of the crude product from ethanol afforded pure **S3-1** as yellow solid. Yield: 28.0 g, 99%; mp 105-106 °C, ^{1}H NMR ($CDCl_3$) δ ppm 3.91 (s, 3H), 3.93 (s, 3H), 3.94 (s, 3H), 3.95 (s, 3H), 6.86-6.92 (m, 2H), 7.14 (s, 1H), 7.21 (dd, 1H, *J* = 8, 2 Hz), 7.40 (d, 1H, *J* = 16 Hz), 7.60 (s, 1H), 7.66 (dd, 1H, *J* = 8, 2 Hz), 7.74 (d, 1H, *J* = 16 Hz); ^{13}C NMR ($CDCl_3$) δ ppm 55.9, 56.05, 56.08, 109.9, 110.2, 110.8, 111.1, 119.5, 122.9, 128.0, 131.5, 144.1, 149.2, 151.2, 153.1, 188.6.

1,3-Bis(3,4-dimethoxyphenyl)-propane-1-one (S3-2). A yellow solution of **S3-1** (6.6 g, 20 mmol) and 10% Pd/C (0.1 g) in ethyl acetate (80 mL) was hydrogenated in a Parr apparatus (45 psi) at 22 ^{o}C for 4 h. Workup as above afforded pure **S3-2** as a white solid. Yield: 5.6 g, 85%; mp 80-81 °C; ^{1}H NMR ($CDCl_3$) δ ppm 3.00 (t, 2H, *J* = 8 Hz), 3.24 (t, 2H, *J* = 8 Hz), 3.85 (s, 3H), 3.86 (s, 3H), 3.92 (s, 3H), 3.94 (s, 3H), 6.77-6.79 (m, 3H), 6.87 (d, 1H, *J* = 8 Hz), 7.52 (s, 1H), 7.57 (dd, 1H, *J* = 8, 2 Hz); ^{13}C NMR ($CDCl_3$) δ ppm 30.3, 40.4, 56.01, 56.09, 56.1, 56.2, 110.1, 110.2, 111.4, 112.0, 120.3, 122.8, 130.3, 134.2, 147.5, 149.0, 149.1, 153.4, 198.1.

1,3-Bis(3,4-dimethoxyphenyl)propane (S3-3). A standard Clemmensen reduction of **S3-2** was performed. Amalgamated zinc (5.2 g) was prepared by stirring for 5 min a mixture of mossy zinc (5.2 g), mercuric chloride (0.52 g), water (10 ml), and

conc. hydrochloric acid (0.5 mL). The solution was then decanted and to the resulting amalgamated Zn was added water (4 ml), conc. hydrochloric acid (9 ml), toluene **(**10 mL), and **S3-2** (3.96 g, 12 mmol), successively. The resulting mixture was heated at reflux for 24 h. The reaction mixture was cooled, diluted with water (50 mL), and extracted with dichloromethane (2 x 50 mL). The organic extracts were washed with water (2 x 50 mL), dried over anhydrous $MgSO_4$ and filtered. Recrystallization from ethanol afforded pure **S3-3** as a white solid. Yield: 3.0 g, 79%; mp 74-75 °C; ^{1}H NMR ($CDCl_3$) δ ppm 1.86-1.96 (m, 2H), 2.59 (t, *J* = 7.8 Hz, 4H), 3.86 (s, 12H), 6.70-6.81 (m, 6H); ^{13}C NMR ($CDCl_3$) δ ppm 33.3, 35.0, 55.8, 55.9, 111.2, 111.8, 120.2, 134.9, 147.1, 148.8.

Preparation of 3. To a cooled (~0 ^{o}C) solution of **S3-3** (1.89 g, 5.9 mmol) in CH_2Cl_2 (45 mL) was added CH_3SO_3H (5 mL) and DDQ (1.14 g, 6 mmol) and the resulting mixture was stirred under an argon atmosphere at ~0 for 30 min. Aqueous workup as above and crystallization from a mixture of ethylacetate/hexane afforded pure **3** as white crystalline solid. Yield: 1.81 g, 98%; mp 152-153 °C (lit**[4]** mp 158-159 °C); ^{1}H NMR ($CDCl_3$) δ ppm 2.10-2.19 (m, 2H), 2.42 (t, *J* = 7 Hz, 4H), 3.91 (s, 12H), 6.76 (s, 2H), 6.88 (s, 2H); ^{13}C NMR ($CDCl_3$) δ ppm 31.2, 34.0, 56.1, 56.3, 111.7, 112.0, 132.2, 133.1, 147.6, 147.9.

Preparation of 4.

Scheme 2. 4: Synthetic scheme for 4

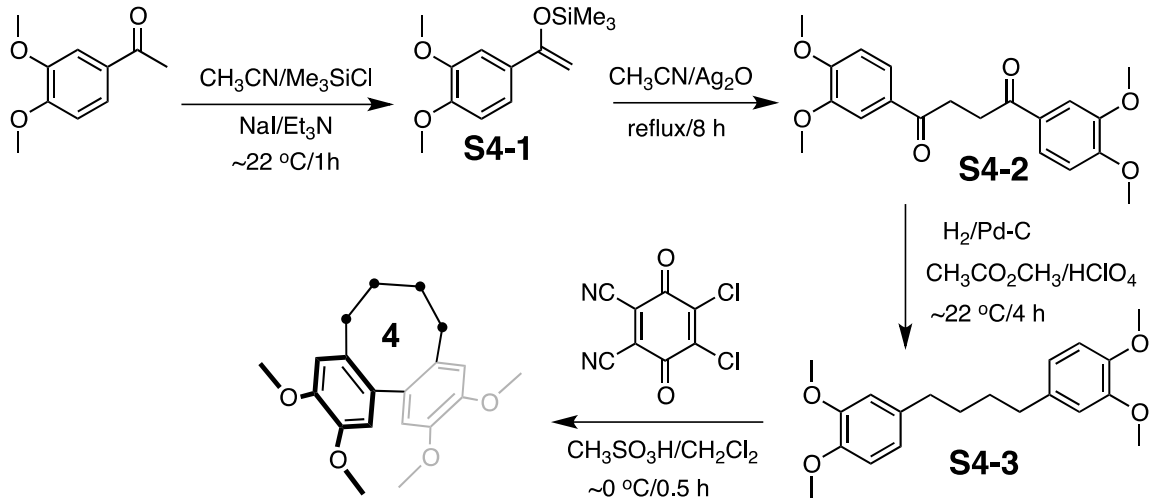

Enol silyl ether S4-1. Following closely a literature procedure,[5] a mixture of 3,4-dimethoxyacetophenone (12 g, 67 mmol) and pre-dried sodium iodide (12 g, 80 mmol) in dry acetonitrile (80 mL) was stirred under an argon atmosphere. To the resulting yellow solution, triethylamine (11 mL, 80 mmol) was added, followed by chlorotrimethylsilane (10 mL, 80 mmol). The reaction mixture was stirred for 1 h at room temperature, during which time the yellow colored solution produced a white suspension. The resulting reaction mixture was quenched with saturated aqueous ammonium chloride (50 mL). The organic layer was separated and the aqueous layer was extracted with prechilled (~0 °C) hexane (2 x 50 mL). The combined organic extract was washed with ice-water (2 x 50 mL), brine (2 x 50 mL) and dried over anhydrous $MgSO_4$ and filtered. Removal of the solvent in vacuo afforded the enol silyl ether **S4-1** in quantitative yield as a pale yellow liquid, which was used in the next step without further purification. Yield: 16.6 g, 98%; ^{1}H NMR ($CDCl_3$) δ ppm 0.26 (s, 9H), 3.88 (s, 3H), 3.89 (s, 3H), 4.36 (d, 1H, *J* = 1.5 Hz),

4.81 (d, 1H, *J* = 1.5 Hz), 6.82 (d, 1H, *J* = 8 Hz), 7.12 (d, 1H, *J* = 2 Hz), 7.17 (dd, 1H, *J* = 8, 2 Hz); ^{13}C NMR ($CDCl_3$) δ ppm 0.0, 55.6, 55.7, 89.7, 108.4, 110.5, 117.9, 130.4, 148.4, 149.1, 155.3.

1,2-Bis(3,4-dimethoxybenzoyl)ethane (S4-2). Following closely a literature procedure,[6] a heterogeneous mixture of **S4-1** (16.4 g, 65 mmol) and Ag_2O (15 g, 65 mmol) in acetonitrile (40 mL) was heated at 75 °C with vigorous stirring for 8 h, during which time a grey metallic silver solid precipitated. The solid was removed by filtration of the reaction mixture through a short pad of celite. The filtrate was washed with brine (2 x 50 mL) and dried over anhydrous $MgSO_4$ and filtered. Evaporation of the solvent in vacuo followed by crystallization of crude **S4-2** from a mixture of dichloromethane/methanol afforded pure **S4-2** as a pale yellow solid. Yield: 9.0 g, 78%; mp 179-180 °C (lit[7] mp 181-182 °C);^{1}H NMR ($CDCl_3$) δ ppm 3.42 (s, 4H), 3.93 (s, 6H), 3.96 (s, 6H), 6.91 (d, 2H, *J* = 8 Hz), 7.57 (d, 2H, *J* = 2 Hz), 7.72 (dd, 2H, *J* = 8, 2 Hz); ^{13}C NMR ($CDCl_3$) δ ppm 32.4, 56.1, 56.2, 110.1, 110.2, 122.9, 130.1, 149.1, 153.4, 197.6.

1,4-Bis(3,4-dimethoxyphenyl)butane (S4-3). A yellow suspension of **S4-2** (3.2 g, 9.0 mmol) and 10% Pd/C (0.2 g) in ethyl acetate (100 mL) with a catalytic amount of perchloric acid was hydrogenated in a Parr apparatus (45 psi) at room temperature for 4 h. An standard workup as above and crystallization from ethanol afforded pure **S4-3** as a white solid. Yield: 3.1 g, 98%; ^{1}H NMR ($CDCl_3$) δ ppm 1.61-1.65 (m, 4H), 2.55-2.59 (m, 4H), 3.84 (s, 6H), 3.85 (s, 6H), 6.68-6.71 (m, 4H), 6.77 (d, 2H, *J* = 8 Hz); ^{13}C NMR ($CDCl_3$) δ ppm 31.4, 35.5, 55.9, 56.1, 111.3, 111.9, 120.3, 135.4, 147.2, 148.9.

Synthesis of 4. A reaction **S4-3** (0.49 g, 1.5 mmol) in CH_2Cl_2 (18 mL) and CH_3SO_3H (2 mL) with DDQ (0.34 g, 1.5 mmol) at 0 ^oC as above afforded pure **4** as crystalline solid after purification by column chromatography using ethylacetate/hexane as. Yield: 0.15 g, 30%; mp 114-115 °C (lit [4] mp 115-116 °C);^{1}H NMR ($CDCl_3$) δ ppm 1.44 (t, 2H, *J* = 10 Hz), 2.00-2.13 (m, 4H), 2.61-2.66 (m, 2H), 3.87 (s, 6H), 3.92 (s, 6H), 6.75 (d, 4H, *J* = 1.3 Hz); ^{13}C NMR ($CDCl_3$) δ ppm 29.5, 32.6, 56.1, 56.2, 112.19, 112.20, 132.5, 135.1, 146.7, 148.5.

Preparation of 5.

Scheme 2. 5: Synthetic scheme for 5

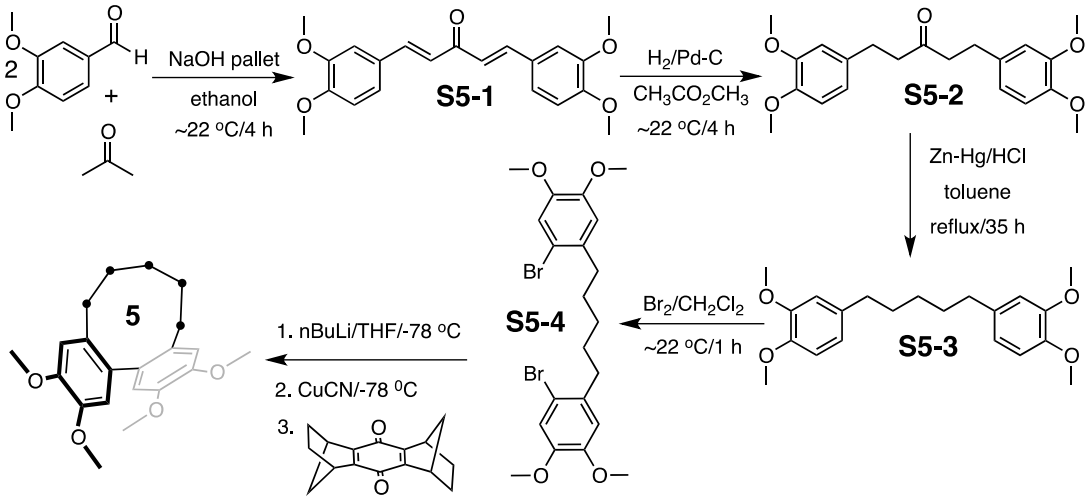

1,5-Bis(3,4-dimethoxyphenyl)-3-pentadienone (S5-1). Following closely the procedure described above for the preparation of **S3-1**, a reaction of 3,4-dimethoxybenzaldehyde (10.0 g, 60 mmol) with analytical grade acetone (1.74 g, 30 mmol) in ethanol (60 mL) in the presence of a pallet of NaOH afforded **S5-1** as yellow solid in excellent yield. Yield: 10.5 g, 99%; mp 121-122 °C (lit [8] mp 122-123 °C); ^{1}H

NMR ($CDCl_3$) δ ppm 3.90 (s, 6H), 3.92 (s, 6H), 6.87 (dd, 2H, *J* = 8, 2 Hz), 6.94 (d, 2H, *J* = 16 Hz), 7.12 (s, 2H), 7.18 (dd, 2H, *J* = 8, 2 Hz), 7.67 (d, 2H, *J* = 16 Hz); ^{13}C NMR ($CDCl_3$) δ ppm 55.9, 56.05, 56.08, 109.9, 110.2, 110.8, 111.1, 119.5, 122.9, 128.0, 131.5, 144.1, 149.2, 151.2, 153.1, 188.6.

1,5-Bis(3,4-dimethoxyphenyl)-3-pentanone (S5-2). Following closely the procedure described above for the preparation of **S3-2**, a yellow solution of **S5-1** (9.9 g, 28 mmol) and 10% Pd/C (0.5 g) in ethyl acetate (100 mL) was hydrogenated in a Parr apparatus (45 psi) for 2 h. Standard workup and crystallization from ethanol-dichloromethane mixture afforded pure **S5-2**. Yield: 6.0 g, 60%; mp 83-84 °C (lit [8] mp 85 °C); ^1H NMR ($CDCl_3$) δ ppm 2.66 (t, 4H, *J* = 8 Hz), 2.80 (t, 2H, *J* = 8 Hz), 3.81 (s, 6H), 3.82 (s, 6H), 6.64-6.75 (m, 6H); ^{13}C NMR ($CDCl_3$) δ ppm 29.4, 44.9, 55.8, 56.09, 55.9, 111.2, 111.7, 120.1, 133.7, 147.3, 148.8, 209.5.

1,5-Bis(3,4-dimethoxyphenyl)pentane (S5-3). Following closely the procedure described above for the preparation of **S3-3**, Clemmensen reduction of **S4-2** (5.0 g, 14 mmol) with amalgamated zinc (6.0 g), water (4.5 ml), conc. hydrochloric acid (11 ml), and toluene (12 mL), at reflux for 35 h afforded pure **S5-3** after purification by column chromatography using ethylacetate/hexane as eluent. Yield: 2.9 g, 60%; mp 55-56 °C (lit [8] mp 56-57 °C); ^1H NMR ($CDCl_3$) δ ppm 1.34-1.42 (m, 2H), 1.56-1.67 (m, 4H), 2.51-2.56 (m, 4H), 3.84 (s, 6H), 3.86 (s, 6H), 6.68-6.79 (m, 6H); ^{13}C NMR ($CDCl_3$) δ ppm 29.1, 31.8, 35.6, 55.9, 56.0, 111.2, 111.8, 120.2, 135.6, 147.1, 148.8.

1,5-Bis(3,4-dimethoxy-6-bromophenyl)pentane (S5-4). To a solution of **S5-3** (2.0 g, 5.8 mmol) in dichloromethane (25 mL) was added drop wise a solution of bromine (2.1 g, 12.8 mmol) in dichloromethane (20 min). The standard aqueous workup as above

afforded pure **S5-4** after crystallization from a mixture of chloroform and methanol. Yield: 2.8 g, 95%; mp 77-79 ^{o}C; ^{1}H NMR ($CDCl_3$) δ ppm 1.62 (m, 4H), 1.64(m, 2H), 2.67(t, *J* = 7.2 Hz, 4H), 3.85(s, 6H), 3.86(s, 6H), 6.71 (s, 2H), 6.99(s, 2H); ^{13}C NMR ($CDCl_3$) δ ppm 28.58, 29.47, 33.24, 56.15, 56.17, 111.81, 112.32, 133.98, 134.51, 146.75, 148.40.

Synthesis of 5. A dry and argon flushed schlenk flask (100 mL), equipped with a magnetic stirrer and a septum was charged with **S5-4** (1.25 g, 2.5 mmol) and anhydrous diethyl ether (60 mL). The reaction mixture was cooled to –78 ^{o}C, and n-BuLi (1.1 mL, 2.75 mmol, 2.5 M in Hexane) was added dropwise. After this the reaction mixture was stirred until it came to room temperature to ensure a complete lithiation, then the reaction mixture was cooled back down to –78 ^{o}C and CuCN (112 mg, 1.25 mmol) was added. The reaction mixture was allowed to warm to room temperature slowly again. The reaction mixture was vigorously stirred till all CuCN dissolved. The quinone DAQ (0.7 g, 3.0 mmol) was added at –78 ^{o}C and the reaction mixture was stirred for overnight. Reaction was quenched by addition of 2N aqueous HCl (30 mL). The organic layer was separated and the aqueous layer was extracted with dichloromethane (2 x 30 mL). The combined organic layers were dried over $MgSO_4$ and then concentrated under reduced pressure. Unreacted DAQ was converted to DAQ-H_2 by heating the DCM solution of the crude products with Zn dust in presence of acetic acid (1mL) until the yellow color of DAQ disappeared (≈ 5min.). The resulting solution was filtered to separate Zn dust and sparingly soluble DMQ-H2, washed with 10 percent aqueous sodium bicarbonate solution (2 x 25 mL), dried over $MgSO_4$ and evaporated under reduced pressure. Purification of residue on silica gel with hexanes/ethylacetate gave the cyclic **5** as a

viscous liquid. Yield: 171 mg, 20%; mp: low melting solid; ^{1}H NMR ($CDCl_3$) δ ppm 1.37 (m, 2H), 1.50 (m, 2H), 1.74 (m, 2H), 2.07 (m, 2 H), 2.58 (m, 2H), 3.84(s, 6H), 3.91(s, 6H), 6.66(s, 2H), 6.72(s, 2H);^{13}C NMR ($CDCl_3$) δ ppm 29.06, 30.24, 35.90, 56.17, 56.23, 113.06, 114.03, 115.56, 133.99, 147.76, 148.37.

Preparation of 6.

Scheme 2. 6: Synthetic scheme for 6

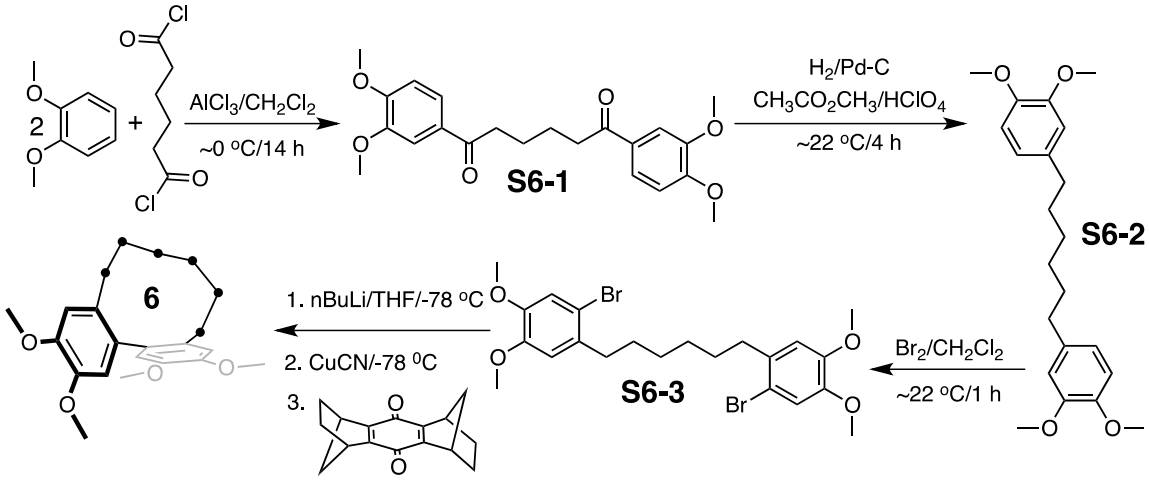

1,6-Bis(3,4-dimethoxyphenyl)-1,6-hexanedione (S6-1). Following closely a literature procedure,[9] a stirred solution of veratrole (13.8 g, 100 mmol) in dry dichloromethane (50 mL) was maintained at ~-10 ºC while anhydrous $AlCl_3$ (13.8 g, 109 mmol) was added in portions. With stirring and cooling at ~0 ºC, adipoyl chloride (8.3 g, 45 mmol) was added dropwise during a 2-h period. After stirring for 12 h, the mixture was poured into a large beaker containing 1 kg of crushed ice, water (100 mL), and conc. hydrochloric acid (50 mL). After stirring for 15 min at 0 ºC, the aqueous layer was extracted with dichloromethane (5 x 150 mL) and the combined organic extracts were washed successively with water (2 x 100 mL), 10% K_2CO_3 (2 x 100 mL), and dried over anhydrous $MgSO_4$ and filtered. After evaporation of the solvent in vacuo, the solid

residue was triturated with ether to remove excess veratrole. The crude residue was then recrystallized from toluene to afford pure **S6-1** as white solid. Yield: 15 g, 86%; mp 148-149 °C (lit [9] mp 149-150 °C); ^{1}H NMR ($CDCl_3$) δ ppm 1.80-1.84 (m, 4H), 2.97-3.00 (m, 4H), 3.92 (s, 6H), 3.94 (s, 6H), 6.87 (d, 2H, *J* = 8 Hz), 7.52 (d, 2H, *J* = 2 Hz), 7.58 (dd, 2H, *J* = 8 Hz); ^{13}C NMR ($CDCl_3$) δ ppm 24.4, 38.1, 56.1, 56.2, 110.0, 110.1, 122.8, 130.3, 149.1, 153.2, 198.8.

1,6-Bis(3,4-dimethoxyphenyl)hexane (S6-2). Following closely the procedure described above for preparation of **S4-3**, **S6-1** (10 g, 26 mmol) and 10% Pd/C (1.0 g) in ethyl acetate (60 mL) was hydrogenated in a Parr apparatus (45 psig) at room temperature for 2 h. After workup and recrystallization from ethanol afforded pure **S6-2** as a white solid. Yield: 8.3 g, 90%; mp 77-78 °C (lit [10] mp 77-78 °C); ^{1}H NMR ($CDCl_3$) δ ppm 1.33-1.37 (m, 4H), 1.55-1.63 (m, 4H), 2.54 (t, 4H, *J* = 7.5 Hz), 3.84 (s, 6H), 3.86 (s, 6H), 6.69-6.78 (m, 6H); ^{13}C NMR ($CDCl_3$) δ ppm 29.3, 31.8, 35.7, 55.9, 56.0, 111.2, 111.8, 120.2, 135.6, 147.1, 148.8.

1,6-Bis(3,4-dimethoxy-6-bromophenyl)hexane (S6-3). To a solution of **S6-2** (2.1 g, 5.8 mmol) in dichloromethane (50 mL) was added drop wise a solution of bromine (13 mmol) in dichloromethane (20 min). The organic layer was washed with aqueous sodium bisulfite (2 x 50 mL) and dried over anhydrous $MgSO_4$. Evaporation of solvent and crystallization from a mixture of chloroform and methanol afforded **S6-3** as white solid. Yield: 92%; mp 83-85 ^{o}C; ^{1}H NMR ($CDCl_3$) δ ppm 1.42 (m, 4H), 1.59(m, 4H), 2.64(t, 4H, *J* = 7.85 Hz), 3.84(s, 6H), 3.85(s, 6H), 6.70(s, 2H), 6.98(s, 2H); ^{13}C NMR ($CDCl_3$) δ ppm 29.30, 30.42, 36.04, 56.22, 56.32, 113.08, 114.11, 115.65, 134.22, 147.81, 148.43.

Synthesis of 6. Following closely the procedure described above for preparation of **5**, **S6-3** (1.3 g, 2.5 mmol) in anhydrous ether (60 mL) was reacted with nBuLi (1.1 mL, 2.75 mmol, 2.5 M in Hexane) and CuCN (112 mg, 1.25 mmol) at –78°C, followed by reaction with DAQ (0.7 g, 3.0 mmol). Workup as above and purification by column chromatography on silica gel with hexanes/ethylacetate as eluent afforded cyclic **6** as viscous oil. Yield: 231 mg, 26 %; mp: low-melting solid; ^{1}H NMR ($CDCl_3$) δ ppm 0.72 (m, 2H), 1.16 (m, 2H), 1.38 (m, 2H), 1.60 (m, 2H), 2.46 (m, 2H), 3.80 (s, 6H), 3.90 (s, 6H), 6.54 (s, 2H), 6.73 (s, 2H); ^{13}C NMR ($CDCl_3$) δ ppm 20.97, 28.36, 29.16, 56.06, 56.11, 111.13, 113.13, 132.87, 134.85, 146.37, 148.53.

Preparation of ^{t}Bu-7.

Scheme 2. 7: Synthetic scheme for ^{t}Bu-7

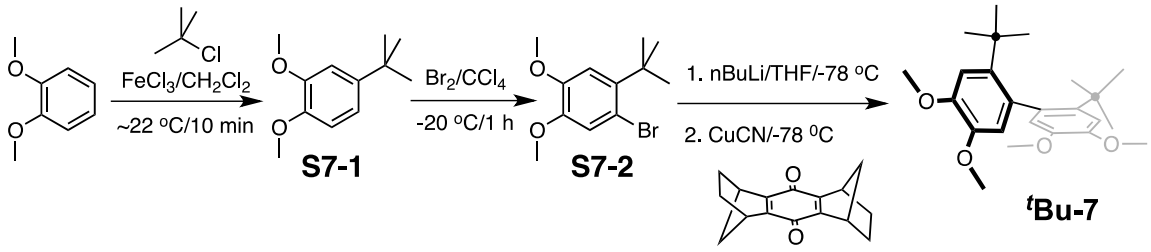

4-*tert*-Butyl-1,2-dimethoxybenzene (S7-1). A catalytic amount of $FeCl_3$ (50 mg) was added to a mixture of 1,2-dimethoxybenzene (10.38 g, 100 mmol) and tert-butyl chloride (10 mL) in dry DCM (100 mL). The reaction mixture was stirred at room temperature for 10-15 min, followed by addition of methanol (10 mL). Standard aqueous workup and filtration through a short pad of silica gel afforded **S7-1** as a low melting solid in quantitative yield. ^{1}H NMR (CDCl3) δ ppm 1.36 (s, 9H), 3.89 (s, 3H), 3.93 (s,

3H), 6.85 (d, 1H, J= 8.2 Hz), 6.93- 7.01 (m, 2H); ^{13}C NMR (CDCl3) δ ppm 31.59, 34.44, 55.89, 109.34, 110.34, 117.18, 143.99, 146.91,148.50.

1-Bromo-2-tert-butyl-4,5-dimethoxybenzene (S7-2). 4-tert-Butyl-1,2-dimethoxybenz-ene (**S7-1**, 4.5 g, 23 mmol) in CCl_4 (25 mL) was cooled to -20 ^{o}C followed by addition of a solution of bromine (24 mmol) in CCl_4 (20 mL) slowly so that the temperature did not rise above –10 ^{o}C. After completion of the reaction (~1h), an aqueous solution of 5% sodium hydrogen sulfate (50 mL) was added, organic layer was separated, dried over $MgSO_4$, evaporated to afford **S7-2** as a low melting solid which was purified by column chromatography on silica gel using hexanes/ethylacetate as eluent. Yield: 5.9 g, 95 %, ^{1}H NMR ($CDCl_3$) δ ppm 1.48 (s, 9H), 3.83 (s, 3H), 3.85 (s, 3H), 6.96 (s, 1H), 7.05 (s, 1H); ^{13}C NMR ($CDCl_3$) δ ppm 29.99, 36.33, 56.11, 117.71, 112.61, 118.72, 140.11, 147.31, 147.56.

2,2'-Di-*tert*-Butyl-4,4',5,5'-tetramethoxybiphenyl (^{t}Bu-7). Biaryl **^{t}Bu-7** was synthesized using the same procedure as described for the preparation of **5** and **6**., using **S7-2** (683 mg, 2.5 mmol). Yield: 241 mg, 25 %, mp: 118-120 ^{o}C; ^{1}H NMR ($CDCl_3$) δ ppm 1.16 (s, 18H), 3.78 (s, 6H), 3.91 (s, 6H), 6.50 (s, 2H), 6.98 (s, 2H). ^{13}C NMR ($CDCl_3$) δ ppm 33.39, 36.99, 55.96, 56.03, 111.65, 115.99, 134.68, 139.35, 145.03, 147.50.

^{1}H/^{13}C NMR spectroscopy of Compounds

All NMR spectra were recorded as $CDCl_3$ solution at ambient temperatures.

^{1}H NMR spectra of **S1-1**.

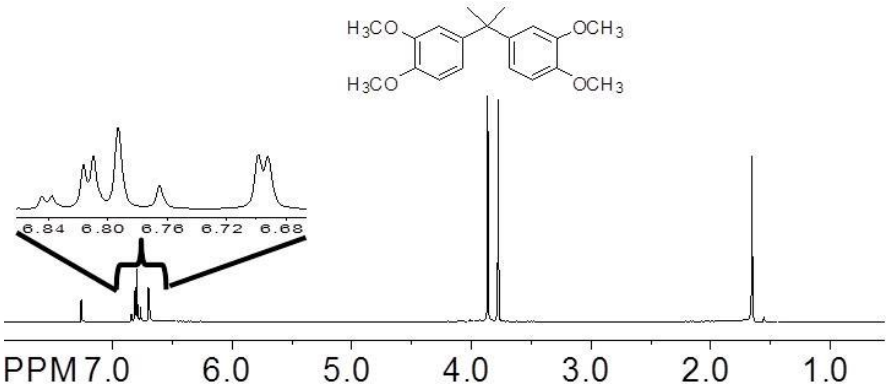

^{13}C NMR spectra of **S1-1**.

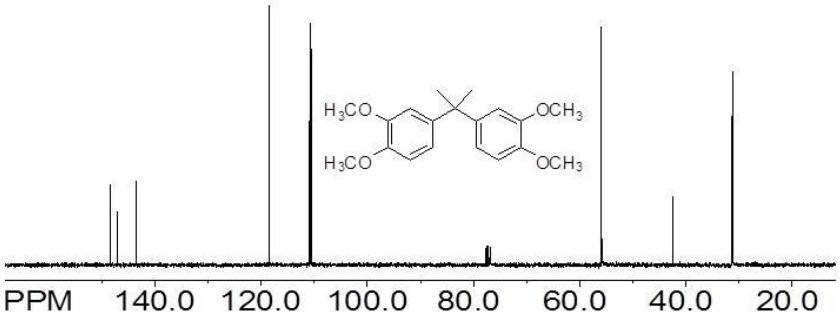

^{1}H NMR spectra of **1**.

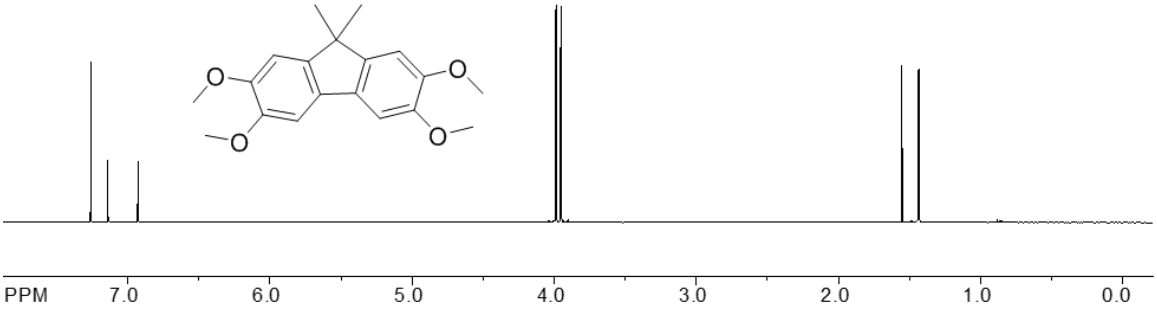

^{13}C NMR spectra of **1**.

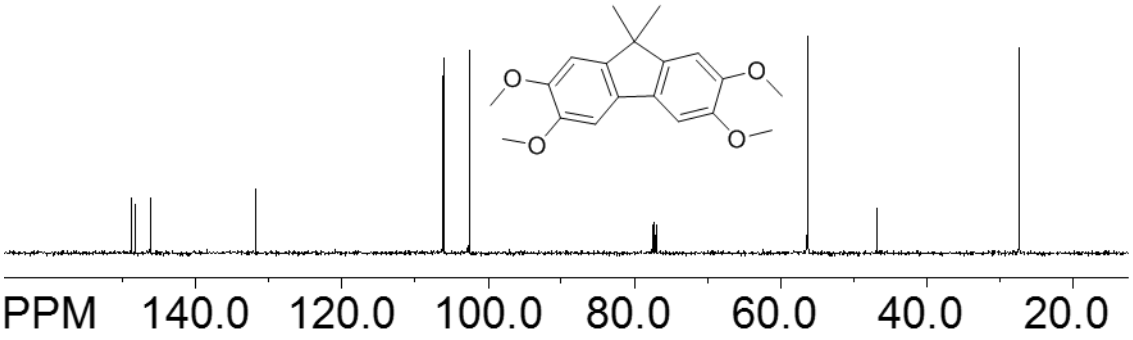

^{1}H NMR spectra of **2S-1**.

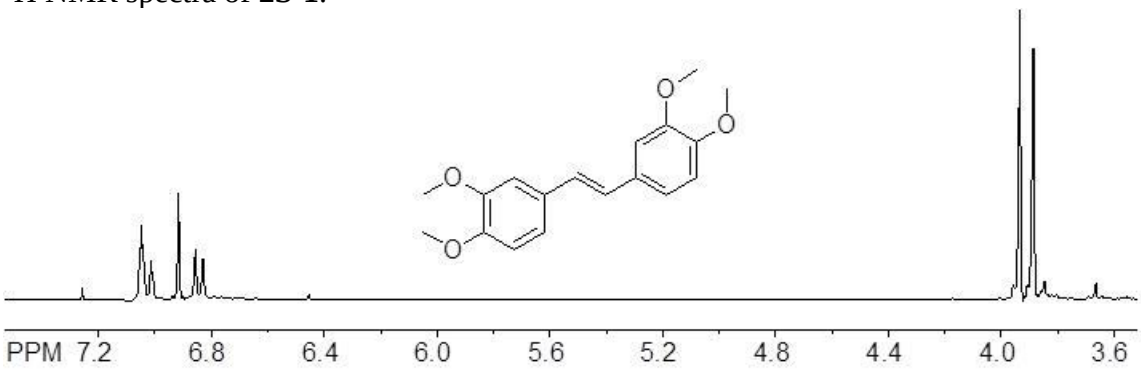

^{13}C NMR spectra of **2S-1**.

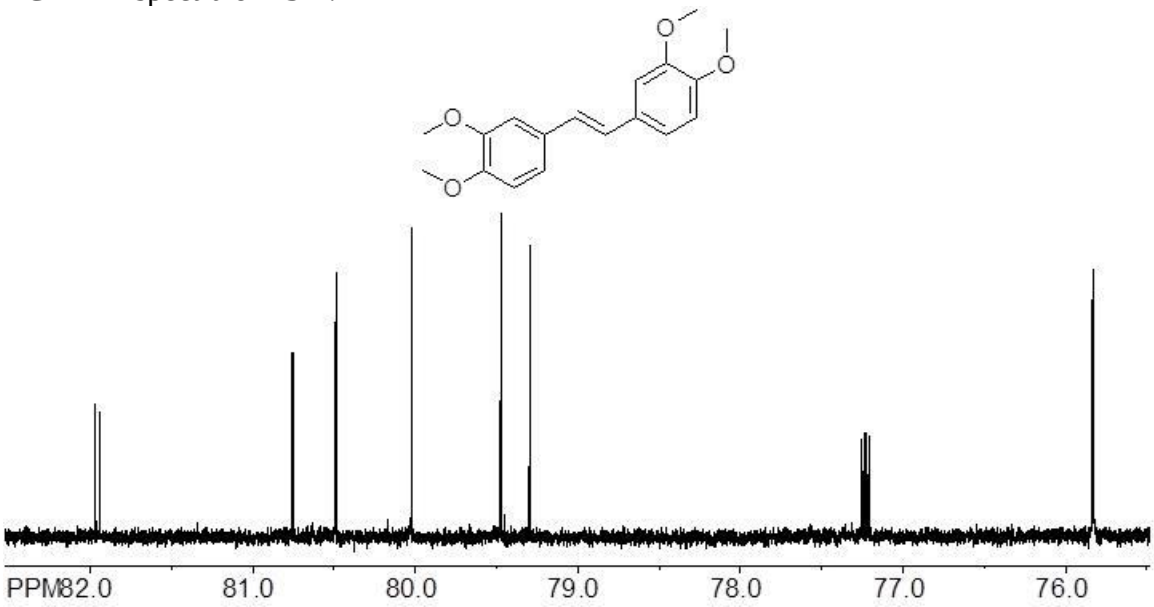

^{1}H NMR spectra of **2S-2**.

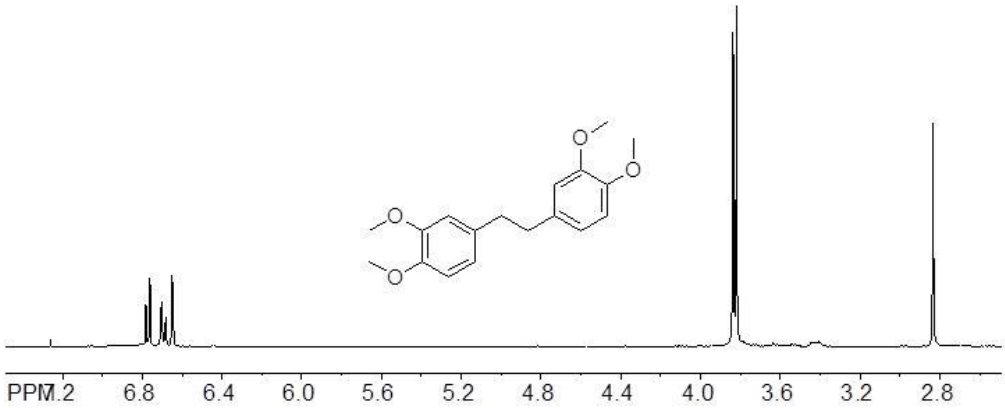

^{13}C NMR spectra of **2S-2**.

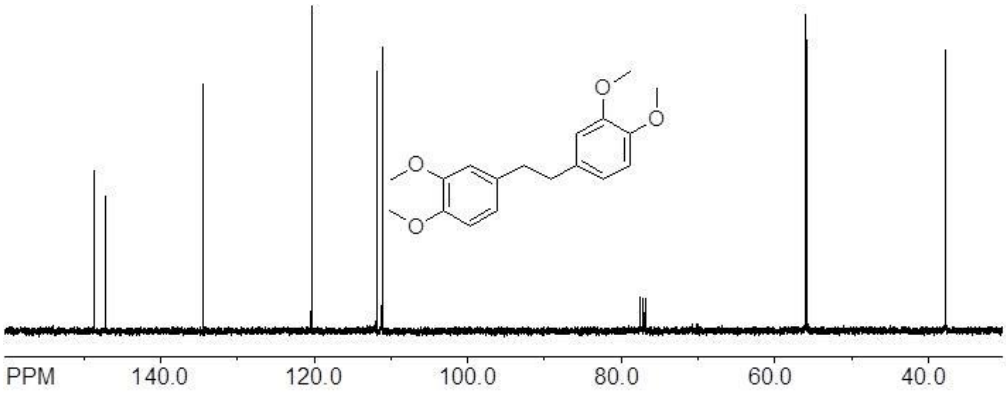

^{1}H NMR spectra of **2S-3**.

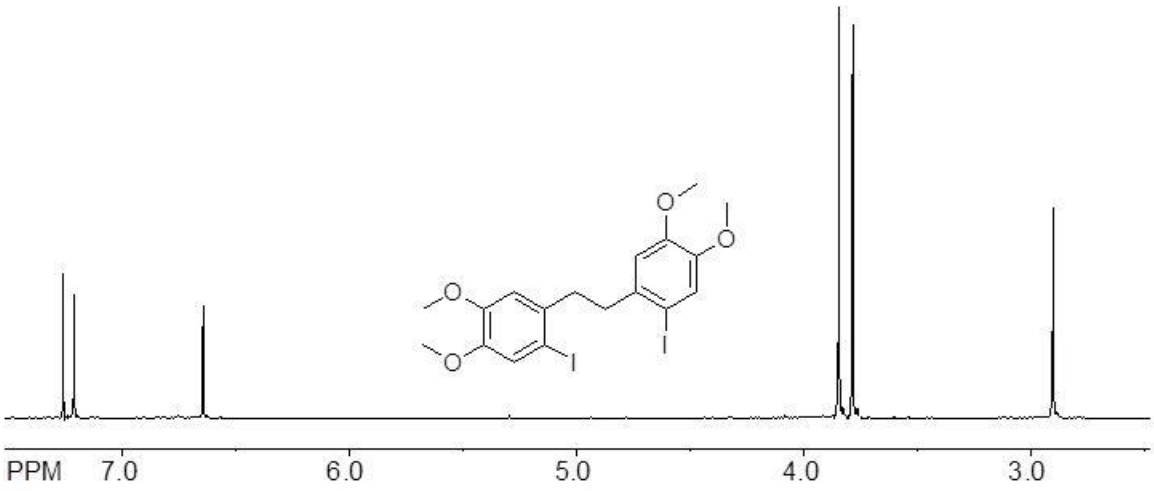

^{13}C NMR spectra of **2S-3**.

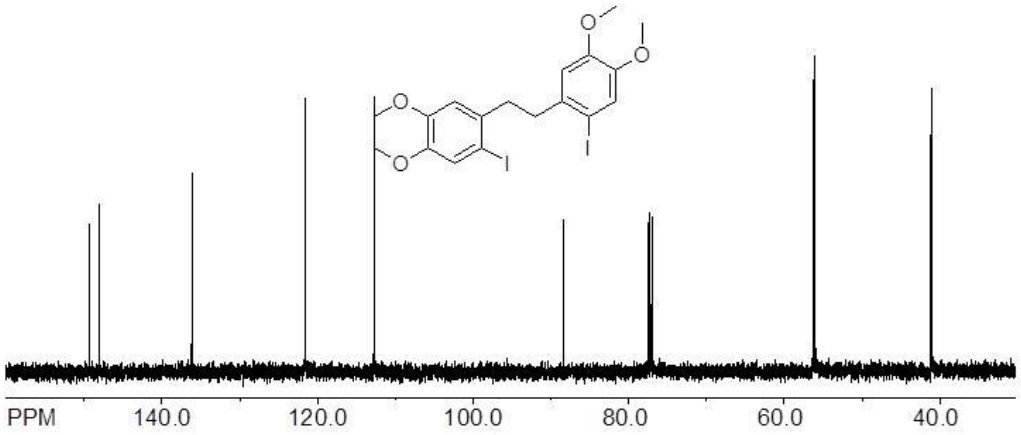

^{1}H NMR spectra of **2**.

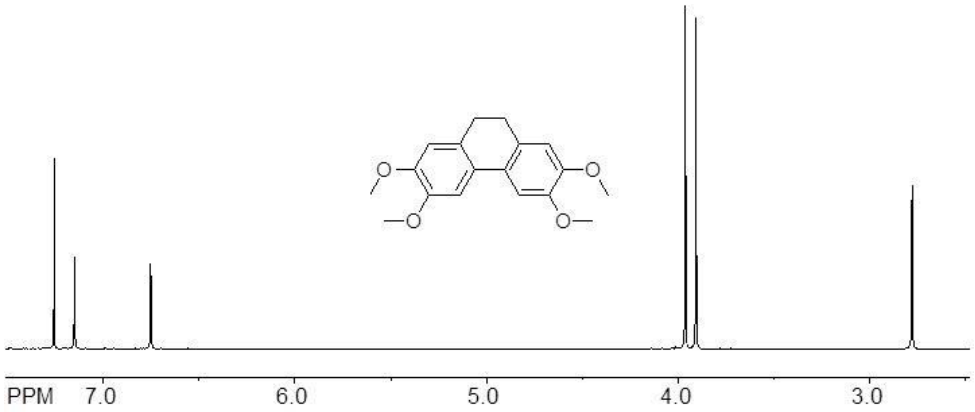

^{13}C NMR spectra of **2**.

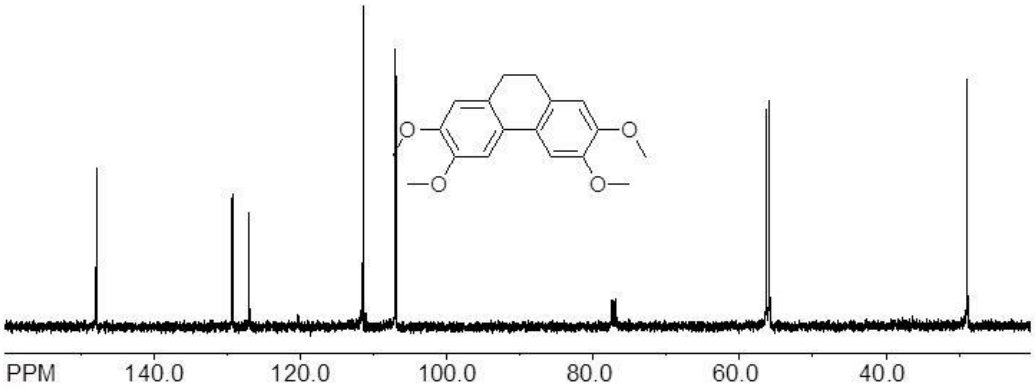

^{1}H NMR spectra of **3S-1**.

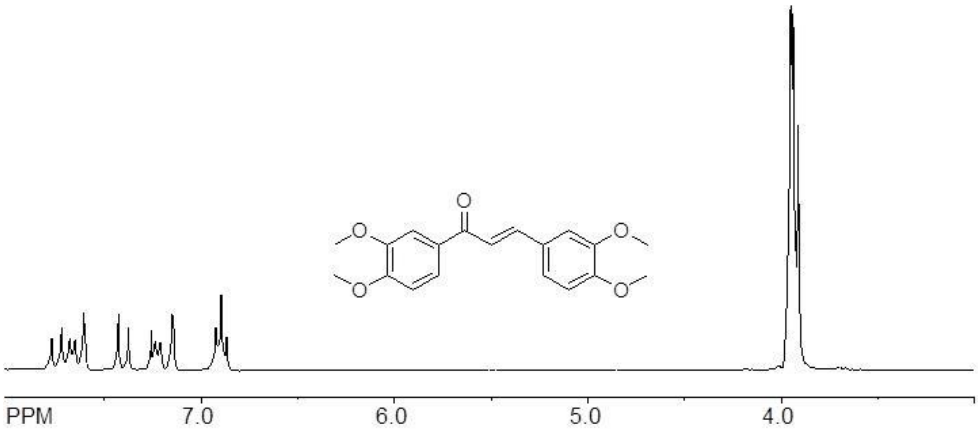

^{13}C NMR spectra of **3S-1**.

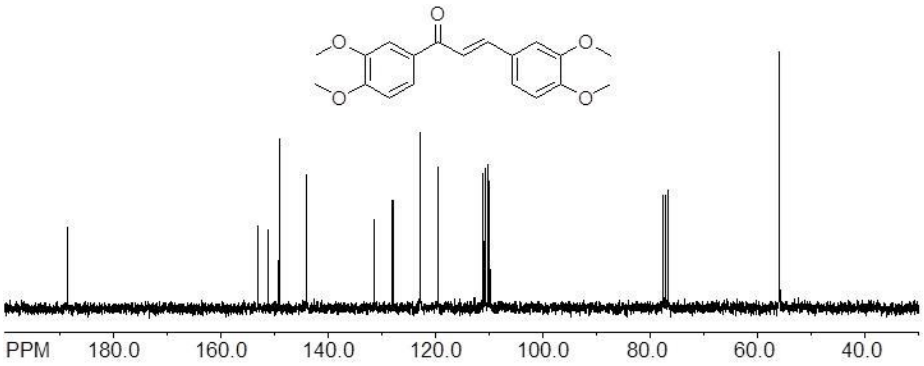

^{1}H NMR spectra of **3S-2**.

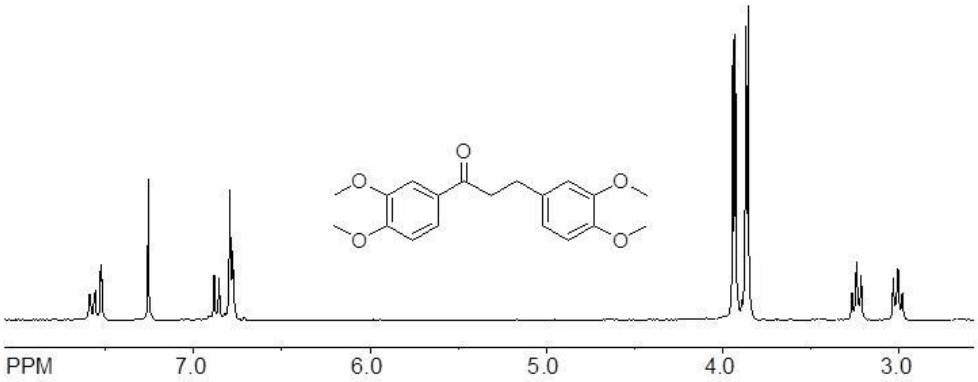

^{13}C NMR spectra of **3S-2**.

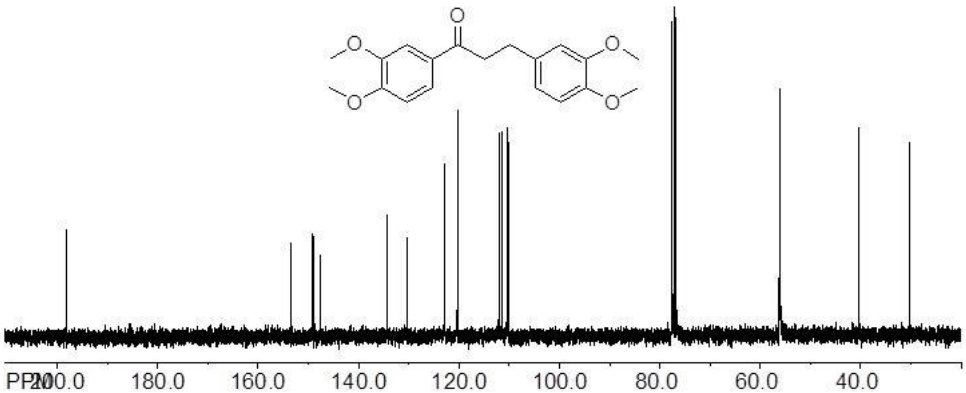

^{1}H NMR spectra of **3S-3**.

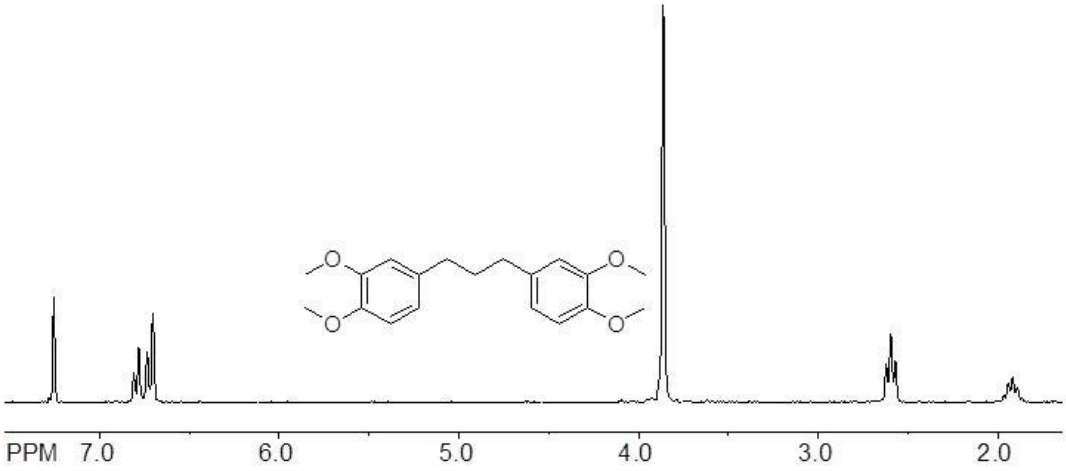

^{13}C NMR spectra of **3S-3**.

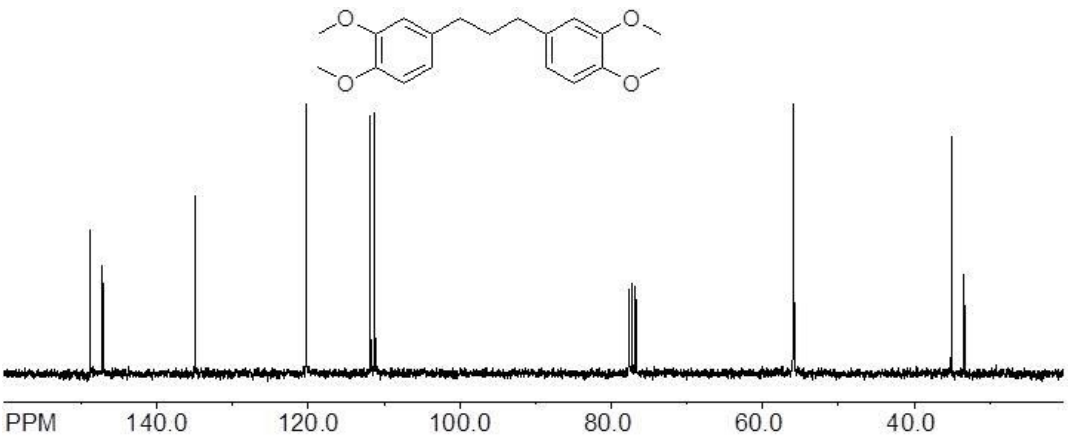

^{1}H NMR spectra of **3**.

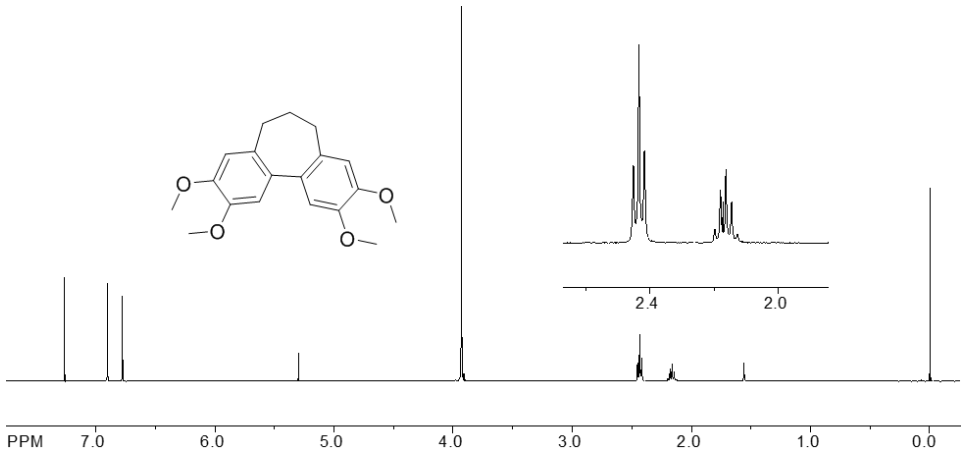

^{13}C NMR spectra of **3**.

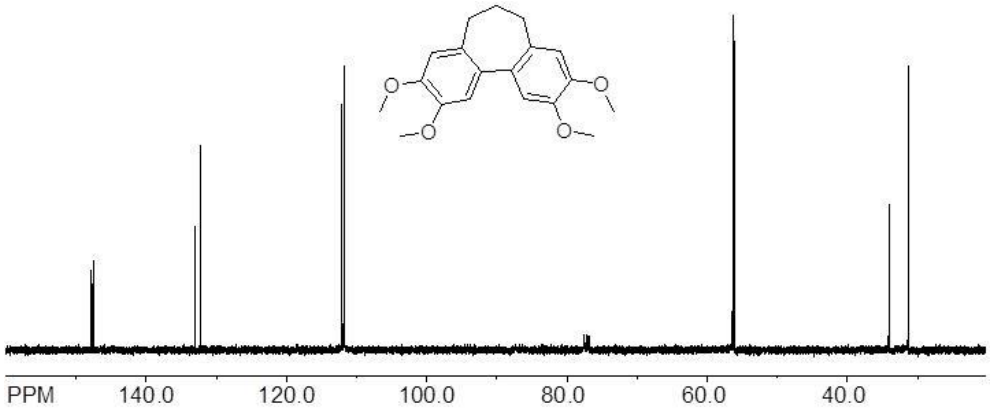

^{1}H NMR spectra of **4S-1**.

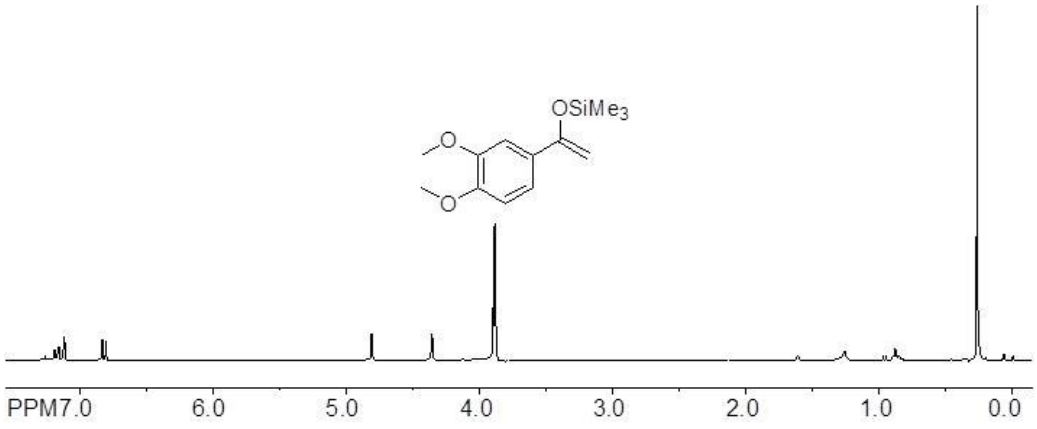

^{13}C NMR spectra of **4S-1**.

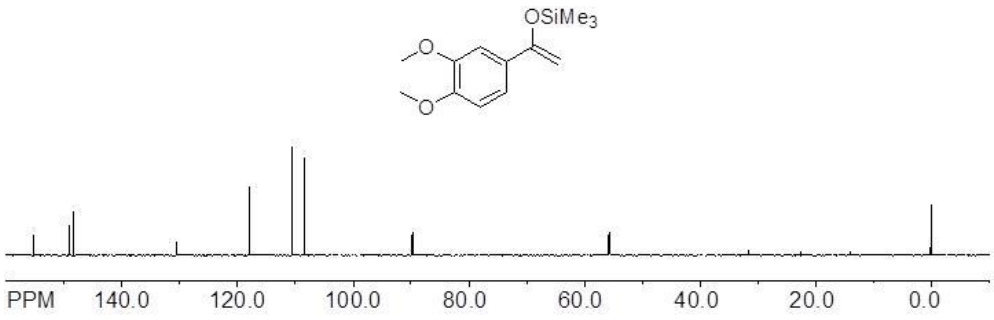

^{1}H NMR spectra of **4S-2**.

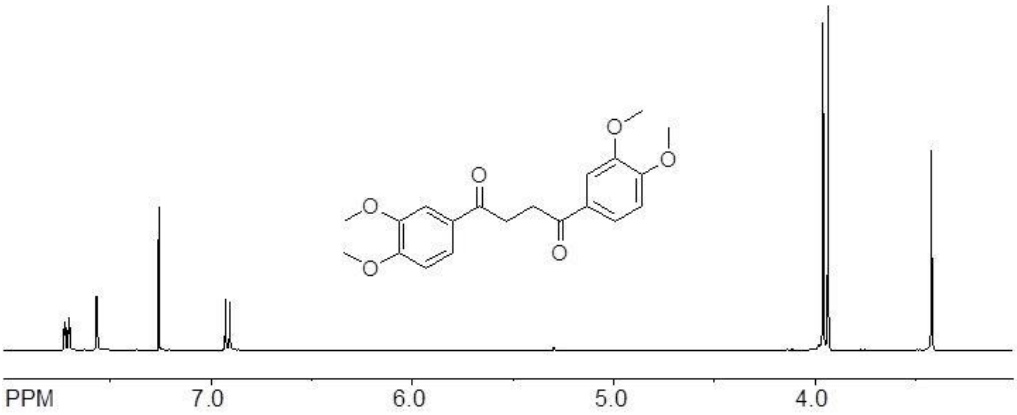

^{13}C NMR spectra of **4S-2**.

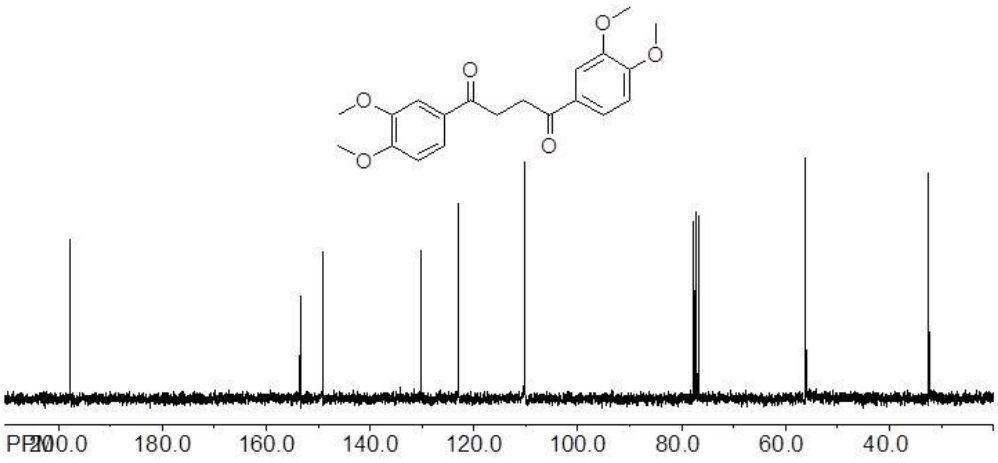

^{1}H NMR spectra of **4S-3**.

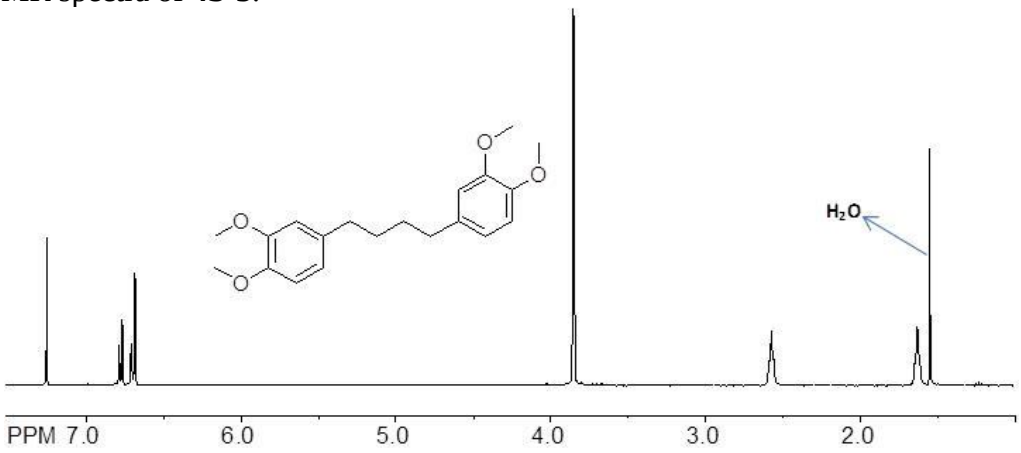

^{13}C NMR spectra of **4S-3**.

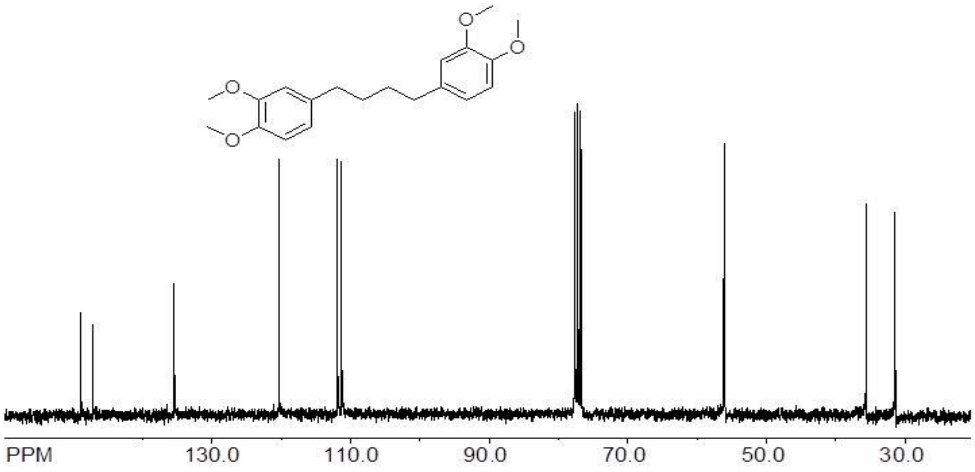

^{1}H NMR spectra of **4**.

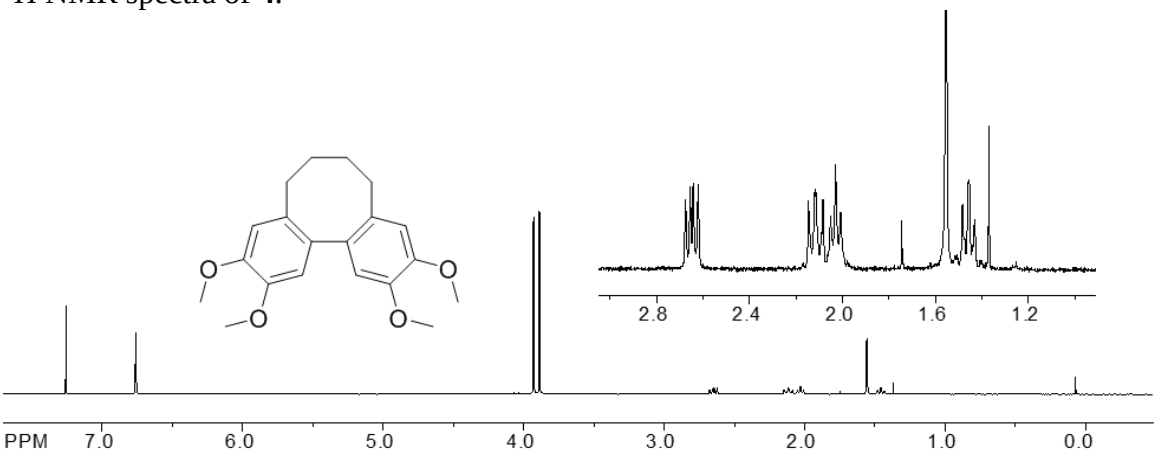

^{13}C NMR spectra of **4**.

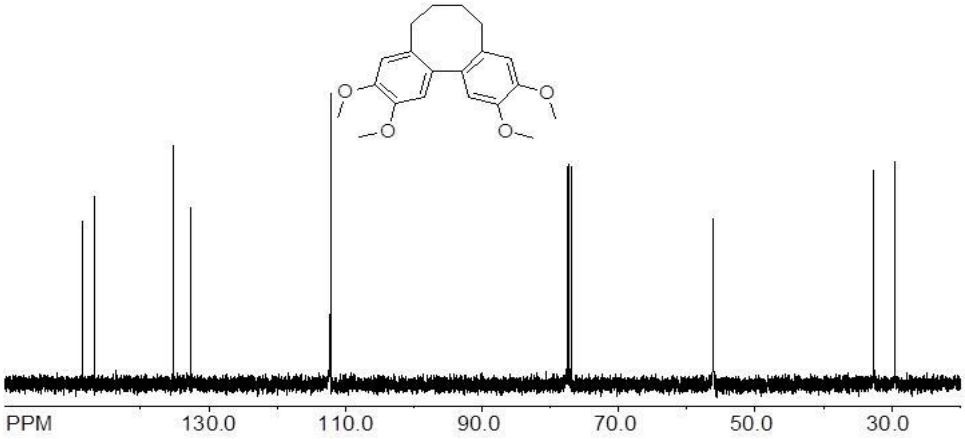

^{1}H NMR spectra of **5S-1**.

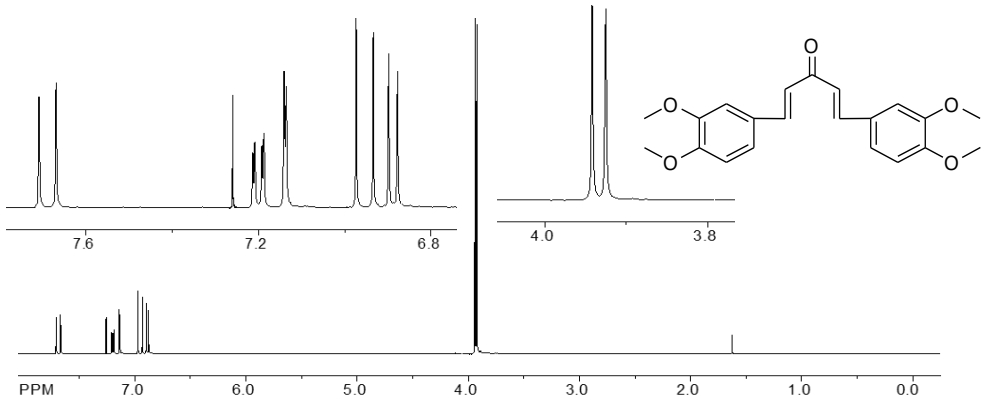

^{13}C NMR spectra of **5S-1**.

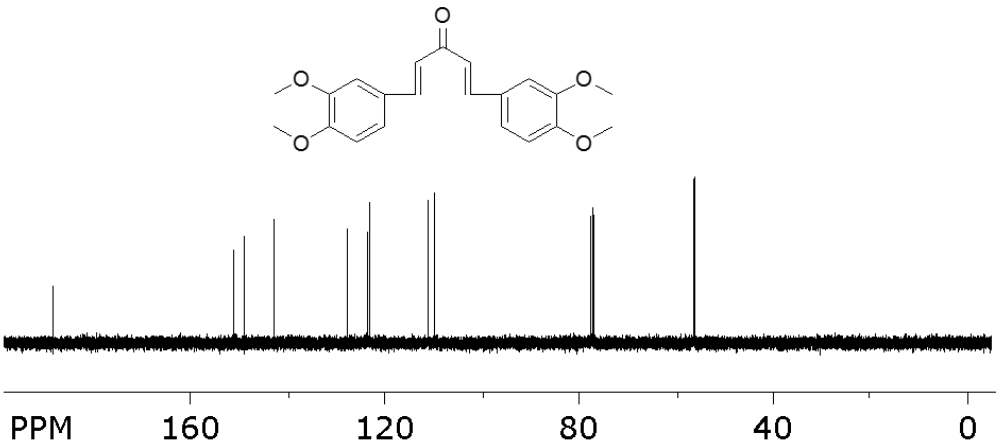

^{1}H NMR spectra of **5S-2**.

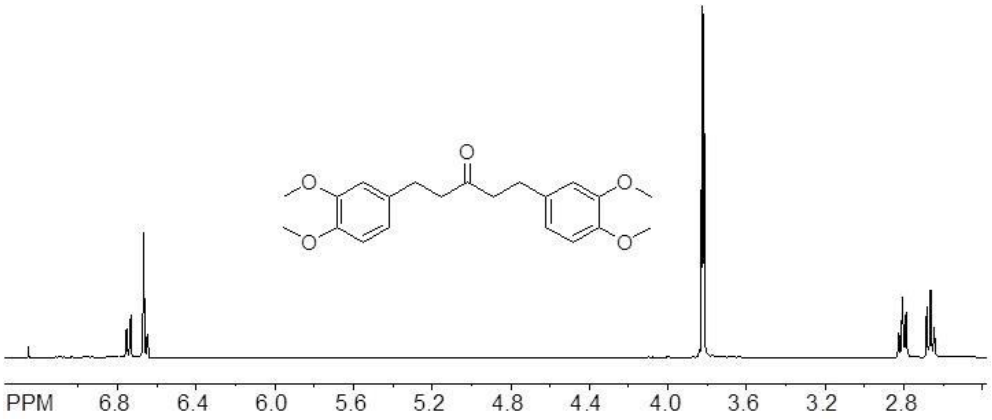

^{13}C NMR spectra of **5S-2**.

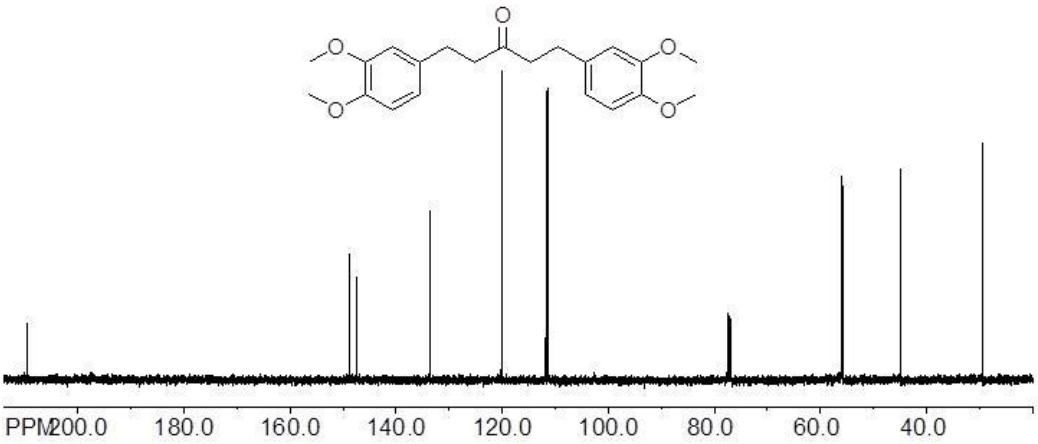

^{1}H NMR spectra of **5S-3**.

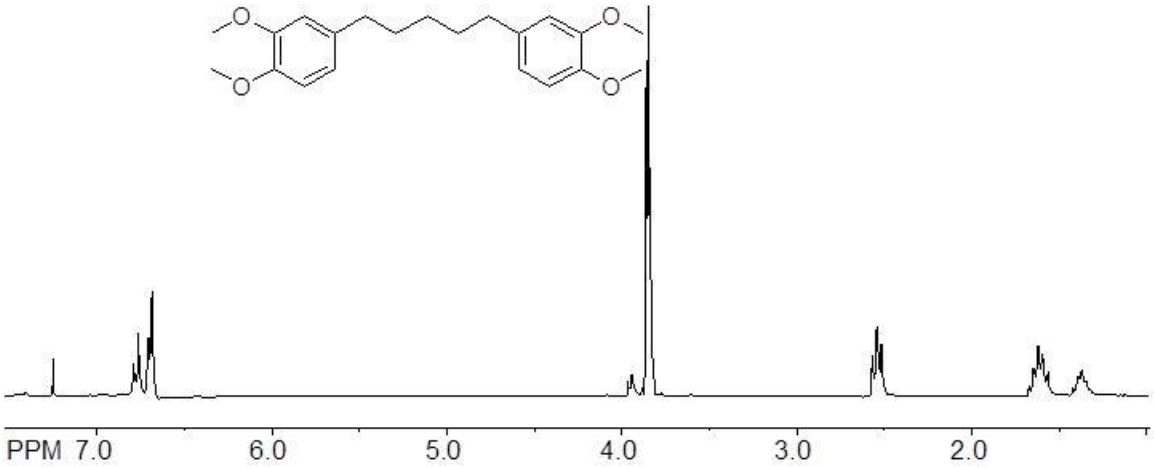

^{13}C NMR spectra of **5S-3**.

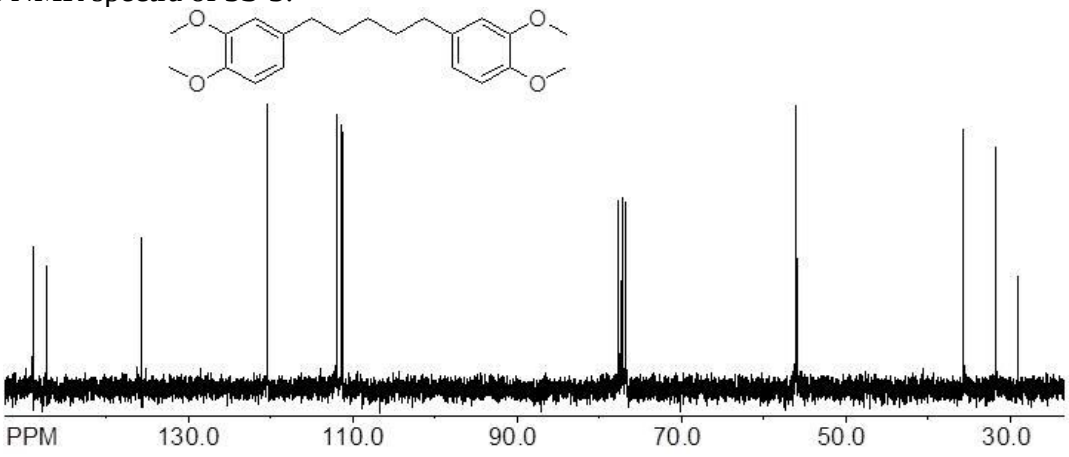

^{1}H NMR spectra of **5S-4**.

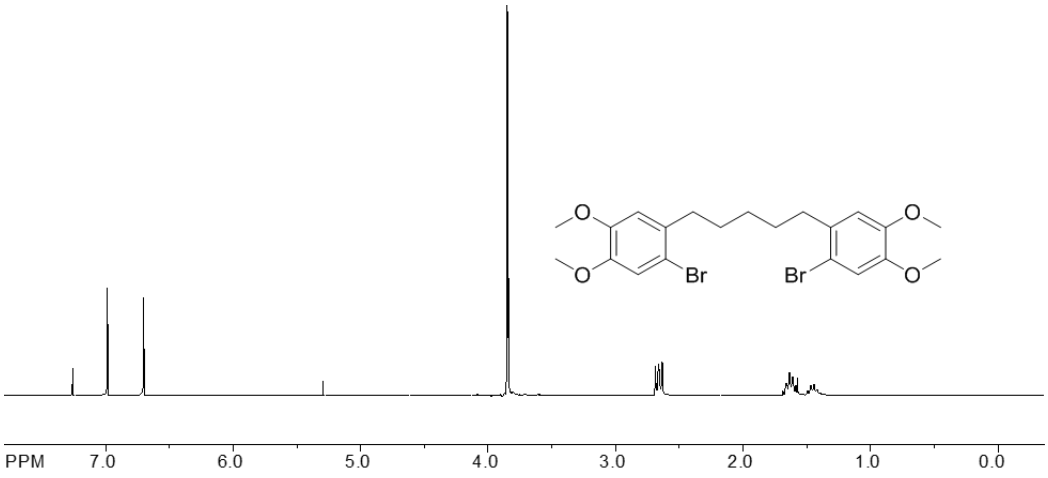

^{13}C NMR spectra of **5S-4**.

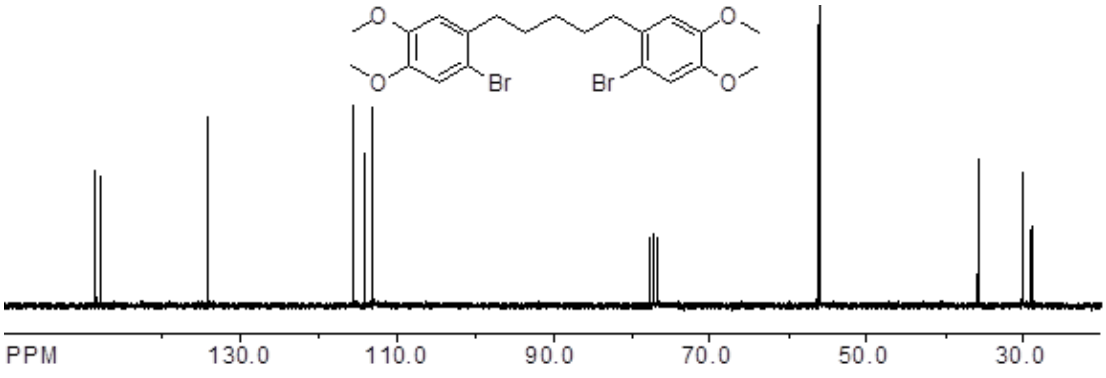

^{1}H NMR spectra of **5**.

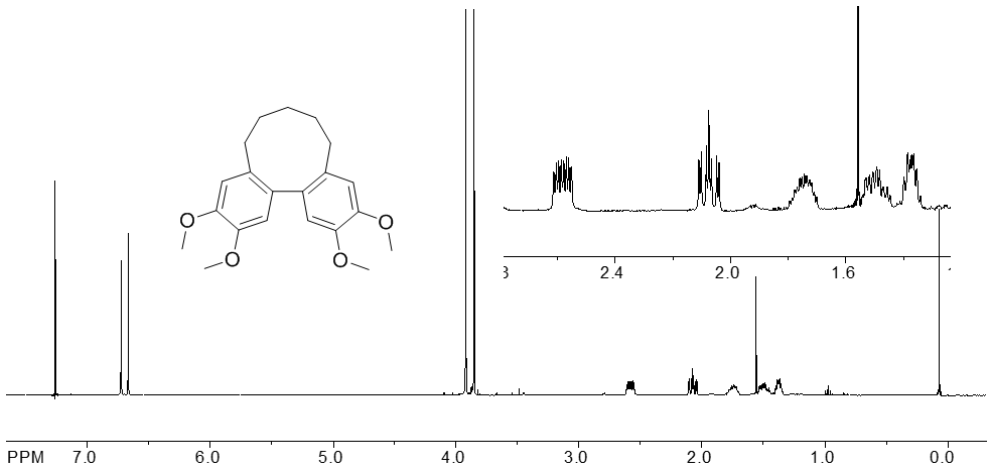

^{13}C NMR spectra of **5**.

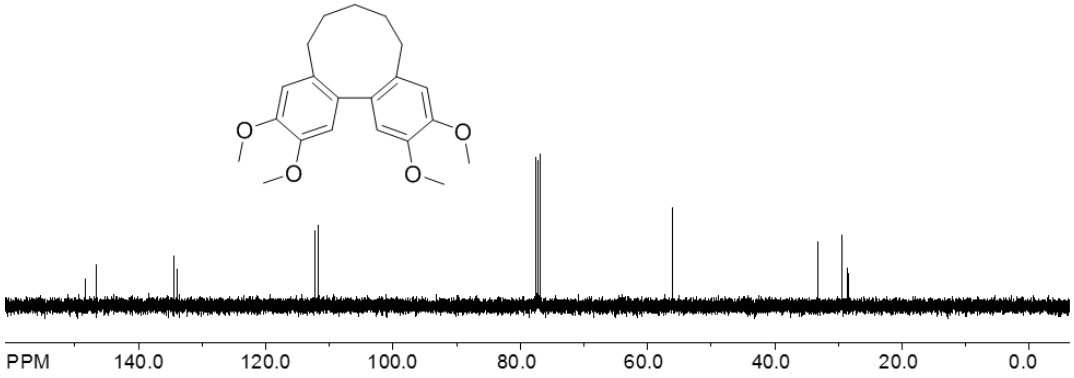

^{1}H NMR spectra of **6S-1**.

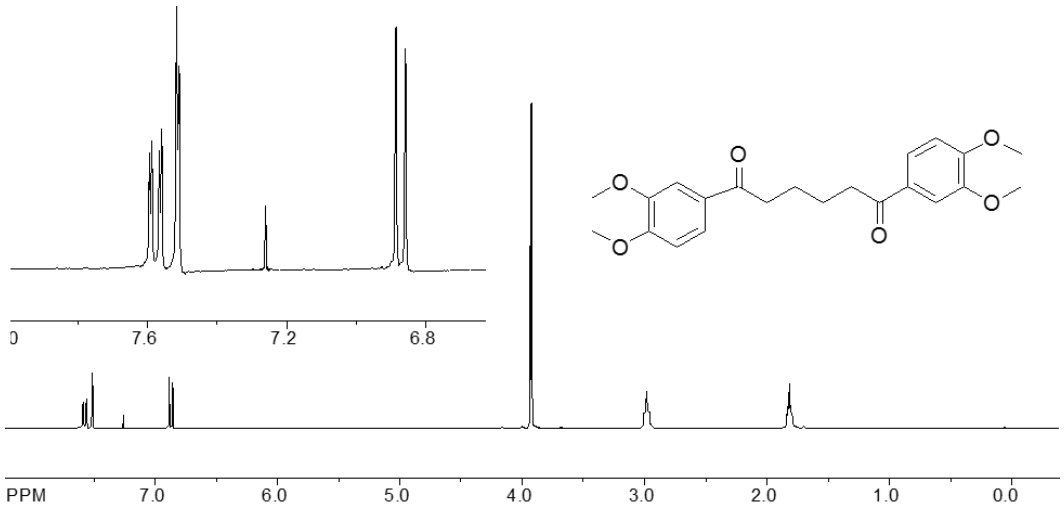

^{13}C NMR spectra of **6S-1**.

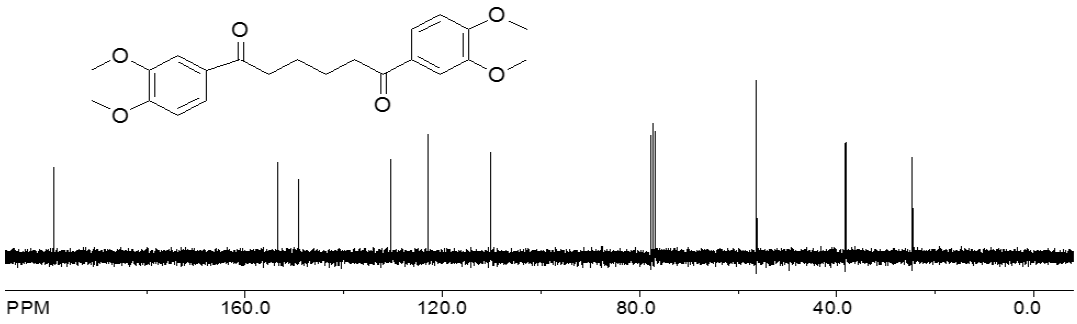

^{1}H NMR spectra of **6S-2**.

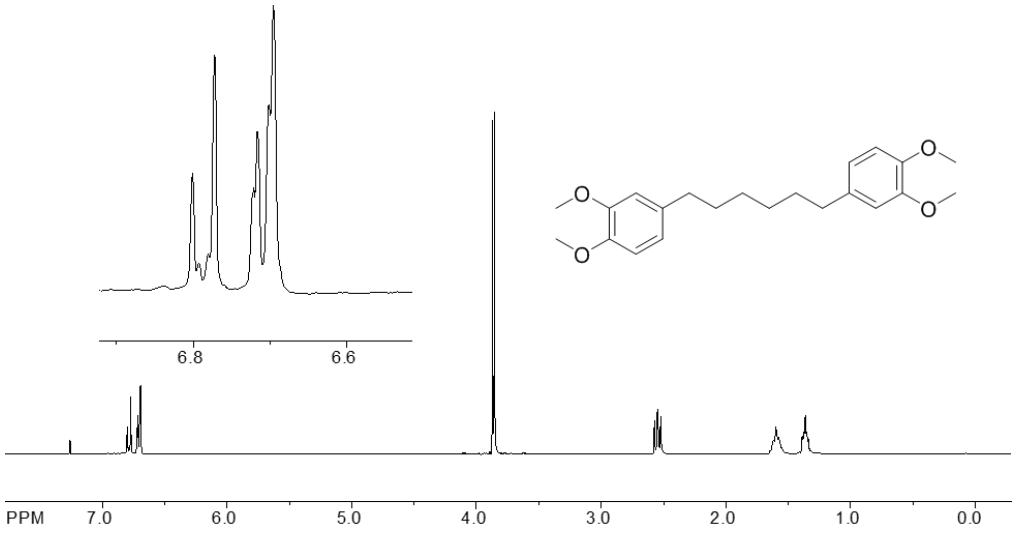

^{13}C NMR spectra of **6S-2**.

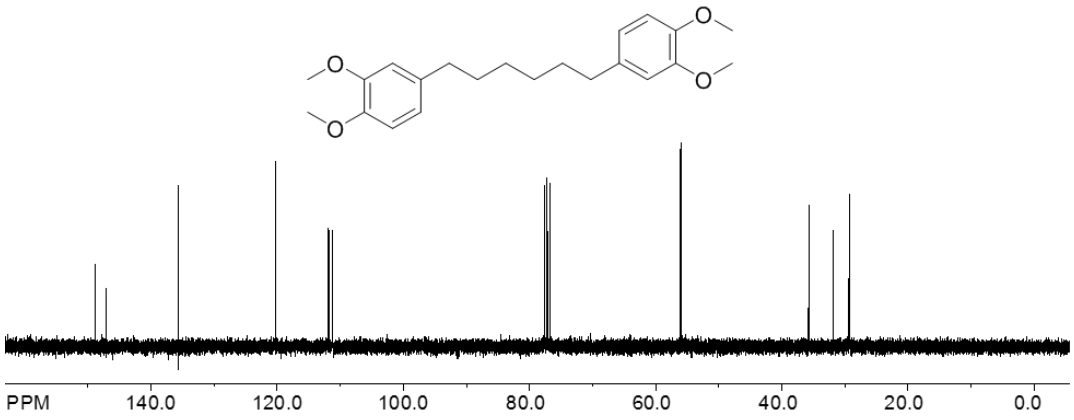

^{1}H NMR spectra of **6S-3**.

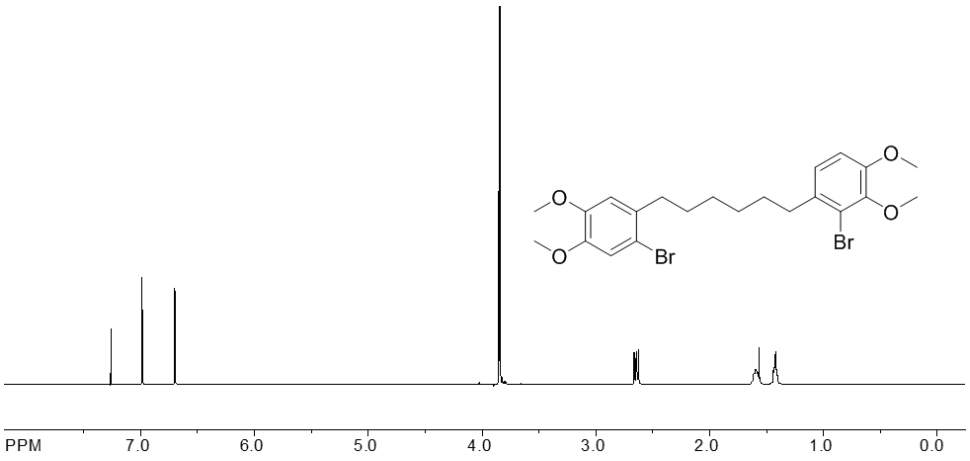

^{13}C NMR spectra of **6S-3**.

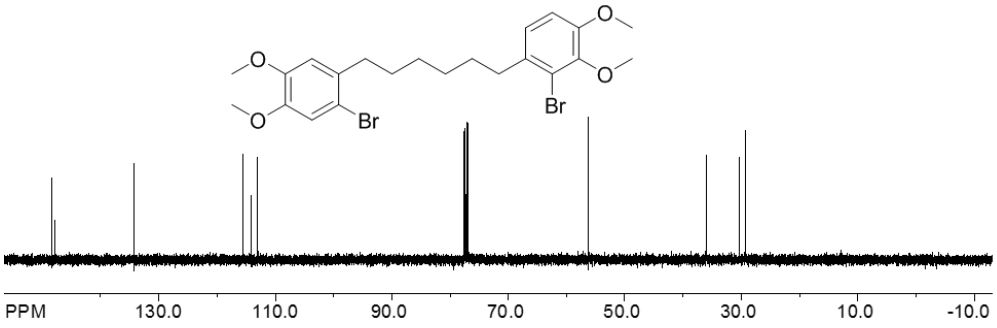

^{1}H NMR spectra of **6**.

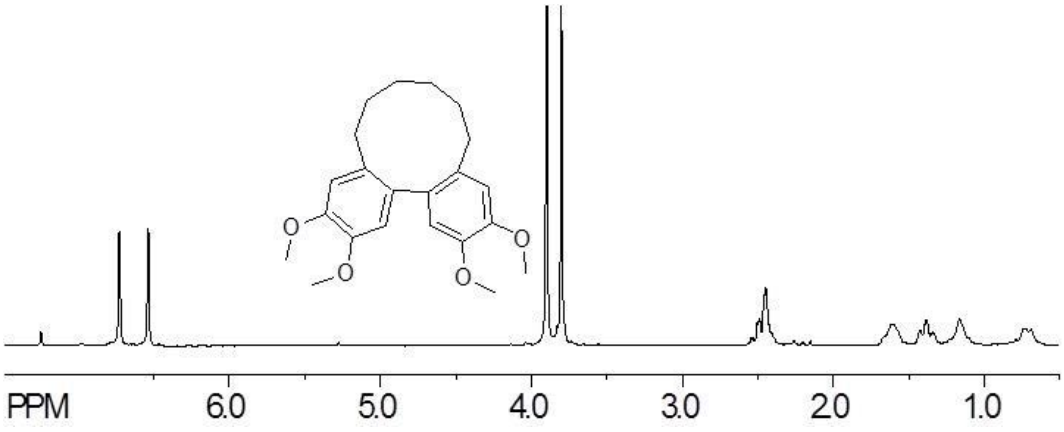

^{13}C NMR spectra of **6**.

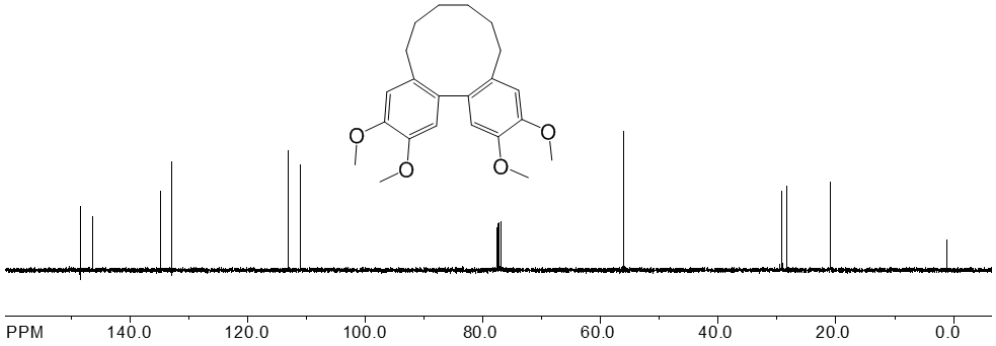

^{1}H NMR spectra of **7S-1**.

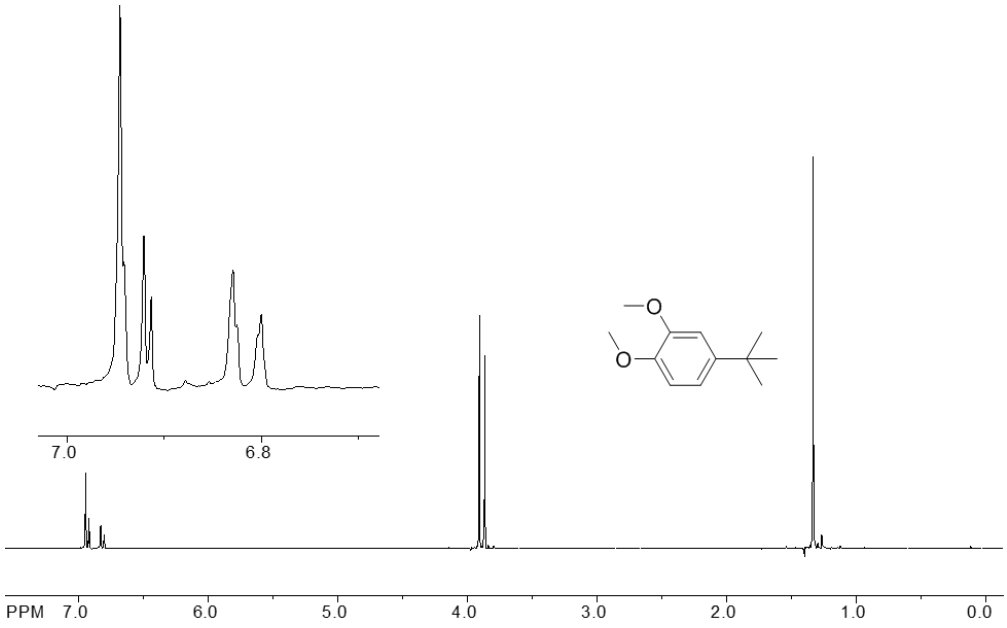

^{13}C NMR spectra of **7S-1**.

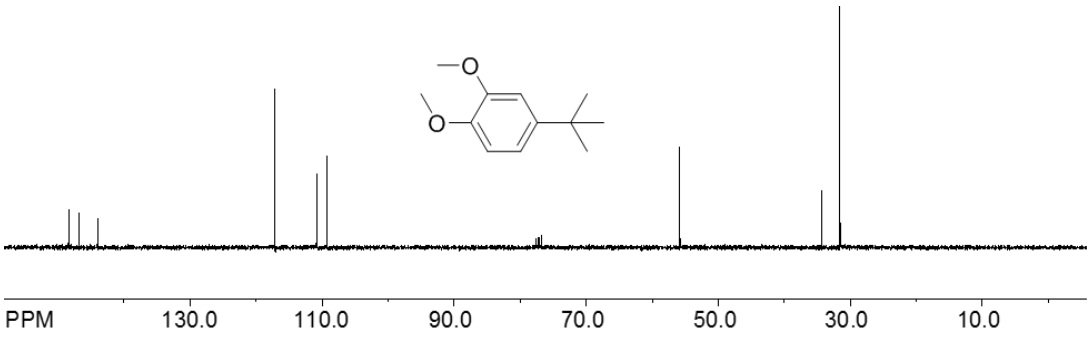

^{1}H NMR spectra of **7S-2**.

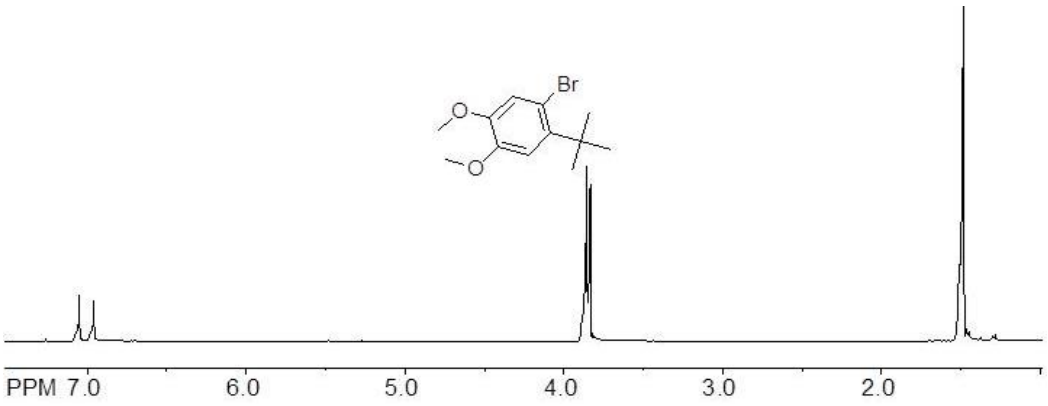

^{13}C NMR spectra of **7S-2**.

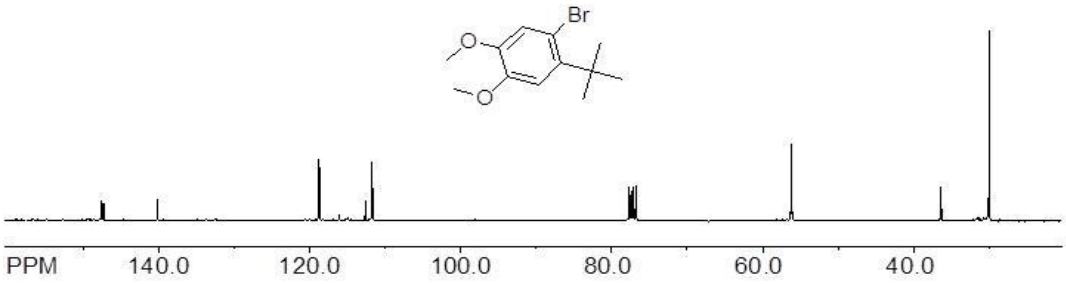

^{1}H NMR spectra of **^{t}Bu-7**.

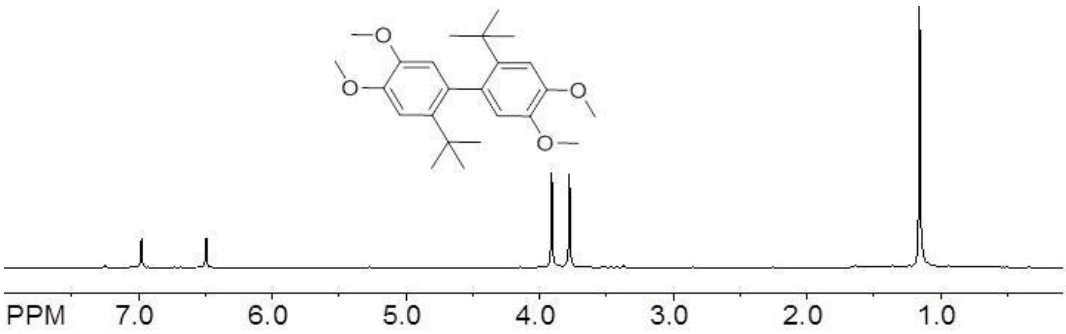

^{13}C NMR spectra of **^{t}Bu-7**.

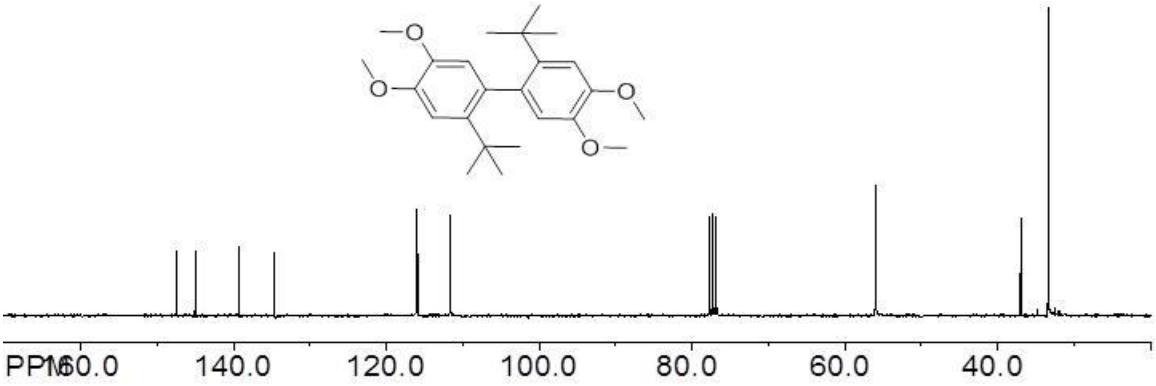

Cyclic voltammetry of biaryls 1-7 and model compound

The CV cell was of an air-tight design with high vacuum Teflon valves and Viton O-ring seals to allow an inert atmosphere to be maintained without contamination by grease. The working electrode consisted of an adjustable platinum disk embedded in a glass seal to allow periodic polishing (with a fine emery cloth) without changing the surface area (~1 mm^2) significantly. The reference SCE electrode (saturated calomel electrode) and its salt bridge were separated from the catholyte by a sintered glass frit. The counter electrode consisted of a platinum gauze that was separated from the working electrode by ~3 mm. The CV measurements were carried out in a solution of 0.1 M supporting electrolyte (*n*-Bu_4NPF_6) and the substrate in dry CH_2Cl_2 under an argon atmosphere at 22 ºC. All the cyclic voltammograms were IR compensated. The oxidation potentials (E_{ox}, calculated by taking the average of anodic and cathodic peaks) were referenced to ferrocene.

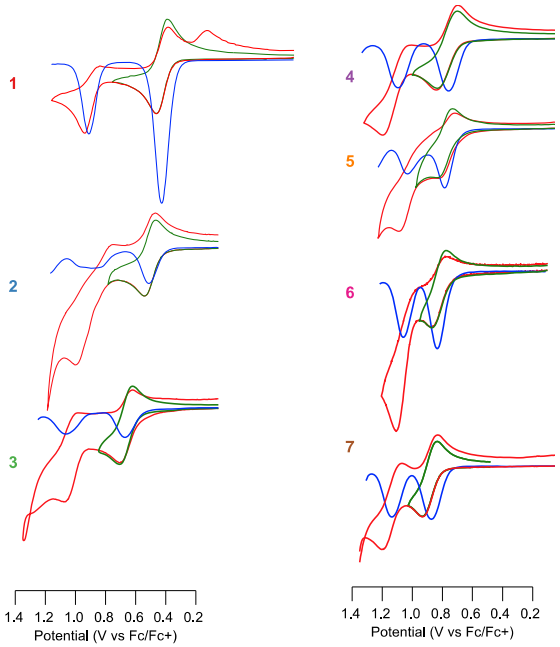

Figure 2. 11. Cyclic (green and red lines) and square-wave (blue lines) voltammograms of 2 mM **1**-**7** in CH_2Cl_2 (0.1 M *n*-Bu_4NPF_6) at a scan rate of 200 mV s^{-1} and 22 ºC.

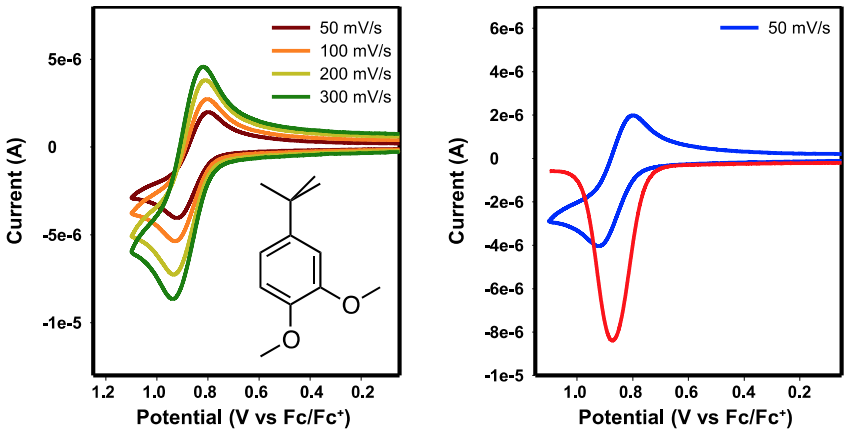

Figure 2. 12. Cyclic voltammograms of model of 2 mM 3,4-dimethoxy-1-*tert*-butylbenzene at various scan rates in CH_2Cl_2 (0.1 M *n*-Bu_4NPF_6) at 22 ºC, and its square-wave voltammogram.

The model monoaryl, i.e. 3,4-dimethoxytoluene, undergoes an expected irreversible electrochemical oxidation because it readily forms the corresponding 2,2-

dimethyl-3,4,3',4'-tetramethoxybiphenyl.[11] Interestingly, replacing the methyl with *tert*-butyl group in 3,4-dimethoxytoluene affords a completely reversible cyclic voltammograms because it prevents oxidation coupling due to the steric hindrance. Note that the oxidation potentials of 3,4-dimethoxytoluene and 3,4-dimethoxy-1-*tert*-butylbenzene are expected to be similar.

Generation of cation radicals of 1-7

The clean one-electron electron transfer from **1-7** to their cation radicals at the equivalence titration point (i.e. 1:1 ratio of electron donor:oxidant) was confirmed by the deconvolution of spectra at each titration point using the clean absorption spectra of $\mathbf{THE}^{+\bullet}$ (or $\mathbf{NAP}^{+\bullet}$) and $\mathbf{1}^{+\bullet}$-$\mathbf{7}^{+\bullet}$ and fitting of the obtained molar fractions to the equilibrium equations of the one- and two-electron oxidation.[12]

Preparation of $\mathbf{NAP}^{+\bullet}\,\mathbf{SbCl_6}^{-}$: In a dry Schlenk tube equipped with a magnetic stir bar, 25.0 mg (0.069 mmol) of NO^+SbCl_6 was taken out from the Glove Box. Then approximately 10 mL of anhydrous CH_2Cl_2 was added into the Schlenk tube under argon atmosphere at room temperature and was kept stirring to dissolve NO^+SbCl_6. The Schlenk tube having light yellow colored solution was placed in an ice bath and was kept stirring for 10 minutes. 23.8 mg (0.068 mmol) of annulated napthyl was added at 0 ^{0}C under argon atmosphere and the resulting solution was kept vigorous stirring with occasional degassing to remove in situ generated NO gas. After 1 hour stirring and occasional degassing the resulting solution turned to deep blue color which was ready to use as oxidant for the redox titration.

Preparation of $THE^{+\bullet}$ $SbCl_6^-$: A stock solution of $THE^{+\bullet}$ was prepared by dissolving [$THE^{+\bullet}$ $SbCl_6^-$] (4.4×10^{-3} mmol) in anhydrous dichloromethane (20 mL) at 22 ^{o}C under an argon atmosphere. A 3-mL aliquot of the red-orange solution was transferred to a 1-cm quartz cuvette equipped with a Schlenk adapter (under an argon atmosphere). The redox titrations were carried out by adding the increments of an electron donor (tetraarylethylenes and tetraarylbenzidine) dissolved in dichloromethane to the above solution of $THE^{+\bullet}$; and the accompanied color changes were monitored by UV-vis-NIR spectroscopy.

1 (2.07 mM) + **THE**$^{+\bullet}$ $SbCl_6^-$ (95 uM) → **1**$^{+\bullet}$ $SbCl_6^-$ + **THE**^{0}

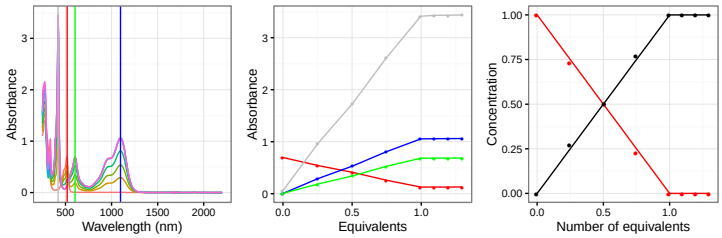

2 (1.93 mM) + **THE**$^{+\bullet}$ $SbCl_6^-$ (94 uM) → **2**$^{+\bullet}$ $SbCl_6^-$ + **THE**^{0}

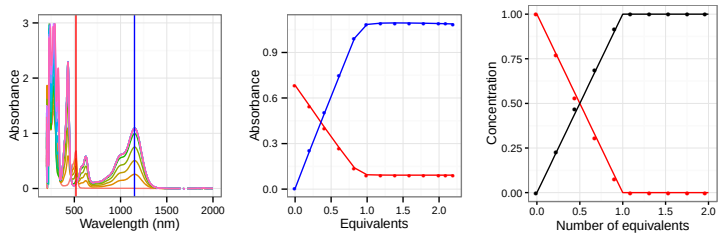

3 (2.67 mM) + **NAP**$^{+\bullet}$ $SbCl_6^-$ (85 uM) → **3**$^{+\bullet}$ $SbCl_6^-$ + **NAP**^{0}

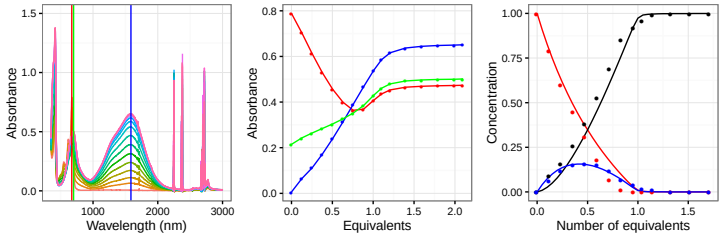

4 (2.67 mM) + **NAP**$^{+\bullet}$ $SbCl_6^-$ (85 uM) → **4**$^{+\bullet}$ $SbCl_6^-$ + **NAP**^{0}

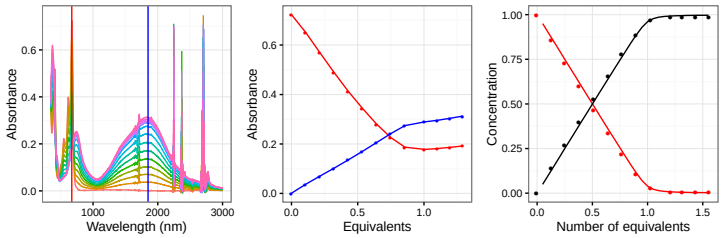

5 (1.64 mM) + **NAP**$^{+\bullet}$ $SbCl_6^-$ (76 uM) → **5**$^{+\bullet}$ $SbCl_6^-$ + **NAP**^{0}

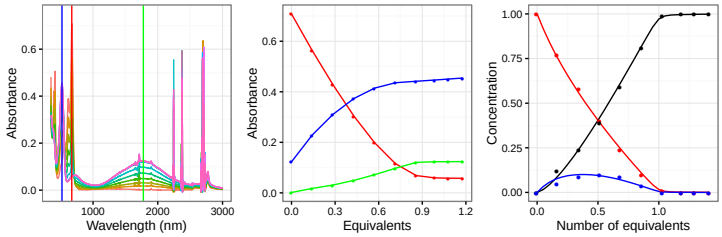

(continued on the next page)

6 (1.54 mM) + **NAP**$^{+\bullet}$ $SbCl_6^-$ (59 uM) → **6**$^{+\bullet}$ $SbCl_6^-$ + **NAP**^{0}

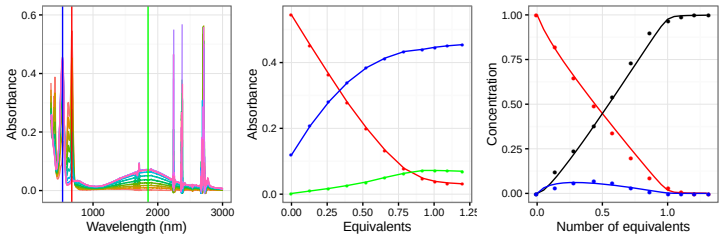

7 (3.18 mM) + **NAP**$^{+\bullet}$ $SbCl_6^-$ (104 uM) → **7**$^{+\bullet}$ $SbCl_6^-$ + **NAP**^{0}

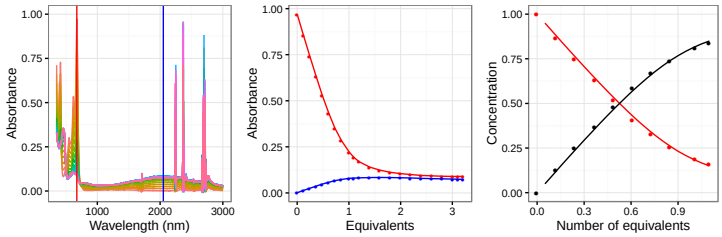

Figure 2. 13. Spectral changes attendant upon the reduction of **1**-**7**, as indicated, (see panel titles for the stock solution concentrations) by **THE**$^{+\bullet}$ $SbCl_6^-$ or **NAP**$^{+\bullet}$ $SbCl_6^-$ in CH_2Cl_2 at 22 ºC.

Note that in cases of large linkers (i.e. **3**$^{+\bullet}$, **5**$^{+\bullet}$, and **6**$^{+\bullet}$), 15%, 10% and 7% of an additional species were identified by spectral deconvolution, which were attributed to the corresponding rearranged dications. Note that formation of these rearranged dicationic species was reversible as they disappeared upon addition of excess neutral biaryl, and thus do not interfere in accurate determination of the spectroscopic characteristics of biaryl cation radicals. The identity of these rearranged dicationic species is under investigation.

Crystal data and structure refinement

Generation and crystallization of cation radicals salts: A 25 mL Schlenk tube was charged with nitrosonium hexachloroantimonate (44 mg, 0.12 mmol), and a cold solution of **1** or **3** (0.12 mmol) in anhydrous dichloromethane (5 mL) was added under an argon atmosphere at -10 ºC. The solution was stirred while slowly bubbling argon through the solution to entrain gaseous NO for 5 min to yield a dark-colored solution of the corresponding cation radical. The resulting cation radical solution was carefully layered with dry toluene (10 mL) and placed in a refrigerator (-10 ºC) which after 2 days produced single crystals suitable for X-ray structure analysis.

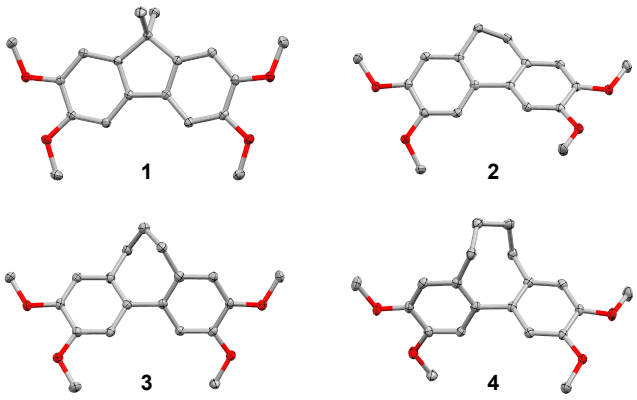

Figure 2. 14. ORTEP diagrams (50% probability) of **1**-**4**.

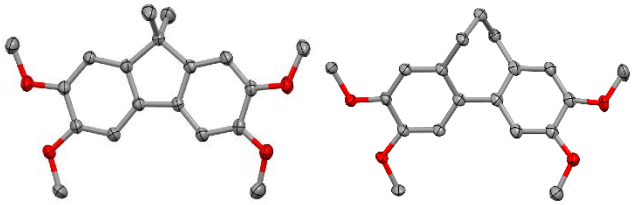

$1^{+\bullet}$ **$3^{+\bullet}$**

Figure 2. 15. ORTEP diagrams (50% probability) of **$1^{+\bullet}$** and **$3^{+\bullet}$**.

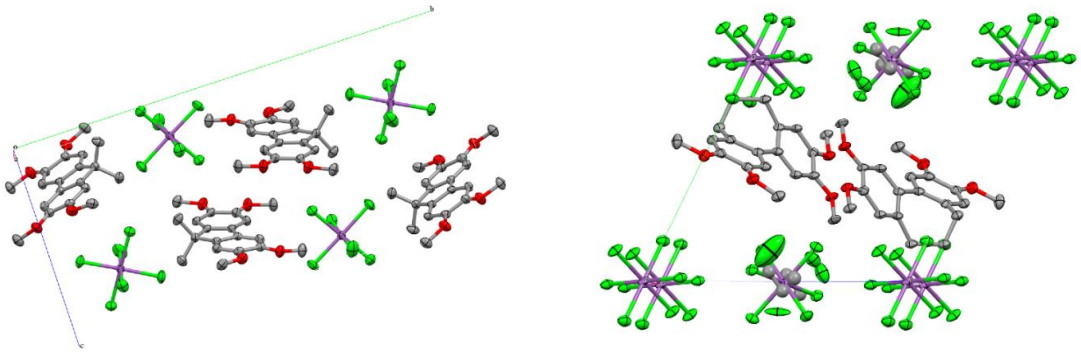

Figure 2. 16. Crystal packing diagrams of $\mathbf{1}^{+\bullet}$ (left) and $\mathbf{3}^{+\bullet}$ (right) together with counteranion (i.e. $SbCl_6^-$) and disordered CH_2Cl_2 molecules.

Table 2. 6. Crystal data and structure refinement for **1**.

Identification code	raj2g	
Empirical formula	C21 H25 N O4	
Formula weight	355.42	
Temperature	100(2) K	
Wavelength	0.71073 Å	
Crystal system	Monoclinic	
Space group	P 21/c	
Unit cell dimensions	a = 17.284(2) Å	a= 90°.
	b = 7.1576(9) Å	b= 118.787(2)°.
	c = 17.852(2) Å	g = 90°.
Volume	1935.5(4) $Å^3$	
Z	4	
Density (calculated)	1.220 Mg/m^3	
Absorption coefficient	0.084 mm^{-1}	
F(000)	760	
Crystal size	0.60 x 0.25 x 0.15 mm^3	
Theta range for data collection	1.34 to 31.88°.	
Index ranges	-25<=h<=22, 0<=k<=10, 0<=l<=26	
Reflections collected	31716	
Independent reflections	6334 [R(int) = 0.0280]	

Completeness to theta = 25.00°	99.8 %
Absorption correction	Semi-empirical from equivalents
Max. and min. transmission	0.989 and 0.950
Refinement method	Full-matrix least-squares on F^2
Data / restraints / parameters	6334 / 0 / 335
Goodness-of-fit on F^2	1.028
Final R indices [I>2sigma(I)]	R1 = 0.0423, wR2 = 0.1158
R indices (all data)	R1 = 0.0523, wR2 = 0.1229
Largest diff. peak and hole	0.460 and -0.225 e.$Å^{-3}$

Table 2. 7. Crystal data and structure refinement for **2**.

Identification code	raj9sa	
Empirical formula	C18 H20 O4	
Formula weight	300.34	
Temperature	100(2) K	
Wavelength	1.54178 Å	
Crystal system	Orthorhombic	
Space group	P 21 21 21	
Unit cell dimensions	a = 7.48390(10) Å	a= 90°.
	b = 8.79450(10) Å	b= 90°.
	c = 22.7959(3) Å	g = 90°.
Volume	1500.36(3) $Å^3$	
Z	4	
Density (calculated)	1.330 Mg/m^3	
Absorption coefficient	0.759 mm^{-1}	
F(000)	640	
Crystal size	0.66 x 0.35 x 0.22 mm^3	
Theta range for data collection	3.88 to 67.17°.	
Index ranges	-8<=h<=8, 0<=k<=10, 0<=l<=26	
Reflections collected	12583	
Independent reflections	2627 [R(int) = 0.0226]	
Completeness to theta = 67.17°	98.9 %	

Absorption correction	Numerical
Max. and min. transmission	0.8508 and 0.6342
Refinement method	Full-matrix least-squares on F^2
Data / restraints / parameters	2627 / 0 / 280
Goodness-of-fit on F^2	0.990
Final R indices [I>2sigma(I)]	R1 = 0.0244, wR2 = 0.0658
R indices (all data)	R1 = 0.0252, wR2 = 0.0666
Absolute structure parameter	0.07(14)
Extinction coefficient	0.0015(3)
Largest diff. peak and hole	0.159 and -0.125 e.$Å^{-3}$

Table 2. 8. Crystal data and structure refinement for **3**.

Identification code	raj7i	
Empirical formula	C19 H22 O4	
Formula weight	314.37	
Temperature	100(2) K	
Wavelength	1.54178 Å	
Crystal system	Orthorhombic	
Space group	P n a 21	
Unit cell dimensions	a = 18.4276(2) Å	a= 90°.
	b = 9.23800(10) Å	b= 90°.
	c = 18.8820(2) Å	g = 90°.
Volume	3214.36(6) $Å^3$	
Z	8	
Density (calculated)	1.299 Mg/m^3	
Absorption coefficient	0.731 mm^{-1}	
F(000)	1344	
Crystal size	0.35 x 0.25 x 0.15 mm^3	
Theta range for data collection	4.68 to 66.98°.	
Index ranges	0<=h<=21, 0<=k<=11, 0<=l<=21	
Reflections collected	26579	
Independent reflections	2889 [R(int) = 0.0177]	
Completeness to theta = 66.98°	97.7 %	

Absorption correction	Semi-empirical from equivalents
Max. and min. transmission	0.8982 and 0.7839
Refinement method	Full-matrix least-squares on F^2
Data / restraints / parameters	2889 / 1 / 415
Goodness-of-fit on F^2	0.994
Final R indices [I>2sigma(I)]	R1 = 0.0542, wR2 = 0.1369
R indices (all data)	R1 = 0.0546, wR2 = 0.1376
Absolute structure parameter	0.1(2)
Largest diff. peak and hole	0.768 and -0.218 e.$Å^{-3}$

Table 2. 9. Crystal data and structure refinement for **4**.

Identification code	raj9x	
Empirical formula	C20 H24 O4	
Formula weight	328.39	
Temperature	100(2) K	
Wavelength	1.54178 Å	
Crystal system	Monoclinic	
Space group	P 21/c	
Unit cell dimensions	a = 9.7582(3) Å	a= 90°.
	b = 16.5351(5) Å	b= 92.560(2)°.
	c = 21.8816(7) Å	g = 90°.
Volume	3527.13(19) $Å^3$	
Z	8	
Density (calculated)	1.237 Mg/m^3	
Absorption coefficient	0.687 mm^{-1}	
F(000)	1408	
Crystal size	0.60 x 0.19 x 0.12 mm^3	
Theta range for data collection	3.35 to 67.18°.	
Index ranges	-11<=h<=11, 0<=k<=19, 0<=l<=25	
Reflections collected	28526	
Independent reflections	5984 [R(int) = 0.0177]	

Completeness to theta = 68.00°	99.8 %
Absorption correction	Semi-empirical from equivalents
Max. and min. transmission	0.9221 and 0.6832
Refinement method	Full-matrix least-squares on F^2
Data / restraints / parameters	5984 / 0 / 626
Goodness-of-fit on F^2	1.029
Final R indices [I>2sigma(I)]	R1 = 0.0312, wR2 = 0.0784
R indices (all data)	R1 = 0.0347, wR2 = 0.0804
Extinction coefficient	0.00054(7)
Largest diff. peak and hole	0.280 and -0.153 e.$Å^{-3}$

Table 2. 10. Crystal data and structure refinement for $\mathbf{1}^{+\bullet}$.

Identification code	raj1p	
Empirical formula	C19 H22 Cl6 O4 Sb	
Formula weight	648.82	
Temperature	100(2) K	
Wavelength	0.71073 Å	
Crystal system	Monoclinic	
Space group	P 21/n	
Unit cell dimensions	a = 8.440(4) Å	a= 90°.
	b = 24.795(11) Å	b= 97.684(7)°.
	c = 12.131(5) Å	g = 90°.
Volume	2516(2) $Å^3$	
Z	4	
Density (calculated)	1.713 Mg/m^3	
Absorption coefficient	1.757 mm^{-1}	
F(000)	1284	
Crystal size	0.20 x 0.15 x 0.08 mm^3	
Theta range for data collection	1.64 to 31.85°.	
Index ranges	-12<=h<=12, 0<=k<=36, 0<=l<=17	
Reflections collected	29955	
Independent reflections	8044 [R(int) = 0.0566]	

Completeness to theta = 25.00°	99.8 %
Absorption correction	Semi-empirical from equivalents
Max. and min. transmission	0.8722 and 0.7202
Refinement method	Full-matrix least-squares on F^2
Data / restraints / parameters	8044 / 0 / 271
Goodness-of-fit on F^2	1.073
Final R indices [I>2sigma(I)]	R1 = 0.0619, wR2 = 0.1392
R indices (all data)	R1 = 0.0868, wR2 = 0.1479
Largest diff. peak and hole	1.957 and -2.322 e.$Å^{-3}$

Table 2. 11. Crystal data and structure refinement for $\mathbf{3}^{+\bullet}$.

Identification code	raj10n	
Empirical formula	C19.50 H23 Cl7 O4 Sb	
Formula weight	691.28	
Temperature	100(2) K	
Wavelength	1.54178 Å	
Crystal system	Triclinic	
Space group	P -1	
Unit cell dimensions	a = 10.1459(4) Å	a= 64.055(2)°.
	b = 11.9103(5) Å	b= 81.580(2)°.
	c = 12.4173(5) Å	g = 75.636(2)°.
Volume	1305.87(9) $Å^3$	
Z	2	
Density (calculated)	1.758 Mg/m^3	
Absorption coefficient	15.187 mm^{-1}	
F(000)	684	
Crystal size	0.40 x 0.20 x 0.10 mm^3	
Theta range for data collection	4.22 to 67.44°.	
Index ranges	-11<=h<=11, -12<=k<=14, 0<=l<=14	
Reflections collected	4258	
Independent reflections	4258 [R(int) = 0.0494]	
Completeness to theta = 67.44°	98.6 %	

Absorption correction	Numerical
Max. and min. transmission	0.3120 and 0.0644
Refinement method	Full-matrix least-squares on F^2
Data / restraints / parameters	4258 / 3 / 324
Goodness-of-fit on F^2	0.991
Final R indices [I>2sigma(I)]	R1 = 0.0392, wR2 = 0.1090
R indices (all data)	R1 = 0.0404, wR2 = 0.1101
Extinction coefficient	0.00043(12)
Largest diff. peak and hole	1.653 and -1.076 e.$Å^{-3}$

Analysis of the NMR chemical shifts of 2,2'-protons of 1-7

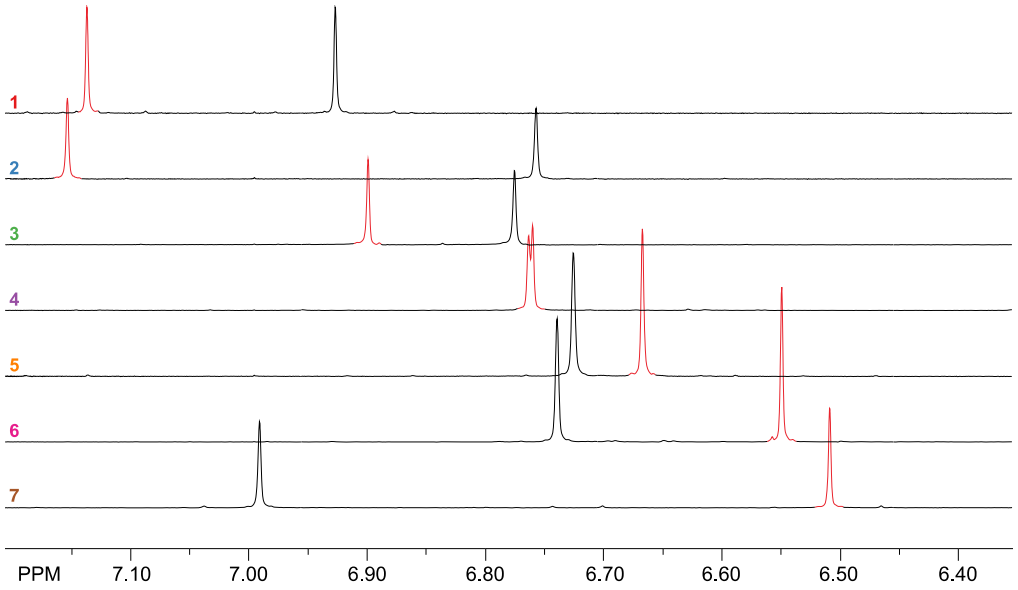

Figure 2. 17. ^{1}H NMR spectra of **1-7** showing the chemical shifts of aromatic protons. The chemical shifts of 2,2'-protons are marked by red color.

Table 2. 12. Comparison of the ^{1}H NMR chemical shifts and calculated chemical shieldings of 2,2'-protons of all identified conformers of **1-7** as well as relative free energies of these conformers

Name	δ(NMR), ppm	Δ*G*, kcal/mol	δ(2),[a] ppm	δ(2'),[a] ppm	δ(DFT),[b] ppm	δ(DFT,scaled),[c] ppm
1	7.14	0.0	24.21	24.21	24.21	7.14
2	7.16	0.0	24.21	24.21	24.21	7.14
3	6.90	0.0	24.50	24.50	24.50	6.92
4	6.76	8.3	24.57	24.93	24.75	6.73
		0.0	24.71	24.71	24.71	6.76
5	6.67	0.0	24.77	24.89	24.83	6.67
		3.9	24.90	24.90	24.90	6.62
		1.6	24.86	24.88	24.87	6.64
6	6.55	0.0	24.96	24.96	24.96	6.57
		2.9	24.86	24.85	24.86	6.65
		2.8	24.80	24.80	24.80	6.69
		5.2	24.82	24.82	24.82	6.67
		4.1	24.82	24.82	24.82	6.67
		6.7	24.76	24.76	24.76	6.72
		10.4	24.78	24.76	24.77	6.71
		13.8	24.84	25.13	24.99	6.55
7	6.50	0.0	25.08	25.09	25.09	6.47

[a] Calculated chemical shieldings of the 2,2'-protons;
[b] Average of δ(2) and δ(2');
[c] Calculated chemical shieldings, scaled according to the linear trend with ^{1}H NMR chemical shifts in Figure 2.2 A, i.e. δ(DFT, scaled) = 25.417-0.75514*δ(DFT).

Computational Details

Electronic structure calculations were performed with the Gaussian 09 package, revision D01.[13] For the density functional theory (DFT) calculations we used calibrated (see Ref. [14] for details, also see refs [12,15-18]) B1LYP functional[19] that contains 40% contribution of the exact exchange with 6-31G(d) basis set by Pople and co-workers.[20] Solvent effects were included using the implicit integral equation formalism polarizable continuum model (IEF-PCM, also referred as PCM)[21-25] with the dichloromethane solvent parameters (ε = 8.93). In all DFT calculations, ultrafine Lebedev's grid was used

with 99 radial shells per atom and 590 angular points in each shell. For the cation radical calculations, wave function stability tests[26,27] was performed to ensure absence of solutions with lower energy. The values of $<S^2>$ operator after spin annihilation were confirmed to be close to the expectation value of 0.75, thus indicating that spin contamination was not an issue for the performed calculations. Atomic charges were calculated using Natural Population Analysis approach,[28] which is a part of the Natural Bond Orbital analysis.[29] Tight cutoffs on forces and atomic displacement were used to determine convergence in geometry optimization procedure. Hessians were calculated for the optimized structures of all neutral and cation radicals to confirm absence of imaginary frequencies. Free energies were computed within harmonic oscillator approximation for T = 298.15 K and P = 1 atm.

Electronic excitation energies were calculated using the time-dependent density functional theory (TD-DFT).[27,30-35] The gauge-independent atomic orbital (GIAO) method[36] was employed for 1H NMR shift calculations;[37] isotropic shielding constants were calculated using the B1LYP-40 functional and polarization-consistent pcS-2 basis set by Jensen.[38] The initial conformations of **3-6** were obtained using ChemAxon Marvin (conformers plugin) conformer generator,[39] which utilizes molecular mechanics calculations.[40] After the removal of duplicates, the conformer structures were optimized by the RM1 method[41] using MOPAC2009[42] and then by the DFT calculations at the B1LYP-40/6-31G(d)+PCM(CH2Cl2) level.

Excitation energies of 3,4,3',4'-tetramethoxybiphenyl as function of the dihedral angle between aryl groups (φ) was performed for the values of φ from 0º to 90º with a

step size of 5°. For every scan point (i.e. for every value of φ), a constrained optimization was performed with all fixed dihedral angles. The optimized geometries/electronic structures were subjected to the stability test (see above) and TD-DFT calculations.

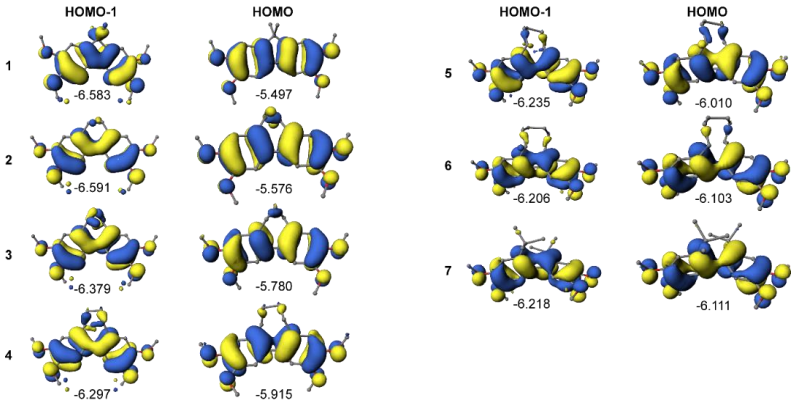

Figure 2. 18. The isovalue (±0.03 a.u.) plots and orbital energies of HOMO and HOMO-1 of **1**-**7** [B1LYP-40/6-31G(d)+PCM (CH_2Cl_2)].

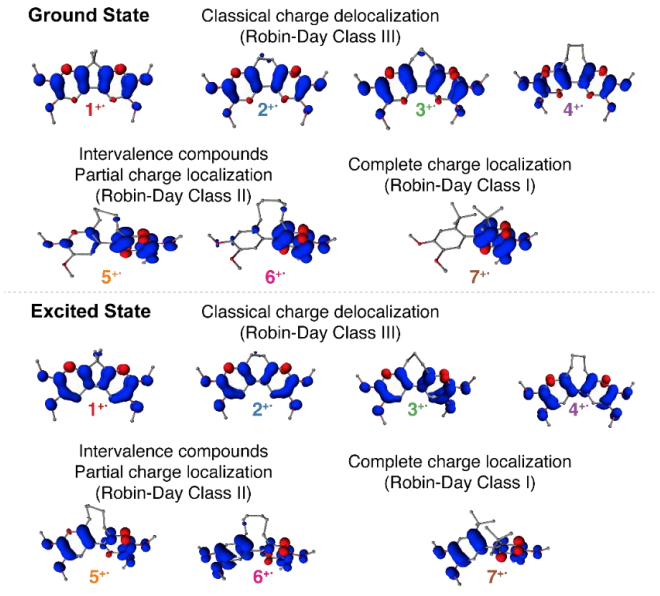

Figure 2. 19. The isovalue (±0.003 a.u.) plots of spin density of $\mathbf{1}^{+\bullet}$-$\mathbf{7}^{+\bullet}$ in their ground (D_0) and excited (D_1) states [B1LYP-40/6-31G(d)+PCM (CH_2Cl_2)].

$1^{+\bullet}$

Excited State 1: 2.030-?Sym 1.3633 eV 909.46 nm f=0.2319 <S**2>=0.780

84A -> 85A -0.13867

81B -> 84B 0.11538

83B -> 84B 0.97781

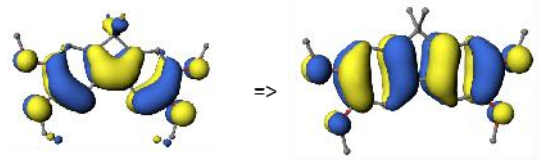

83B **84B**

$2^{+\bullet}$:

Excited State 1: 2.021-?Sym 1.2761 eV 971.61 nm f=0.2415 <S**2>=0.771

80A -> 81A 0.13383

77B -> 80B 0.10949

79B -> 80B 0.98020

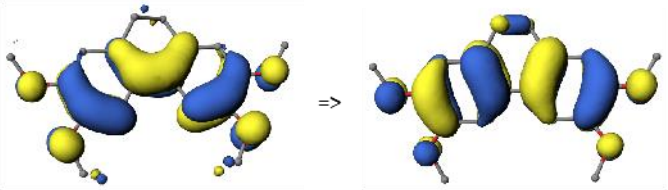

79B **80B**

$3^{+\bullet}$

Excited State 1: 2.013-?Sym 0.9078 eV **1365.75** nm f=0.1950 <S**2>=0.763

81B -> 84B 0.11016

83B -> 84B 0.98645

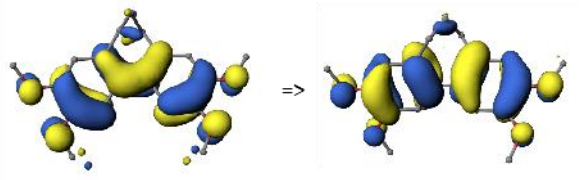

83B **84B**

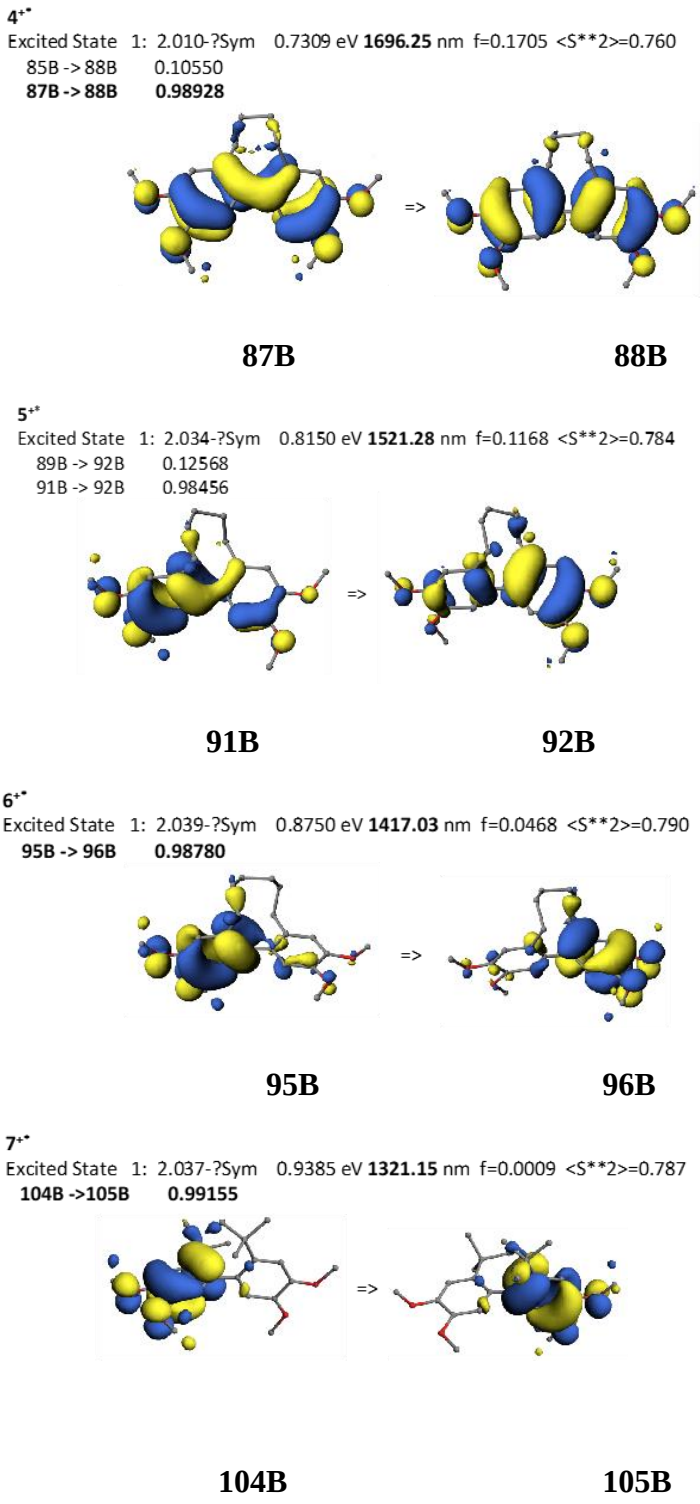

Figure 2. 20. Showing the nature of the $D_0 \rightarrow D_1$ electronic transition in $\mathbf{1}^{+\bullet}$-$\mathbf{7}^{+\bullet}$ as well as the isovalue plots (±0.03 a.u.) of the most relevant orbitals.

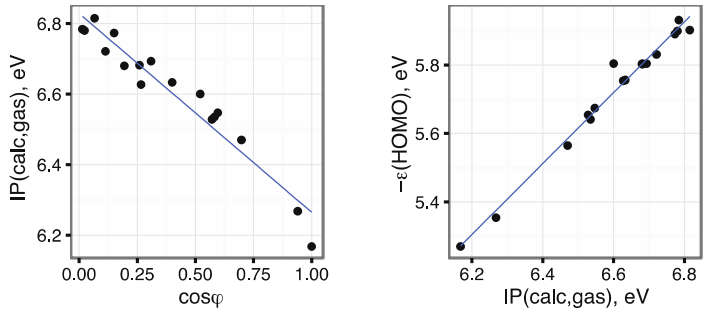

Figure 2. 21. Left: Showing the linear correlation between the calculated [B1LYP-40/6-31G(d)+PCM(CH2Cl2)] gas-phase ionization potentials of identified conformers of **1**-**7**, listed in Tables S10/S11, and cos φ_{CR} in the full range of angles from 0º to 90º. Right: Showing the linear correlation between the energies of highest occupied molecular orbitals of identified conformers of **1**-**7** and their ionization potentials.

CHAPTER 3

Hexa-peri-hexabenzocoronene-fluorene hybrid: A platform for highly soluble, easily functionalizable HBCs with expanded graphitic core

Abstract: Materials based upon hexa-*peri*-hexabenzocoronenes (**HBC**s) show significant promise in a variety of photovoltaic applications. There remains the need, however, for a soluble, versatile, **HBC**-based platform, which can be tailored via incorporation of electro-active groups or groups that can prompt self-assembly. Herein, we report the successful synthesis of a new **HBC**-fluorene hybrid with expanded graphitic core that is highly soluble, resists aggregation, and can be readily functionalized at its vertices. We also show that this new **HBC** platform can be tailored to incorporate six electro-active groups at its vertices, as exemplified by a facile synthesis of a representative hexaaryl derivative of ***F*HBC**. Synthesis of new ***F*HBC** derivatives, containing electro-active functional groups which can allow controlled self-assembly, may serve as potential long range charge-transfer materials for photovoltaic applications.

Disclaimer: The results discussed in this chapters were further supplimented by DFT calculations and relevant computational works by my coworkers Dr. Maxim V. Ivanov. My contribution to this chapter is limited to synthesis of various molecules and spectroscopic studies with my co–worker Dr. Tushar S Navale.

INTRODUCTION

Hexa-*peri*-hexabenzocoronenes (**HBC**s) are promising materials for application in thin film electronic devices, field effect transistors, and photovoltaic applications.[1,2] Indeed, the design and synthesis of improved **HBC**s continues to garner tremendous attention,[3] as expanding the size of the flat π-conjugated graphitic core is expected to result in high charge carrier mobility.[4,5] While the parent **HBC** (**Figure 3.1**) can be readily accessed via oxidative cyclodehydrogenation of hexaphenyl-benzene, it is insoluble in common organic solvents.[5,6] **HBC**s incorporating alkyl groups at the vertices (^{R}**HBC**, **Figure 3.1**) display improved solubility, yet often form aggregates in solution, as evidenced by broadened signals in their $^{1}H/^{13}C$ NMR spectra at ambient temperatures.[7,8] Unfortunately, the incorporation of solubilizing groups at the vertices of **HBC**s restrict their further functionalization with desired electro-active groups.

To address this issue, we will show that incorporating six fluorene rings, substituted with solubilizing groups at their C9 methylenes, into the 'bay areas' of the parent **HBC** core produces a hybrid structure that eliminates the issues plaguing **HBC** (see **Figure 3.1**). Specifically, the hybrid structure provides (i) an expanded graphitic core, (ii) increased solubility, and (iii) contains unsubstituted vertices for subsequent functionalization (*vide infra*). Accordingly, we describe the successful synthesis of a highly-soluble **HBC**–fluorene hybrid, hereafter referred to as **FHBC**, and show that it can be readily functionalized at all six vertices (**Figure 3.1**). We will also show that expansion of the graphitic core of **HBC** affords multiple (reversible) 1-e^- oxidation, producing a stable, non-aggregated cation-radical salt in solution. The successful synthesis of this new, readily functionalizable graphitic platform detailed here, offers potential for the design

and syntheses of next-generation materials for applications in modern photovoltaic devices.

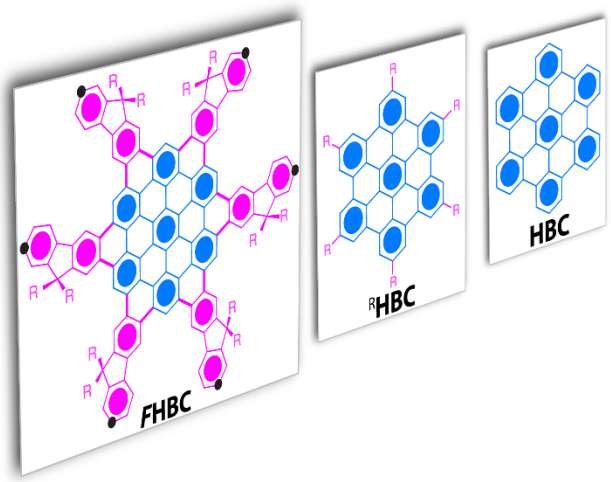

Figure 3. 1. A comparison of the relative sizes of the parent **HBC**, **HBC** functionalized at its vertices with solubilizing groups (e.g. R = *n*-alkyl or *tert*-butyl), and newly designed **HBC**–fluorene hybrid (***F*HBC**, R = *n*-alkyl) with provisions for both solubility and sites for on-demand functionalization (indicated by black dots).

RESULTS AND DISCUSSION

The strategy for the preparation of ***F*HBC** involves an oxidative cyclodehydrogenation of a hexaphenylbenzene derivative **5,** in which alternate phenyl groups (i.e. 1,3,5 phenyls) are functionalized with two fluorenyl rings (**Scheme 3.1**). Initially, we attempted to access **5** via the selective conversion of readily available *hexakis*(4-bromophenyl)benzene[9] (**1**) to a symmetrical 1,3,5-TMS derivative **2** by lithiation with ^{t}BuLi at -90 ^{o}C followed by reaction with TMSCl.[10,11] Although **2** was easily prepared in high yield, a series of functional group transformations onto **2** (**Scheme 3.1**) returned the desired hexabromo derivative **4** in meager yield, largely due to the poor

solubility of **4** and its precursors. The solubility issues forced us to abandon this route for accessing ***F*HBC** (see **Scheme 3.1** and **Scheme 3.2** and Experimental section for additional details).

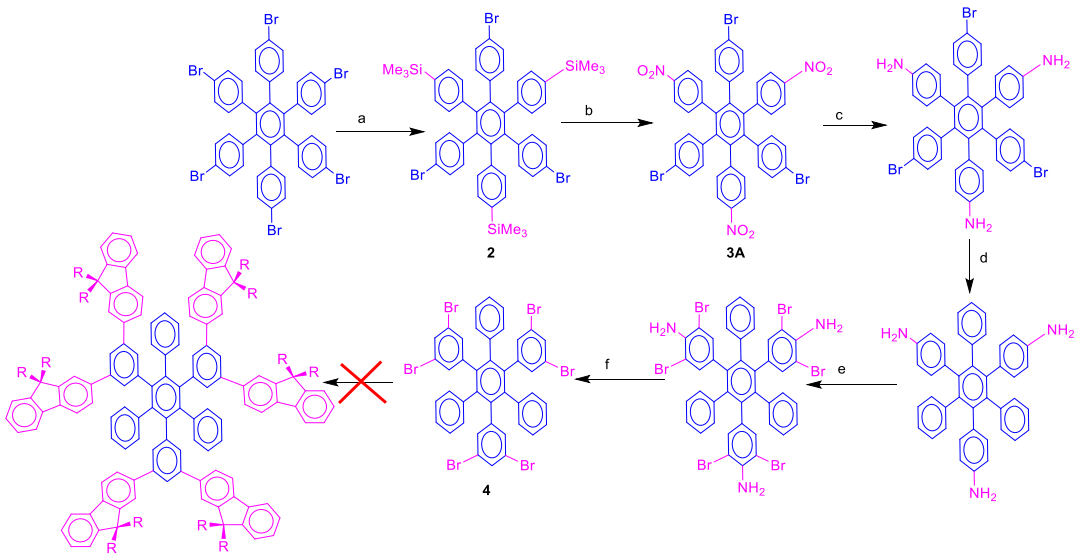

Scheme 3. 1: Two different synthetic approaches for the preparation of ***F*HBC**. **a**. i) *t*BuLi (6 equiv)/-90°C; ii) Me_3SiCl/-90°C, yield: 76%. **b**. 70% HNO_3/Ac_2O/80 °C, yield: 40%. **c.** (i) Sn/HCl/DME/90 °C**, yield:** 74**%**; d. $Pd(OAc)_2/PPh_3$/aq K_2CO_3/***n***-butanol/100 °C, yield: 68%. **e**. aq. HBr (48%)/H_2O_2 **(30%)**/THF/ H_20, yield: ~76%. **f**. i) $NaNO_2/H_2SO_4$; ii) H_3PO_2, produced a highly insoluble mixture of products which could not be fully characterized.

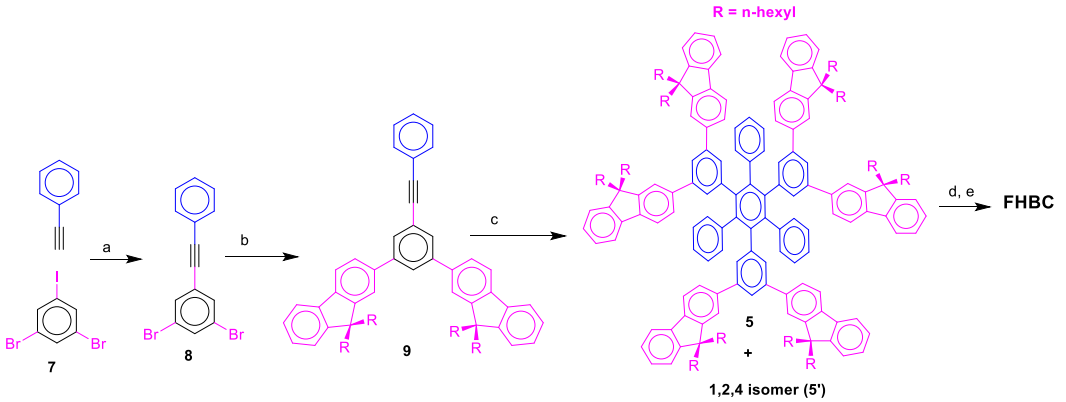

Scheme 3. 2: a. $PdCl_2(PPh_3)_2$/CuI/diisopropylamine/40 °C/4h, yield: 97%. **b**. 9,9-dihexylfluorene-2-boronic acid pinacol ester/$Pd(PPh_3)_4$/aq. K_2CO_3/ ethanol/toluene/ reflux/24h, yield: 89%. **c**. $Co_2(CO)_8$/p-dioxane/ reflux/14h, Yield: ~96%. **d**. DDQ (22

equiv)/CH_2Cl_2-CH_3SO_3H (9:1) mixture/0 ^oC/6h, yield: 28% (after chromatographic purification). **e**. $FeCl_3$ (100 equiv)/ CH_2Cl_2/CH_3NO_2/22 ^oC, yield: 18%.

In an alternative strategy, **5** could be prepared as an isomeric mixture in 3 simple steps (**Scheme 3.2**), via a practical if non-elegant route. First, a Sonogashira coupling of phenylacetylene (**6**) with readily-available 1,3-dibromo-5-iodobenzene[12] (**7**) returned alkyne **8** in excellent yield. A 2-fold Pd-catalyzed Suzuki coupling of **8** with 9,9-dihexylfluorene-2-boronic acid afforded alkyne derivative **9** in 86% yield in two steps. Finally, a $Co_2(CO)_8$-catalyzed cyclotrimerization of **9** afforded **5** (1,3,5-isomer) and **5'** (1,2,4-isomer) as a statistical mixture[13] in nearly quantitative yield (**Scheme 3.2**). Repeated attempts to separate highly soluble isomeric mixture of **5**/**5'**, using flash chromatography and fractional crystallizations, were unsuccessful.

We subjected the isomeric mixture of **5**/**5'** to oxidative cyclodehydrogenation, using $FeCl_3$ as an oxidant, which afforded a deep-red solid. A chromatographic purification of the red-solid using hexanes as eluents easily separated ***F*HBC** as an orange-red microcrystalline solid in 18% yield.[14] A much higher yield and purer ***F*HBC** (28%) was obtained by oxidative cyclodehydrogenation of **5**/**5'**, using our recently developed procedure with [DDQ/acid] as an oxidant system in CH_2Cl_2.[15,16] Note that oxidative cyclodehydrogenation of only **5** (1,3,5 isomer) can produce ***F*HBC**, and as the isomeric mixture of **5**/**5'** contains only ~33% of **5**, use of [DDQ/acid][15,16] as oxidant produces a nearly quantitative yield of ***F*HBC**.

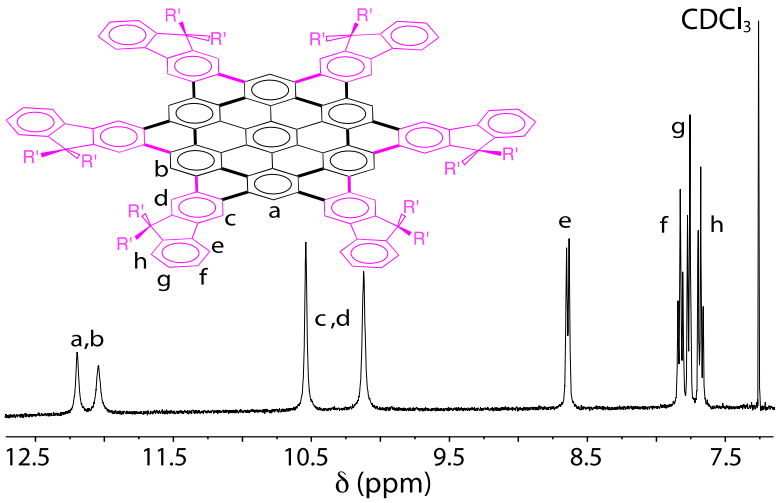

Figure 3. 2. Partial ^{1}H NMR spectrum of 10 mM ***F*HBC** in $CDCl_3$ at 22 ^{o}C showing well-resolved resonances for equivalent aromatic protons (labeled).

The **HBC**-*fluorene* hybrid (***F*HBC**) was found to be highly soluble in common organic solvents, such as hexanes, CH_2Cl_2, $CHCl_3$, THF, DMF, etc., and its structure was established by ^{1}H/^{13}C NMR spectroscopy and MALDI-TOF mass spectrometry (see experimental Information). A ^{1}H NMR spectrum of ***F*HBC** in $CDCl_3$ showed well-resolved resonances for all unique protons, indicating minimal or no aggregation at ambient temperatures (**Figure 3.2**). This is distinct from the solution-phase NMR spectra of other **HBC**s, which generally show broad signals owing to extensive aggregation.[7,8]

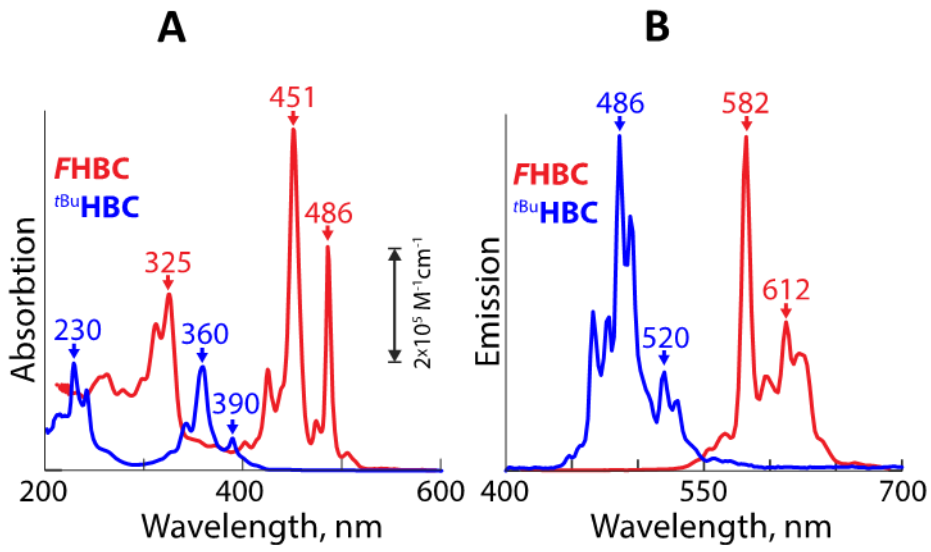

Figure 3. 3. A. Comparison of the UV-vis absorption (10^{-6} M) and **B.** emission spectra of **FHBC** (red) and **tBuHBC** (blue) in CH_2Cl_2 at 22 °C.

The UV-visible absorption spectrum of ***F*HBC** is compared with well-known $^{t\text{Bu}}$**HBC** [6,17] in CH_2Cl_2 in **Figure 3.3 A**. Each shows characteristic well-resolved vibronic structure; however, the significant expansion of the graphitic core in ***F*HBC**, leads to a large red shift (by ~90 nm) of its absorption bands (325, 451, and 486 nm; ε_{451} = 6.0 x 10^5 $M^{-1}cm^{-1}$) and increased molar absorptivity compared to $^{t\text{Bu}}$**HBC** (230, 360, and 390 nm; ε_{360} = 1.9 x 10^5 $M^{-1}cm^{-1}$). Normalized emission spectra of ***F*HBC** and $^{t\text{Bu}}$**HBC**, at the same concentrations, **Figure 3.3.B**, show a red-shift of the emission bands of ***F*HBC** (582, 612 nm) compared to $^{t\text{Bu}}$**HBC** (486, 520 nm). At higher concentrations, $^{t\text{Bu}}$**HBC** shows a broad emission (at ~560 nm) indicating aggregate (i.e., dimer) formation.[17] In contrast, the emission spectrum of ***F*HBC** does not show the appearance of a new excimeric band.

Electrochemical analysis showed that ***F*HBC** displays four reversible oxidation waves at 0.40, 0.76, 1.01 and 1.19 V (vs. Fc/Fc^+) corresponding to the formation of

monocation, dication, trication and tetracation, respectively (**Figure 3.4. A**). In contrast, $^{t\text{Bu}}$**HBC** exhibits a single oxidation wave at 0.64 V vs Fc/Fc^{+} in CH_2Cl_2 (see **Figure 3.10**).[6,17] Moreover, the expansion of the size of the graphitic core in ***F*HBC** results in a significant lowering of the first oxidation potential (by ~240 mV) in comparison to $^{t\text{Bu}}$**HBC**.

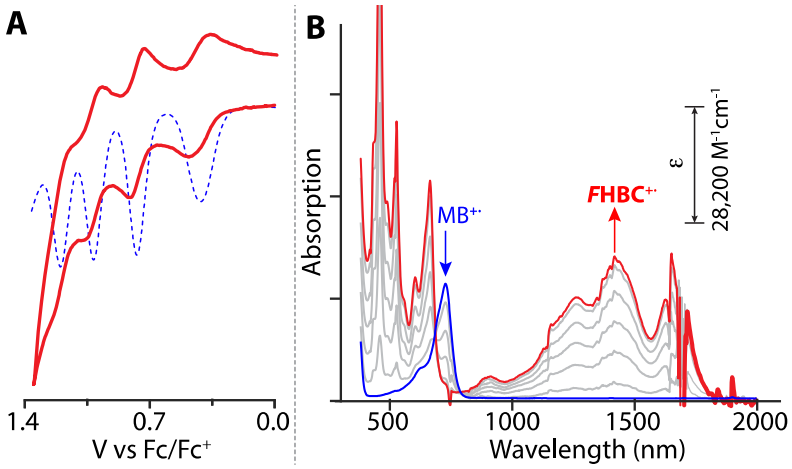

Figure 3. 4. (A) Cyclic (solid red line) and square-wave (dashed blue line) voltammograms of ***F*HBC** (0.63 mM) in CH_2Cl_2 containing 0.2 M *n*-Bu_4NPF_6 at a scan rate of 200 mV s^{-1} and 22 ºC. (B) The spectral changes observed upon the reduction of 5.5 x 10^{-6} M $\mathbf{MB}^{+\bullet}SbCl_6^-$ by an incremental addition of sub-stoichiometric amounts of ***F*HBC** in CH_2Cl_2 at 22 ºC.

The cation radical of ***F*HBC** was generated in solution via quantitative redox titrations using magic blue (i.e., $\mathbf{MB}^{+\bullet}$ or tris-4-bromophenylamminium cation radical, E_{red} = 0.70 V vs Fc/Fc^{+}, λ_{max} = 728 nm, ε_{max} = 28,200 cm^{-1} M^{-1}) as an oxidant.[18,19] The spectrum of $\mathbf{FHBC}^{+\bullet}$ remained unchanged at tenfold higher concentration, as well as in the presence of excess (up to 10 equivalents) neutral ***F*HBC**, suggesting a lack of

aggregation either between the molecules of ***F*HBC**$^{+\bullet}$ or ***F*HBC**$^{+\bullet}$/***F*HBC** in solution. In contrast, $^{t\text{Bu}}$**HBC**$^{+\bullet}$ readily forms a dimeric cation radical in solution, i.e. $^{t\text{Bu}}$**HBC**$^{+\bullet}$ + $^{t\text{Bu}}$**HBC** → [$^{t\text{Bu}}$**HBC**]$_2^{+\bullet}$ with an equilibrium constant K = 1100 M^{-1} (see **Figure 3.5**). Expansion of the chromophoric size of ***F*HBC**$^{+\bullet}$ (λ_{max} = 460, 528, 664, 1261, and 1418 nm, ε_{1418} = 36,000 cm^{-1} M^{-1}) leads to an increased molar absorptivity (by a factor of ~6) when compared to $^{t\text{Bu}}$**HBC**$^{+\bullet}$ (λ_{max} = 550, 836, 1570, 1740, 2100 nm, ε_{2100} = 5700 cm^{-1} M^{-1}), see **Figure 3.13**.[6,17]

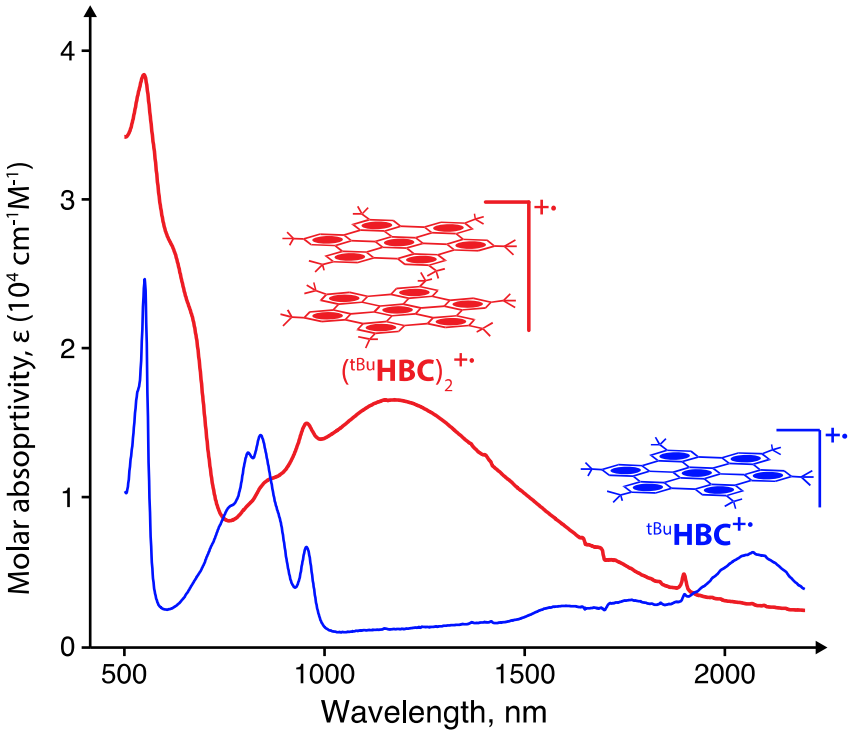

Figure 3. 5. Electronic absorption spectrum of $^{t\text{Bu}}$**HBC**$^{+\bullet}$ (blue) and its spectrum in the presence of neutral $^{t\text{Bu}}$**HBC** (red).[7,8]

Summarizing, while $^{t\text{Bu}}$**HBC** forms aggregates in neutral, excited, and cation radical states, as judged by, respectively, broad NMR spectra, observation of excimeric emission (at ~560 nm),[6,17] and observation of intervalence transition (at 1200 nm)[6,17] in its cation radical spectrum in the presence of neutral $^{t\text{Bu}}$**HBC** (see **Figures 3.4/ 3.6**), such spectroscopic signatures of aggregation were completely absent in the case of ***F*HBC**. A cursory examination of the molecular structures of ***F*HBC** and $^{t\text{Bu}}$**HBC** suggests that the narrow bay areas in ***F*HBC** do not afford arrangement of two hexyl chains in a staggered (sandwich-like) dimer. On the other hand, the relatively wider bay areas in $^{t\text{Bu}}$**HBC** provide sufficient space for smaller methyl groups to be accommodated in a sandwich-like (staggered) dimeric structure (**Figure 3.6.A**).

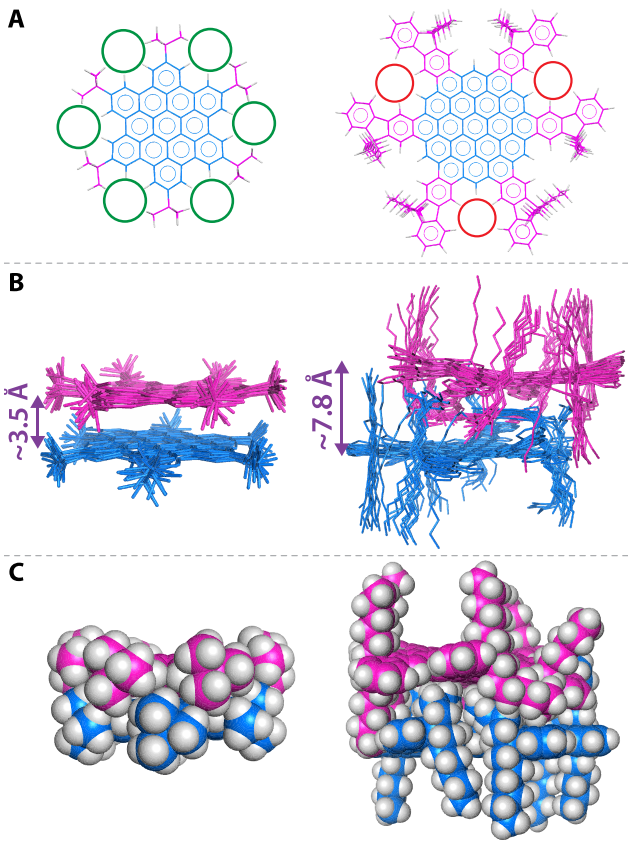

Figure 3. 6. (A) Structures of $^{t\text{Bu}}$**HBC** and ***F*HBC** showing the different sizes of the bay areas with the aid of circles. (B) Superimposed structures of $^{t\text{Bu}}$**HBC** and ***F*HBC** dimers obtained from molecular dynamics simulations (see Supporting Information for details). (C) Space-filling representation of $^{t\text{Bu}}$**HBC** and ***F*HBC** dimers.

As a further probe of the lack of aggregation in ***F*HBC**, we performed (1-ns long) molecular dynamics (MD) simulations at ambient temperature, which showed that neutral $^{t\text{Bu}}$**HBC** indeed forms a stable dimer (with the interplanar separations between the aromatic cores close to van der Waals contact (~3.5 Å), while in dimeric ***F*HBC** the pair of nanographenes lie at a separation of ~7.8 Å (**Figure 3.6 B-C**). Indeed, the presence of the long hexyl chains in ***F*HBC** hinders the approach of the graphitic cores in the dimer in favor of multiple CH-π interactions between the large π-system and alkyl chains (**Figure 3.6 B/C**). It is important to emphasize that access to ***F*HBC** platform, which

resists self aggregation, will open new avenues for the preparation of 2-dimensional extended aggregates via π-π contacts between the outer phenylenes of fluorene moieties that can be functionalized with appropriate groups at its vertices.

Functionalization of ***F*HBC** at its vertices would require access to its hexabromo derivative **7** (**Scheme 3. 8**). Initial attempts of a six-fold bromination of ***F*HBC** in CH_2Cl_2 using bromine resulted in an inseparable mixture of polybrominated products.[20] However, a bromination of the *isomeric mixture* of **5**/**5'** (i.e. the precursor to ***F*HBC**) in CH_2Cl_2 with bromine, in the presence of a catalytic amounts of iodine (in ~4h), afforded isomers **10**/**10'**, appropriately brominated at the desired positions of all fluorenes (**Scheme 3.8**). An oxidative cyclodehydrogenation of this isomeric mixture (**10**/**10'**) using DDQ/acid oxidant system followed by column chromatography returned ***F*HBC**-Br_6 in 26% yield as a dark-red solid (**Scheme 3.9**). The structure of ***F*HBC**-Br_6 was established by $^1H/^{13}C$ NMR spectroscopy and further confirmed by MALDI mass spectrometry (**Figure 3.8**).

As a proof of concept experiment, a six-fold Suzuki coupling of ***F*HBC**-Br_6 with 2,5-dimethoxy-4-methylphenylboronic acid, under standard reaction conditions, afforded ***F*HBC**-Ar_6 as a deep-red solid in 91% yield (**Scheme 3.10**). The structure of ***F*HBC**-Ar_6 was established by $^1H/^{13}C$ NMR spectroscopy and MALDI mass spectrometry. A ^1H NMR spectrum of ***F*HBC**-Ar_6 in $CDCl_3$ showed well-resolved resonances (see Experimental Information) similar to ***F*HBC**.

CONCLUSION

In conclusion, we have developed a highly soluble versatile **HBC** platform (i.e. ***F*HBC**) that contains an expanded graphitic core containing 19 Clar sextets and affords the ready

introduction of multiple electro-active groups at its vertices. This ready tailoring of electro-active groups at vertices of ***F*HBC**, as demonstrated by a facile synthesis of a hexaarylbenzene derivative (i.e. ***F*HBC**-Ar_6), will allow the preparation of molecules with desirable electro-active functional groups suited for controlled assembly to form aggregates with tunable properties such as long-range charge transport for applications in the modern area of photovoltaics.[21,22]

GENERAL EXPERIMENTAL METHODS

FHBCs were synthesized using literature procedures and were characterized by NMR spectroscopy, mass spectrometry, and X-ray crystallography. The reversible cyclic and square-wave voltammograms of **FHBCs** and the corresponding model compounds were recorded by the electrochemical oxidation at a platinum electrode in CH_2Cl_2 containing 0.1 M *n*-Bu_4NPF_6 at 22 ºC at scan rate of 200 mV s^{-1} and were referenced to ferrocene as an added internal standard.

Materials. All reactions were performed under argon atmosphere unless otherwise stated. Anhydrous tetrahydrofuran (THF) was prepared by refluxing commercial tetrahydrofuran over lithium aluminum hydride under an argon atmosphere for 24 hours followed by distillation under an argon atmosphere. It was stored in a Schlenk flask equipped with a Teflon valve fitted with Viton O-rings. Dichloromethane was repeatedly stirred with fresh aliquots of conc. sulfuric acid (~10 % by volume) until

the acid layer remained colorless. After separation, it was washed successively with water, aqueous sodium bicarbonate, water, and aqueous sodium chloride, and dried over anhydrous calcium chloride. The dichloromethane was distilled twice from P_2O_5 under an argon atmosphere and stored in a Schlenk flask equipped with a Teflon valve fitted with Viton O-rings. The hexanes and toluene were distilled from P_2O_5 under an argon atmosphere and then refluxed over calcium hydride (~12 h). After distillation from CaH_2, the solvents were stored in Schlenk flasks under an argon atmosphere. NMR spectra were recorded on 300 and 400 MHz NMR spectrometers.

Synthesis

Synthetic scheme for the preparation of 1,3-dibromo-5-iodobenzene (7).[23] A large-scale synthesis of 1,3-dibromo-5-iodobenzene was accomplished in three high yielding steps from commercially-available 2,6-dibromo-4-nitroaniline (see **Scheme 3.3** below) using standard literature procedures. [23]

Scheme 3. 3: Synthesis of 1,3-dibromo-5-iodobenzene (7)

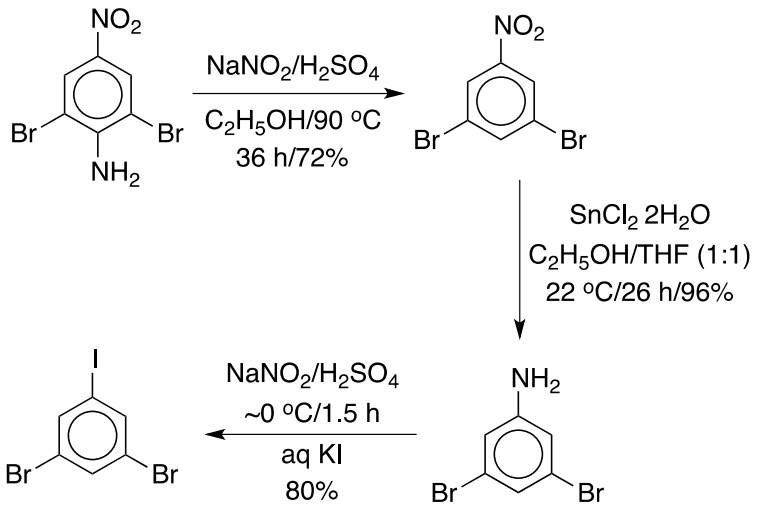

Synthesis of 1,3-dibromo-5-nitrobenzene. To a refluxing solution of 2,6-dibromo-4-nitroaniline (40 g, 135 mmol) in a mixture of ethanol (450 mL) and conc. H_2SO_4 (45 mL) was added solid $NaNO_2$ (30 g, 435 mmol) in small portions (5 g portions over 5 h) to prevent excessive foaming. After all $NaNO_2$ was added, the resulting reaction mixture was stirred at ~90 ^oC for an additional 36 h. The reaction mixture was cooled to room temperature and poured into ice-cold water (500 mL), which then resulted in the precipitation of the product. The solid was filtered using a Buchner funnel and repeatedly washed with water (3 x 100 mL). The crude solid was dissolved in boiling ethanol and cooled to room temperature to crystallize out pure 1,3-dibromo-5-nitrobenzene as orange needles. Yield: 27 g, 72%; mp 95 ^oC; ^1H NMR ($CDCl_3$) δ ppm 7.99 (t, 1H, J = 1.7 Hz), 8.32 (d, 2H, J = 1.7 Hz); ^{13}C NMR ($CDCl_3$) δ ppm 123.68, 125.79, 140.27.

Synthesis of 3,5-dibromophenylamine. To a solution of 1,3-dibromo-5-nitrobenzene (27 g, 96 mmol) in a mixture of THF (200 mL) and ethanol (200 mL) was

added slowly $SnCl_2.2H_2O$ (108 g, 480 mmol) in several portions and the resulting mixture was stirred for 20 h at ambient temperature. The solvent was removed on a rotavap and the resulting semisolid material was treated with aqueous NaOH (2 M, 250 mL), stirred for 2 h, and then extracted with diethyl ether (3 x 100 mL). The combined ether layers were dried over $MgSO_4$, filtered, and evaporated to afford 3,5-dibromophenylamine which was used in the next step without further purification. Yield: 24 g, 96 %; ^{1}H NMR ($CDCl_3$) δ ppm 3.76 (s, 2H), 6.76 (s, 2H), 7.01 (s, 1H).

Synthesis of 1,3-dibromo-5-iodobenzene (7). The 3,5-dibromophenylamine (13 g, 52 mmol), obtained above, was dissolved in conc. H_2SO_4 (100 ml) by stirring in a heated (~50 ^{o}C) water bath. The resulting solution was cooled to ~0 ^{o}C and solid sodium nitrite (7.85 g, 113.9 mmol) was added in small portions with continuous stirring and maintaining the temperature below 5 ^{o}C. The reaction mixture was allowed to stir for an additional 2 h at ~0 ^{o}C and then poured onto ice-cold solution of KI (25 g, 150 mmol) in water (120 mL). The resulting mixture was slowly warmed to room temperature (~1 h) and then heated to ~80 ^{o}C for an additional 15 minutes. The resulting reaction mixture produced a lot of solid which was filtered and washed with cold water (3 x 50 mL). Drying and crystallization of the solid product from ethanol afforded the desired 1,3-dibromo-5-iodobenzene (**7**) in good yield (15 g, 80%). mp 123-124 ^{o}C ; ^{1}H NMR ($CDCl_3$) δ ppm 7.63 (s, 1H), 7.79 (s, 2H); ^{13}C NMR ($CDCl_3$) δ ppm 94.67, 123.58, 133.85, 138.70.

Scheme 3. 4: Synthesis of 1,3-dibromo-5-phenylethynylbenzene (8)[24]

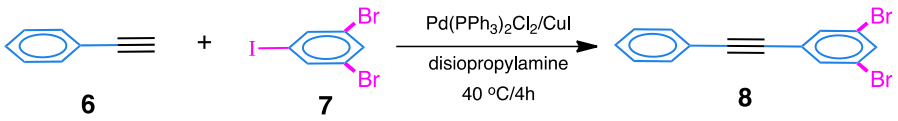

To a solution of 1,3-dibromo-5-iodobenzene (6.0 g, 16.6 mmol) in diisopropylamine (30 mL) was added $PdCl_2(PPh_3)_2$ (0.29 g, 0.40 mmol), CuI (0.08 g, 0.40 mmol), and phenylacetylene (1.82 mL, 16.6 mmol) were added successively at room temperature and under an argon atmosphere. The resulting mixture was stirred at ~40 ^oC (water bath) for 4 h. The mixture was then cooled to room temperature and diluted with hexanes (100 mL). The contents were filtered through a short pad of silica gel and silica pad was washed with hexanes (3 x 25 mL). Evaporation of the solvent *in vacuo* led to an oil which was purified by flash chromatography using a mixture of ethyl acetate and hexanes (1:9) as eluent to afford the pure 1,3-dibromo-5-phenylethynylbenzene (**8**) as a white solid (5.4 g, 97%). mp 106- 108 ^oC; ^1H NMR ($CDCl_3$) δ ppm 7.34-7.40 (m, 3H), 7.49-7.54 (m, 2H), 7.60 (d, 2H, J = 1.78 Hz), 7.63 (t, 1H, J = 1.78 Hz); ^{13}C NMR ($CDCl_3$) δ ppm 86.58, 92.14, 122.42, 122.82, 126.90, 128.67, 129.17, 131.94, 133.17, 134.07.

Scheme 3. 5: Synthesis of 1,3-difluoranyl-5-phenylethynylbenzene (9).

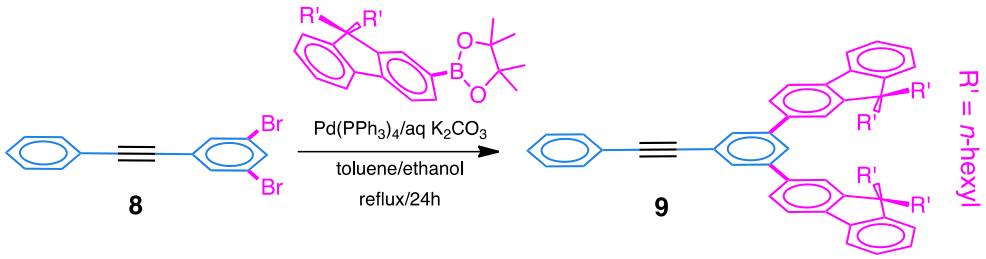

To a degassed solution of **8** (1.1 g, 3.3 mmol), 2-(4,4,5,5-tetramethyl-1,3,2-dioxaborolan)-9,9-dihexylfluorene (4.0 g, 8.7 mmol), and $Pd(PPh_3)_4$ (0.09 g, 0.08 mmol) in a mixture of pre-degassed toluene (50 mL) and ethanol (13 mL) in a Schlenk flask, was added a degassed solution of potassium carbonate (2 M, 20 mL) with the aid of a syringe. The resulting mixture was refluxed for 24 hours while protected from light by encasing the flask in aluminum foil. The reaction mixture was then cooled to room temperature, poured onto 5% aqueous HCl (50 mL) and extracted with dichloromethane (3 x 30 mL). The combined extracts were washed with water (50 mL) and brine (50 mL) and dried over anhydrous $MgSO_4$. Removal of the solvent in *vacuo* afforded crude product which was purified by flash chromatography on silica gel using a mixture of ethyl acetate and hexanes (1:99) as eluent to afford 1,3-difluoranyl-5-phenylethynylbenzene **9** as a viscous oil (2.5 g, 89%). ^{1}H NMR ($CDCl_3$) δ ppm 0.60-0.73 (m, 8H), 0.77 (t, 12H, *J* = 6.7 Hz), 1.02- 1.16 (m, 24H), 2.0- 2.08 (m, 4H), 7.32-7.41 (m, 10H), 7.60- 7.65 (m, 4H), 7.68 (dd, 2H, *J* = 8.0 Hz, 1.6 Hz), 7.73- 7.77 (m, 2H), 7.80 (d, 2H, *J* = 8.0Hz), 7.82 (d, 2H, J= 1.7 Hz), 7.90 (t, 1H, *J* = 1.7 Hz); ^{13}C NMR ($CDCl_3$) δ ppm 14.24, 22.80, 23.96, 29.92, 31.70, 40.64, 55.45, 89.73, 89.80, 120.03, 120.05, 120.22, 123.12, 124.27, 126.30, 127.02, 127.39, 128.64, 129.22, 131.91, 139.43, 140.84,141.10, 142.76, 151.20, 151.76.

Scheme 3. 6: Trimerization of 1,3-difluoranyl-5-phenylethynylbenzene 9 to an isomeric mixture of hexaarylbenzenes 5 and 5'.

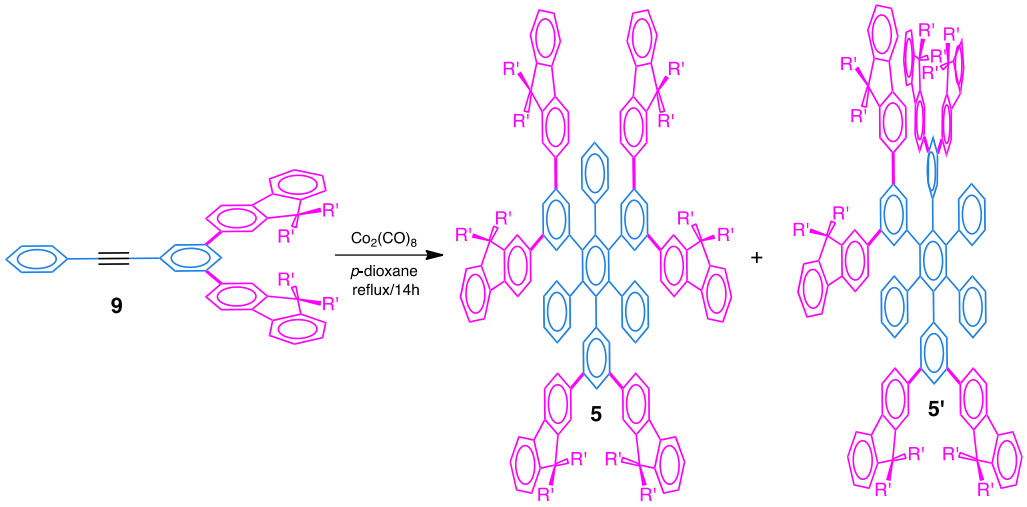

To a degassed solution of **9** (3.52 g, 4.2 mmol) in *p*-dioxane (80 mL) was added octacarbonyldicobalt (0.48 g, 1.4 mmol) under a strict inert atmosphere. The resulting mixture was refluxed for 14 hours and then evaporated *in vacuo*. The resulting solid was dissolved in dichloromethane (100 mL) and filtered through a short pad of celite, and the celite pad was washed with dichloromethane (25 mL). Evaporation of the dichloromethane and repeated precipitations from a mixture of dichloromethane and ethanol afforded a light brown solid which contained a mixture of isomeric **5** and **5'** (3.4 g, 96%) as confirmed by MALDI mass spectrometry and $^{1}H/^{13}C$ NMR spectroscopy (see spectra below). Multiple attempts to separate the isomeric mixture of **5** and **5**' by chromatography and crystallizations were unsuccessful.

Scheme 3. 7: Synthesis of *F*HBC from a mixture of 5 and 5' using $FeCl_3$ or DDQ.

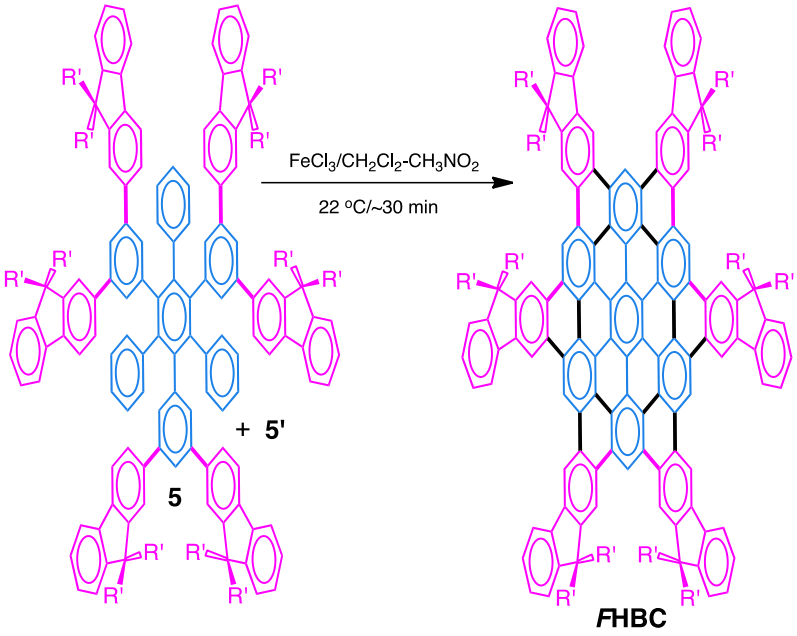

$FeCl_3$ procedure: To a solution of **5** and **5'** (1.5 g, 0.6 mmol) in dry dichloromethane (50 mL) was added dropwise a solution of ferric chloride (3.3 g, 20 mmol) in nitromethane (30 mL) at ~0 ºC during the course of 20 min. The ice bath was removed and the resulting mixture was stirred for an additional 30 minutes at ~22 °C and was then quenched by an addition of methanol (25 mL) followed by water (100 mL). The organic layer was separated and the aqueous layer was further extracted with dichloromethane (3 x 50 mL). The combined organic layers were washed with water (3 x 50 mL) and dried over anhydrous magnesium sulfate and filtered. The resulting dark-red solution was then passed through a short pad of silica gel to remove iron containing impurities, and the solvent was evaporated to afford dark red solid. A careful flash column chromatography using a mixture of benzene and hexanes (1:19) as eluent afforded ***F*HBC** (0.27 g, 18%) as a dark-red solid. mp >450 ºC; ^{1}H NMR ($CDCl_3$) δ ppm 0.79 (s, 6H), 1.1- 1.5 (m, 14H), 2.45- 2.85 (m, 4H), 7.17 (t, 1H, *J* = 7.2 Hz), 7.79 (d, 1H,

J = 7.2 Hz), 7.86 (t, 1H, *J* = 7.2 Hz), 8.67 (d, 1H, *J* = 7.2 Hz), 10.12 (s, 1H), 10.56 (s, 1H), 12.04 (s, 1H), 12.22 (s, 1H); ^{13}C NMR ($CDCl_3$) δ ppm 14.25, 22.88, 24.58, 30.25, 31.88, 41.66, 55.93, 115.57, 116.07, 118.61, 121.06, 121.12, 121.61, 122.94, 122.97, 123.77, 127.70, 127.73, 127.87, 128.58, 130.85, 131.00, 141.23, 142.20, 151.39, 152.24. MS: MALDI-TOF (M^+) = 2505.

DDQ procedure: A solution of a mixture of **5** and **5'** (0.5 g, 0.2 mmol) in dichloromethane (18 mL) containing a protic acid (e.g. CH_3SO_3H, 10% v/v) or Lewis acid ($BF_3.OEt_2$, ~25 equiv.) at ~0 ^oC was treated with DDQ (4.4 mmol, 22 equiv), and the solution immediately took on a dark-red coloration. The progress of the reaction was monitored by TLC. After completion of the reaction (~6 h), it was quenched with a saturated aqueous solution of $NaHCO_3$ (40 mL). The dichloromethane layer was separated and washed with water and brine solution and dried over anhydrous $MgSO_4$ and filtered. Removal of the solvent in vacuo followed by flash column chromatography using a mixture of benzene and hexanes (1:19) as eluent afforded ***F*HBC** (0.14 g, 28%) as a dark-red solid.

Scheme 3. 8: Synthesis of hexabrominated 10 and 10' by bromination of isomeric mixture 5 and 5'.

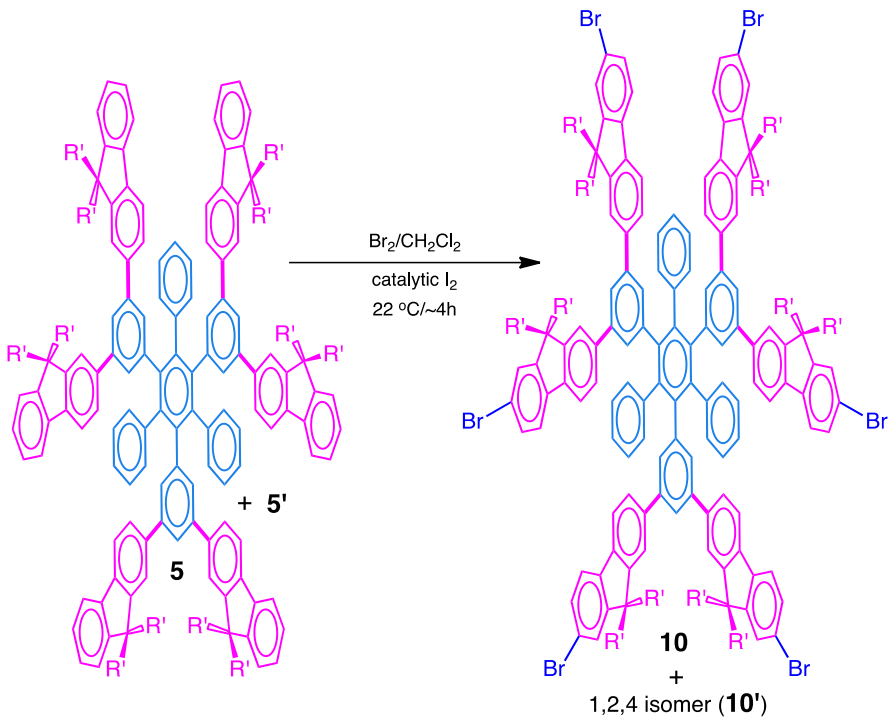

To a solution of mixture of **5** and **5'** (1.2 g, 0.48 mmol) in dichloromethane (100 mL) containing a crystal of iodine was added dropwise a solution of bromine (0.46 g, 2.9 mmol) in dichloromethane (50 mL), with the aid of a dropping funnel during a course of 15 minutes. The resulting mixture was stirred for an additional 3.5 h at room temperature. The reaction was quenched by addition of aqueous NaOH (1 M, 100 mL). The dichloromethane layer was separated and the aqueous layer was further extracted with dichloromethane (2 x 25 mL). The combined organic layers were washed with saturated aqueous sodium bisulfite (2 x 30 mL) solution, followed by water (50 mL) and brine (30 mL) and dried over anhydrous magnesium sulfate. The solvent was evaporated under vacuum to afford a mixture of **10** and **10'** as a light brown solid (1.42 g, 99%). This mixture was used in the next step without further purification.

Scheme 3. 9: Synthesis of Synthesis of *F*HBC-Br$_6$ from mixture of 10 and 10' using FeCl$_3$ or DDQ.

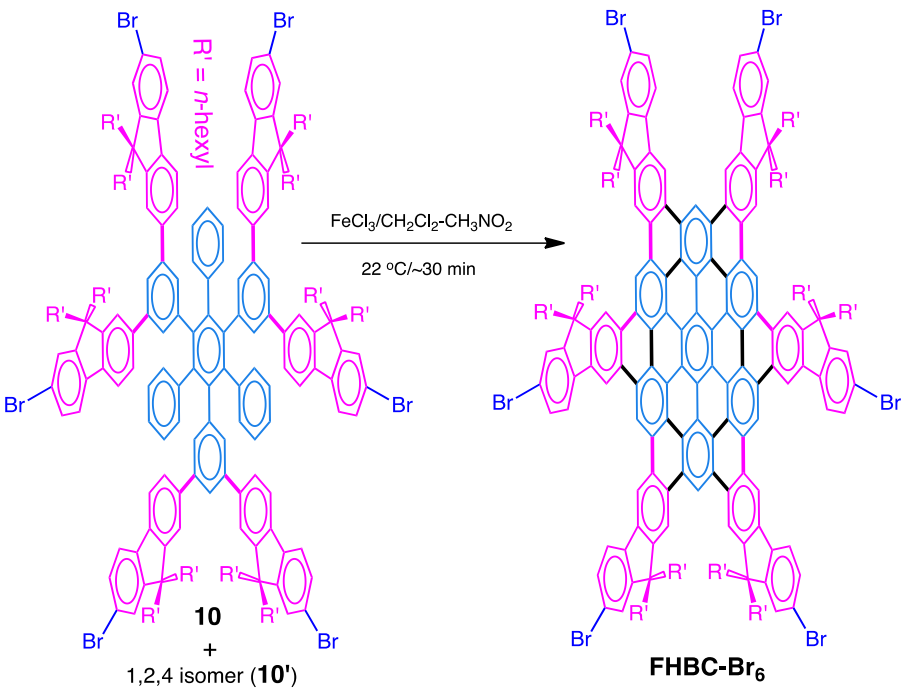

FeCl$_3$ procedure: To a solution of **10** and **10'** (0.81 g, 0.27 mmol), from above, in dry dichloromethane (100 mL) was added dropwise a solution of ferric chloride (2.7 g, 17 mmol) in nitromethane (25 mL) at ~0 °C during the course of 20 min. The ice bath was removed and the resulting mixture was stirred for an additional 3 h at ~22 °C and was then quenched by an addition of methanol (30 mL) followed by water (100 mL). The organic layer was separated and the aqueous layer was further extracted with dichloromethane (3 x 50 mL). The combined organic layers were washed with water (3 x 50 mL) and dried over anhydrous magnesium sulfate and filtered. The resulting dark-red solution was then passed through a short pad of silica gel to remove iron containing impurities, and the solvent was evaporated to afford dark red solid. A careful flash column chromatography using ethyl acetate, which eluted only the undesired products,

followed by dichloromethane that eluted the desired ***F*HBC-Br$_6$** (0.16 g, 20%) as a dark-red solid. mp > 450 ^{o}C, ^{1}H NMR ($CDCl_3$) δ ppm 0.70–0.80 (m, 36H), 1.10-1.40 (m, 96H), 2.44-2.75 (m, 24H), 7.87 (s, 6H), 7.93 (d, 6H, *J* = 8.0 Hz, 1.5 Hz), 8.47 (d, 6H, J = 8.0 Hz), 10.07 (s, 6H), 10.47 (s, 6H), 12.00 (s, 3H), 12.12 (s, 3H). See MALDI and ^{1}H/^{13}C NMR spectra below.

DDQ procedure: A solution of a mixture of **10** and **10'** (0.6 g, 0.2 mmol) in dichloromethane (18 mL) containing CF_3SO_3H, 10% v/v) at ~0 ^{o}C was treated with DDQ (4.4 mmol, 22 equiv), and the resulting mixture was stirred for ~4 h. It was quenched with a saturated aqueous solution of $NaHCO_3$ (40 mL). The dichloromethane layer was separated and washed with water and brine solution and dried over anhydrous $MgSO_4$ and filtered. Removal of the solvent in vacuo followed by flash column chromatography as above (used for the material generated by $FeCl_3$ method) afforded desired ***F*HBC-Br$_6$** (0.17 g, 26%) as a dark-red solid.

Scheme 3. 10: Synthesis of ***F*HBC-Ar$_6$**.

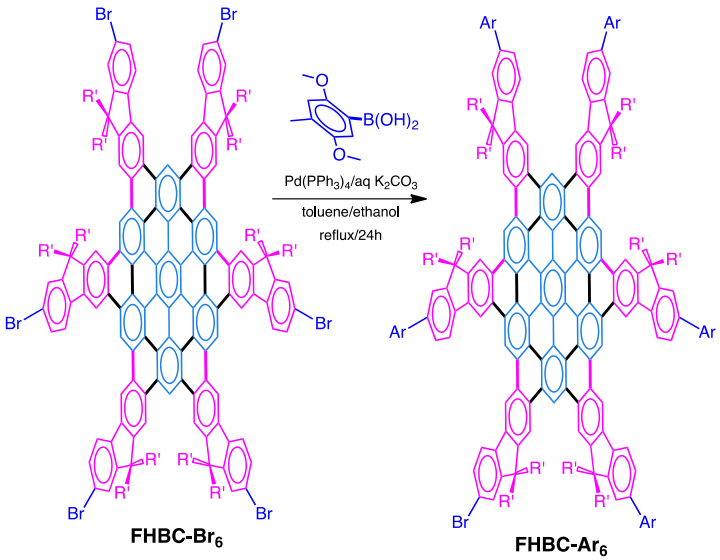

To a degassed solution of ***F*HBC-Br$_6$** (50 mg, 0.017 mmol), 2,5-dimethoxy-4-methylphenylboronic acid (0.04 g, 0.20 mmol), Pd (PPh_3)$_4$ (0.06 g, 0.005 mmol) in a mixture of dry toluene (25 mL) and ethanol (7 mL), was added a degassed solution of potassium carbonate (2 M, 10 mL) using a syringe. The resulting mixture was refluxed for 24 h under a complete exclusion of light. The reaction mixture was then cooled to room temperature, poured into 5% aqueous HCl (50 mL), and extracted with dichloromethane (3 x 30 mL). The combined extracts were washed with water (50 mL) and brine (50 mL) and dried over anhydrous $MgSO_4$. Removal of the solvent in *vacuo* afforded a solid that was purified using column chromatography on silica gel using a mixture of ethyl acetate and hexanes (1:19) as eluent to afford ***F*HBC-Ar$_6$** as a deep red solid (48 mg, 85%). m.p >400 ^oC. ^1H NMR ($CDCl_3$) δ ppm 0.76- 0.84 (m, 36H), 1.20-1.48 (m, 96H), 2.56- 2.82 (m, 24H), 3.94 (s, 18H), 4.03 (s, 18H), 7.02 (s, 6H), 7.19 (s, 6H), 7.92-8.02 (m, 12H), 8.69 (d, 6H, J = 8.7 Hz), 10.17 (s, 6H), 10.59 (s, 6H), 12.09 (s, 3H), 12.25 (s, 3H). ^{13}C NMR ($CDCl_3$) δ ppm 14.24, 16.64, 22.90, 24.67, 30.31, 31.89, 41.62, 55.92, 56.47, 57.26, 113.55, 115.53, 116.26, 118.73, 120.66, 121.19, 121.26, 121.62, 121.72, 123.03, 125.25, 127.17, 127.81, 127.90, 128.90, 129.52, 130.78, 131.11, 138.91, 139.87, 142.11, 150.74, 151.88, 152.54. See MALDI and $^1H/^{13}C$ NMR spectra below.

Scheme 3. 11: Synthetic scheme for the preparation of 4

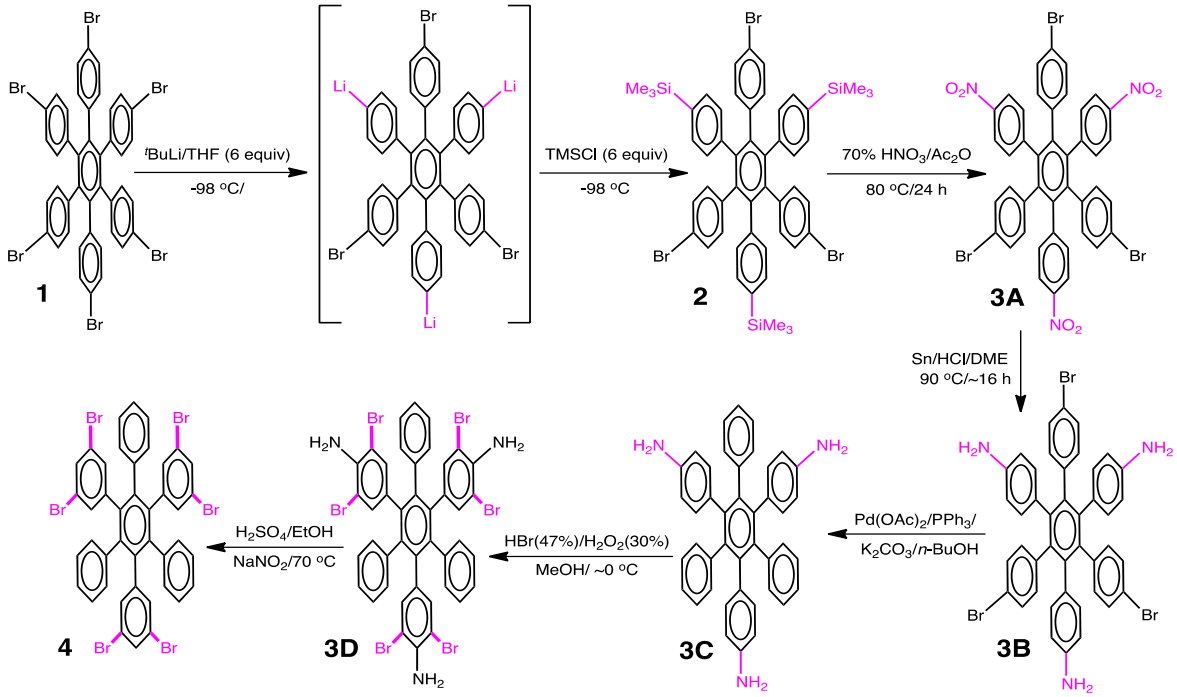

Synthesis of 2[25,26]

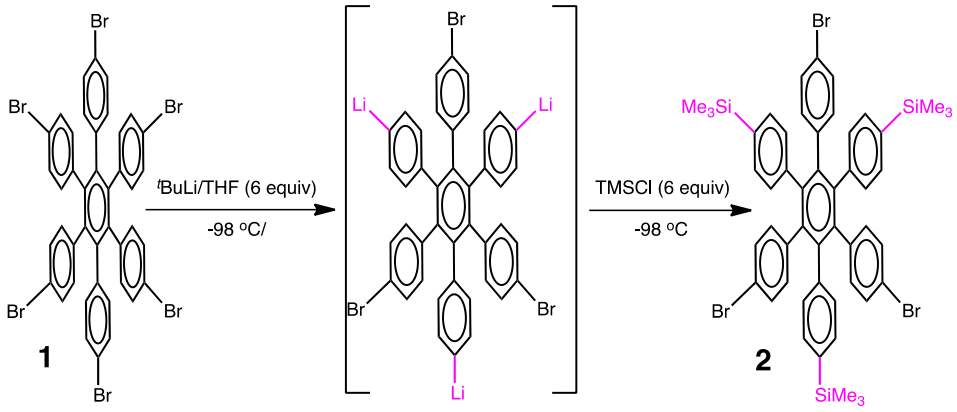

A dry Schlenk flask containing *hexakis*(4-bromophenyl)benzene[27] (10.0 g, 9.92 mmol) and THF (100 mL) was cooled to -98 °C in a liquid nitrogen/methanol bath (~15 min). A hexane solution of ^{t}BuLi (6 equivalent, 35.3 mL, 60 mmol) was added slowly with the aid of syringe under an argon atmosphere. The resulting mixture was stirred for an additional 10 minutes at -98 °C. The cooling bath was then removed and the reaction mixture was stirred for an additional 1 hour. During this time, the color of reaction mixture turned from greenish yellow to pink. The pink solution was cooled again to -98 °C and maintained at this temperature for 10 minutes before slowly adding trimethylsilylchloride (TMSCl) (6 eq, 7.6 mL, 60 mmol) with the aid of a syringe. After completing the addition of TMSCl, the cooling bath was removed. The color of the reaction mixture changed from colorless to pink to white. This mixture was stirred for an additional hour before quenching by addition of aqueous ammonium chloride (40 mL). The resulting mixture was extracted with chloroform (3 x 50 mL) and the combined organic extracts were dried over $MgSO_4$ and solvent was evaporated under reduced pressure. The resulting solid was recrystallized from a mixture of $CHCl_3$/EtOH (70:30) to afford pure **2** (7.43 g, 76%). ^{1}H NMR ($CDCl_3$, 400 MHz) δ ppm 6.62 (d, 2H, J = 8.46

Hz), 6.72 (d, 2H, *J* = 8.08 Hz), 6.95 (d, 2H, *J* = 8.45 Hz), 7.03 (d, 2H, *J* = 8.08 Hz). ^{13}C NMR ($CDCl_3$, 400 MHz) δ ppm -0.99, 119.66, 129.94, 130.69, 132.08, 133.09, 137.70, 139.43, 139.45. 140.33, 140.69.

Synthesis of 3A

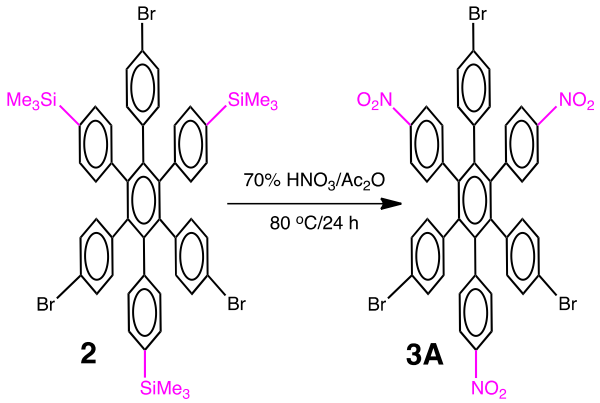

In a dry Schlenk flask containing **2** (2.5 g, 2.53 mmol) was added acetic anhydride (10 mL) followed by a dropwise addition of 70% HNO_3 (2.5 mL) with the aid of a syringe at ambient temperatures. The resulting mixture was heated at ~80 °C for 24 h, cooled to room temperature, and poured onto a cold (~0 °C) 10% aqueous NaOH solution (100 mL). The reaction mixture was extracted with dichloromethane (3 x 25 mL) and the combined organic extracts were dried over $MgSO_4$ and the solvent was removed under reduced pressure. The resulting crude solid was purified by column chromatography using silica gel and hexane : ethyl acetate (80 : 20) mixture as eluent to return pure **3A** (1.0 g, 44%). ^{1}H NMR ($CDCl_3$, 400 MHz) δ ppm 6.63 (d, 2H, *J* = 8.66 Hz), 6.97 (d, 2H, *J* = 8.92 Hz), 7.07 (d, 2H, *J* = 8.57 Hz), 7.84 (d, 2H, *J* = 8.88 Hz). ^{13}C NMR ($CDCl_3$, 400 MHz) δ ppm 121.61, 122.94, 131.25, 131.86, 132.29, 137.26, 139.37, 140.03. 146.18, 146.30.

Synthesis of 3B

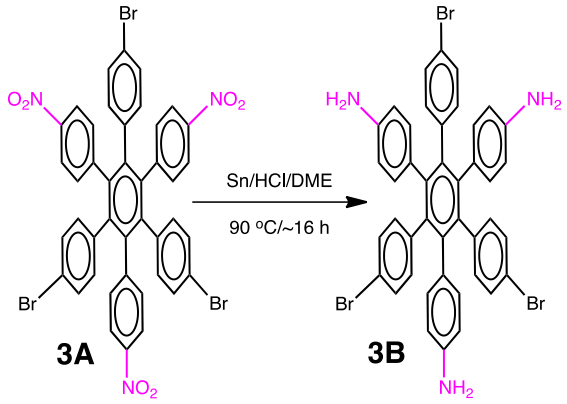

To a mixture of trinitro derivative **3A** (0.8 g, 0.9 mmol), concentrated HCl (20 mL), and 1,2-dimethoxyethane (20 mL) powdered tin (0.94 g, ~8 mmol) was added in small portions. The resulting mixture was stirred for ~13 h at 90 °C. After which time, more HCl (15 mL) and powdered tin (200 mg) were added and the stirring was continued for additional 3 h at 90 °C. The reaction mixture was cooled to room temperature and 10% aqueous NaOH solution was added until the solution turned basic (pH = 9, pH paper). This solution was extracted with diethyl ether (3 x 40 mL) and the combined ether extracts were dried over anhydrous $MgSO_4$. The solvent was removed under reduced pressure and the crude product was treated with concentrated HCl to form a solid precipitate, which was washed by a mixture of ethyl acetate/hexanes (10:90). The resulting solid was filtered and treated with pyridine until the solid dissolve and then the solution was extracted with diethyl ether and the solvent was removed under reduced pressure to afford brown color compound **3B** (0.53 g, 74%). ^{1}H NMR ($CDCl_3$, 400 MHz), δ in ppm 6.23 (d, 2H, *J* = 8.56 Hz), 6.47 (d, 2H, *J* = 8.57 Hz), 6.64 (d, 2H, *J* = 8.56 Hz), 7.00 (d, 2H, *J* = 8.50 Hz), 3.369 (-NH_2, br hump). ^{13}C NMR ($CDCl_3$, 400 MHz), δ in ppm 114.28, 119.36, 130.02, 130.62, 132.26, 133.27, 139.70, 140.25, 140.51, 143.83.

Synthesis of 3C

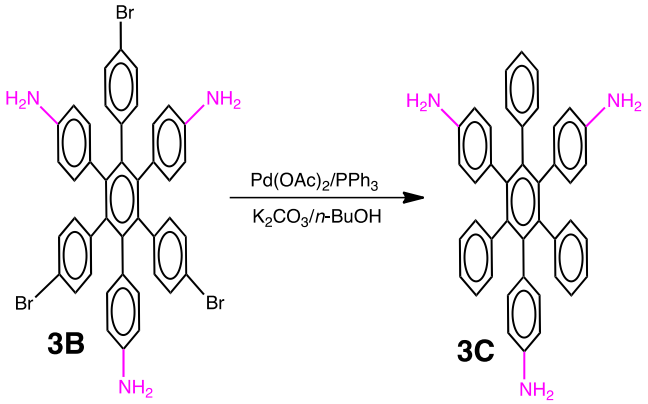

To a dry Schlenk flask **3B** (0.97 g, 1.2 mmol), $Pd(OAc)_2$ (27 mg, 0.12 mmol), PPh_3 (124 mg, 0.472 mmol), K_2CO_3 (372 mg, 2.36 mmol) and *n*-butanol (35 mL) were successively added under argon atmosphere and the resulting mixture was subjected to additional degassing and purging with argon. The reaction mixture was then stirred at 100 °C for overnight. The reaction was quenched by addition of water (100 mL) and extracted with dichloromethane (4 x 30 mL). The combined organic extracts were dried over $MgSO_4$ and the solvent was removed under reduced pressure. The crude product was treated with concentrated HCl (5 mL) and the oily residue formed was washed with benzene and then added pyridine and dichloromethane (100 mL) and evaporated. The resulting solid was washed by a mixture of hexane and ethyl acetate (4:1) to afford pure compound **3C** (0.46 g, 68%). ^{1}H NMR ($CDCl_3$, 400 MHz), δ in ppm 6.18 (d, 2H, *J* = 8.66 Hz), 6.54 (d, 2H, J = 8.50 Hz), 6.73- 6.99 (m, 5H). ^{13}C NMR ($CDCl_3$, 400 MHz), δ in ppm 113.88, 124.90, 126.74, 131.62, 131.79, 132.49, 140.35, 140.70, 141.59, 143.35.

Synthesis of 3D

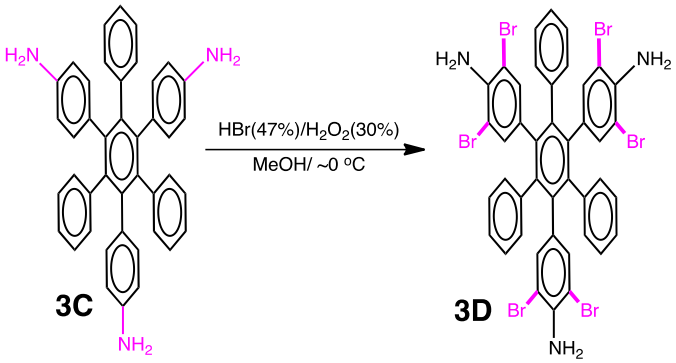

Compound **3C** (0.65 g, 1.12 mmol) in MeOH (110 mL) was taken in a Schlenk flask and 1.7 mL (10 mmol) concentrated aqueous HBr (47% wt/wt) was carefully added. To this resulting mixture, 30% aqueous H_2O_2 (0.76 mL, 6.7 mmol) was added slowly at 0°- 4 °C during the course of 15 minutes and was allowed to stir overnight. The reaction was quenched with aqueous NaOH solution (2 g, 100 mL water) and the resulting solid thus formed was filtered and washed with water. The solid was dissolved in $CHCl_3$ (100 mL) and dried over $MgSO_4$, filtered and the solvent was removed under reduced pressure to afford **3D** (0.9 g, 76%). ^{1}H NMR ($CDCl_3$, 400 MHz), δ in ppm 4.25 (br hump –NH_2), 6.78 (s, 2H), 6.79-6.85 (m, 2H), 6.89-7.08 (m, 3H). ^{13}C NMR ($CDCl_3$, 400 MHz), δ in ppm 107.40, 126.15, 127.46, 131.07, 131.96, 134.54, 138.00, 139.38, 139.75, 141.35.

Synthesis of 4[28]

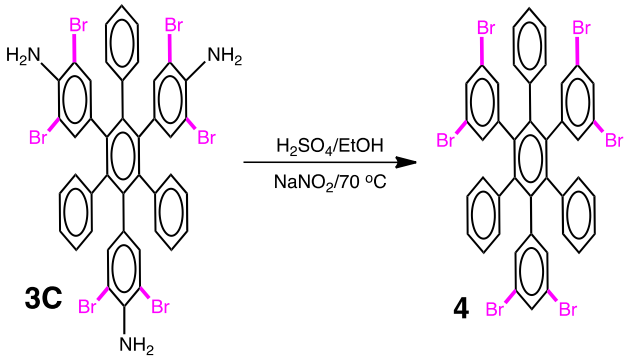

Compound **3D** (0.9 g, 0.86 mmol) from above was suspended in EtOH (100 mL) and heated to 50 °C. To this solution was added dropwise concentrated H_2SO_4 (5 mL) and the temperature was raised to 70 °C. To this mixture, solid $NaNO_2$ (0.7 g, 10 mmol) was added in portions over 45 minutes and it was heated at 80 °C for overnight, cooled to room temperature, and poured into ice water. The resultant highly colored solid was filtered and could not be characterized due to rather poor solubility.

^{1}H/^{13}C NMR spectroscopy of Compounds

^{1}H NMR of 1,3-dibromo-5-nitrobenzene

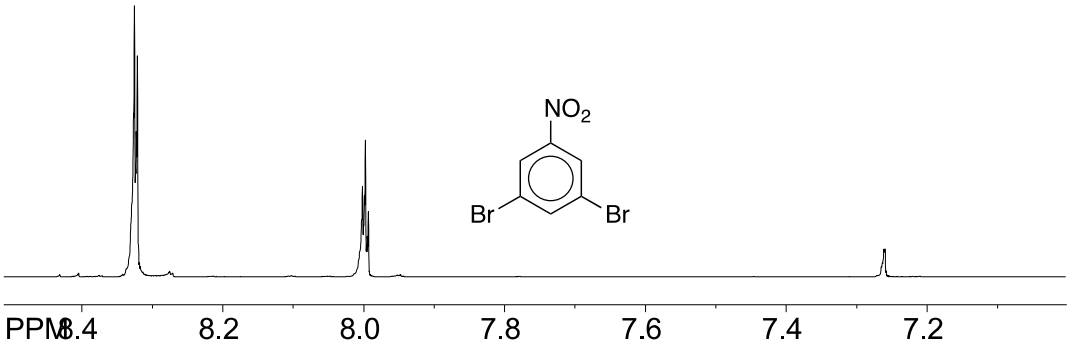

^{13}C NMR of 1,3-dibromo-5-nitrobenzene

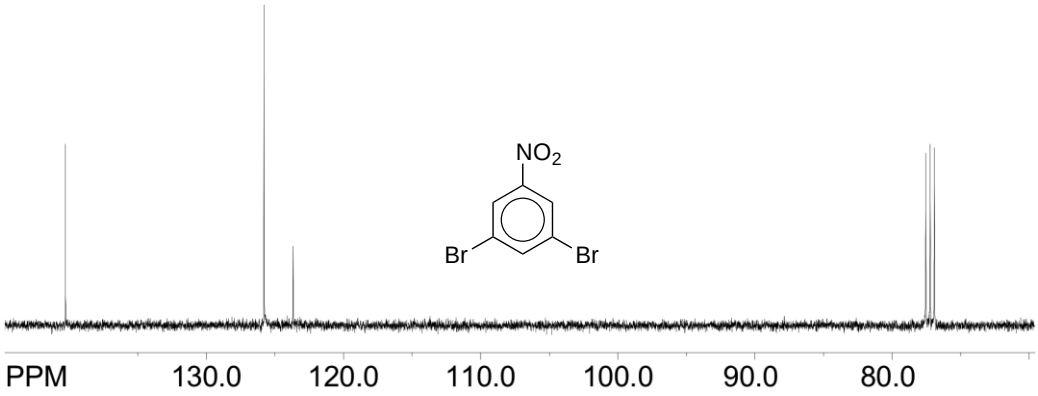

^{1}H NMR of 3,5-dibromo-phenylamine

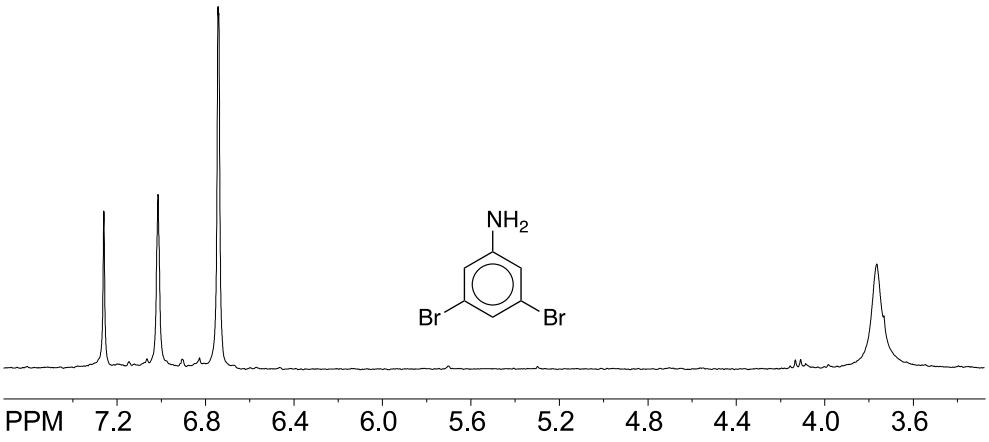

^{1}H NMR of 1,3-dibromo-5-iodobenzene (**7**)

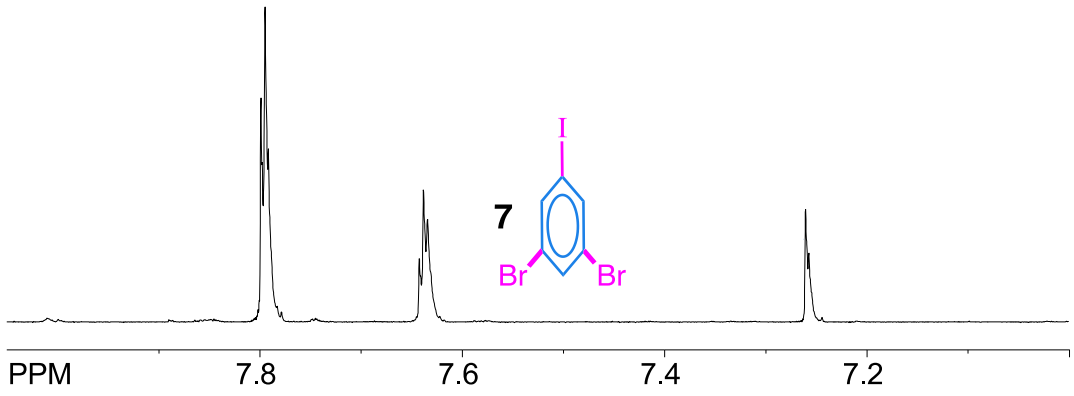

^{13}C NMR of 1,3-dibromo-5-iodobenzene (**7**)

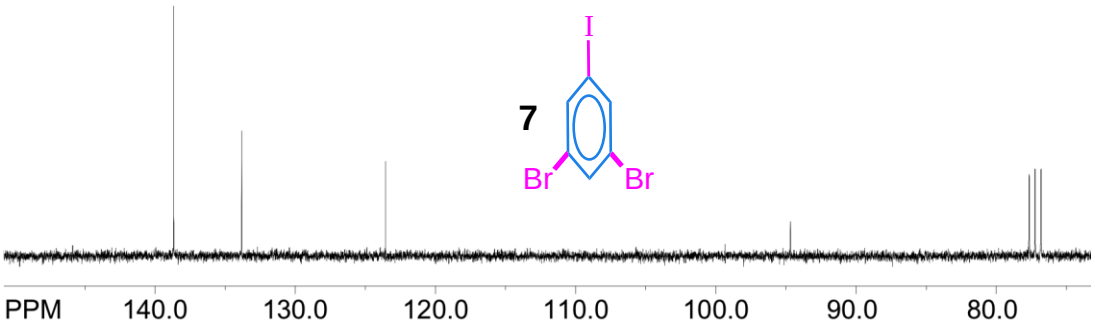

^{1}H NMR of 1, 3-dibromo-5-phenylethynylbenzene (**8**)

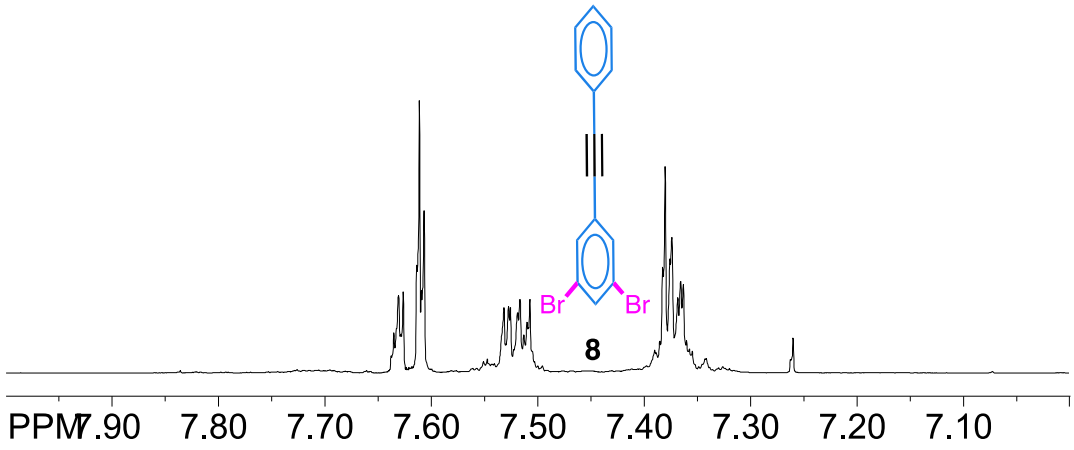

^{13}C NMR of 1, 3-dibromo-5-phenylethynylbenzene (**8**)

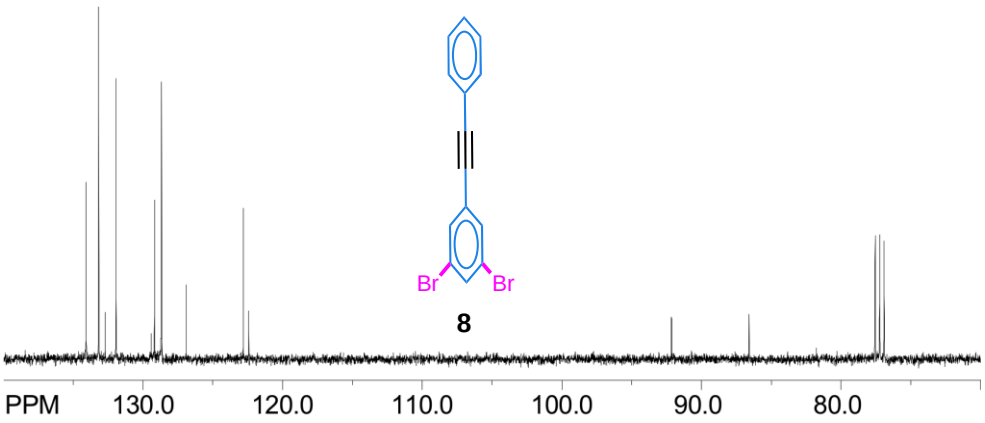

^{1}H NMR of 1,3-difluoranyl-5-phenylethynylbenzene (**9**)

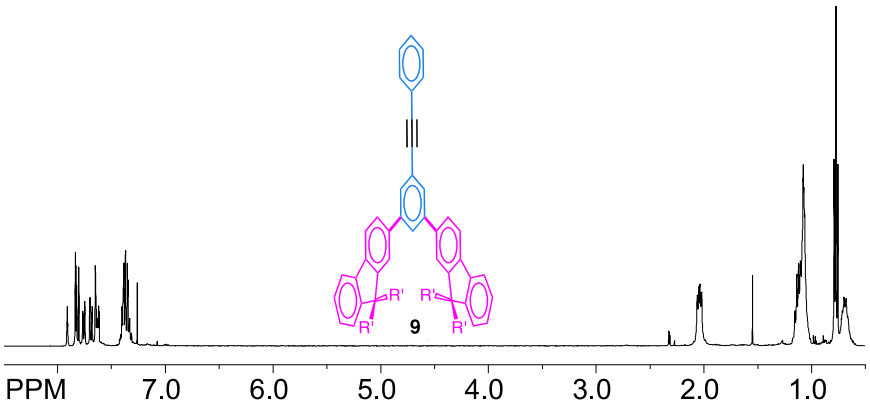

Expanded ^{1}H NMR of 1,3-difluoranyl-5-phenylethynylbenzene (**9**)

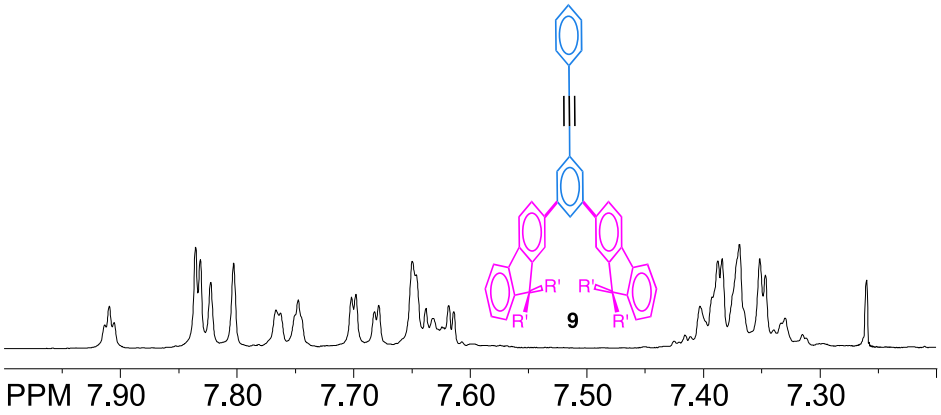

^{13}C NMR of of 1,3-difluoranyl-5-phenylethynylbenzene (**9**)

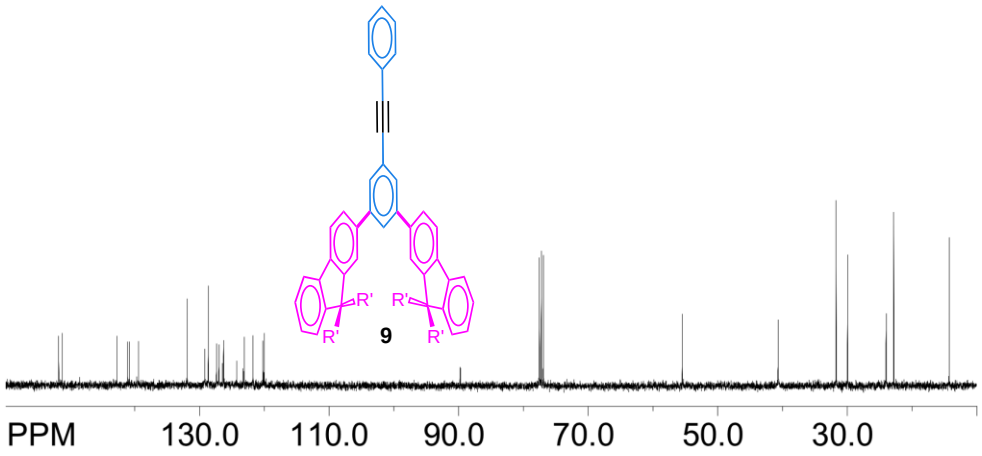

^{1}H NMR of the mixture of hexaarylbenzenes **5** and **5'**

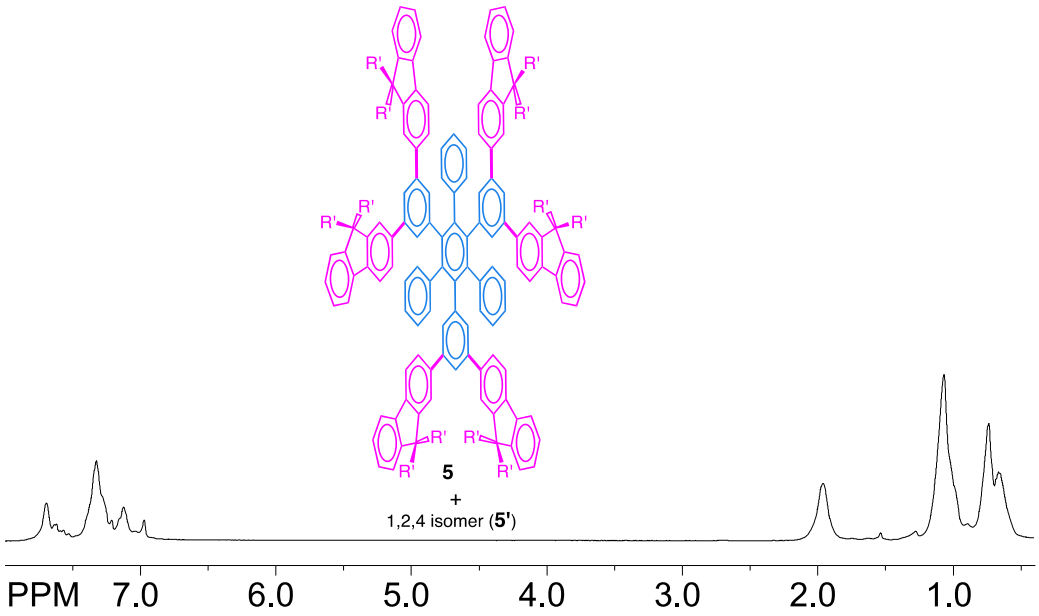

^{13}C NMR of the mixture of hexaarylbenzenes **5** and **5'**

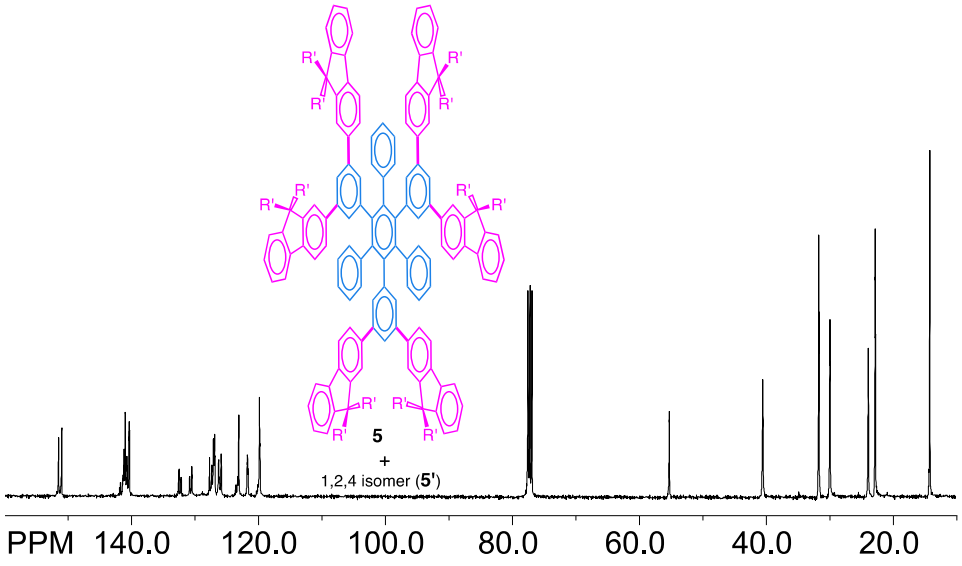

Expanded ^{13}C NMR of the mixture of hexaarylbenzenes **5** and **5'**

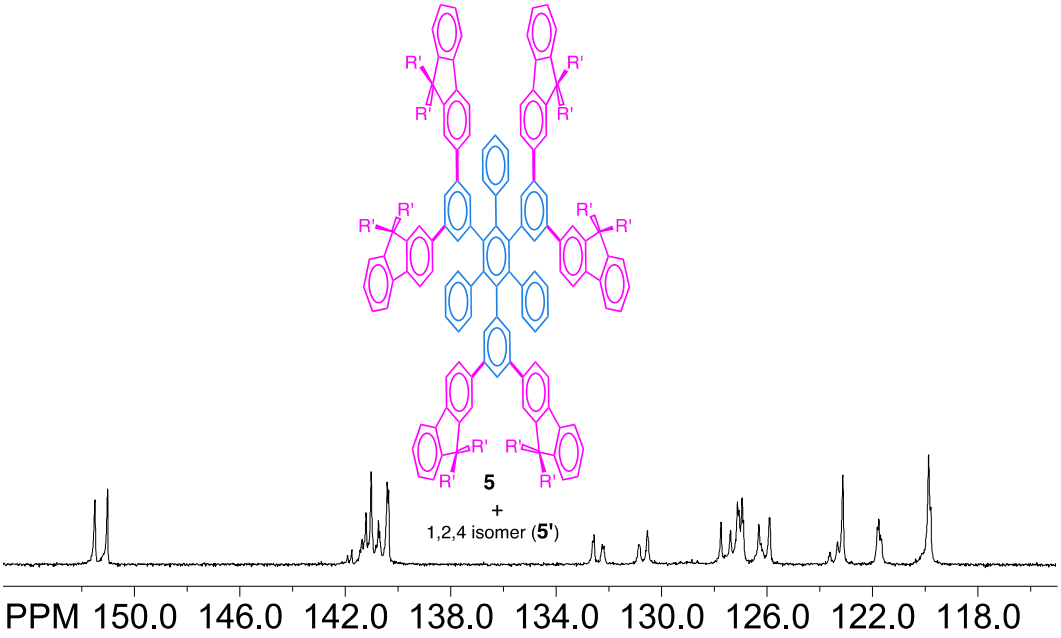

^{1}H NMR of **FHBC**

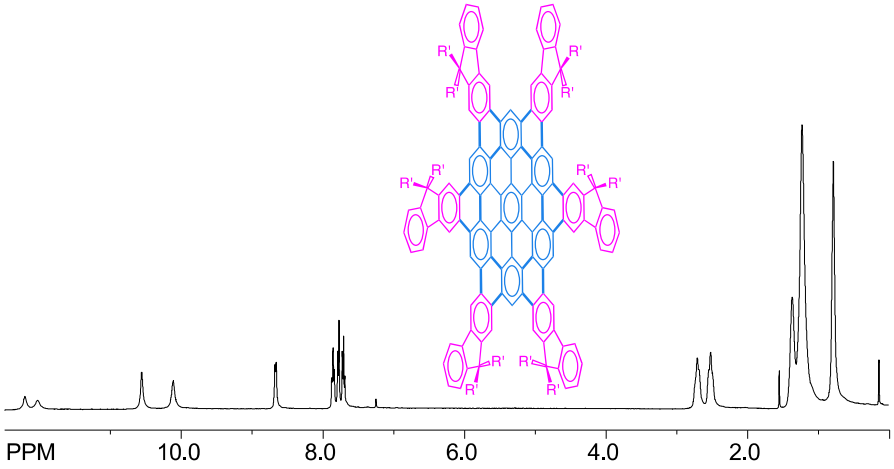

Expanded ^{1}H NMR of **FHBC**

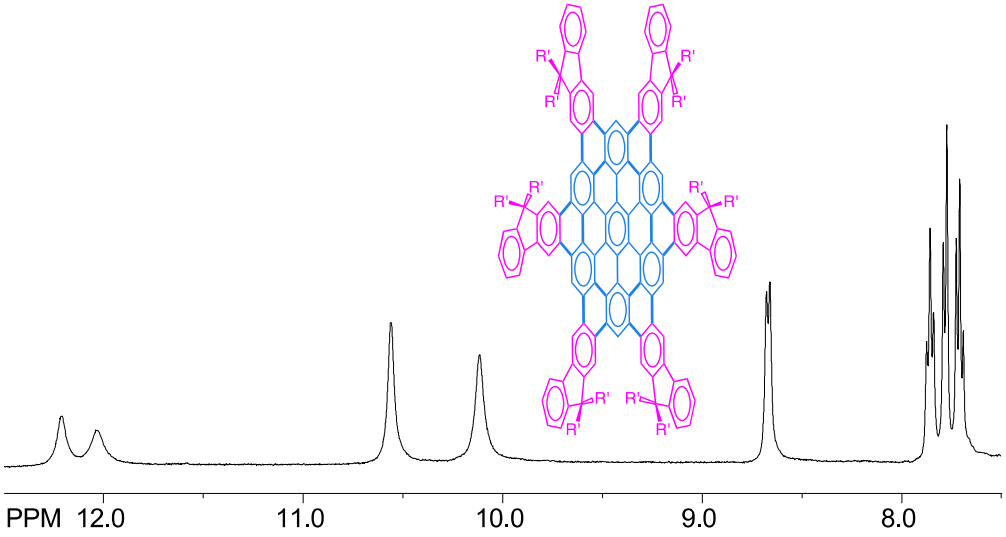

Expanded ^{1}H NMR of **FHBC**

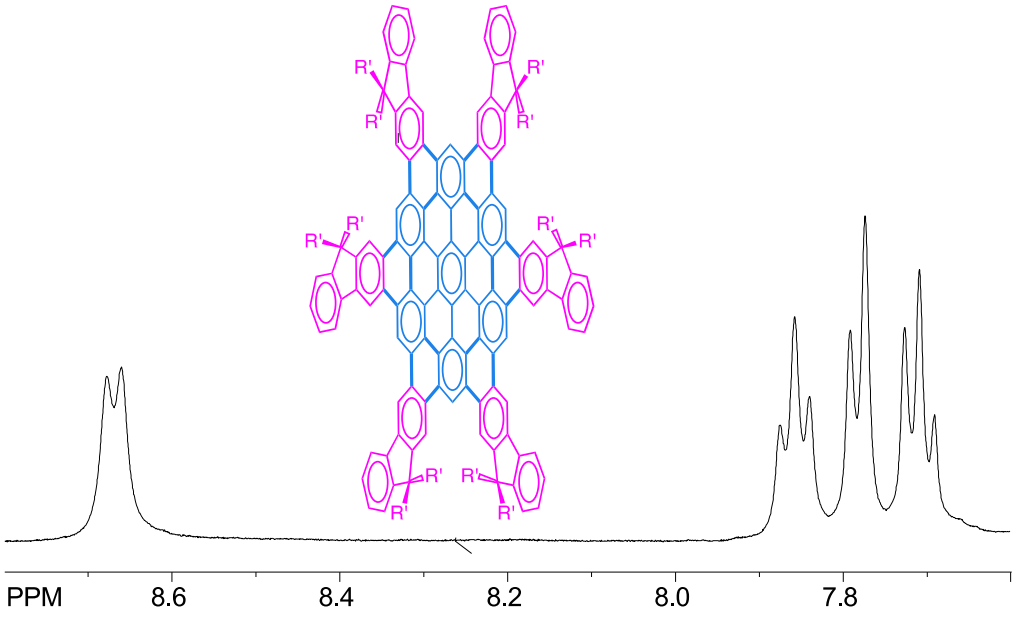

^{13}C NMR of **FHBC**

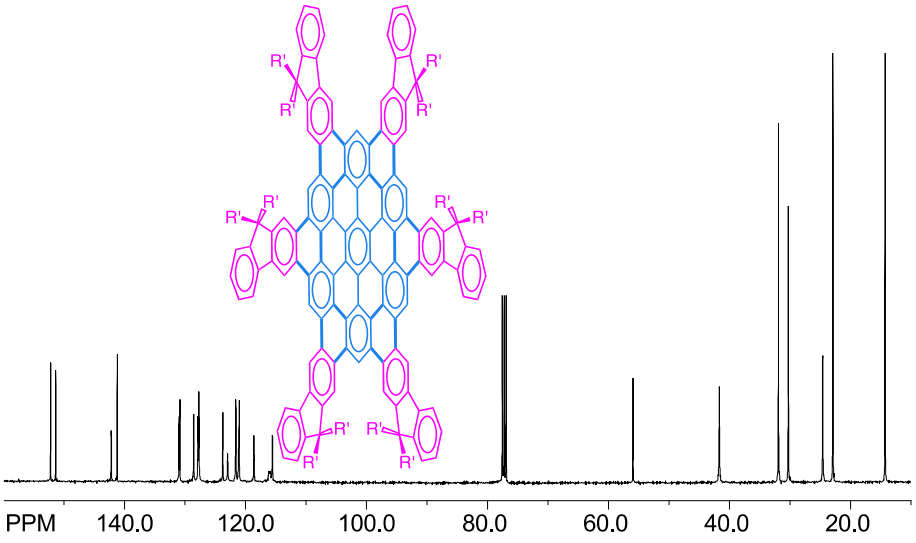

Expanded ^{13}C NMR of **FHBC**

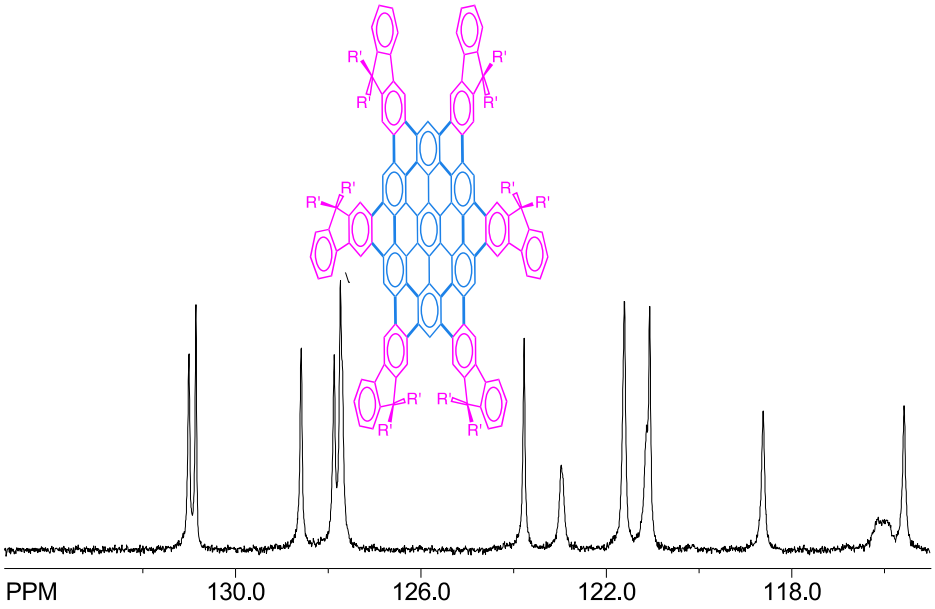

^{1}H NMR of **FHBC**-Br_6

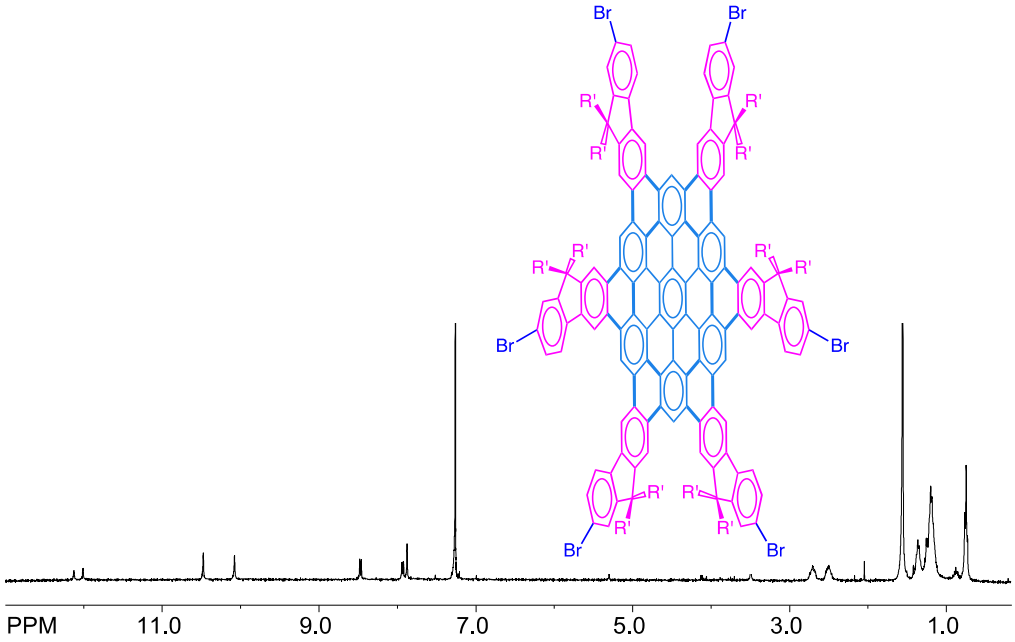

Expanded ^{1}H NMR of **FHBC**-Br_6

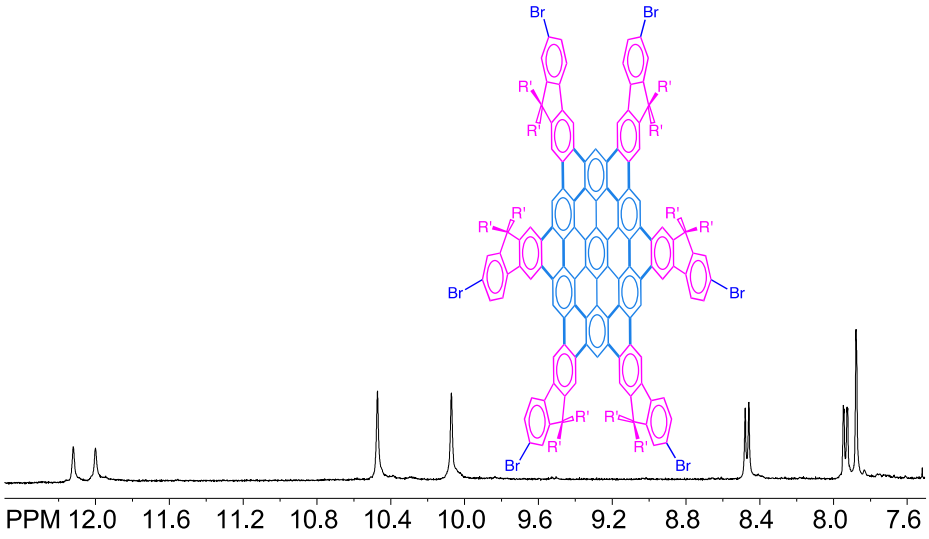

^{1}H NMR of **FHBC**-Ar$_6$

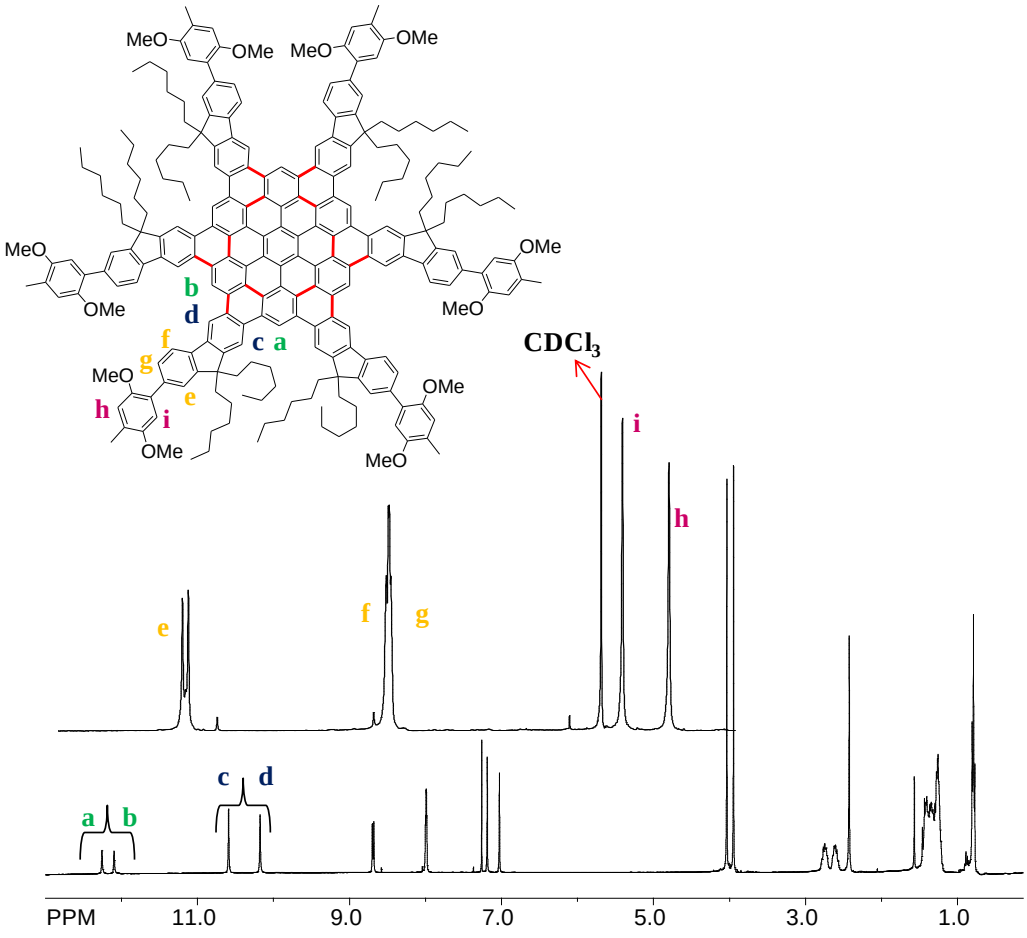

^{13}C NMR of **FHBC**-Ar$_6$:

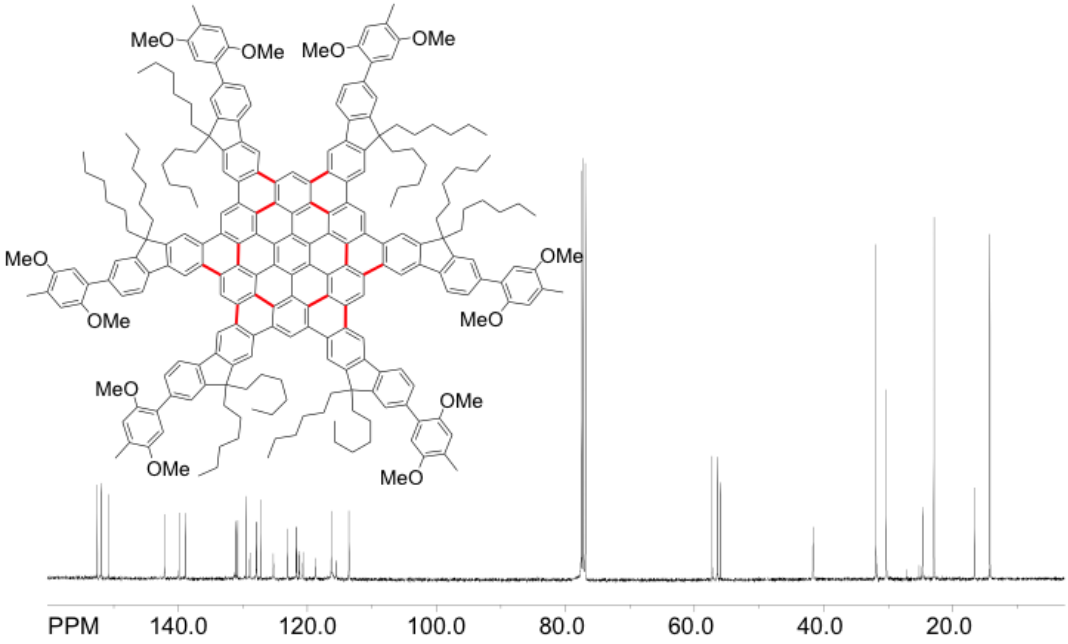

Expanded ^{13}C NMR of **FHBC**-Ar6:

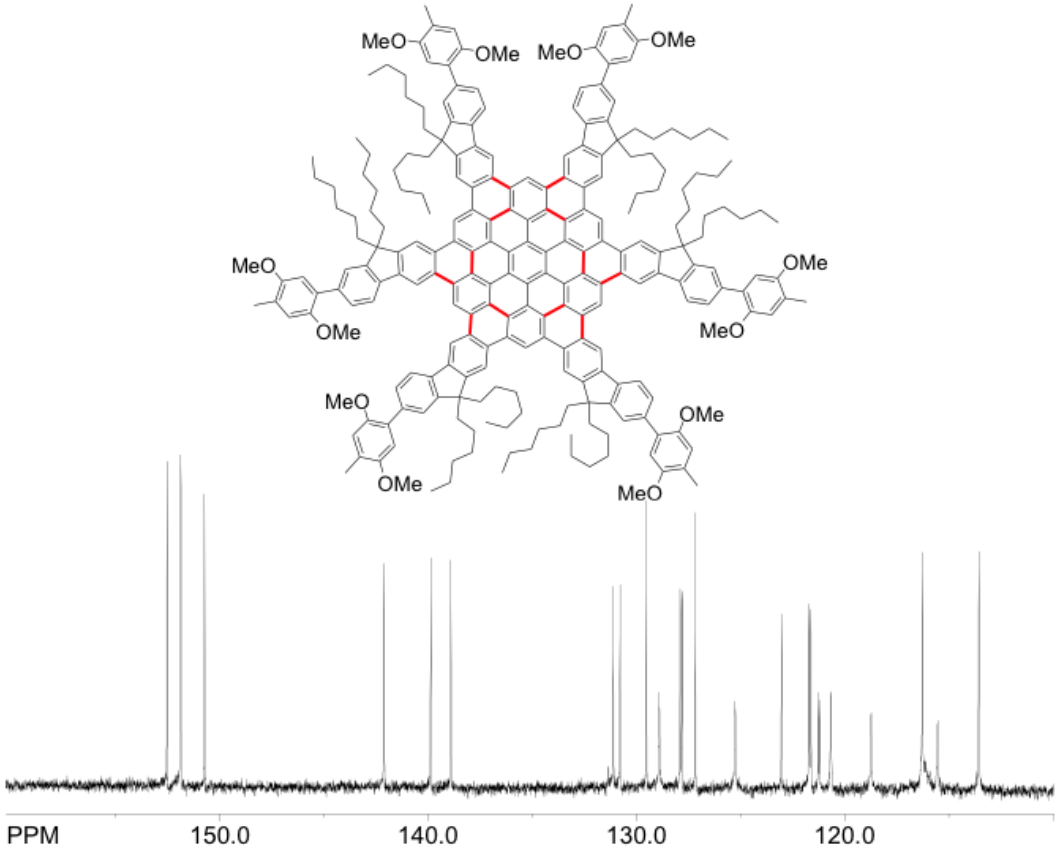

MALDI-TOF mass spectrometry

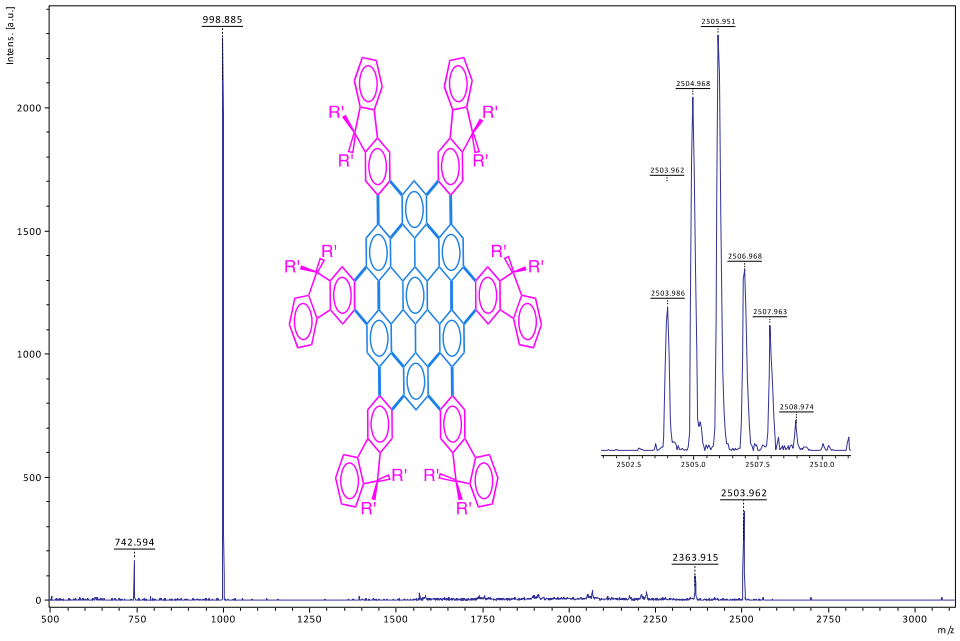

Figure 3. 7. MALDI-TOF mass spectra of ***F*HBC** obtained using dithranol as a matrix. Inset showing the isotope distribution for the molecular ion of ***F*HBC**.

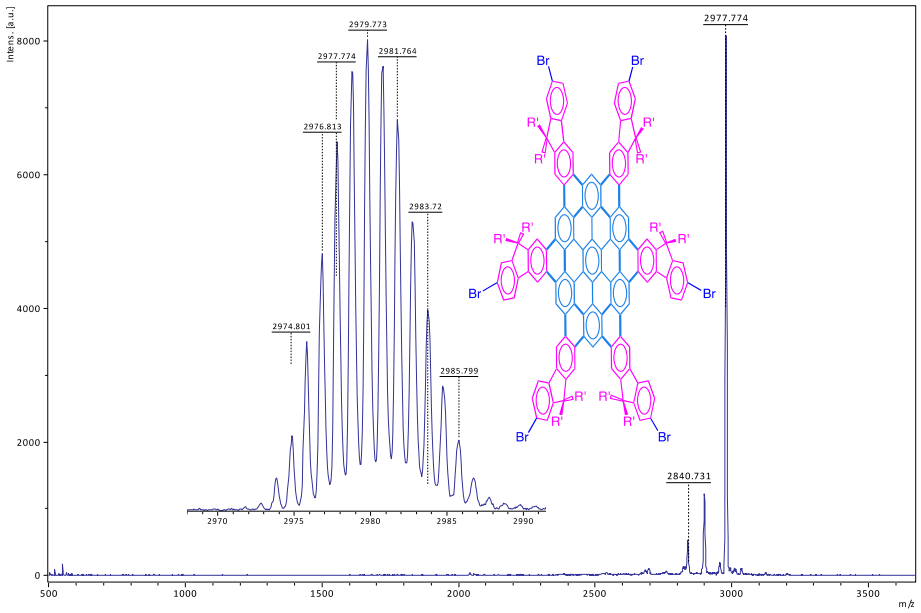

Figure 3. 8. MALDI-TOF mass spectra of ***F*HBC**-Br_6 obtained using dithranol as a matrix. Inset showing the isotope distribution for the molecular ion of ***F*HBC** -Br_6.

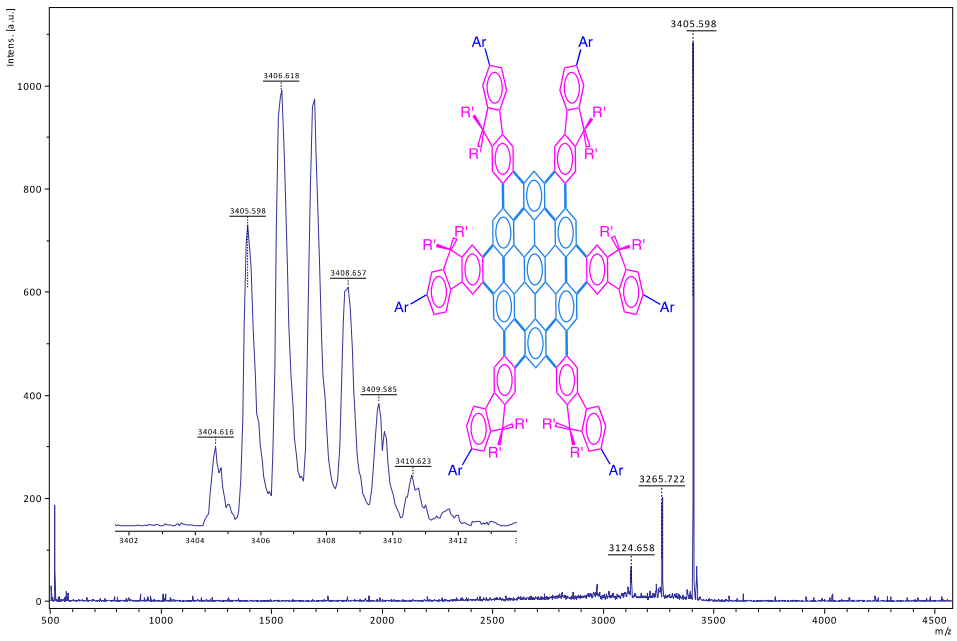

Figure 3. 9. MALDI-TOF mass spectra of ***F*HBC**-Ar_6 obtained using dithranol as a matrix. Inset showing the isotope distribution for the molecular ion of ***F*HBC** -Ar_6.

^{1}H NMR spectrum of **2**

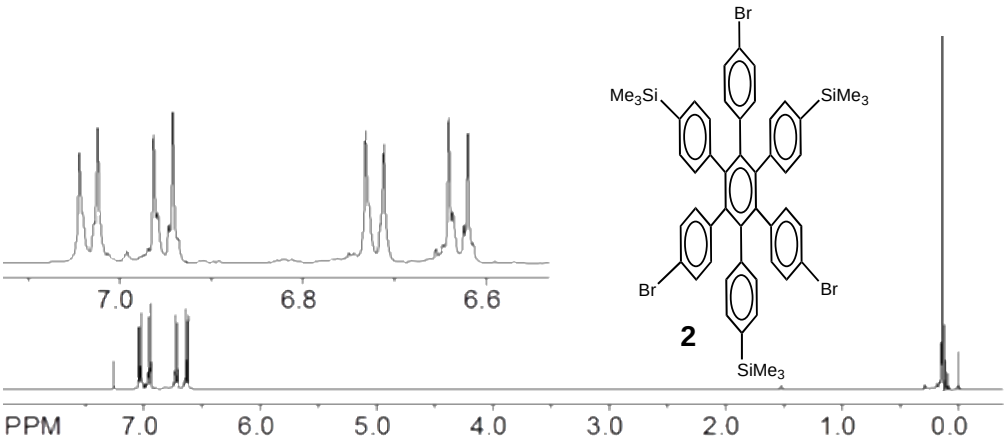

^{13}C NMR spectrum of **2**

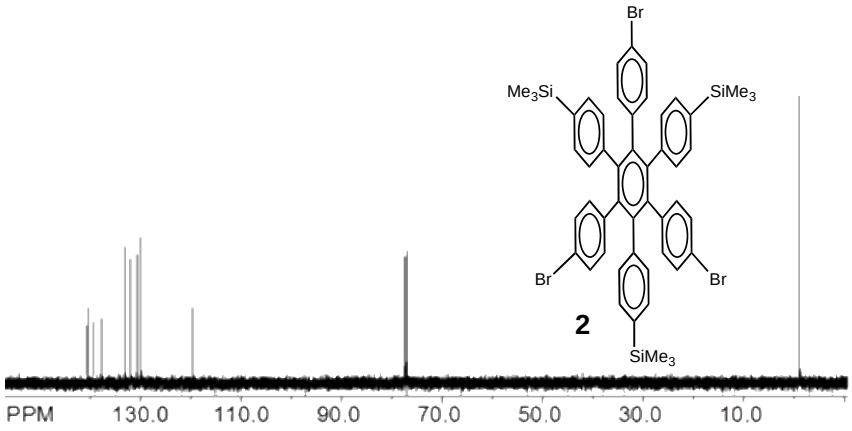

^{1}H NMR spectrum of **3A**

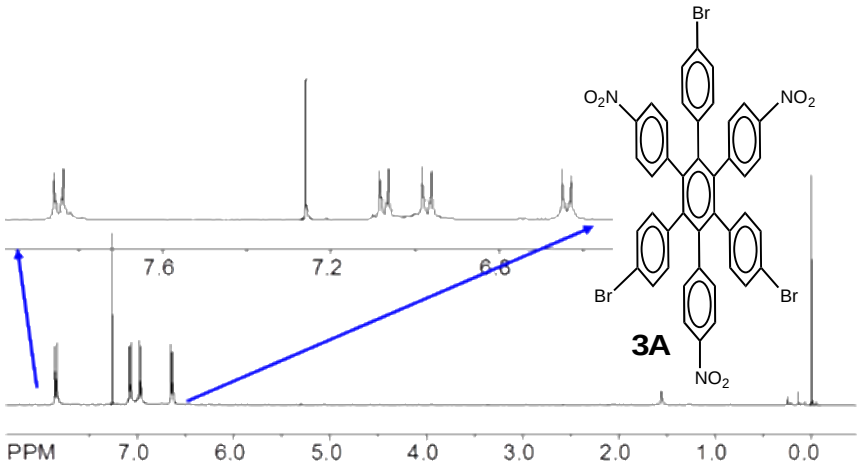

^{13}C NMR spectrum of **3A**

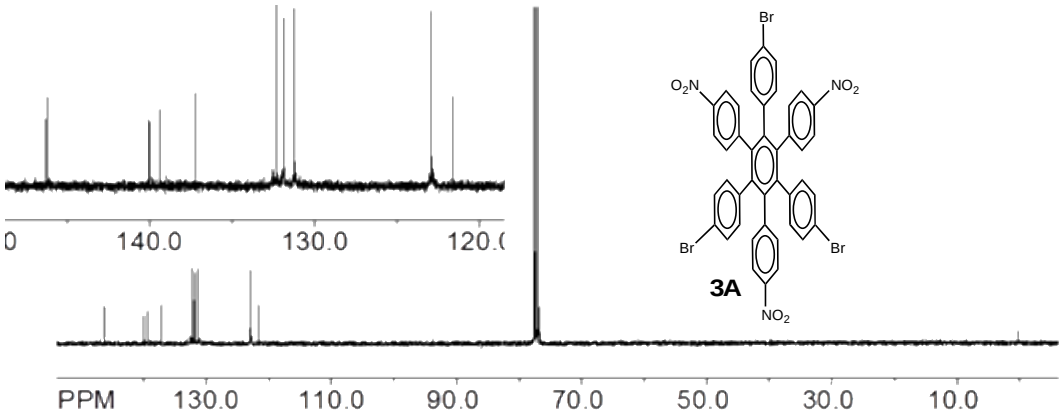

^{1}H NMR spectrum of **3B**

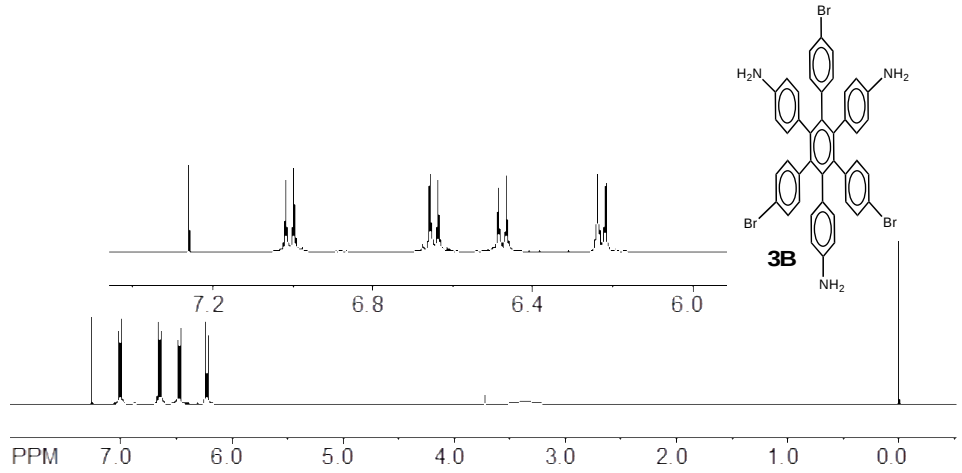

^{13}C NMR spectrum of **3B**

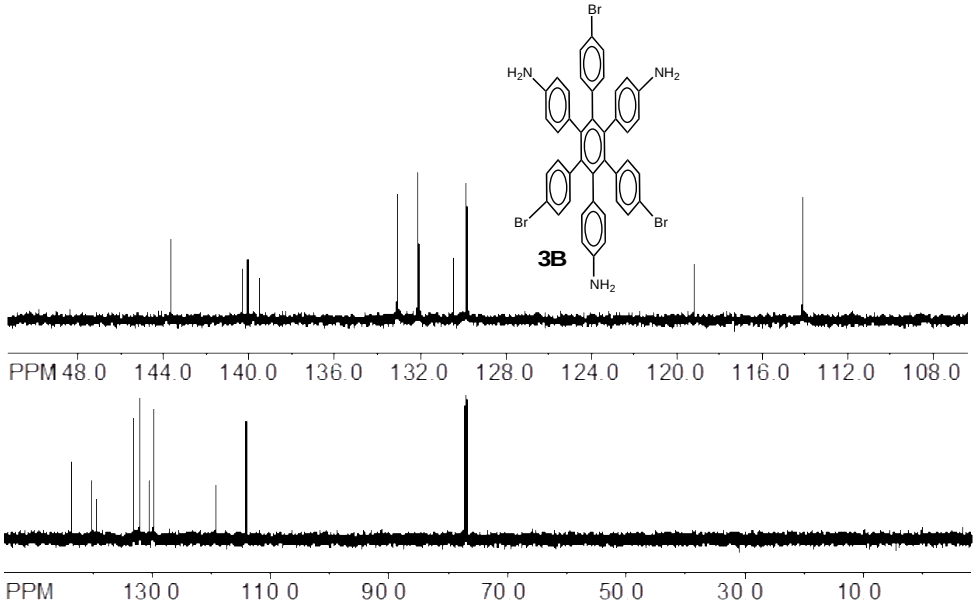

^{1}H NMR spectrum of **3C**

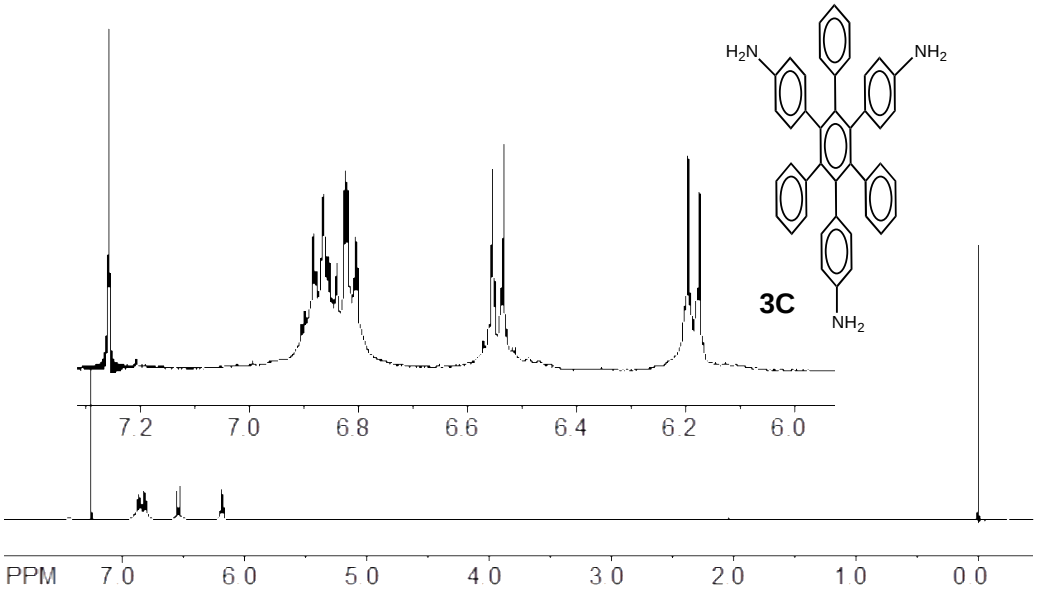

^{13}C NMR spectrum of **3C**

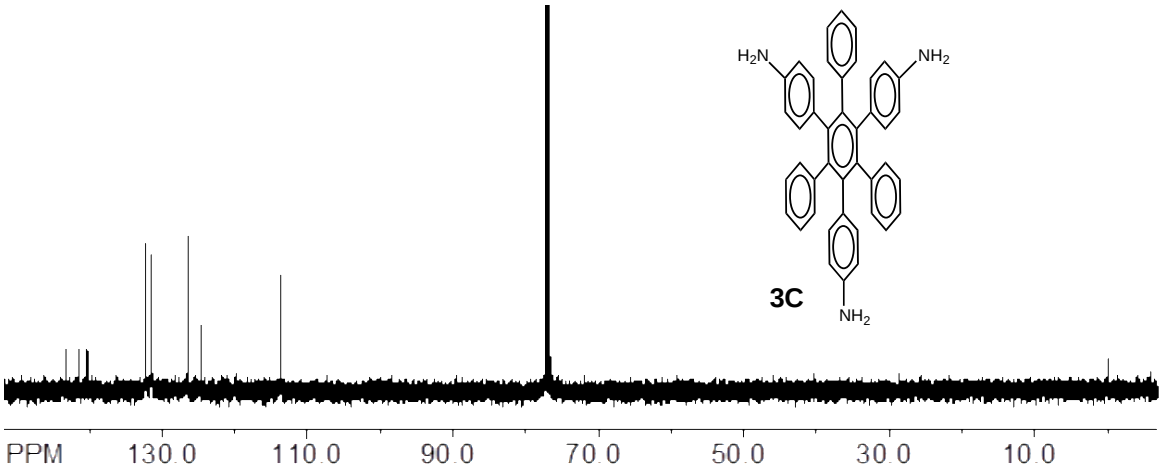

^{1}H NMR spectrum of **3D**

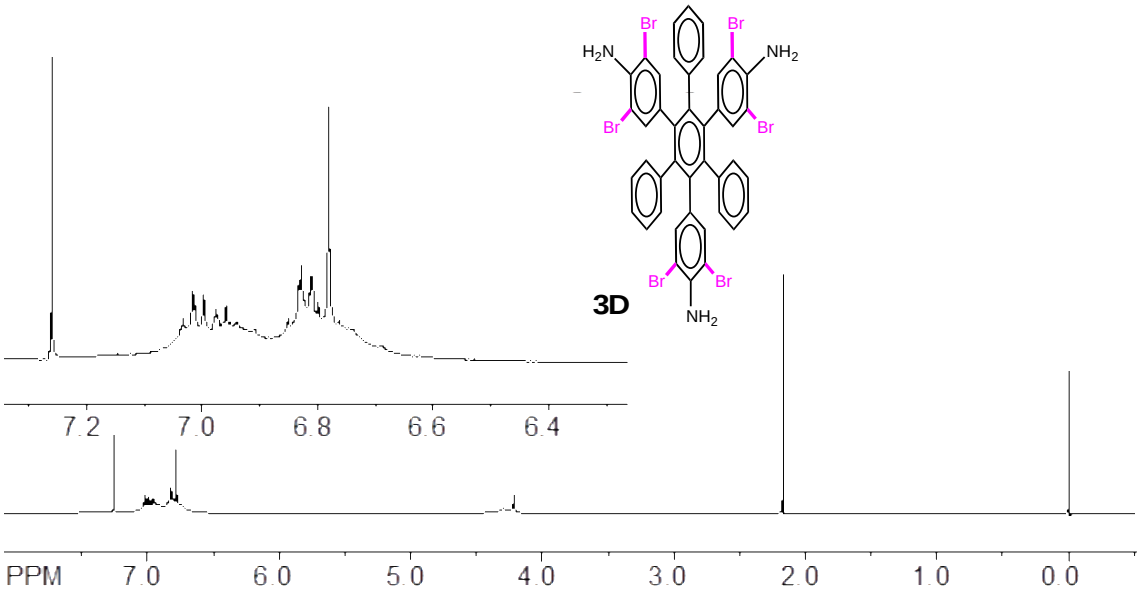

^{13}C NMR spectrum of **3D**

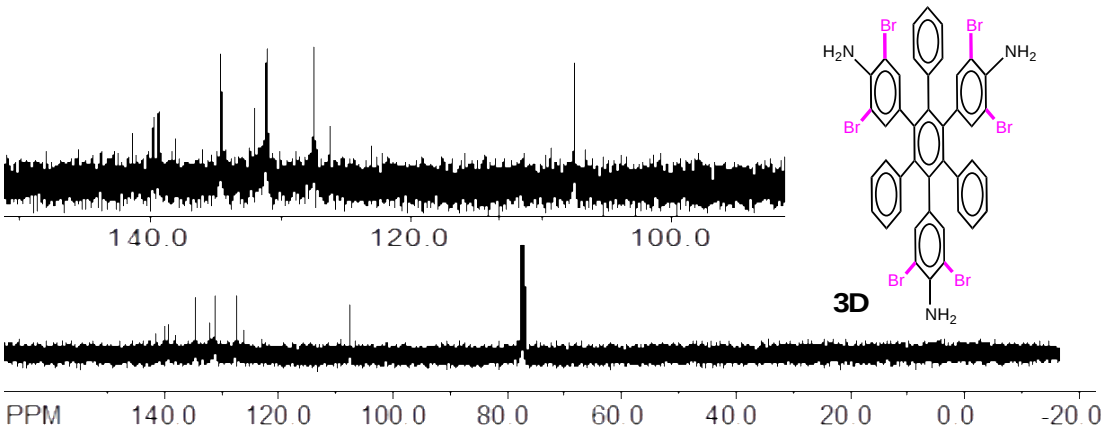

Electrochemistry

The electron donor strength of ***F*HBC** and $^{t\text{Bu}}$**HBC** was evaluated by electrochemical oxidation at a platinum electrode in dichloromethane containing 0.2 M *n*-Bu_4NPF_6 as the supporting electrolyte. The cyclic voltammograms of ***F*HBC**, when

terminated before the start of the fifth oxidation event, showed three reversible oxidation waves, which consistently met the reversibility criteria at various scan rates of 200-500 mV/s, as they all showed cathodic/anodic peak current ratios of i_a/i_c=1.0 (theoretical) as well as the differences between anodic and cathodic peak potentials of E_{pa}-E_{pc} ~ 70 mV at 22 ^{o}C. The reversible oxidation potentials of ***F*HBC** were calibrated with ferrocene as internal standard (E_{ox} = 0.45 V *vs* SCE) and were found to be 0.40, 0.76, 1.01 and 1.19 V vs Fc/Fc^+ corresponding to the formation of mono, di, tri and tetracation respectively. It is noted that the fourth oxidation wave in the cyclic voltammogram of ***F*HBC** displays a quasi-reversible oxidation wave. In contrast, ^{t}Bu**HBC** exhibits a single oxidation wave at (E_{ox} =) 0.64 V vs Fc/Fc^+ in CH_2Cl_2 (**Figure 3.11**).[29, 30]

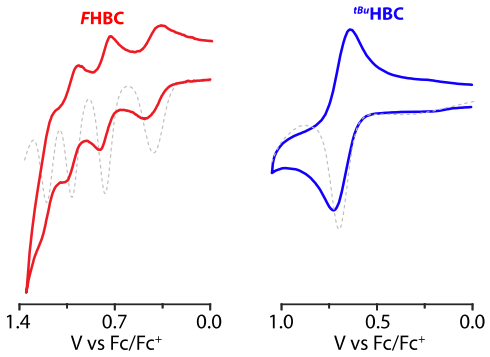

Figure 3. 10. Cyclic (solid lines) and square-wave (dashed lines) voltammograms of ***F*HBC** (red) and ^{tBu}**HBC** (blue) in CH_2Cl_2 containing 0.2 M *n*-Bu_4NPF_6 at a scan rate of 200 mV s^{-1} and 22 ^{o}C.

Generation of *F*HBC cation radical

Reproducible spectra of ***F*HBC** cation radical were obtained in CH_2Cl_2 solution at 22 ºC by quantitative redox titrations using magic blue (tris-4-bromophenylamminium cation radical, $\mathbf{MB}^{+\bullet}$, E_{red} = 0.70 V vs Fc/Fc^+, λ_{max} = 728 nm, ε_{max} = 28200 cm^{-1} M^{-1}).[31,32]

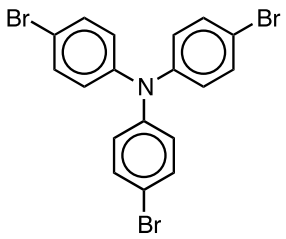

Figure3. 11. Chemical structure of magic blue.

Redox titration experiment was carried out by an incremental addition of sub-stoichiometric amounts of electron donor (***F*HBC**) to the solution of $\mathbf{MB}^{+\bullet}$. The 1-e^- oxidation of ***F*HBC** to $\mathbf{FHBC}^{+\bullet}$ and reduction of $\mathbf{MB}^{+\bullet}$ to **MB** can be described by an equilibrium equation:

$$\mathbf{MB}^{+\bullet} + \mathbf{FHBC} \rightleftarrows \mathbf{MB} + \mathbf{FHBC}^{+\bullet} \quad \text{(eq. 1)}$$

Depletion of $\mathbf{MB}^{+\bullet}$ and formation of $\mathbf{FHBC}^{+\bullet}$established that $\mathbf{MB}^{+\bullet}$ was completely consumed (**Figure 3.12**).

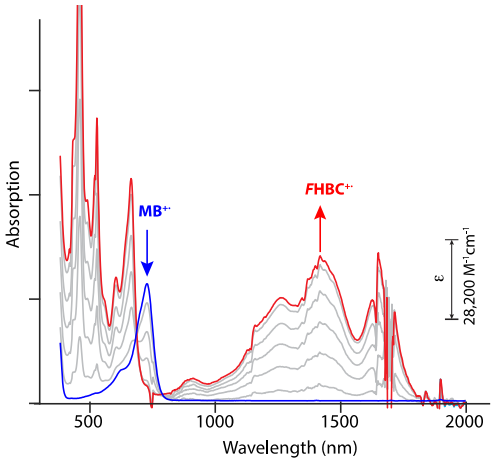

Figure 3. 12. The spectral changes observed upon the reduction of 5.5 x 10^{-6} M **MB**$^{+\bullet}$ by an incremental addition of substoichiometric amounts of ***F*HBC** in CH_2Cl_2 at 22 ^{o}C.

Numerical deconvolution[9,10] of the UV-VIS absorption spectrum at each increment of the titration produced the individual spectra of ***F*HBC**$^{+\bullet}$ and **MB**$^{+\bullet}$. Obtained electronic spectrum of ***F*HBC**$^{+\bullet}$ shows a significant increase of molar absorptivity (by a factor of ~6) as compared to $^{t\text{Bu}}$**HBC**$^{+\bullet}$ (**Figure 3.13**).

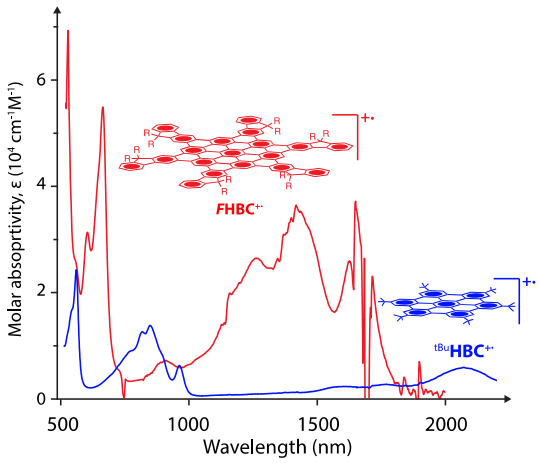

Figure 3. 13. Comparison of the electronic absorption spectra of ***F*HBC**$^{+\bullet}$ and $^{t\text{Bu}}$**HBC**$^{+\bullet}$.

CHAPTER 4

Spreading Electron Density Thin: Increasing the Chromophore Size in Polyaromatic Wires Decreases Interchromophoric Electronic Coupling

Disclaimer: The results discussed in this chapters were further supplimented by DFT calculations and relevant computational works by my coworkers Dr. Maxim V. Ivanov. My contribution to this chapter is limited to synthesis of various molecules and spectroscopic studies.

INTRODUCTION

Poly-*p*-phenylene-based wires are prototypical systems for charge-transfer studies with potential applications in photovoltaic and molecular electronics devices.[1-5] Electronic coupling between a pair of phenylenes in a poly-*p*-phenylene-based wire is a crucial parameter that controls its redox and optical properties, as well as the rates of electron transfer in corresponding donor-wire-acceptor systems.[6-9] For example, unsubstituted poly-*p*-phenylene wires are characterized by strong interchromophoric electronic coupling due to the favorable nodal arrangement of the HOMO lobes and relatively small interplanar dihedral angles, which promote effective orbital overlap between adjacent phenylenes.[10,11] This strong electronic coupling is reflected in the sensitivity of redox/optical properties to the wire length, as can be judged by large slopes in their $1/n$ or $\cos[\pi/(n+1)]$ dependences,[10,12] where n is number of chromophoric units in a wire.

In this context, an interesting question concerns how many phenylenes should be included in a single chromophore. For example, a poly-*p*-phenylene-based wire shown in **Figure 4.1** can be either considered as a poly-fluorene (i.e., $\mathbf{PF}_n$) or poly-*p*-phenylene (i.e., $\mathbf{PP}_n$). Irrespective of how the chromophore is defined, the absorption band of $\mathbf{PF}_n$ or $\mathbf{PP}_n$ shifts red with increasing wire length, indicating that interchromophoric electronic coupling is significant (**Figure 4.1**).[10] But can the value of the electronic coupling depend on how one defines the chromophore?

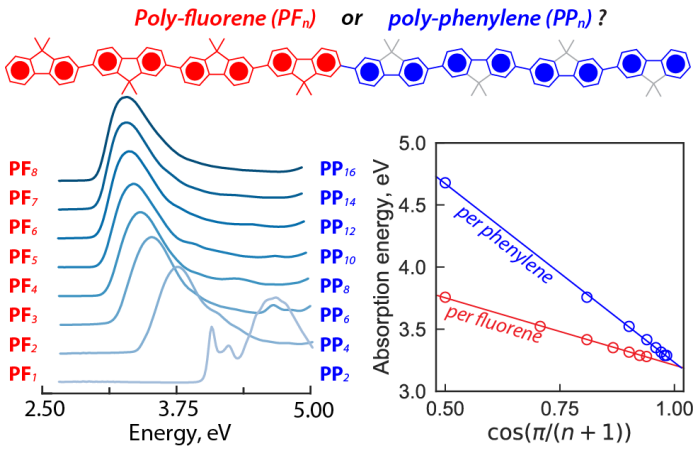

Figure 4. 1. Depending on the choice of the monomeric unit, a molecular wire on the top can be either considered as poly-fluorene (**PF**$_n$) or poly-phenylene (**PP**$_n$). Left. Absorption spectra of **PF**$_n$ (or **PP**$_n$). Right: Energies of maximum absorption plotted against cos[π/(*n*+1)], where *n* is number of phenylenes (blue) or fluorenes (red).

According to the Hückel molecular orbital theory, the energy of the HOMO to LUMO transition scales linearly with cos[π/(*n*+1)] and the scaling factor depends on the electronic coupling.[10,13] Remarkably, the slope of the linear ν-vs-cos[π/(*n*+1)] plot is smaller by nearly a factor of two when *n* is number of fluorenes as compared to the plot where *n* is number of phenylenes (**Figure 4.1**), suggesting that the electronic coupling between fluorenes is by a factor of two smaller than between a pair of phenylenes for the same wire.

As the magnitude of the electronic coupling directly impacts the redox/optical properties of the wire and the extent of hole (i.e., polaron) delocalization in the corresponding cation radicals, a choice of the chromophore size seems to be an important additional parameter. Indeed, a recent study showed on the example of biaryls with

varied chromophore size that as the chromophore size increases, the mechanism of hole delocalization changes from static delocalization to dynamic hopping.[14]

In order to systematically probe the curious dependence of the chromophore size on the electronic coupling, herein we designed a set of poly-*p*-phenylene-based mono- and bichromophores (i.e., ***n*PP** and ***n*PP$_2$**, **Chart 4.1**) where the size of the chromophore is varied from n = 2 to 4 phenylenes. Aided by the electrochemical properties of ***n*PP**/***n*PP$_2$** and spectroscopic signatures of their cation radicals with the support from DFT calculations we conclude that as the size of the chromophore increases the interchromophoric electronic coupling gradually decreases and may reach nearly non-existent values at the polymeric limit. We show that this initially surprising result becomes obvious when one considers this problem with the aid of Hückel molecular orbital theory, which predicts that at the polymeric limit the energies of the molecular orbitals become nearly degenerate and energy bands are formed, leading to the inevitability of decreasing interchromophoric electronic coupling as the chromophore expands.

Chart 4. 1. Structures of monochromophoric *n***PP** and bichromophoric *n***PP**$_2$ studied in this work. *R* = hexyl.

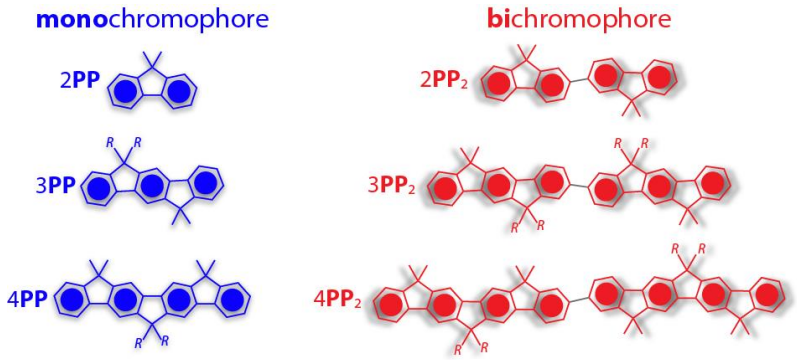

RESULTS AND DISCUSSION

Synthesis. Monochromophores n**PP** and bichromophores n**PP**$_2$ (n = 2-4) were synthesized by adaptation of the literature procedures. All compounds were characterized by ^{1}H/^{13}C NMR spectroscopy and MALDI mass spectrometry.

The strategy for the preparation of ladder type planer fluorene involves the key steps (i) Pd(0)-catalyzed Suzuki coupling or Suzuki type coupling of the fluorene and phenylene subunits to assemble the definite number of aromatic units, (ii) alkylation of the carbonyl group of ester function to form the diols (and mono alcohol) and (iii) an acid catalyzed Friedel-Crafts type intramolecular annulation that results in the formation of the planarized π-system.

The simplest member of the series, i.e 2**PP** or 9,9-dihexylfluorene which is made trivially by alkylation of commercially available fluorene. To synthesize 3**PP** and 4**PP**, a

bromo (mono or di) derivatives of 9,9-dihexylfluorene was used to couple with phenylene subunits followed by methylation of carbonyl group of ester functional towards its mono or diols. Subsequently mono or diols are treated with methane sulphonic acid in dichloromethane to form planarized 3**PP** and 4**PP** by Friedel-Crafts type intramolecular annulation. The synthesis of 3$\mathbf{PP}_2$ required to make mono bromo 3**PP** which started with alkylation of simple 2-bromo fluorene followed by nitration by using fuming HNO_3 acid which in turn coupled with 3,3-dimethyl-3H-benzo[c][1,2]oxaborol-1-ol, to form the desired alcohol intermediate to afford 2-Nitro-6,6-dihexyl-12,12-dimethylindenofluorene, **S5**. The nitro compound was reduced with Sn in presence of HCl in the solution of 1,2 dimethoxy ethane and ethanol which was used to prepare 2-Bromo-6,6-dihexyl-12,12-dimethylindenofluorene, **S6** by Sandmeyer reaction. The bromo compound was used to synthesize pinacolato boronic ester which was coupled with the same bromo compound to prepare 3$\mathbf{PP}_2$.

The synthesis of 4$\mathbf{PP}_2$ is started with the bromination of 4**PP** to afford dibromo 4**PP**, **S10a** which was converted to monobromo by subsequent lithiation by using n-BuLi followed by TMSCl in THF. The produced silyl compound was treated with CF_3COOH in dichloromethane to make mono bromo 4**PP**, **S11**. Albeit this reaction afforded the mixture of 4**PP**, dibromo 4**PP** and mono bromo 4**PP**. The purified mono bromo 4**PP** was used to prepare pinacolato boronic ester which was coupled with mono bromo 4**PP** by Suzuki coupling reaction to afford 4$\mathbf{PP}_2$. (**Scheme 4.1**, More details in the experimental section)

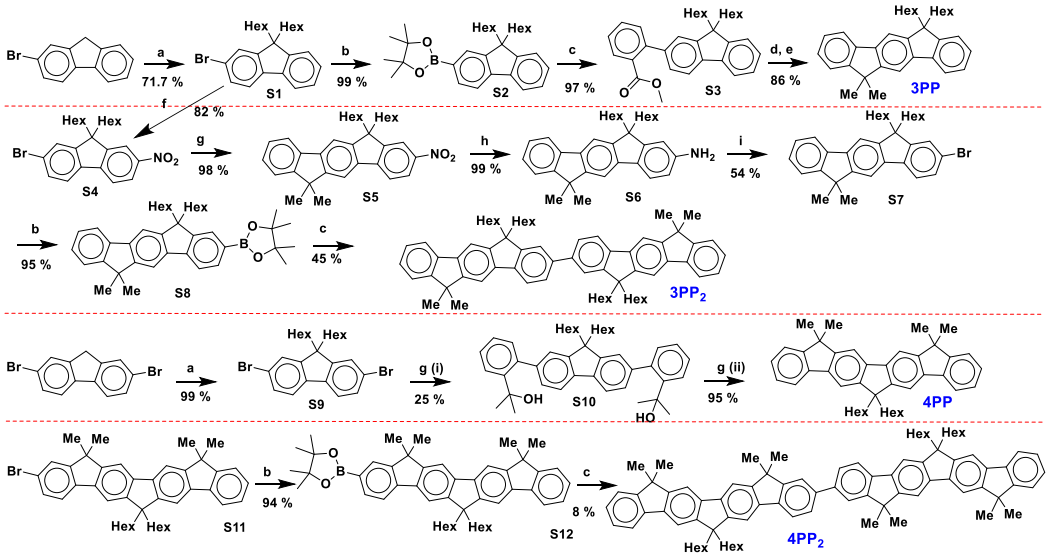

Scheme 4. 1: Synthetic scheme for the preparation of monomers and dimers of planer fluorene.

a. *t*BuOK, 1-bromohexane, THF, 0 ^{o}C 30 min, 20 ^{o}C 3 h; b. $(Bpin)_2$, $Pd(dppf)Cl_2$, KOAc, 1,4-dioxane, 90 ^{o}C; c. Methyl 2-bromobenzoate, $Pd(PPh_3)_4$, Na_2CO_3, toluene, H_2O, reflux; d. MeMgBr, THF, reflux 12 h; e. CH_2Cl_2/CH_3SO_3H = 9/1, 0 ^{o}C 30 min, 20 ^{o}C 3 h; f. HNO_3 (fuming)/0 ^{o}C in AcOH 10 min, 20 ^{o}C 14 h; g. (i) 3,3-dimethyl-3H-benzo[c][1,2]oxaborol-1-ol, $Pd(dppf)Cl_2$, Na_2CO_3, DME, H_2O, reflux; (ii) CH_2Cl_2/CH_3SO_3H = 9/1, 0 ^{o}C 30 min, 20 ^{o}C 3 h; h. Sn powder, HCl, DME, EtOH, reflux; i. HBr (48%), H_2O, MeCN, 90 ^{o}C; prechilled aqueous $NaNO_2$ 1h, CuBr in HBr (48%) 0 ^{o}C 1h, reflux 12 h.

Electrochemistry. The electron donor strengths of n**PP** and n**PP**$_2$ (n = 2-4) were evaluated by electrochemical oxidation at a platinum electrode as a 2 mM solution in CH_2Cl_2 containing 0.1 M n-Bu_4NPF_6 as the supporting electrolyte. The cyclic voltammograms (CV) of n**PP** showed that that upon increasing the number of phenylenes, the first oxidation potential decreases from E_{ox} = 1.27 V vs Fc/Fc^+ in 2**PP**, to 0.89 V in 3**PP**, to 0.68 V in 4**PP** (**Figure 4.2**). Noteworthy, while 2**PP** (expectedly) displays an irreversible CV due to the presence of the substitution-labile carbons that

render the cation radicals susceptible to dimerization, the CVs of 3**PP** and 4**PP** were found to be completely reversible.

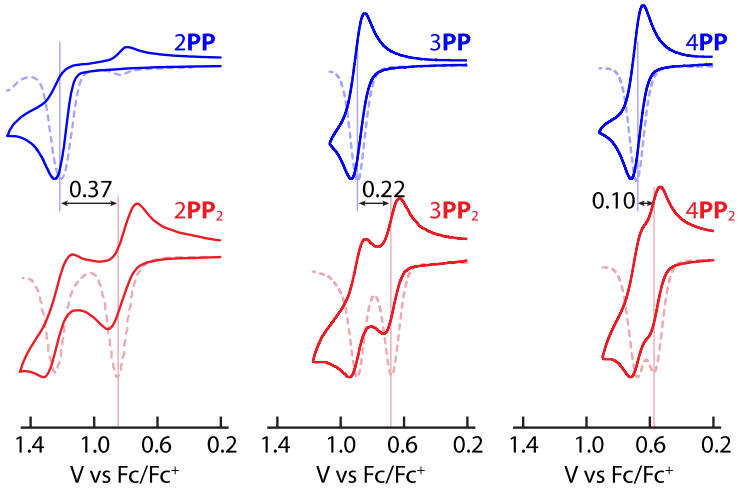

Figure 4. 2. Cyclic (solid lines) and square-wave (dashed lines) voltammograms of 2 mM *n***PP** (blue) and *n***PP**$_2$ (red) in CH_2Cl_2 (0.1 M *n*-Bu_4NPF_6) at 200 mV s^{-1} and 22 ºC.

The reversible CVs of *n***PP**$_2$ (*n* = 2-4) showed two well-separated oxidation waves that correspond to formation of the cation radical and dication (**Figure 4.2**). As the number of phenylenes in each chromophore increases, the first oxidation potential of *n***PP**$_2$ decreases from E_{ox} = 0.90 V vs Fc/Fc^+ in 2**PP**$_2$ to 0.67 V in 3**PP**$_2$ to 0.58 V in 4**PP**$_2$. Because the E_{ox} of monochromophoric *n***PP** decreases faster with increasing *n* than E_{ox} of bichromophoric *n***PP**$_2$, the amount of hole stabilization, measured as the difference ΔE_{ox} = E_{ox}[*n***PP**] – E_{ox}[*n***PP**$_2$], decreases from 0.37 to 0.22 to 0.10 V, indicating that the interchromophoric electronic coupling decreases with increasing *n* (**Table 4.1**). Consistent with this conclusion, we also note that the separation between two oxidation

waves in *n***PP**$_2$ decreases with increasing chromophore size, signifying that that the repulsive interactions between the positive charge densities in *n***PP**$_2^{2+}$ also decrease with increasing chromophore size.[15-18]

Table 4. 1. Oxidation potentials (E_{ox}, V vs Fc/Fc$^+$) of *n***PP** and *n***PP**$_2$; experimental (ΔE_{ox}, V) and computed using B1LYP40/6-31G(d)+PCM(CH_2Cl_2) (ΔG_{ox}, eV) hole stabilizations; wavelengths (λ, nm) of maximum absorption of *n***PP**$^{+\bullet}$ and *n***PP**$_2^{+\bullet}$. Data for λ[2**PP**$^{+\bullet}$] and λ[2**PP**$_2^{+\bullet}$] was taken from literature.[10]

n	E_{ox}[*n***PP**]	E_{ox}[*n***PP**$_2$]	ΔE_{ox}	ΔG_{ox}	λ[*n***PP**$^{+\bullet}$]	λ[*n***PP**$_2^{+\bullet}$]
2	1.27	0.9	0.37	0.37	690	1240
3	0.89	0.67	0.22	0.19	872	1784
4	0.68	0.58	0.10	0.08	1100	2330

In order to further probe the electronic structure of *n***PP**$_2$ we resorted to electronic spectroscopy of their cation radicals. The cation radicals are expected to display an intervalence transition in the near-IR region, the position and intensity of which are sensitive to the degree of electronic coupling.[19-21] Cation radicals of *n***PP**$_2$ and *n***PP** (*n* = 3 and 4) were generated via quantitative[22,23] redox titrations using two aromatic oxidants: **THEO**$^{+\bullet}SbCl_6^-$ (**THEO** = tetrasubstituted *p*-hydroquinone ether, E_{red1} = 0.67 V vs Fc/Fc$^+$, λ_{max} = 518 nm, ε_{max} = 7300 cm^{-1} M^{-1})[24] and **NAP**$^{+\bullet}SbCl_6^-$ (**NAP** = cycloannulated naphthalene derivative, E_{red1} = 0.94 V vs Fc/Fc$^+$, λ_{max} = 672 nm, ε_{max} = 9300 cm^{-1} M^{-1}).[25,26] Each redox titration experiment was carried out by an incremental addition of sub-stoichiometric amounts of the electron donor (**D**, i.e., *n***PP**$_2$ or *n***PP**) to the solution of an oxidant cation radical (**Ox**$^{+\bullet}$, i.e., **THEO**$^{+\bullet}$ or **NAP**$^{+\bullet}$). The one-electron oxidation of **D** to **D**$^{+\bullet}$ and reduction of **Ox**$^{+\bullet}$ to **Ox** can be described by an equilibrium shown in eq. 1.

$$\mathbf{Ox}^{+\bullet} + \mathbf{D} \rightleftarrows \mathbf{Ox} + \mathbf{D}^{+\bullet} \text{……..(eq. 1)}$$

The reproducible spectra of $n\mathbf{PP}^{+\bullet}/n\mathbf{PP}_2^{+\bullet}$ were obtained by a robust numerical deconvolution procedure[22,23] at each titration point that produced the mole fraction plots of each species involved in the redox reaction. The plots show that, in the case of 3**PP**, 4**PP** and 3$\mathbf{PP}_2$, addition of a neutral donor leads to exclusive formation of the corresponding cation radical and complete consumption of the oxidant (**Figure 4.3**). In the case of 4$\mathbf{PP}_2$, the redox titrations involved two successive one-electron oxidations with multiple equilibria as shown in **Figure 4.3G**. Upon addition of 0.5 equivalents of 4$\mathbf{PP}_2$, the oxidant is consumed completely and only the dication 4$\mathbf{PP}_2^{2+}$ is formed, due to the similar values of its first and second oxidation energies (**Table 4.1**). Upon further addition of 0.5 equivalents of neutral 4$\mathbf{PP}_2$, 4$\mathbf{PP}_2^{2+}$ is completely converted into the 4$\mathbf{PP}_2^{+\bullet}$ via a disproportionation reaction.[22]

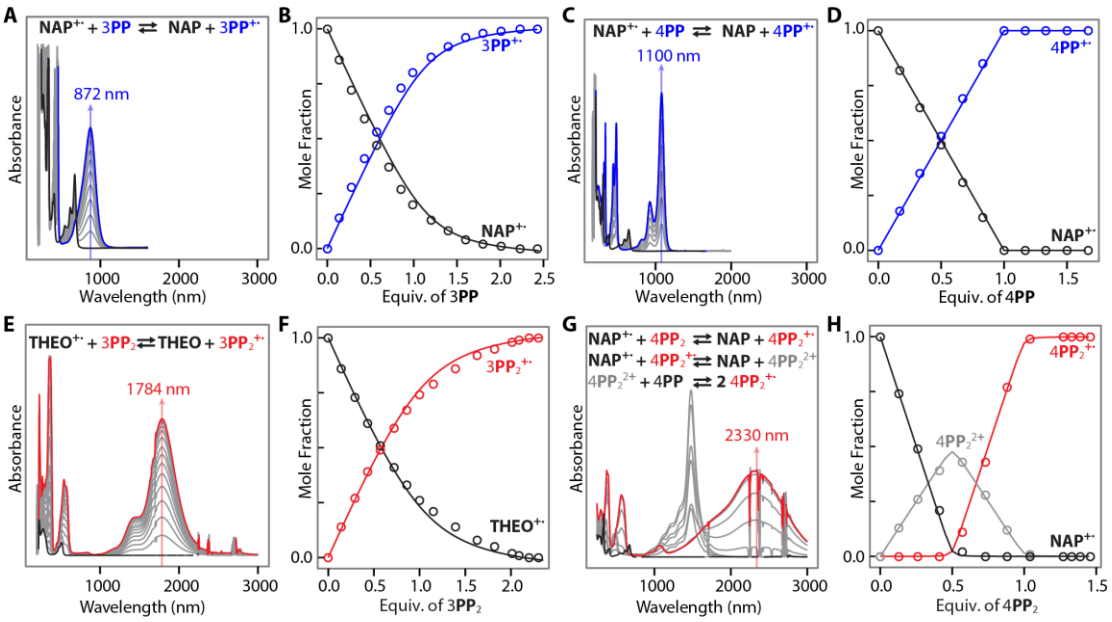

Figure 4. 3. A. Spectral changes observed upon the reduction of 0.036 mM **NAP**$^{+\bullet}$ in CH_2Cl_2 by incremental addition of 2.2 mM solution of 3**PP** in CH_2Cl_2. B. Mole fraction plot of **NAP**$^{+\bullet}$ (black) and 3**PP**$^{+\bullet}$ (blue) against the added equivalents of 3**PP**. Symbols represent experimental points, while the solid lines show best-fit to the experimental points using ΔG_1 = -0.08 V.[22] C. Spectral changes observed upon the reduction of 0.021 mM **NAP**$^{+\bullet}$ in CH_2Cl_2 by incremental addition of 2.1 mM solution of 4**PP** in CH_2Cl_2. D. Mole fraction plot of **NAP**$^{+\bullet}$ (black) and 4**PP**$^{+\bullet}$ (blue) against the added equivalents of 4**PP**. Symbols represent experimental points, while the solid lines show best-fit to the experimental points using ΔG_1 = -1.16 V. E. Spectral changes observed upon the reduction of 0.027 mM **THEO**$^{+\bullet}$ in CH_2Cl_2 by incremental addition of 0.77 mM solution of 3**PP**$_2$ in CH_2Cl_2. F. Mole fraction plot of **THEO**$^{+\bullet}$ (black) and 3**PP**$_2^{+\bullet}$ (red) against the added equivalents of 3**PP**$_2$. Symbols represent experimental points, while the solid lines show best-fit to the experimental points using ΔG_1 = -0.06 V. G. Spectral changes observed upon the reduction of 0.018 mM **NAP**$^{+\bullet}$ in CH_2Cl_2 by incremental addition of 0.45 mM solution of 4**PP**$_2$ in CH_2Cl_2. H. Mole fraction plot of **NAP**$^{+\bullet}$ (black), 4**PP**$_2^{2+}$ (grey) and 4**PP**$_2^{+\bullet}$ (red) against the added equivalents of 4**PP**$_2$. Symbols represent experimental points, while the solid lines show best-fit to the experimental points using ΔG_1 = -0.39 V and ΔG_{12} = 0.22 mV.

Electronic absorption spectra of *n***PP**$_2^{+\bullet}$ (*n* = 3-4), obtained from the deconvolution, show the presence of a characteristic broad band that is red-shifted (i.e., shifted to longer wavelength) as compared to the corresponding monochromophoric *n***PP**$^{+\bullet}$ (**Figure 4.3**), signifying extensive hole delocalization in *n***PP**$_2^{+\bullet}$. At the same time,

as the number of phenylenes in the chromophore increases, the position of the near-IR band shifts to longer wavelengths, indicating that the electronic coupling is decreasing. In order to further probe the evolution of electronic coupling with chromophore size, we resorted to density functional theory (DFT) calculations.

Accurate description of the electronic structure of π-conjugated cation radicals is challenging for DFT due to the self-interaction error (SIE), which may lead in unfavorable cases to artificial hole delocalization, artificially low oxidation energies and an incorrect description of the excited states.[27-30] The SIE can be partially corrected by inclusion of a calibrated amount of the exact Hartree−Fock (HF) exchange term into the hybrid density functional.[19,31] In our past studies, B1LYP[32] functional with 40% of HF exchange term (i.e., B1LYP-40)[33] was introduced where the amount of Hartree-Fock exchange term was fine-tuned to reproduce experimental oxidation potentials and cation radical excitation energies of poly-*p*-phenylenes with increasing number of *p*-phenylenes. Noteworthy, it was later shown that B1LYP-40/6-31G(d) performs exceptionally well in reproducing the experimental redox/optoelectronic properties of a variety of π-conjugated[10-12] and π-stacked assemblies[33-35] that were not included in the original training set. Therefore, in this manuscript we performed DFT calculations of *n***PP**/*n***PP**$_2$ and their cation radical using B1LYP-40/6-31G(d) method and account for the solvent effects using the polarizable continuum model (PCM)[36] with CH_2Cl_2 parameters. X-ray crystallography of numerous neutral aromatic hydrocarbons and their cation radicals has established that oxidation induces significant structural reorganization in the form of elongations and contractions of the C-C bonds as well as in decrease of dihedral angles between adjacent aromatic moieties.[37,38] Indeed, calculations showed that upon

oxidation, the molecular structure of *n***PP**$_2$ undergoes a quinoidal distortion, as exemplified for 2**PP**$_2$ in **Figure 4.4A** below.

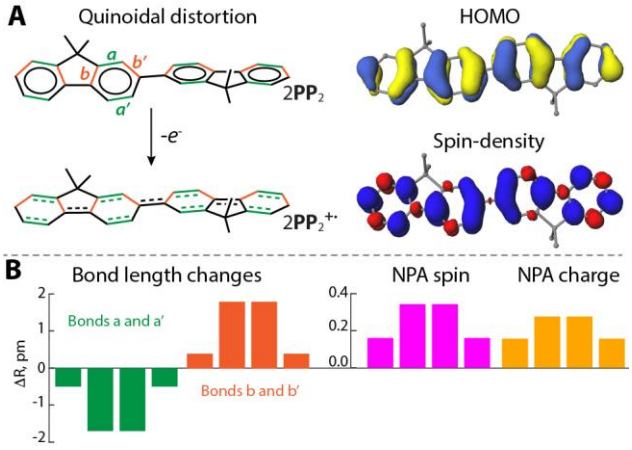

Figure 4. 4. A Schematic representation of the quinoidal distortion in 2**PP**$_2$→2**PP**$_2^{+\bullet}$ transformation, HOMO of 2**PP**$_2$ and spin-density of 2**PP**$_2^{+\bullet}$. B. Per-phenylene bar-plot representation of the distributions of the bond length changes, NPA spins and charges in 2**PP**$_2^{+\bullet}$.

Importantly, oxidation-induced bond length changes track in the accordance with the disposition of the lobes of HOMO, i.e., bonds that correspond to the bonding lobes undergo contraction and bonds that correspond to the antibonding lobes undergo contraction, e.g. the average of bonds *a* and *a*' contracts by 0.5-1.7 pm, while the average of bonds *b* and *b*' elongates by 0.4-1.8 pm (**Figure 4.4B**). The natural population analysis (NPA) of the electron density in 2**PP**$_2^{+\bullet}$ further showed that the spin and charge distributions parallel the distribution of the bond-length changes indicating polaron formation[39-41] (**Figure 4.4B**).

A simple yet intuitive model to describe the polaron (i.e., hole) delocalization in various mixed-valence compounds is the two-state Marcus-Hush theory, which predicts that the extent of polaron delocalization depends on the interplay between electronic coupling (H_{ab}) and reorganization energy (λ).[19,20,42,43] In the large electronic coupling limit ($2H_{ab} \geq \lambda$), the polaron is evenly delocalized between two sites (i.e., class III or 'static' delocalization), while in the limit of small electronic coupling ($2H_{ab} < \lambda$), the polaron is partially delocalized with the distribution maximum centered on one of the sites (i.e., class II or 'dynamic' hopping). When electronic coupling is non-existent ($H_{ab} = 0$, class I), the polaron is fully localized on one site.

Partitioning the spin, charge and structural reorganization distributions in $2\mathbf{PP}_2^{+\bullet}$ between a pair of fluorenes rather than four phenylenes suggests that the polaron is evenly delocalized between the fluorenes, hence the mechanism of polaron delocalization is 'static' delocalization according to the two-state representation (**Figure 4.5**).

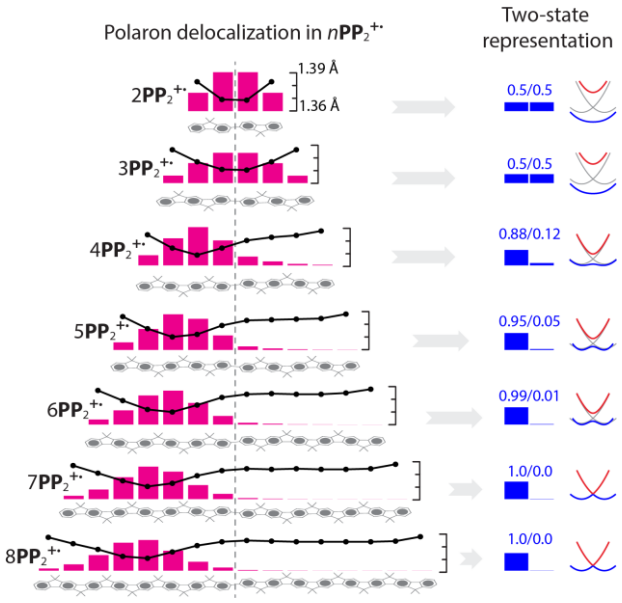

Figure 4. 5. Left. Per-phenylene bar-plot representation of the distributions of the NPA spin (magenta) superimposed with the plot of C-C bond length (average of *a* and *a*', Figure 4) in $n\mathbf{PP}_2^{+\bullet}$. Right: Two-state representation of polaron delocalization in $n\mathbf{PP}_2^{+\bullet}$.

Similarly, in $3\mathbf{PP}_2^{+\bullet}$ the spin/charge/bond length changes are delocalized along the entire bichromophore, and thus the mechanism of polaron delocalization is also static delocalization. However, further increase of the chromophore size shifts the polaron distribution towards one side of $n\mathbf{PP}_2^{+\bullet}$ ($n > 3$), indicating that the mechanism of polaron delocalization evolves into dynamic hopping, i.e. class II (**Figure 4.5**). In the case of even longer $n\mathbf{PP}_2^{+\bullet}$ ($n > 5$), the polaron is fully localized on a single chromophore, i.e., this bichromophore belong to the class I. Thus, depending the chromophore size, the mechanism of hole delocalization in two-state representation may switch from static delocalization to dynamic hopping to a complete localization, akin to the switchover

observed for biaryls with varied interplanar angle.[43] As the extent of hole delocalization depends on the interplay between electronic coupling (H_{ab}) and reorganization energy (λ), the switchover in the delocalization mechanism arises due to the decreasing H_{ab} and/or increasing λ.[42]

In order to confirm that the switchover in the delocalization mechanism occurs due to the decreasing electronic coupling, we first compare computed oxidation free energies (G_{ox}) of *n***PP** and *n***PP**$_2$ (*n* = 2-8). Calculations showed that as the number of phenylenes in the chromophore increases, oxidation energies of both *n***PP** and *n***PP**$_2$ decrease (**Figure 4.6A**). Furthermore, hole stabilization, measured as the difference $\Delta G_{ox} = G_{ox}[n\mathbf{PP}] - G_{ox}[n\mathbf{PP}_2]$, is the largest for *n* = 2 and decreases with increasing *n*. Comparing the computed ΔG_{ox} with the available experimental values of ΔE_{ox} for *n* = 2-4 (**Table 4.1**), it is clear that the B1LYP40 method shows a remarkable performance in reproducing hole stabilization for these systems, as the error in the computed ΔG_{ox} values is less than 0.03 eV. This suggests that calculations can provide reliable information on the extent hole stabilization for the longer bichromophores, for which experimental data is unavailable. Calculations show that for longer *n***PP**$_2$ increase in the chromophore size reduces the hole stabilization to nearly non-existent values, i.e., $\Delta G_{ox} < 0.01$ for $n > 5$, which is consistent with complete localization of the polaron on a single chromophore.

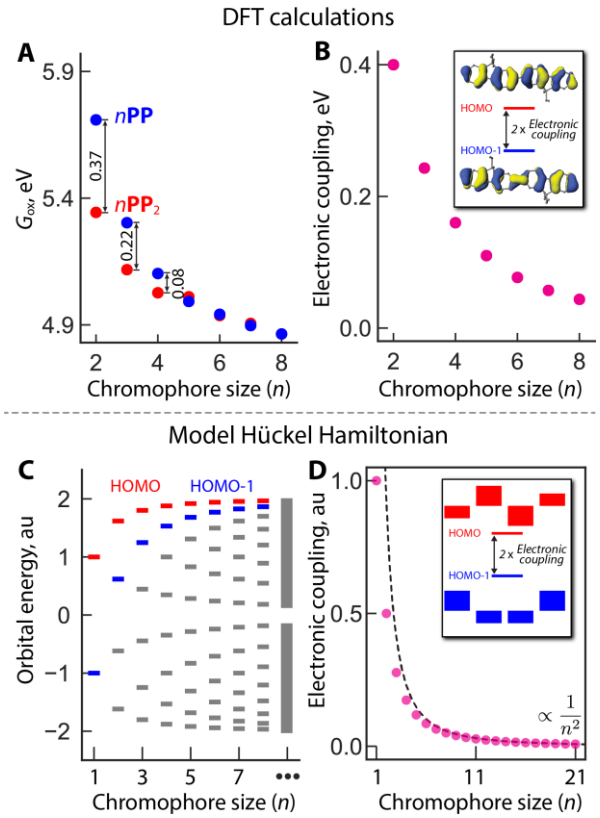

Figure 4. 6. A. Oxidation energies (G_{ox}) of *n***PP** (blue) and *n***PP**$_2$ (red) against the chromophore size measured in the number of phenylene units (*n*) computed using B1LYP40/6-31G(d)+PCM(CH_2Cl_2). B Interchromophoric electronic coupling of *n***PP**$_2$ measured as a half of the HOMO/HOMO-1 energy gap against chromophore size (*n*). Inset shows HOMO and HOMO-1 of 2**PP**$_2$. C. Orbital energies calculated for a model Hückel Hamiltonian matrix (eq. 2) against number of phenylene units. D. Electronic coupling measured as a HOMO/HOMO-1 energy gap from a model Hückel Hamiltonian matrix against number of phenylene units. Dashed line corresponds to the $3\pi^2/8n^2$ dependence derived in the limit of $n\rightarrow\infty$; see Supporting Information for details. Inset shows per-phenylene barplot representation of HOMO and HOMO-1 wavefunctions of 2**PP**$_2$ obtained from Hückel Hamiltonian.

Following Hückel's approach of representing molecular orbitals (MO) as a linear combination of atomic orbitals, the two frontier MOs of *n***PP**$_2$ can be represented as symmetric and antisymmetric linear combinations of the HOMO of a single

chromophore. Then the energy difference between HOMO and HOMO-1 equals twice the electronic coupling, and thus can be quickly determined from the DFT calculations of neutral *n***PP**$_2$. Following this approach, electronic couplings were computed for each *n***PP**$_2$, which showed decreasing dependence with the chromophore size (**Figure 4.6B**). In order to provide an intuitive rationale for this observation we resorted to a theoretical model. Following Hückel theory, each bichromophore *n***PP**$_2$ can be represented as a set of 2*n* electronically coupled phenylenes with the Hamiltonian matrix **H**:

$$\mathbf{H} = \begin{bmatrix} \alpha & \beta & \cdots & 0 & 0 \\ \beta & \alpha & \cdots & 0 & 0 \\ \vdots & \vdots & \ddots & \vdots & \vdots \\ 0 & 0 & \cdots & \alpha & \beta \\ 0 & 0 & \cdots & \beta & \alpha \end{bmatrix} \quad (eq.2),$$

where **H** is the 2*n*×2*n* tight-binding matrix, α is the orbital energy of a single phenylene, and β is the electronic coupling between a pair of adjacent phenylenes. Note that analytical expressions of eigenvalues (i.e., MO energies) and eigenvectors (i.e., MO wavefunctions) of Hückel Hamiltonian matrix are known from the original works.[44,45] Here, for the sake of simplicity, we set α = 0 and β = -1.

Diagonalization of the Hamiltonian **H** produced eigenvalues of a bichromophore, among which two largest eigenvalues correspond to the energies of HOMO and HOMO-1 (**Figure 4.6C**). The corresponding eigenvectors can be represented as symmetric and antisymmetric linear combinations of the HOMO of a single chromophore. Thus, based on the simple Hückel Hamiltonian, the energy gap between HOMO and HOMO-1 decreases with increasing number of phenylenes in a chromophore, leading to nearly isoenergetic values and thus negligible electronic coupling at large *n* (**Figure 4.6D**). This

is fully consistent with results obtained from DFT calculations (**Figure 4.6B**). In contrast to DFT calculations, solution to the Hückel Hamiltonian matrix is available in an analytic form,[44,45] and thus allows a derivation of the analytic formula for the electronic coupling, which in the limit of $n \to \infty$ follows a simple $3\pi^2/8n^2$ dependence (**Figure 4.6D**);

We note that while in a discrete molecule the MO energies are clearly distinguished, at the polymeric limit the energy *bands* are formed that can be described by a continuous density of states (**Figure 4.6B**).[46,47] It is thus inevitable that as the oligomer size increases, the spacing between its MO energies (HOMO and HOMO-1 included) will decrease and reach near-degenerate values at the polymeric limit, which in case of a bichromophoric oligomer can be interpreted as decreasing the electronic coupling between chromophores.

Following a recent study[14] on the mechanism of hole delocalization in biaryls with varied donor strength of the substituent and varied size of the chromophore, an alternative explanation of decreasing electronic coupling in *n***PP**$_2$ is warranted. This study showed that upon increase in the chromophore size a total of two electrons per orbital spreads over a larger area, thus decreasing the amount of the electron density at the coupling-mediating carbons at the biaryl linkage and leading to a diminished electronic coupling. Likewise, as the number of phenylenes in each chromophore of *n***PP**$_2$ increases, the electron density of HOMO spreads over a larger number of carbons, decreasing the electron density at the coupling-mediating carbons and thereby decreasing interchromophoric electronic coupling.

CONCLUSION

Motivated by the question whether a set of linearly connected fluorenes is better termed a poly-fluorene or poly-phenylene wire (**Figure 4.1**), we performed a combined experimental/theoretical study on a series of phenylene-based bichromophores *n***PP**$_2$ of increasing size. We found that as the number of phenylenes in a chromophore increases from n = 2 to 4, the amount of hole stabilization measured electrochemically decreases and the absorption band in the electronic spectra of *n***PP**$_2^{+\bullet}$ shifts to longer wavelength, indicating that the interchromophoric electronic coupling decreases. Aided by the benchmarked DFT calculations of a series of long *n***PP**/*n***PP**$_2$ (n = 2-8) we have shown that the electronic coupling decreases to nearly non-existent values when n > 5, leading to a complete localization of a polaron (i.e., hole) on a single chromophore in corresponding *n***PP**$_2^{+\bullet}$. Finally, using a model Hückel Hamiltonian we showed that the decreasing electronic coupling is a consequence of the clustering of MO energy level as the length of the oligomer increases. This obvious, yet fundamental understanding that the interchromophoric electronic coupling decreases with increasing chromophore size is crucial during the rational design of novel electron donors for photovoltaic and molecular electronic applications.

GENERAL EXPERIMENTAL METHODS

All reactions were performed under argon atmosphere unless otherwise noted. All commercial reagents were used without further purification unless otherwise noted. Dichloromethane (Aldrich) was repeatedly stirred with fresh aliquots of concentrated sulfuric acid (~10 % by volume) until the acid layer remained colorless. After separation it was washed successively with water, aqueous sodium bicarbonate, water, and aqueous sodium chloride and dried over anhydrous calcium chloride. The dichloromethane was distilled twice from P_2O_5 under an argon atmosphere and stored in a Schlenk flask equipped with a Teflon valve fitted with Viton O-rings. The hexanes and toluene were distilled from P_2O_5 under an argon atmosphere and then refluxed over calcium hydride (~12 h). After distillation from CaH_2, the solvents were stored in Schlenk flasks under an argon atmosphere. Tetrahydrofuran (THF) was dried initially by distilling over lithium aluminum hydride under an argon atmosphere. The THF was further refluxed over metallic sodium in the presence of benzophenone until a persistent blue color was obtained and then it was distilled under an argon atmosphere and stored in a Schlenk flask equipped with a Teflon valve fitted with Viton O-rings. NMR spectra were recorded on Varian 300 and 400 MHz NMR spectrometers. Mass spectra were recorded on Bruker Daltonics MALDI-TOF mass spectrometer and Electronic absorption (UV−vis/NIR) measurements were made on a Cary 5000 instrument.

Synthetic schemes for the preparation of compounds in **Chart 4.1** are presented below in individual schemes S2-S5 together with the detailed experimental procedures for each step of synthesis and their characterization data (i.e. numerical spectroscopic data) as well as $^{1}H/^{13}C$ NMR spectra are given below. Note that identity of each molecule was further confirmed by MALDI mass spectrometry.

Scheme 4. 2:. Synthesis of 3PP

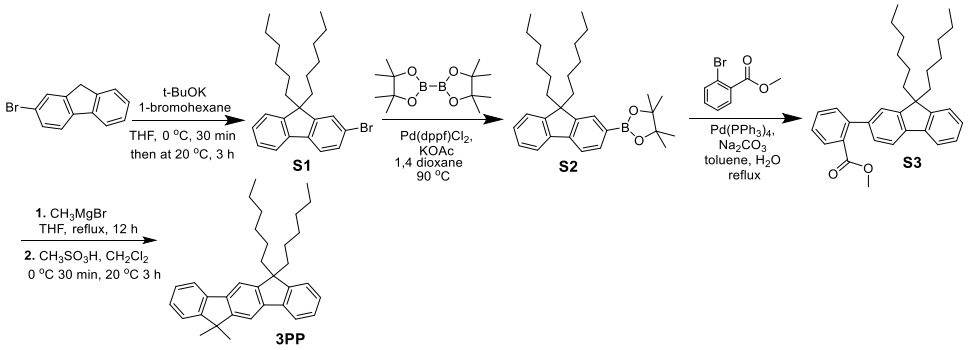

Synthesis of 2-bromo-9,9-dihexyl-fluorene, **S1**[48]:

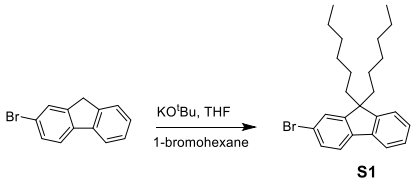

To an ice cooled solution of 2-bromofluorene (5 g, 20.4 mmol, 1.0 eq.) in dry THF (30 mL) under an argon atmosphere was added potassium *tert*-butoxide (6.90 g, 61.5 mmol, 2.56 eq.) and then the solution was stirred at room temperature for 15 min. 1-bromohexane (8.41 g, 50.94 mmol, 2.5 eq.) was added dropwise into the solution and continued stirring the reaction mixture for additional 3 h. The reaction mixture was

neutralized with 5 % aqueous HCl solution (40 mL). After the reaction mixture was extracted with CH_2Cl_2 (3×40 mL), combined organic extracts were dried over anhydrous $MgSO_4$ and the solvent was removed under reduced pressure. The thick crude liquid was purified by silica gel column chromatography using hexane as eluent to afford 6.05 g (yield 71.7 %) pure gummy **S1**. ^{1}H NMR (400 MHz, $CDCl_3$) δ ppm 0.63-0.74 (m, 4H), 0.83 (t, 6H), 1.04-1.22 (m, 12 H), 1.96-2.09 (m, 4H), 7.34-7.41 (m, 3H), 7.50 (dd, *J* = 1.84 Hz, 8.00 Hz, 1H), 7.55 (d, *J* = 1.77 Hz, 1H), 7.60 (d, *J* = 8.06 Hz, 1H), 7.69-7.74 (m, 1 H); ^{13}C NMR (400MHz, $CDCl_3$) δ ppm 14.15, 22.72, 23.80, 29.80, 31.61, 40.45, 55.47, 119.86, 121.12, 122.94, 126.22, 127.03, 127.57, 130.00, 140.12, 140.23, 150.37, 153.05.

Synthesis of **S2**[49]:

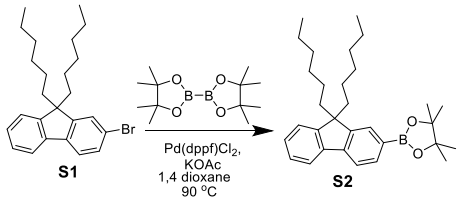

2-bromo-9,9-dihexyl-fluorene (**S1**, 6.50 g, 15.72 mmol, 1.0 eq.), bis(pinacolato)diboron (4.39 g, 17.28 mmol, 1.1 eq.), potassium acetate (4.62 g, 47.16 mmol, 3.0 eq), and Pd(dppf)Cl_2 (667 mg, 0.91 mmol, 0.058 eq.) were mixed in dry dioxane (100 mL) under an argon atmosphere and the mixture were heated at 90 °C for 12 hours. After adding 50 mL of water to quench the reaction, the mixture was extracted with dichloromethane (2×30 mL). Combined organic layers were dried over anhydrous $MgSO_4$ and solvent was removed under reduced pressure. The crude product was filtered through silica using 70:30 mixture of hexane and ethyl acetate to give the title compound **S2** as a thick liquid (7.16 g, 99% yield). ^{1}H NMR (400MHz, $CDCl_3$) δ ppm 0.5-0.64 (m,

4H), 0.75 (t, 6H, *J* = 7.27 Hz), 0.95-1.14 (m, 12H), 1.39 (s, 12 H), 1.89-2.07 (m, 4H), 7.27-7.37 (m, 3H), 7.66-7.76 (m, 3H), 7.80 (dd, 1H, *J* = 7.54 Hz, 0.95 Hz); ^{13}C NMR (400MHz, $CDCl_3$) δ ppm 14.16, 22.72, 23.78, 25.09, 29.82, 31.62, 40.38, 55.21, 83.83, 119.09, 120.21, 123.06, 126.78, 127.60, 128.95, 133.82, 141.04, 144.25, 150.00, 151.43.

Synthesis of **S3**:

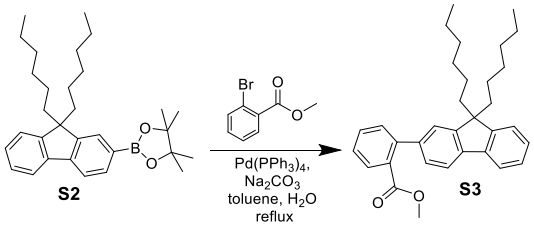

Compound **S2** (3.50 g, 7.60 mmol, 1.0 eq), methyl 2-bromobenzoate (2.66 g, 12.37 mmol, 1.62 eq), $Pd(PPh_3)_4$ (50 mg) and 50 mL of toluene were placed in a dried Schlenk flask. Then an aqueous solution of Na_2CO_3 (5 g in 20 mL water) was added in the Schlenk flask. The reaction mixture was evacuated and filled with argon for three times. The reaction mixture was then heated to reflux for overnight. After completion of the reaction, the reaction was quenched by adding 30 mL of water and then extracted with dichloromethane (4×50 mL). The combined organic extracts were dried over anhydrous $MgSO_4$ and the solvent was removed under reduced pressure. The crude product was purified through silica gel column chromatography using hexane to afford **S3** as solid (3.45 g, 97 %). m.p. 50-52 °C. ^{1}H NMR (300MHz, $CDCl_3$) δ ppm 0.57-0.72 (m, 4H), 0.76 (t, 6H, *J* = 7.13 Hz), 1.00-1.19 (m, 12 H), 1.89-2.07 (m, 4H), 3.59 (s, 3H), 7.28-7.40 (m, 5H), 7.41-7.50 (m, 2H), 7.58 (td, 1H, *J* = 7.35 Hz, 1.46 Hz), 7.71-7.78 (m, 2H), 7.85 (ddd, 1H, *J* = 7.71 Hz, 1.42 Hz, 0.42 Hz); ^{13}C NMR (400MHz, $CDCl_3$) δ ppm 14.13, 22.71, 23.83, 29.86, 31.66, 40.62, 51.94, 55.21, 119.47, 119.86, 122.93, 123.00,

126.88, 127.12, 127.33, 129.82, 130.88, 131.23, 131.35, 140.31, 140.39, 140.90, 140.95, 142.91, 150.72, 150.95, 169.62.

Synthesis of **3PP** [49]:

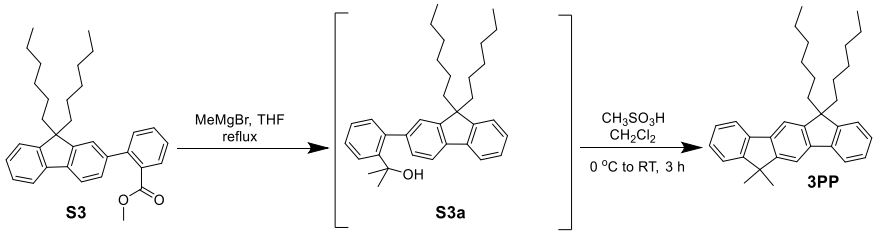

Compound **S3** (4.11g, 8.76 mmol, 1.0 eq.) was dissolved in 60 mL of anhydrous THF under argon and CH_3MgBr (3 M in diethyl ether, 29.2 mL, 87.69 mmol, 10.0 eq.) was added. After refluxing for 10 h, the reaction mixture was cooled to 0 °C by using ice bath. Water (100 mL) was added into flask very slowly [**Caution**: It is exothermic reaction] and the mixture was extracted with diethyl ether (3×30 mL). The organic phase was dried over anhydrous $MgSO_4$ and the solvent was removed under reduced pressure. The intermediate crude alcohol **S3a** (without purification) was treated with CH_3SO_3H/CH_2Cl_2 (6 mL/54 mL) at 0 °C for 30 minutes and stirred at room temperature for 4 hours. The reaction mixture was quenched with aqueous saturated $NaHCO_3$ solution and extracted with dichloromethane. The organic phase was washed with water and dried over anhydrous $MgSO_4$. The solvent was removed under reduced pressure and purified through silica gel column chromatography using hexane as solvent to afford pure **3PP** as thick liquid (3.42 g, 86 %). ^{1}H NMR (400MHz, $CDCl_3$) δ ppm 0.57-0.85 (m, 10H), 1.00-1.19 (m, 12H), 1.61 (s, 6H), 1.99-2.11 (m, 4H), 7.29-7.42 (m, 5H), 7.48-7.50 (m, 1H), 7.70 (s, 1H), 7.78-7.84 (m, 3H); ^{13}C NMR (400MHz, $CDCl_3$) δ ppm 14.17, 22.77, 23.92, 27.61, 29.94, 31.68, 40.86, 46.66, 54.83, 113.91, 114.38, 119.46, 119.80, 122.77, 122.94,

126.86, 126.82, 126.84, 126.99, 138.65, 139.74, 140.82, 141.41, 150.25, 151.27, 152.95, 154.22.

Scheme 4. 3: Synthesis of $3PP_2$.

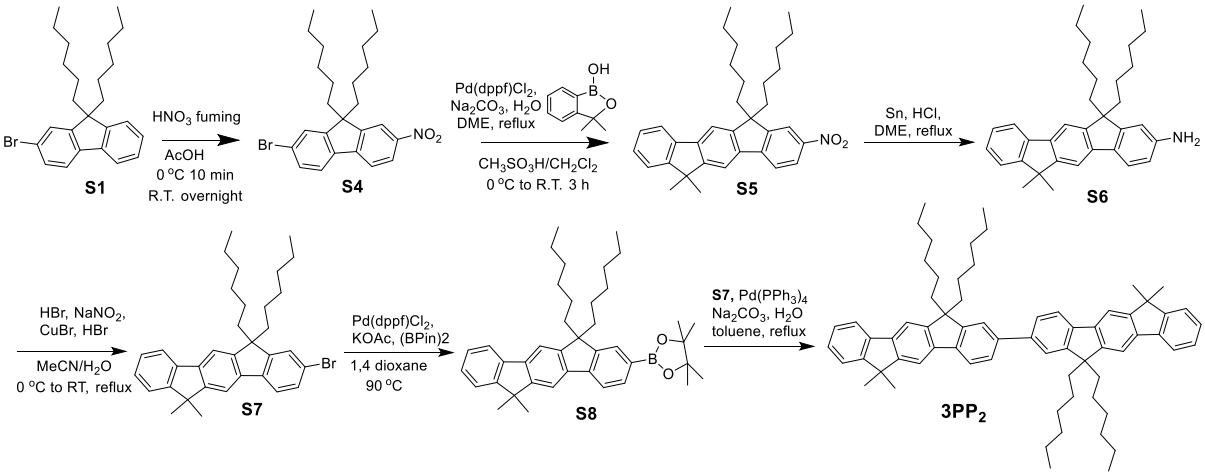

Synthesis of **S4**[51]:

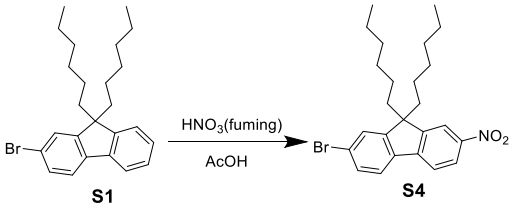

2-bromo-9,9-dihexylfluorene, **S1** (5g, 12.13 mmol) was dissolved in 85 mL of glacial acetic acid. To the formed solution, 20 mL of fuming nitric acid were added dropwise over 10 min at 0 °C upon vigorous stirring. After addition was completed, reaction mixture was further stirred at 20 °C for overnight. The yellow color solution was poured into 600 mL of water and extracted with dichloromethane (4×50 mL). The combined dichloromethane extracts were washed with saturated aqueous $NaHCO_3$ solution and water and the organic layer was dried over anhydrous $MgSO_4$. The solvent was removed under reduced pressure. Yellow thick liquid was passed through silica pad

column using hexane and give yellow colored crude product. Through multiple crystallization from methanol afforded 4.55 g (82% yield) of pure **S4**. m.p. 52 - 54° C, Lit.[2] 54-57 ° C. ^{1}H NMR (400MHz, $CDCl_3$) δ ppm 0.48-0.63 (m, 4H), 0.76 (t, *J* = 7.23 Hz, 6H), 0.96-1.16 (m, 12H), 1.91-2.08 (m, 4H), 7.50-7.55 (m, 2H), 7.64 (d, *J* = 8.56 Hz, 1H), 7.76 (d, *J* = 8.41 Hz, 1H), 8.18 (d, *J* = 2.08 Hz, 1H), 8.26 (dd, *J* = 8.40, 2.08 Hz, 1H); ^{13}C NMR (400MHz, $CDCl_3$) δ ppm 14.11, 22.66, 23.83, 29.61, 31.56, 40.13, 56.12, 118.40, 120.10, 122.62, 123.56, 123.82, 126.67, 130.84, 137.83, 146.58, 147.49, 151.72, 154.49.

Synthesis of **S5**[49,50]:

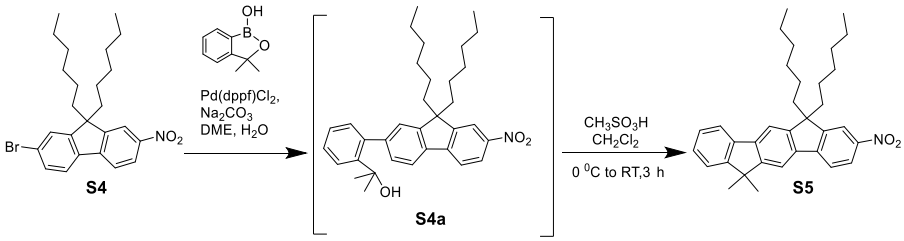

To a mixture of 3,3-dimethyl- 3H-benzo[c][1,2]oxaborol-1-ol (5.30g, 32.71 mmol, 3.0 eq.), **S4** (5.0g, 10.90 mmol, 1.0 eq.), sodium carbonate (6.93g, 65.4 mmol, 6.0 eq), and $Pd(dppf)Cl_2$ (0.797 g, 1.09 mmol, 0.1 eq.) in a 250 mL Schlenk flask equipped with air condenser was added 60 mL of anhydrous DME and 30 mL of water. The mixture was evacuated and filled with argon three times. After heating at 100 °C for overnight, the reaction mixture was then cooled to room temperature and 50 mL of water was added. The blackish solution was transferred to a 1 L separatory funnel and extracted with diethyl ether (4×50 mL). The combined organic layers were dried over anhydrous $MgSO_4$ and the solvent was removed under reduced pressure. The blackish brown

colored crude liquid was dissolved in a 1:1 mixture of hexane and ethyl acetate and filtered through $MgSO_4$ pad to remove black palladium content. Then the solvent was removed under reduced pressure and the resulting thick brown colored compound (**S4a**) was subjected to CH_3SO_3H acid (5 mL) catalyzed cyclization reaction in anhydrous dichloromethane (45 mL) at 0 °C (30 min) and at room temperature 3 hours to afford **S5** as gummy yellow liquid (5.30 g, 98%). ^{1}H NMR (300MHz, $CDCl_3$) δ ppm 0.54-0.69 (m, 4H), 0.75 (t, 6H, *J* = 7.14 Hz), 0.93-1.16 (m, 12H), 1.58 (s, 6H), 1.97-2.14 (m, 4H), 7.32-7.43 (m, 2H), 7.44-7.51 (m, 1H), 7.70 (d, 1H, *J* = 0.63 Hz), 7.82 (dd, 3H, *J* = 8.51, 1.60 Hz), 8.21 (d, 1H, *J* = 2.04 Hz), 8.28 (dd, 1H, *J* = 8.37, 2.1 Hz); ^{13}C NMR (300MHz, $CDCl_3$) δ ppm 14.09, 22.69, 23.91, 27.52, 29.74, 31.61, 40.50, 46.78, 55.48, 114.61, 115.48, 118.30, 119.48, 120.34, 122.93, 123.48, 127.27, 127.92, 138.23, 138.95, 141.12, 146.86, 148.11, 152.16, 152.40, 153.59, 154.45.

Synthesis of **S6**[52]:

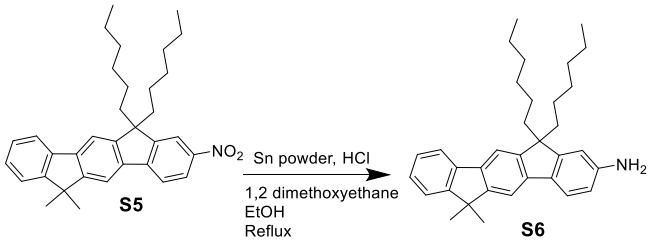

To a solution of **S5** (4.51 g, 9.09 mmol, 1.0 eq.) in 50 mL of 1,2-dimethoxyethane and 20 mL of ethanol, 50 mL of concentrated HCl and Sn (4.32 g, 36.39 mmol, 4.0 eq.) were added carefully and the mixture was stirred at 90 °C for overnight. The reaction mixture was poured into ice cold water and extracted with dichloromethane (3×50 mL). The combined organic extracts were washed with water (3×50 mL) and dried over anhydrous $MgSO_4$. The solvent was removed under reduced pressure to afford pure **S6** as

a thick liquid (4.20 g, 99 %), which was used for the next reaction without purification. ^{1}H NMR (300MHz, $CDCl_3$) δ ppm 0.64-0.77 (m, 4H), 0.81 (t, 6H, *J* = 7.03 Hz), 1.03-1.22 (m, 12H), 1.59 (s, 6H), 1.80-2.12 (m, 4H), 3.76 (bs, 2H), 6.66-6.73 (m, 2H), 7.31 (td, 1H, *J* = 7.27 Hz, 1.26 Hz), 7.38 (td, 1H *J* = 7.40 Hz, 1.26 Hz), 7.47 (d, 1H, *J* = 7.32 Hz), 7.56 (d, 1H, *J* = 8.75 Hz), 7.64 (d, 2H *J* = 0.85 Hz), 7.79 (d, 1H, *J* = 6.91 Hz); ^{13}C NMR (400MHz, $CDCl_3$) δ ppm 14.17, 22.80, 23.87, 27.59, 29.99, 31.71, 41.11, 46.57, 54.57, 109.95, 112.56, 114.04, 114.16, 119.45, 120.25, 122.66, 126.51, 126.95, 132.75, 136.94, 140.01, 141.35, 145.84, 149.24, 152.89, 153.20, 154.03.

Synthesis of **S7**[53]:

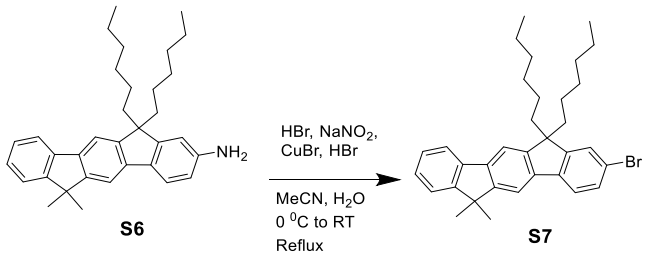

Compound **S6** (3.87 g, 8.30 mmol, 1.0 eq.) was added to a mixture of hydrobromic acid (50 mL, 48 %), water (80 mL) and acetonitrile (80 mL). The mixture was heated to 90 °C to dissolve **S6**, then cooled to 0 °C. The pre-chilled sodium nitrite (0.86 g, 12.46 mmol, 1.5 eq.) in water (20 mL) was added dropwise to the reaction mixture and the mixture was stirred at 0 °C for 1 h. A solution of CuBr (1.3 g, 9.13 mmol, 1.1 eq.) in hydrobromic acid (80 mL, 48 %) was added dropwise at 0 °C and the mixture was stirred vigorously at 0 °C for 1 h. The solution was allowed to warm to room temperature and heated at reflux for 12 h. After the reaction was completed, the mixture was washed with deionized water and extracted with chloroform. The product **S7** (2.40 g, 54 %) was obtained as a colorless thick liquid by silica gel column chromatography using

hexane as an eluent. ^{1}H NMR (400MHz, $CDCl_3$) δ ppm 0.57-0.71 (m, 4H), 0.76 (t, 6H, *J* = 7.17 Hz), 0.94-1.16 (m, 12H), 1.56 (s, 6H), 1.90-2.08 (m,4H), 7.27-7.40 (m, 2H), 7.42-7.49 (m, 3H), 7.55-7.61 (m, 1H), 7.63 (s, 1H), 7.69 (s, 1H), 7.79 (dd, 1H, *J* = 7.01 Hz, 1.42 Hz); ^{13}C NMR (400MHz, $CDCl_3$) δ ppm 14.16, 22.77, 23.88, 27.57, 29.87, 31.66, 40.75, 46.69, 55.20, 114.04, 114.39, 119.90, 120.82, 120.80, 122.91, 126.21, 127.11, 127.21, 129.98, 139.16, 139.49, 139.66, 140.48, 149.90, 153.16, 153.52, 154.21.

Synthesis of **S8**[49]:

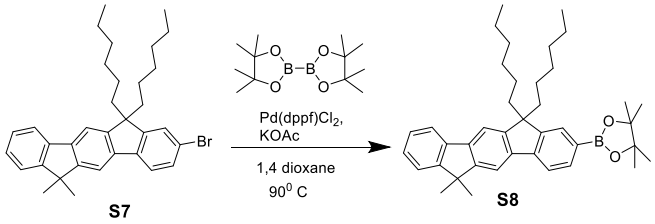

Compound **S7** (0.56 g, 1.057 mmol, 1 eq.), bis(pinacolato)diboron (0.294 g, 1.157 mmol, 1.1 eq.), potassium acetate (0.311 g, 3.16 mmol, 3.0 eq.), and $Pd(dppf)Cl_2$ (23.2 mg, 0.0317 mmol, 3 mmol%) were mixed in dry dioxane (25 mL) under an argon atmosphere and heated at 90 °C for 12 h. The crude reaction mixture was filtered through silica using 1:1 mixture of hexane and ethyl acetate to give **S8** as a thick liquid (0.58 g, 95% yield). ^{1}H NMR (400MHz, $CDCl_3$) δ ppm 0.56-0.69 (m, 4H), 0.74 (t, 6H, *J* = 7.09 Hz), 0.93-1.13 (m, 12H), 1.41 (s, 12H), 1.56 (s, 6H), 1.96-2.09 (m, 4H), 7.27-7.40 (m, 2H), 7.45 (dd, 1H, *J* = 6.52 Hz, 1.26 Hz), 7.65 (s, 1H), 7.70-7.76 (m, 3H), 7.80 (t, 2H, *J* = 8.28 Hz); ^{13}C NMR (400MHz, $CDCl_3$) δ ppm 14.17, 22.75, 23.84, 25.10, 27.60, 29.89, 31.65, 40.68, 46.64, 54.89, 83.79, 114.37, 114.41, 118.79, 119.89, 122.76, 127.05, 127.09, 128.89, 133.88, 139.17, 139.65, 140.61, 144.47, 150.43, 150.90, 152.87, 154.26.

Synthesis of planer fluorene **3PP$_2$**

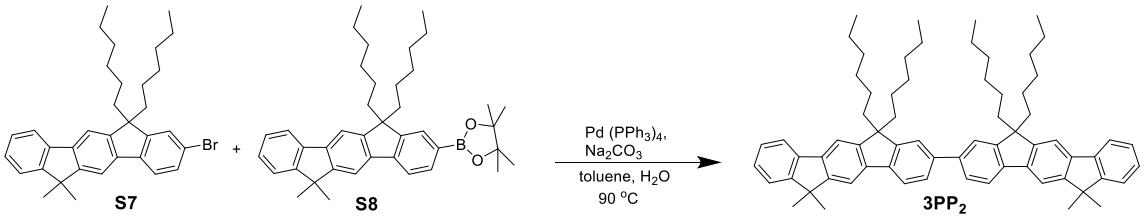

Compound **S7** (0.24 g, 0.46 mmol, 1.0 eq.), **S8** (0.48 g, 0.842 mmol, 1.8 eq.), $Pd(PPh_3)_4$ (50 mg) and 50 mL of toluene were placed in a dried Schlenk flask. Then an aqueous solution of Na_2CO_3 (5 g in 20 mL water) was added into the Schlenk flask. The reaction mixture was evacuated and filled with argon for three times. After refluxed at 90 °C for 24, the reaction mixture was cooled to room temperature and quenched with water. The reaction mixture was extracted with dichloromethane (4×50 mL) and organic layer was dried over anhydrous $MgSO_4$. The solvent was removed under reduced pressure and the crude product was purified through silica gel column chromatography using hexane to afford **3PP$_2$** as white solid (0.19 g, 45 %). m.p. 106-108 °C. ^{1}H NMR (400MHz, $CDCl_3$) δ ppm 0.70-0.82 (m, 20H), 1.01-1.16 (m, 24 H), 1.58 (s, 12H), 2.02-2.13 (m, 8H), 7.31 (td, 2H, *J* = 7.26 Hz, 1.27 Hz), 7.37 (td, 2H, *J* = 7.32 Hz, 1.34 Hz), 7.46 (d, 2H, *J* = 7.58 Hz), 7.63 (d, 2H, *J* = 1.35 Hz), 7.65-7.69 (m, 4H), 7.76 (s, 2H), 7.78-7.82 (m, 4H); ^{13}C NMR (400MHz, $CDCl_3$) δ ppm 14.17, 22.75, 23.97, 27.64, 29.91, 31.66, 40.81, 46.71, 54.99, 113.98, 114.47, 119.70, 119.81, 121.43, 122.79, 126.09, 127.01, 127.12, 138.65, 139.76, 140.29, 140.53, 140.61, 150.60, 152.06, 153.07, 154.26.

Scheme 4. 4: Synthesis of 4PP

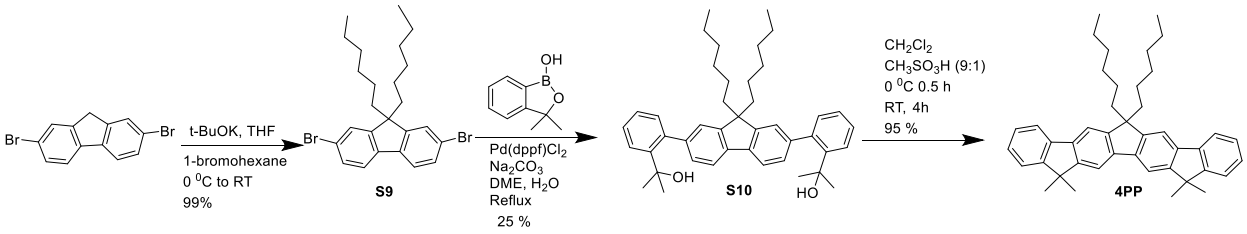

Synthesis of **S9**[48]:

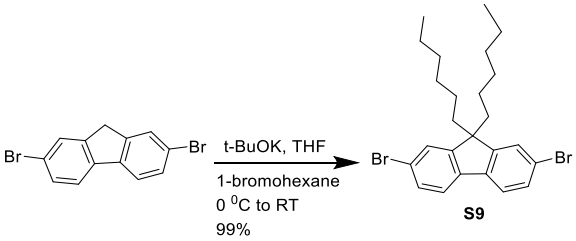

2,7- dibromofluorene (25 g, 77.15 mmol, 1 eq.) was dissolved in dry THF (200 mL) and cooled to 0 °C. Potassium *tert*-butoxide (21.64 g, 192.85 mmol, 2.5 eq.) was added and the mixture was stirred for 10 min. Then 1-bromohexane (29.23 mL, 208.30 mmol, 2.7 eq.) was added dropwise through a dropping funnel. The solution was allowed to warm to room temperature and continually stirred for additional 5 hours. The reaction was quenched with adding 100 mL of 1% aqueous HCl (v/v) and the mixture was extracted with dichloromethane (4×50 mL). The combined organic extracts were dried over anhydrous $MgSO_4$. Upon removing the solvent, the crude product remained as a light-yellow color liquid. Pure **S9** can be obtained after further purification with column chromatography (hexane) gave 37.6 g (99% yield) as a white solid. m.p. 56-58 °C, Lit.[57] 52°C. ^{1}H NMR (400MHz, $CDCl_3$) δ ppm 0.53-0.63 (m, 4H), 0.78 (t, 6H, J = 7.27 Hz), 0.98-1.17 (m, 12H), 1.87-1.95 (m, 4H), 7.43-7.46 (m, 4H), 7.50-7.53 (m, 2H); ^{13}C NMR

(400MHz, $CDCl_3$) δ ppm 14.15, 22.72, 23.77, 29.72, 31.60, 40.34, 55.81, 121.25, 121.59, 126.28, 130.26, 139.17, 152.66.

Synthesis of **S10**[50]:

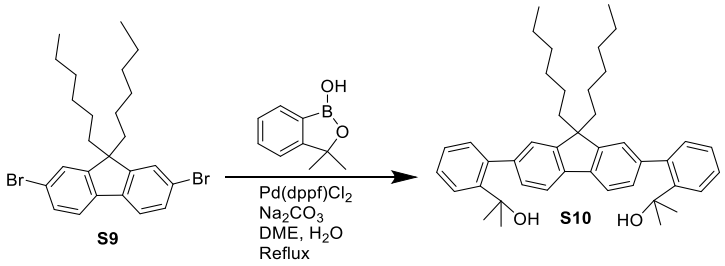

To a mixture of **S9** (5.0g, 10.15 mmol, 1.0 eq.), sodium carbonate (10.76 g, 101.6 mmol, 10.0 eq.), and $Pd(dppf)Cl_2$ (1.48 g, 2.03 mmol, 0.2 eq.) in a 250 mL Schlenk flask equipped with air condenser, was added 60 mL of anhydrous DME and 30 mL of water. The reaction mixture was evacuated and filled with argon three times and refluxed at 100 °C for 12 h. After 50 mL of water was added, the blackish solution was transferred to a 1 L separatory funnel and extracted with diethyl ether (4×50 mL). The combined organic layers were dried over anhydrous $MgSO_4$ and the solvent was removed under reduced pressure. The blackish brown colored crude liquid was dissolved in a 50:50 mixture of hexane and ethyl acetate and filtered through $MgSO_4$ pad to remove black palladium content. Then the solvent was removed under reduced pressure and the resulting thick brown colored compound was purified through silica gel column chromatography using hexane/EtOAc (95:5) to afford compound **S10** as white solid (1.55 g, 25%). m.p. 126-128 °C. ^{1}H NMR (400MHz, $CDCl_3$) δ ppm 0.61-0.73 (m,4H), 0.77 (t, 6H, *J* = 7.28 Hz), 0.96-1.17 (m, 12H), 1.46 (s, 12H), 1.83 (bs, 2H), 1.90-2.00 (m, 4H), 7.16 (dd, 2H, *J* = 7.54 Hz, 1.50 Hz), 7.26-7.32 (m, 6H), 7.38 (td, 2H, *J* = 8.03 Hz, 1.58 Hz), 7.70-7.76 (m, 4H); ^{13}C

NMR (400MHz, $CDCl_3$) δ ppm 14.15, 22.63, 23.91, 29.74, 31.65, 32.64, 40.54, 55.34, 74.05, 119.19, 124.33, 125.96, 126.21, 127.56, 128.39, 132.22, 139.83, 140.48, 142.71, 146.57, 150.40.

Synthesis of **4PP** [52]:

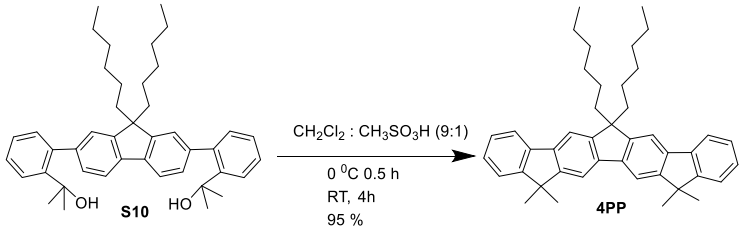

To an ice cooled solution of **S10** (1.0 g, 1.65 mmol, 1.0 eq.) in anhydrous dichloromethane (40 mL), CH_3SO_3H acid (7 mL) was added. After stirring at 0 ^{0}C for 30 minutes, the reaction mixture was allowed to warm up to room temperature and continued stirring for additional 3.5 h. The reaction mixture was neutralized with saturated aqueous $NaHCO_3$ solution and extracted with dichloromethane (4×50 mL). The combined organic layers were washed with water and dried over anhydrous $MgSO_4$. The solvent was removed under reduced pressure and the resulting residue was passed through a short silica pad using hexane as solvent to afford pure **4PP** as white solid (0.90 g, 95 %). m.p.: 150-152 ^{0}C. ^{1}H NMR (400MHz, $CDCl_3$) δ ppm 0.65-0.78 (m, 10H), 0.96-1.15 (m, 12H), 1.58 (s, 12H), 2.01-2.11 (m, 4H), 7.31 (td, *J* = 7.30 Hz, 1.15 Hz, 2H), 7.37 (td, *J* = 7.40 Hz, 1.27 Hz, 2H), 7.46 (d, *J* = 7.31 Hz, 2H), 7.66 (s, 2H), 7.79 (d, *J* = 7.31 Hz, 4H); ^{13}C NMR (400MHz, $CDCl_3$) δ ppm 14.16, 22.81, 23.96, 27.62, 30.00, 31.71, 41.19, 46.68, 54.56, 113.59, 114.41, 119.77, 122.78, 126.94, 127.07, 138.41, 139.82, 141.01, 150.74, 153.02, 154.20.

Scheme 4. 5:Synthesis of $4PP_2$

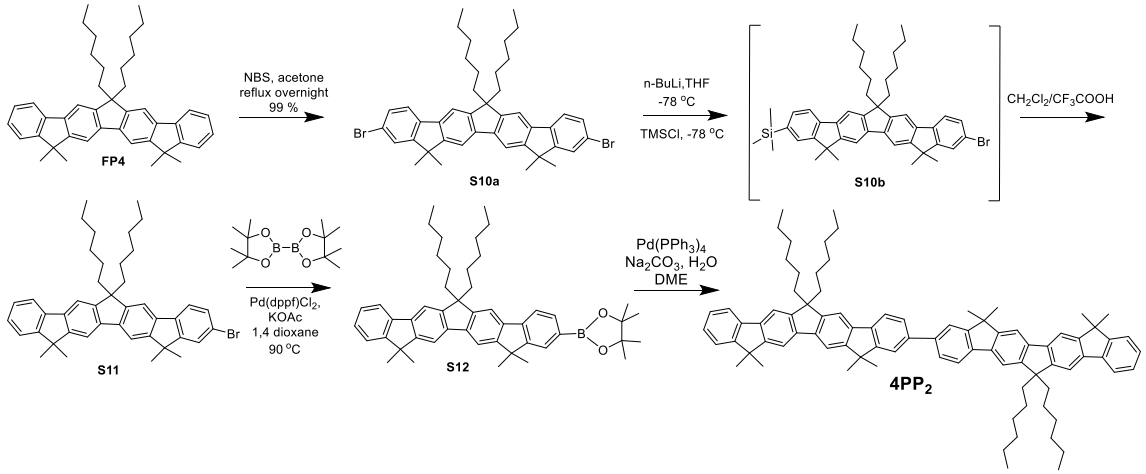

Synthesis of **S11**[56]:

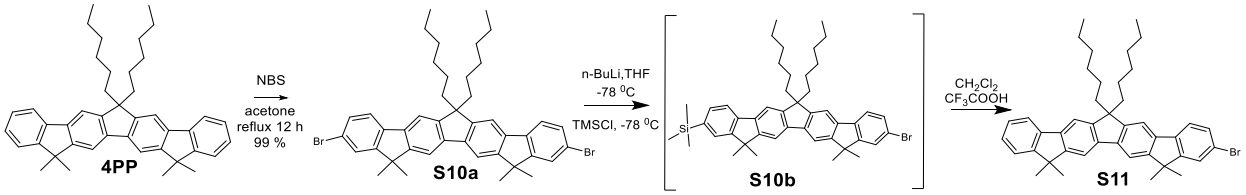

To a Schlenk flask, **4PP** (3.85 g, 6.79 mmol, 1.0 eq.), NBS (4 g, 22.46 mmol, 3.30 eq.) and acetone (40 mL) were added to give a yellow suspension. The reaction mixture was refluxed for 3h. After added another portion of NBS (3.0 g, 16.85 mmol, 2.48 eq.), the mixture was refluxed for additional 12 h. The reaction was quenched with water and the mixture was extracted with CH_2Cl_2 (3×50mL). The combined organic layers were dried over anhydrous $MgSO_4$ and the solvent was removed under reduced pressure. The resulting crude was recrystallized from ethanol to afford pure crystal of compound **S10a**. Yield: 4.92 g (99 %). m.p. 194-196 °C. ^{1}H NMR (400 MHz, $CDCl_3$) δ ppm 0.64-0.76 (m, 10H), 0.99-1.13 (m, 12H), 1.55 (s, 12H), 2.00-2.08 (m,4H), 7.48 (dd, 2H, *J* = 8.06 Hz, 1.76 Hz), 7.56 (d, 2H, *J* = 1.76 Hz), 7.60 (s, 2H), 7.63 (d, 2H, *J* = 8.06 Hz), 7.76 (s, 2H);

^{13}C NMR (400MHz, $CDCl_3$) δ ppm 14.09, 22.69, 23.94, 27.35, 29.86, 31.65, 40.96, 46.87, 54.58, 113.61, 114.37, 120.56, 121.11, 126.14, 130.04, 137.42, 138.65, 141.08, 150.92, 152.65, 156.14.

n-Butyllithium in hexane (1.29 mL, 1.6 M, 2.06 mmol, 1.0 eq.) was added to a solution of **S10a** (1.5 g, 2.06 mmol, 1.0 eq.) in anhydrous THF (20 mL) at -78 ºC under argon atmosphere and the mixture was stirred for 1 h at the same temperature. Then chlorotrimethylsilane (0.38 mL, 3.02 mmol, 1.46 eq.) was added slowly at -78 ºC. After keeping at cooling bath for 10 minutes, the mixture was allowed to warm to room temperature and stirred for overnight. The reaction mixture was quenched with water and the resulting solution was extracted by CH_2Cl_2 (3×50 mL). The organic layer was dried over anhydrous $MgSO_4$. After removing the solvent, the crude product was subjected to desilylation reaction by stirring in the mixture of anhydrous CH_2Cl_2/trifluoroacetic acid (36 mL/4 mL) for 4 hours afford crude mixture of **S11**, which was purified through silica gel column chromatography using hexane as an eluent. (Yield = 0.69g, 51 %). m.p. 178-180 °C. ^{1}H NMR (400 MHz, $CDCl_3$) δ 0.65-0.77 (m, 10H), 0.98-1.14 (m, 12H), 1.56 (s, 6H), 1.58 (s, 6H), 2.02-2.10 (m, 4H), 7.31 (td, 1H *J* = 7.32 Hz, 1.27 Hz), 7.37 (td, 1H, *J* = 7.34 Hz, 1.30 Hz), 7.44-7.50 (m, 2H), 7.57 (d, 1H, *J* = 1.65 Hz), 7.62 (s, 1H), 7.62-7.67 (m, 2H), 7.75-7.82 (m, 3H); ^{13}C NMR (400 MHz, $CDCl_3$) δ 14.15, 22.80, 23.97, 27.48, 27.62, 29.98, 31.70, 41.12, 46.69, 46.96, 54.60, 113.63, 113.70, 114.46, 119.82, 120.60, 121.19, 122.80, 126.25, 127.03, 127.10, 127.14, 130.13, 137.29, 138.65, 138.88, 139.74, 140.77, 141.48, 150.77, 151.02, 152.70, 153.09, 154.22, 156.26.

Synthesis of **S12**[49]:

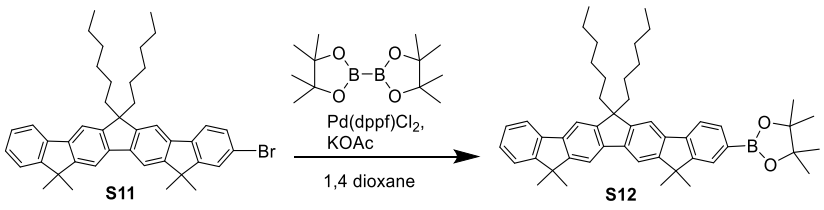

Compound **S11** (0.26 g, 0.403 mmol, 1.0 eq.), bis(pinacolato)diboron (0.112 g, 0.441 mmol, 1.1 eq.), potassium acetate (0.118 g, 1.202 mmol, 3.0 eq.), and Pd(dppf) Cl_2 (8.82 mg, 0.012 mmol, 3 mmol%) were mixed in dry dioxane (25 mL) under an argon atmosphere and heated at 90 °C for 12 h. After removed the dioxane, the oily residue was filtered through silica using 50:50 mixture of hexane/ethyl acetate to give the crude **S12** as a thick liquid, which was further purified by recrystallization from ethanol to afford light yellowish crystal **S12** (0.264 g, 94% yield). m.p. 153-155 °C. ^{1}H NMR (400MHz, $CDCl_3$) δ ppm 0.66-0.75 (m,10H), 0.98-1.13(m,12H), 1.40 (s,12H), 1.58 (s, 6H), 1.59 (s, 6H), 2.01-2.10 (m, 4H), 7.31 (td, 1H, *J* = 7.14 Hz, 1.35 Hz), 7.37 (td, 1H, *J* = 7.42 Hz, 1.35 Hz), 7.46 (dq, 1H, *J* = 7.20 Hz, 1.35 Hz, 0.64 Hz), 7.67 (dd, 2H, *J* = 9.5 Hz, 0.64 Hz), 7.77-7.81 (m, 4H), 7.84 (dd, 1H, *J* = 7.53 Hz, 0.98 Hz), 7.89 (t, 1H, *J* = 0.77 Hz); ^{13}C NMR (400 MHz, CDCl3) δ ppm 14.15, 22.79, 23.96, 25.07, 27.53, 27.61, 29.98, 31.69, 41.14, 46.68, 46.70, 54.55, 83.87, 113.60, 113.70, 114.44, 114.88, 119.17, 119.80, 122.78, 126.69, 127.07, 128.88, 134.07, 138.16, 138.53, 139.79, 140.92, 141.55, 142.90, 150.74, 150.84, 153.02, 153.33, 153.79, 154.22.

Synthesis of **4PP$_2$**

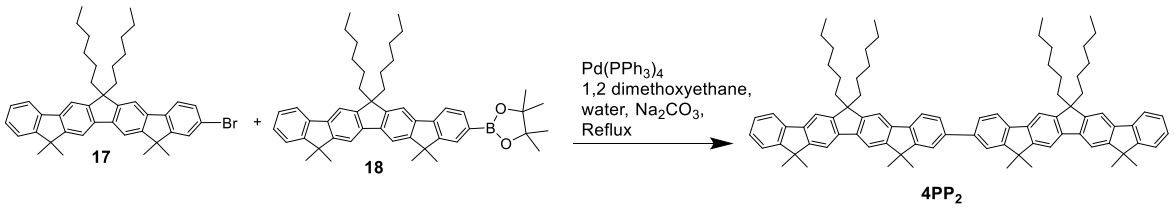

Compounds **S11** (0.157 g, 0.243 mmol, 1.0 eq.), **S12** (0.185 g, 0.267 mmol, 1.1 eq.), $Pd(PPh_3)_4$ (50 mg) and 50 mL of 1,2-dimethoxyethane were placed in a dried Schlenk flask. Then an aqueous solution of Na_2CO_3 (5 g in 20 mL water) was added into this Schlenk flask. The reaction mixture was evacuated and filled with argon for three times. The reaction mixture was refluxed at 90 °C for 48 hours and quenched with water. Then reaction mixture was extracted with dichloromethane (4×50 mL) and organic layer was dried over anhydrous $MgSO_4$. The solvent was removed under reduced pressure and the crude residue was purified through silica gel column chromatography using hexane to afford **4PP$_2$** as white solid (0.024 g, 8 %). m.p. 200-202 °C. ^{1}H NMR (400MHz, $CDCl_3$) δ ppm 0.68-0.90 (m, 20H), 1.00-1.16 (m, 24H), 1.59 (s, 12H), 1.67 (s, 12H), 2.05-2.13 (m, 8H), 7.32 (td, 2H, *J* = 7.38 Hz, 1.28 Hz), 7.38 (td, 2H, *J* = 7.45 Hz, 1.34 Hz), 7.47 (d, 2H, *J* = 7.28 Hz), 7.67 (s, 2H), 7.68-7.61 (m, 4H), 7.73 (d, 2H, *J* = 1.24 Hz), 7.78-7.83 (m, 6H), 7.87 (d, 2H, *J* = 7.81 Hz); ^{13}C NMR (400 MHz, CDCl3) δ ppm 14.17, 22.81, 23.99, 27.63, 27.77, 30.01, 31.72, 41.20, 46.69, 46.85, 54.60, 113.63, 114.49, 119.79, 120.11, 121.55, 122.79, 126.41, 126.96, 127.09, 128.42, 130.22, 132.57, 138.12, 138.45, 138.99, 139.82, 140.62, 141.04, 150.77, 150.89, 153.05, 153.38, 154.22, 154.92.

^{1}H and ^{13}C NMR spectra of compounds

^{1}H NMR of **S1**

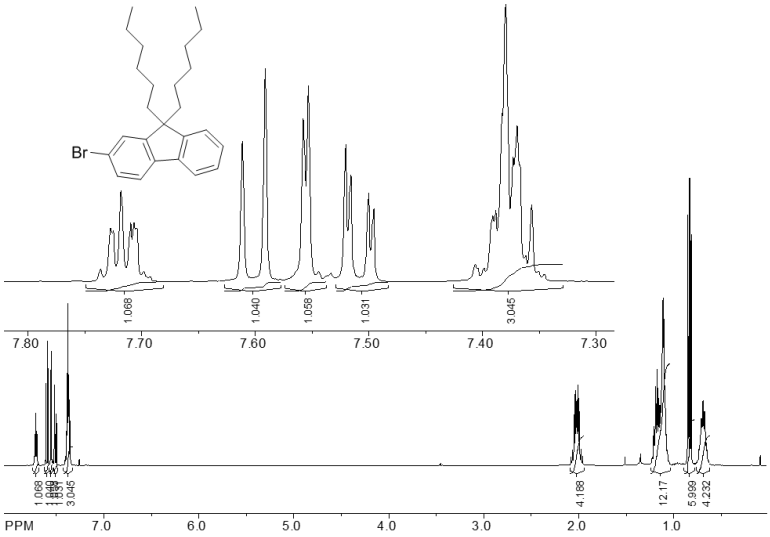

^{13}C NMR of **S1**

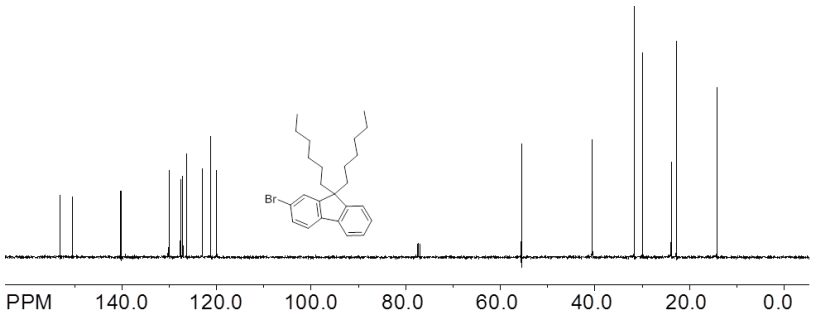

^{1}H NMR of **S2**

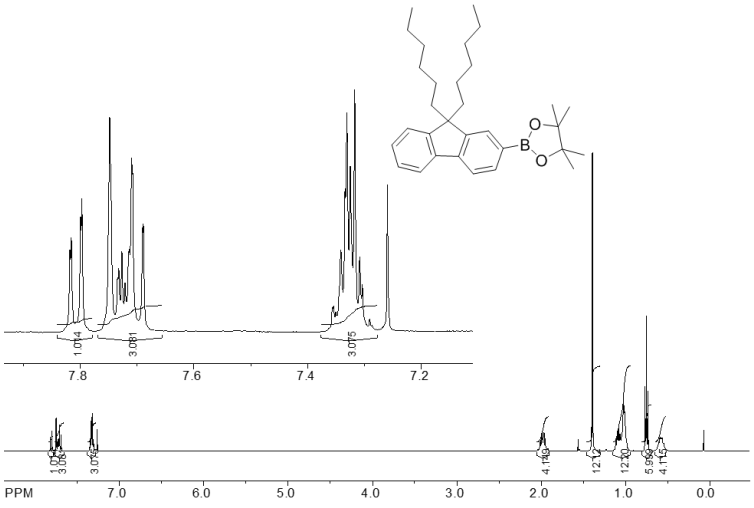

^{13}C NMR of **S2**

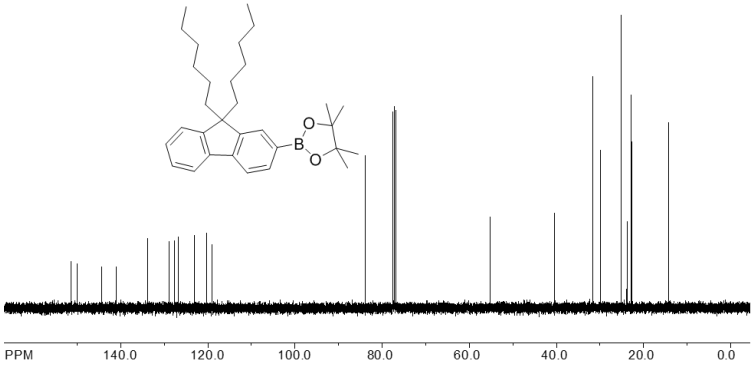

^{1}H NMR of **S3**

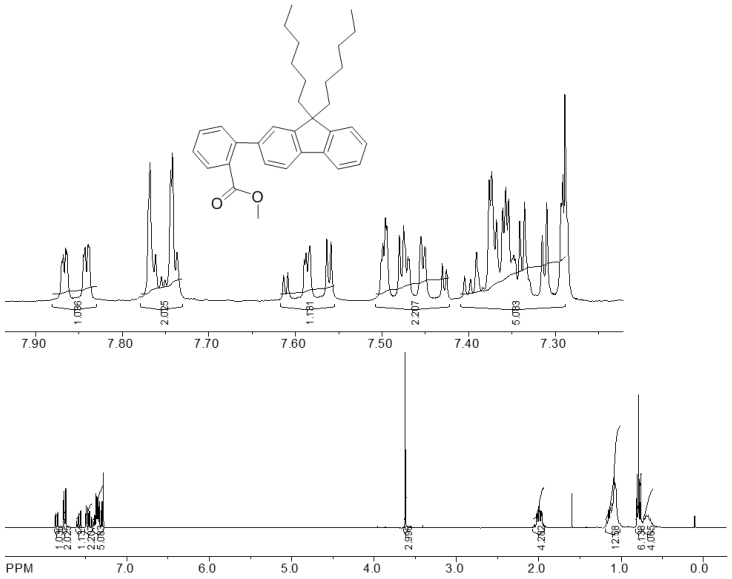

^{13}C NMR of **S3**

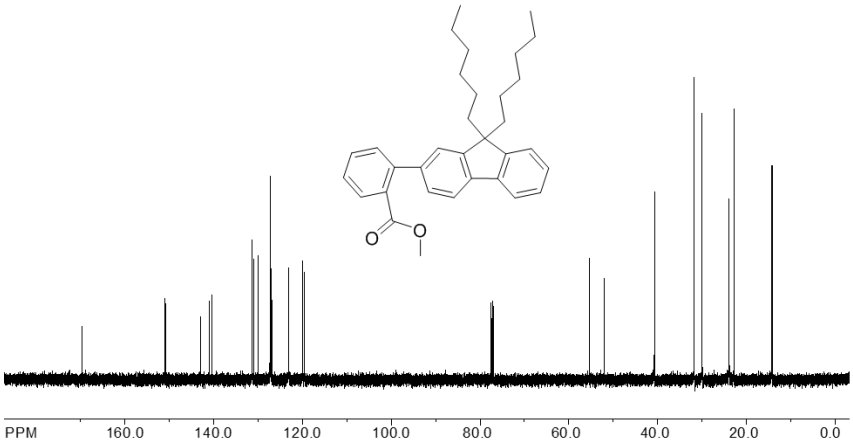

^{1}H NMR of **S4**

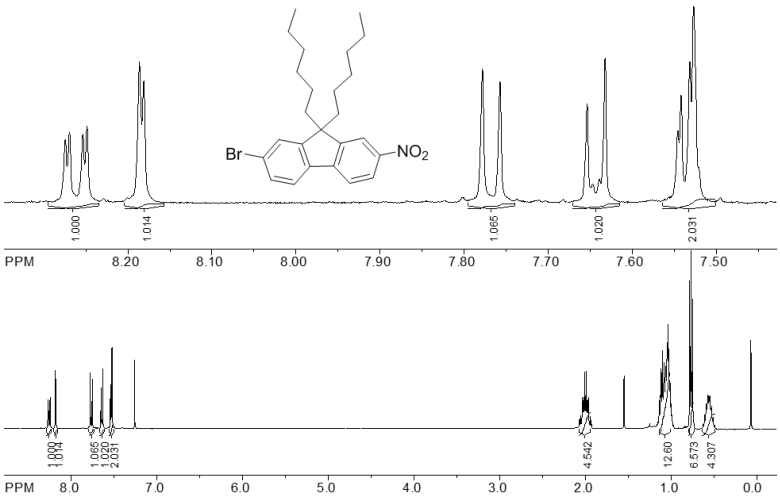

^{13}C NMR of **S4**

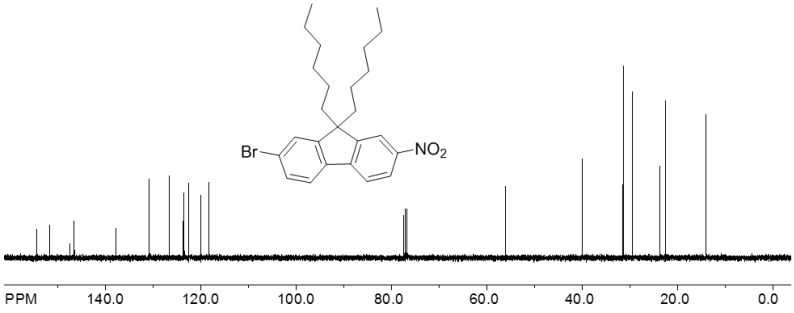

^{1}H NMR of **S5**

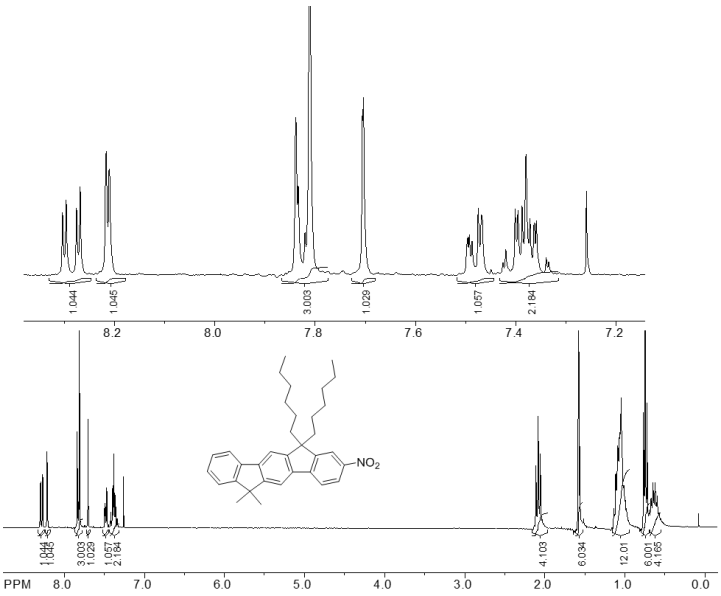

^{13}C NMR of **S5**

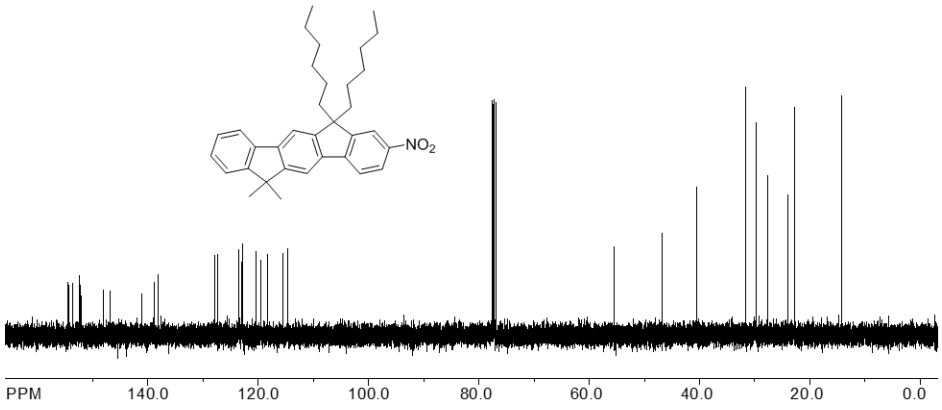

^{1}H NMR of **S6**

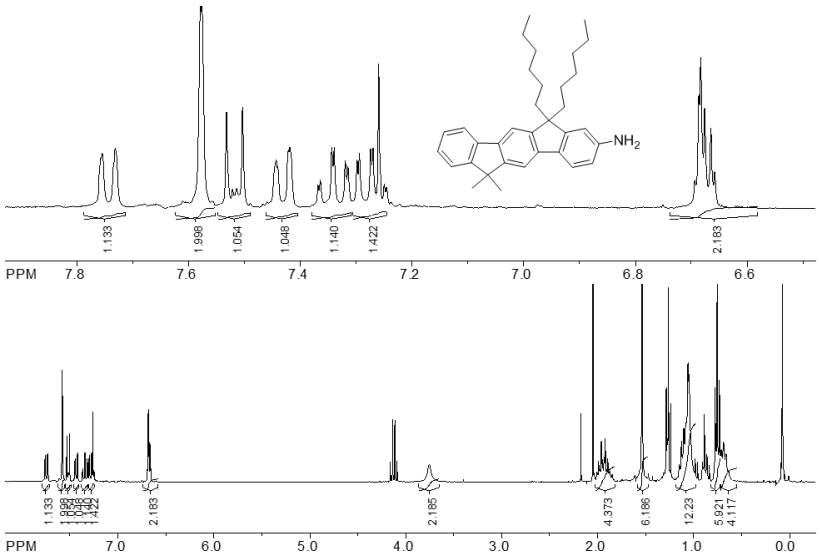

^{13}C NMR of **S6**

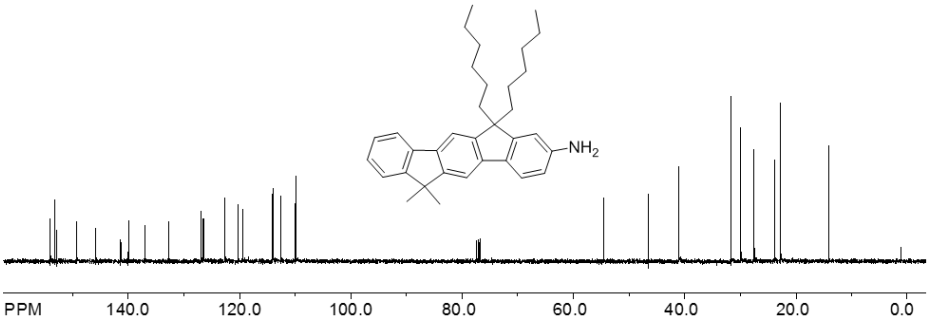

^{1}H NMR of **S7**

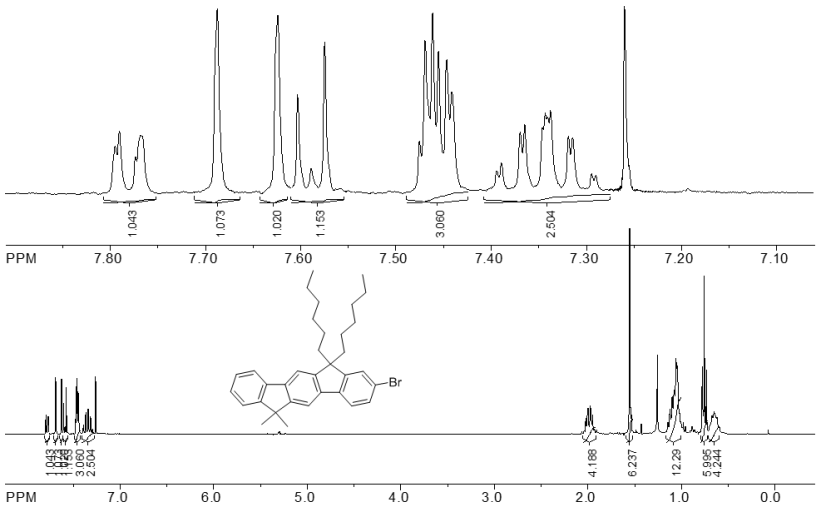

^{13}C NMR of **S7**

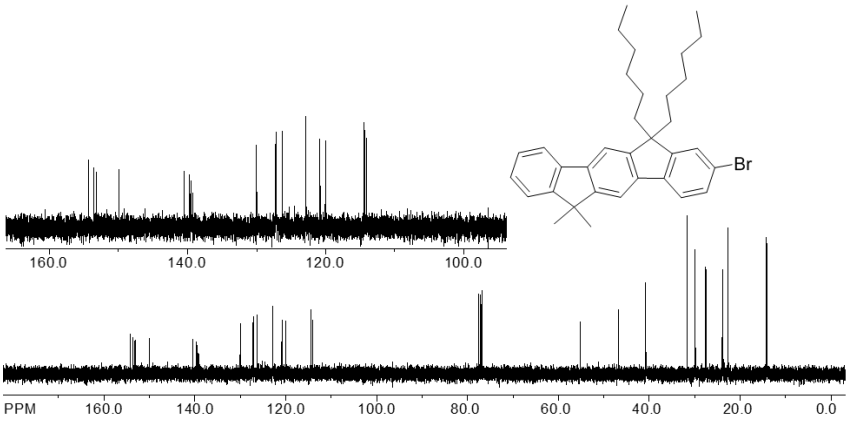

^{1}H NMR of **S8**

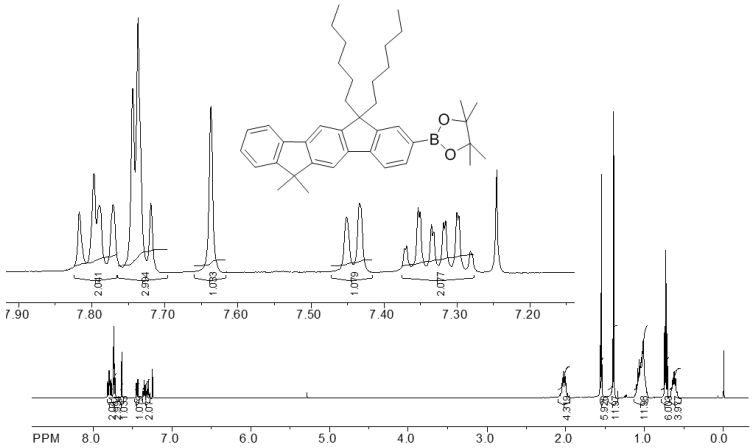

^{13}C NMR of **S8**

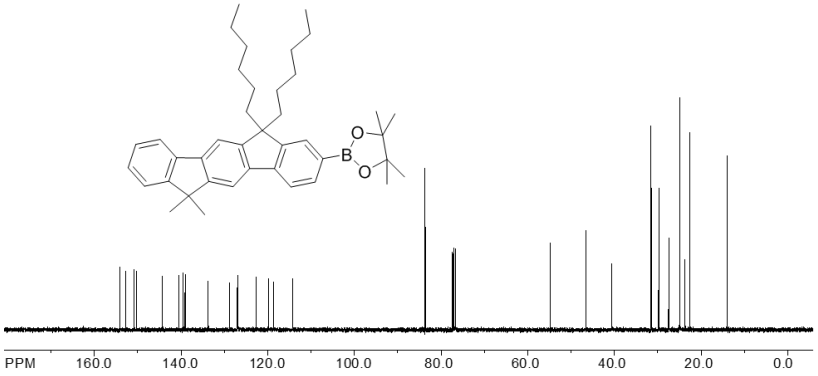

^{1}H NMR of **S9**

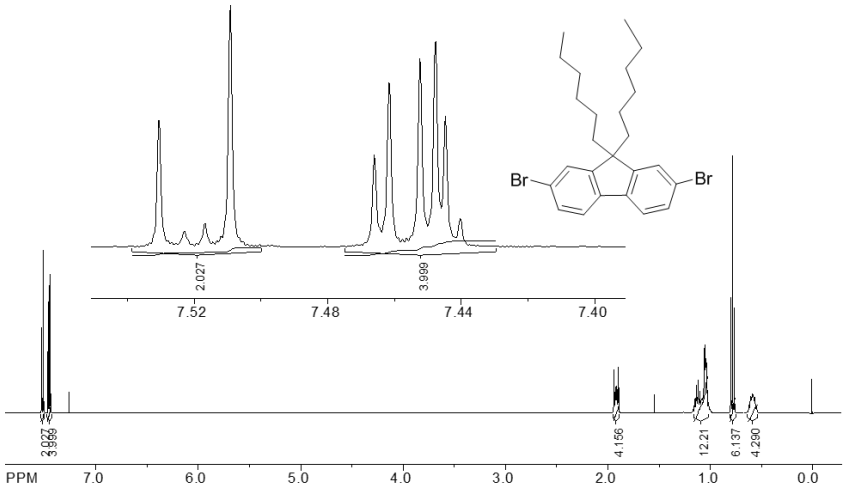

^{13}C NMR of **S9**

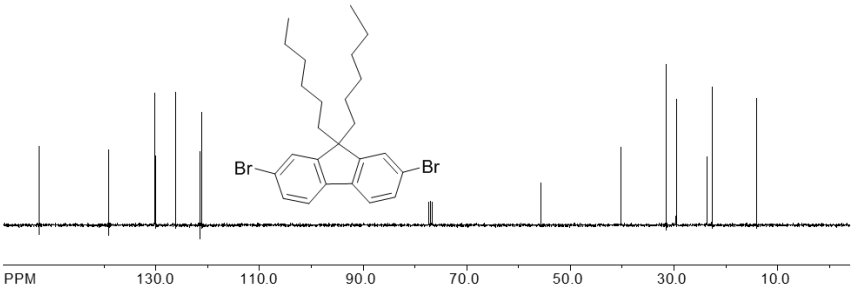

^{1}H NMR of **S10**

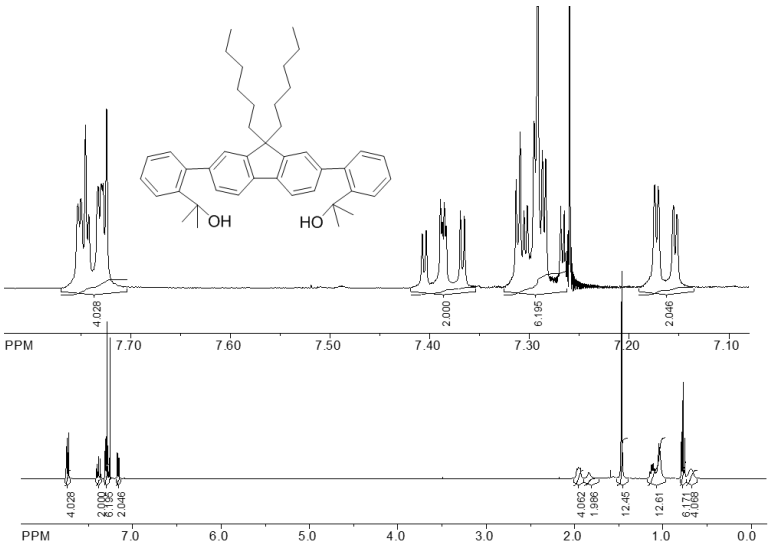

^{13}C NMR of **S10**

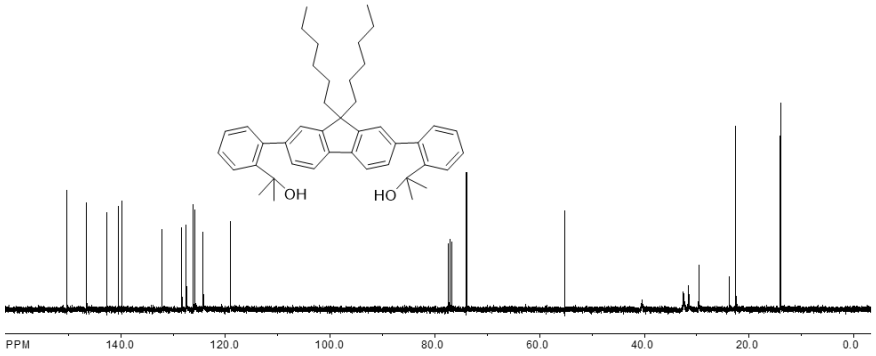

^{1}H NMR of **S10a**

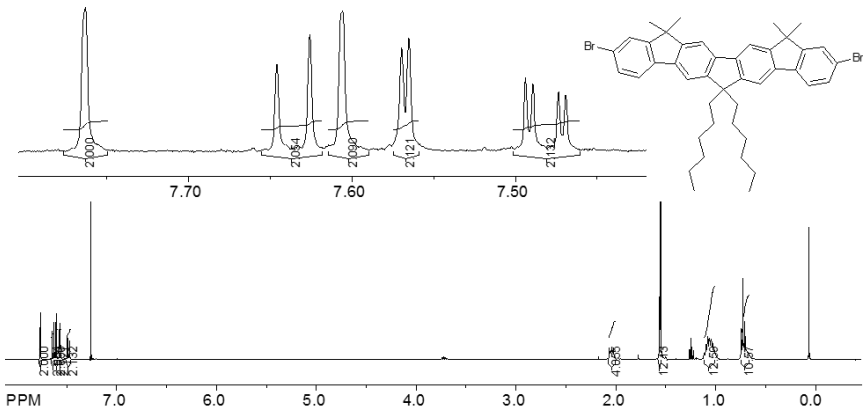

^{13}C NMR of **S10a**

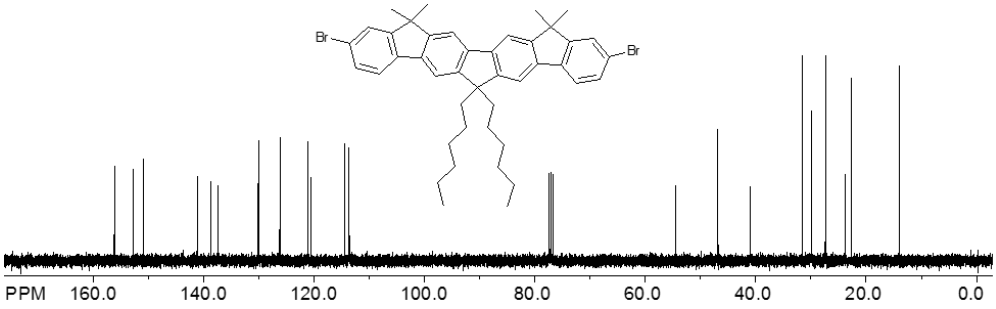

^{1}H NMR of **S11**

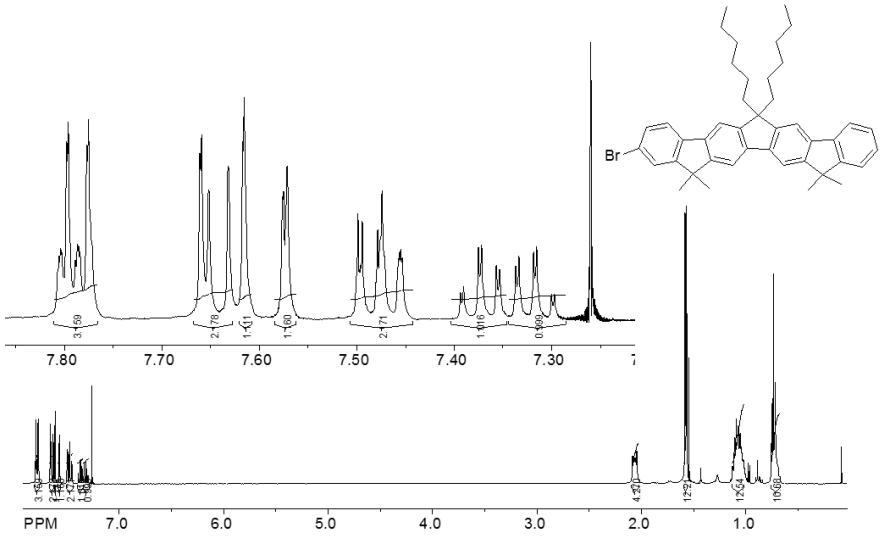

^{13}C NMR of **S11**

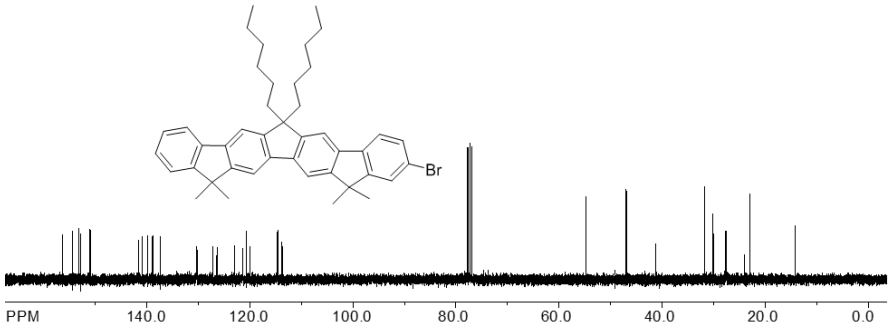

^{1}H NMR of **S12**

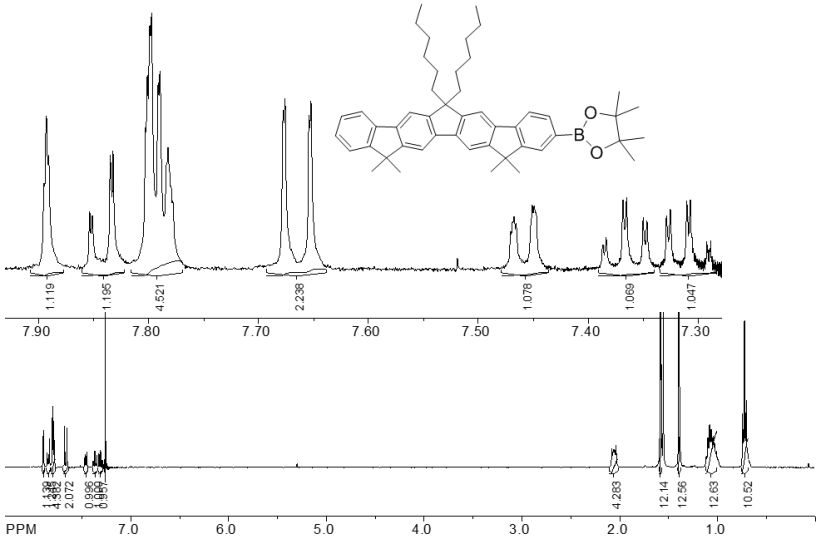

^{13}C NMR of **S12**

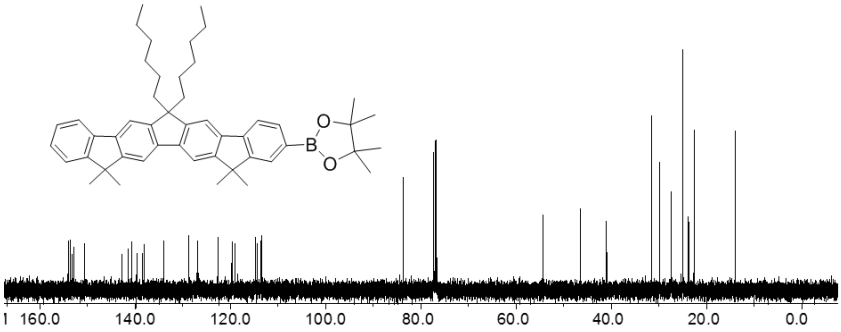

^{1}H NMR of **3PP**

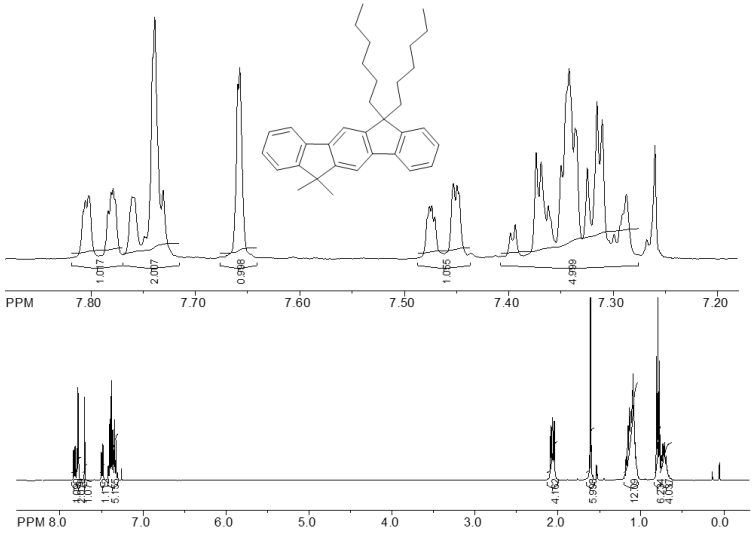

^{13}C NMR of **3PP**

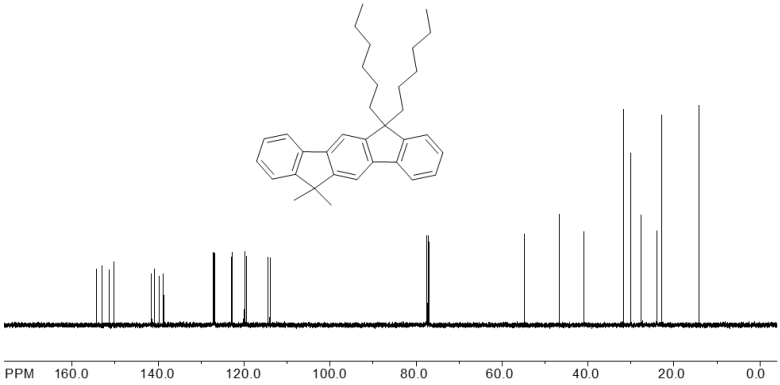

^{1}H NMR of **3PP$_2$**

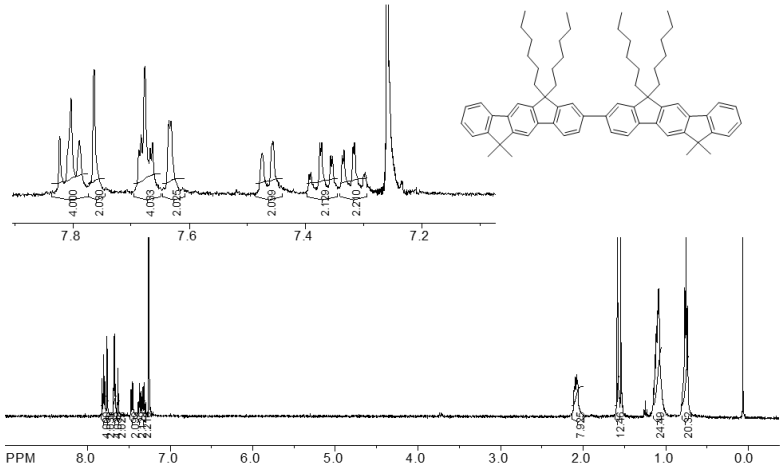

^{13}C NMR of **3PP$_2$**

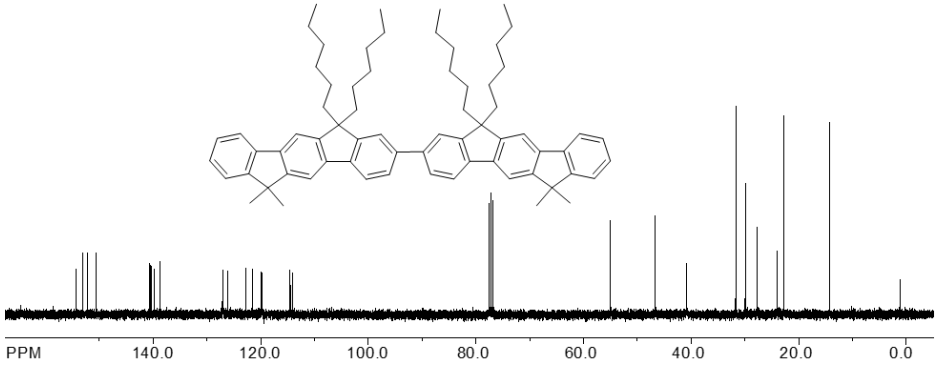

^{1}H NMR of **4PP**

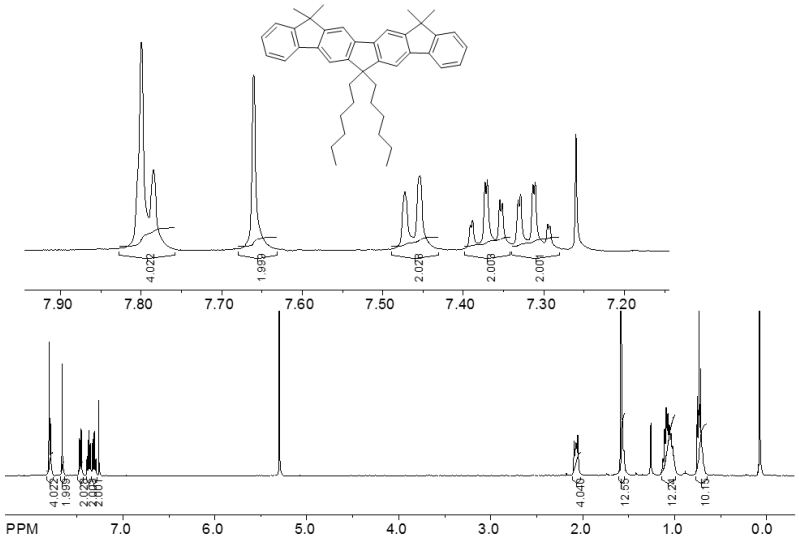

^{13}C NMR of **4PP**

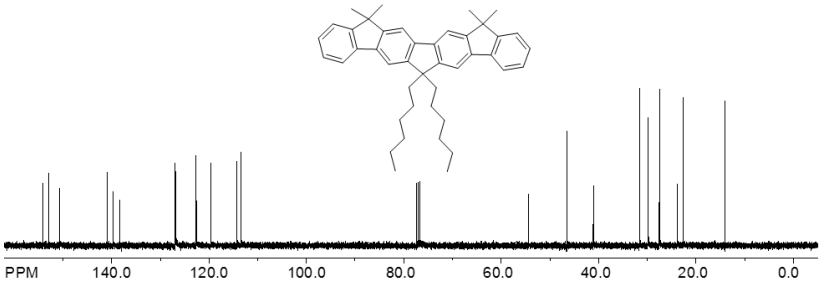

^{1}H NMR of **4PP$_2$**

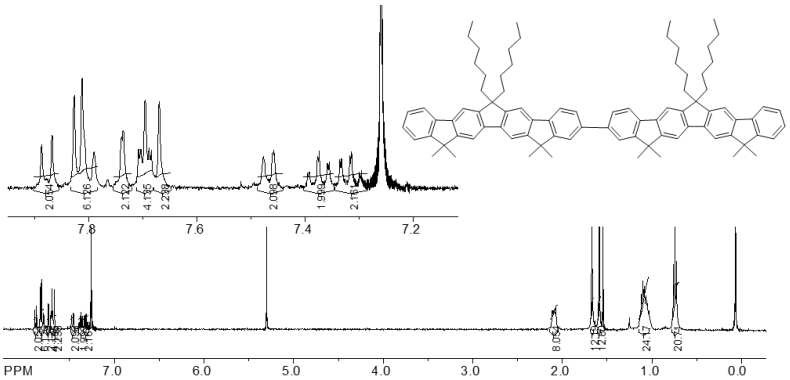

^{13}C NMR of **4PP$_2$**

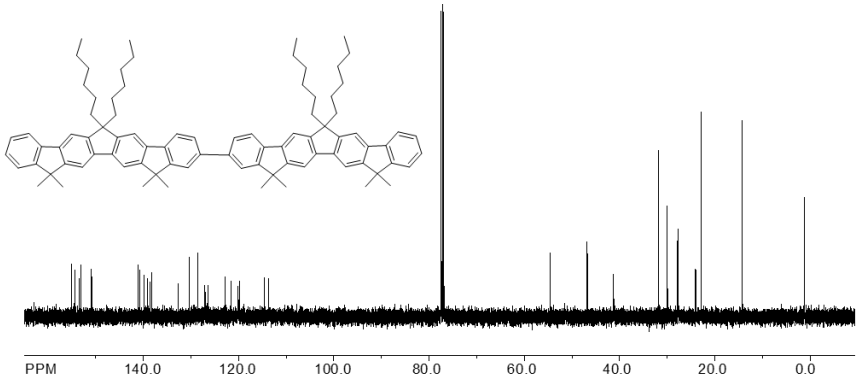

S4. MALDI-TOF mass spectra

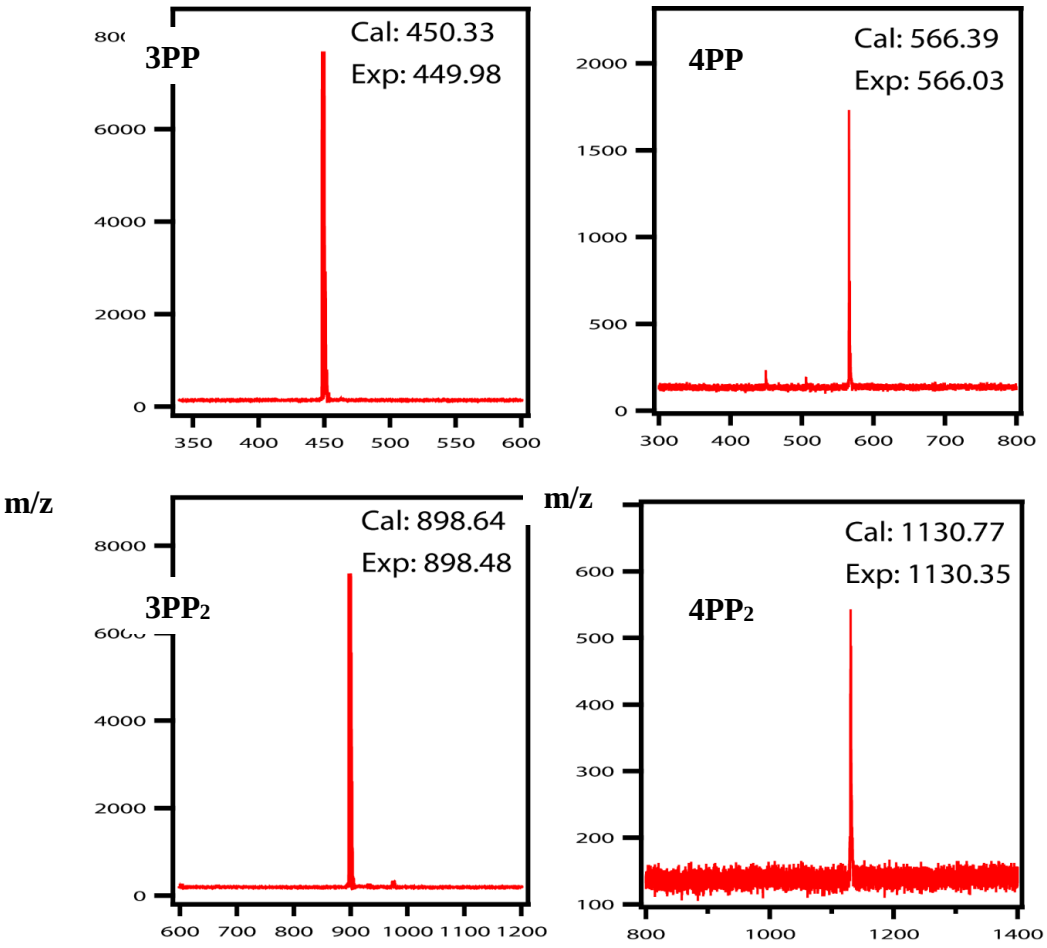

SUMMARY AND CONCLUSION OF THE THESIS

The goal of this work has been motivated towards synthesizing the next generation of organic molecules which are suitable to be used in the photovoltaic devices. In this context, it is important to develop an intuitive understanding of the mechanism of the charge delocalization in electroactive organic molecules. In particular, during the rational design of novel charge-transfer molecular assemblies it becomes crucial to consider how various geometrical factors control the mechanism of charge delocalization. In this work we demonstrated for a set of biaryls with systematically varied interplanar dihedral angles that the mechanism of hole delocalization is governed by the interplay between the energetic gain from the delocalization and energetic penalty from structural reorganization. These factors can be rationalized via two-state Marcus-Hush theory using two empirical parameters: electronic coupling (H_{ab}) and reorganization energy (λ). We showed that in biaryl cation radicals the interplanar angle, where switchover in the mechanisms of hole delocalization occurs, corresponds to the case when $2H_{ab} = \lambda$.

Proper understanding the charge transport mechanism and the hole delocalization requires availability of robust aromatic oxidants. Among these oxidants, magic blue has been widely used as an aromatic oxidant for the one electron oxidation to its commercial availability and a reasonable oxidizing power. However, stability of the $MB^{+\bullet}$ $SbCl_6^-$ salt is a primary concern which leads to a slow decomposition to produce unknown impurities, which have been named “blues brothers”. In this work we demonstrated a synthetic approach to synthesis of the oxidant with the whose electron donor properties are equivalent to those of original magic blue, yet it does not undergo the decomposition.

Hexa-peri-hexabenzocoronene (HBC) is among the most well studied PAHs due to its promise in the application of photoelectronic devices. HBC has a unique graphitic structure and large flat π-systems which enables them to be columnar shape by self-assembly in a crystal and thus provide the suitable platform to delocalize the electron/hole throughout the entire crystal. On the other hand, HBC not only show the troubles like-aggregations and the less solubility to study their properties, but also limit the further functionality to prepare large extended π-systems. The goal of this work is driven to solve these issues by designing and synthesizing new hexa-peri-hexabenzocoronene-fluorene hybrid named as FHBCs that allow the free vertices for further functionalization of FHBCs. Also, by introducing long chain alkyl group in the FHBCs core we improved the solubility and decrease the aggregations in the solution.

Finally, motivated by the question whether a set of linearly connected fluorenes is better termed a poly-fluorene or poly-phenylene wire, we performed a detailed study on a series of phenylene-based bichromophores $n\mathbf{PP}_2$ of increasing size. We found that as the number of phenylenes in a chromophore increases from $n = 2$ to 4, the amount of hole stabilization measured electrochemically decreases and the absorption band in the electronic spectra of $n\mathbf{PP}_2^{+\bullet}$ shifts to longer wavelength, indicating that the interchromophoric electronic coupling decreases. We further showed that the electronic coupling decreases to nearly non-existent values when $n > 5$, leading to a complete hole localization on a single chromophore in corresponding $n\mathbf{PP}_2^{+\bullet}$. This fundamental understanding that the interchromophoric electronic coupling decreases with increasing chromophore size is crucial during the rational design of novel electron donors for photovoltaic and molecular electronic applications.

BIBLIOGRAPHY

INTRODUCTION

1. (a) A. P. Kulkarni; C. J. Tonzola; A. Babel; S. A. Jenekhe. *Chem. Mater.* **2004**, *16*, 4556. (b) W.-L. Yu; H. Meng; J. Pei; S.-J. Chua; W. Huang; Y.-H. Lai. *Chem. Commun.* **1998**, *18*, 1957.

2. C. W. Tang; S. A. VanSlyke; C. H. Chen. *J. Appl. Phys*. **1989**, *65*, 3610. (b) C. H. Chen; J. Shi; C. W. Tang; K. P. Klubek. *Thin Solid Films.* **2000**, *363*, 327. (c) X. T. Tao; S. Miyata; H. Sasabe; G. J. Zhang; T. Wada; M. H. Jiang *Appl. Phys. Lett*. **2001**, *78*, 279.

3. C. Xia; R. C. Advincula. *Macromolecules*. **2001**, *34*, 6922.

4. D. M. Adams; L. Brus; C. E. Chidsey; S. Creager; C. Creutz; C. R. Kagan; P. V. Kamat; M. Lieberman; S. Lindsay; R. A. Marcus. *J. Phys. Chem. B* **2003,** *107*, 6668-6697.

5. E. A. Weiss; M. R. Wasielewski; M. A. Ratner. *Top. Curr. Chem.* **2005,** *257,* 103-133.

6. J. L. Brédas; D. Beljonne; V. Coropceanu; J. Cornil. *Chem. Rev.* **2004,** *104,* 4971-5004.

7. V. Coropceanu; J. Cornil; D. A. da Silva Filho; Y. Olivier; R. Silbey; J. L. Brédas. *Chem. Rev.* **2007,** *107*, 926-952.

8. M. N. Paddon-Row. "Electron and Energy Transfer": in *Stimulating Concepts in Chemistry* (Eds.: F. Vögtle, J. F. Stoddart, M. Shibasaki), Willey-VCH, Weinheim, **2000**, pp. 267–291.

9. M.V. Ivanov; S. H. Wadumethrige; D. Wang; R. Rathore. *J. Phys. Chem. C.* **2017**, *121(29),* 15639-15643.

10. F. A. Khan; D. Wang; B. Pemberton; M. R. Talipov; R. Rathore. *J. Photochem. Photobiol A. Chemistry.* **2016**, *331*, 153-159.

11. J. Vura-Weis; S. H. Abdelwahed; R. Shukla; R. Rathore; M. A. Ratner; M. R. Wasielewski. *Science*. **2010**, *328*, 1547-1550.

12. M. B. Robin; P. Day. *Adv. Inorg. Chem. Radiochem*. **1967**, *10*, 247-422.

13. N. S. Hush. *Prog. Inorg. Chem*. **1967**, *8*, 391-444.

14. M. Parthey; M. Kaupp. *Chem. Soc. Rev*. **2014**, ***43***, 5067-5088.

15. K. D. Demadis; C. M. Hartshorn; T. J. Meyer. *Chem. Rev*. **2001**, *101*, 2655-2685.

16. (a) C. Creutz; H. Taube. *J. Am. Chem. Soc.* **1969**, *91*, 3988. (b) C. Creutz; H. Taube. *J. Am. Chem. Soc.* **1973**, *95*, 1086.

17. A. A. Bugaev; S. E. Nikitin. *Technical Physics Letters.*, **2001**, *27 (2)*, 104–107

18. J. Bonvoisin; J.-P. Launay; C. Rovira; J. Veciana. *Angew. Chem. Int. Ed*. **1994**, *33*, 2106.

19. C. Lambert; G. Nöll. *J. Am. Chem. Soc*. **1999**, *121 (37)*, 8434-8442.

20. S. Barlow; C. Risko; S.-J. Chung; N. M. Tucker; V. Coropceanu; S. C. Jones; Z. Levi; J. L. Brédas; S. R. Marder. *J. Am. Chem. Soc*. **2005**, *127*, 16900-16911.

21. M. R. Talipov; A. Boddeda; Q. K. Timerghazin; R. Rathore. *J. Phys. Chem. C* **2014**, *118*, 21400−21408.

22. M. R. Talipov; M. V. Ivanov; R. Rathore. *J. Phys.Chem. C* **2016**, *120(12)*, 6402-6408.

23. D. Wang; M. R. Talipov; M. V. Ivanov; R. Rathore. *J. Am. Chem. Soc*. **2016**, *138*, 16337−16344.

24. M. V. Ivanov; M. R. Talipov; A. Boddeda; S. H. Abdelwahed; R. Rathore. *J. Phys. Chem. C* **2017**, *121*, 1552−1561.

25. J. Grimme; U. Scherf. Macrornol. *Chem. Phys.* **1996**, *197*, 2297-2304.

26. S. Setayesh; D. Marsitzky; and K. Mùllen. *Macromolecules*. **2000**, *33 (6)*, 2016-2020.

27. E. Wang, C. Li, W. Zhuang, J. Peng and Y. Cao. *J. Mater. Chem*. **2008**, *18*, 797–801.

28. I. Le´vesque; P-O. Bertrand; N. Blouin; M. Leclerc; S. Zecchin; G. Zotti; C. I. Ratcliffe; D. D. Klug; X. Gao; F. Gao; and J. S. Tse. *Chem. Mater*. **2007**, *19*, 2128-2138.

29. J. Jacob; S. Sax; M. Gaal; E. J. W. List; A. C. Grimsdale; and K. Mu1llen. *Macromolecules* **2005**, *38*, 9933-9938.

30. A. K. Mishra; M. Graf; F. Grasse; J. Jacob; E. List; K. Müllen. *Chemistry of materials*. **2006**, *18*(12), 2879-2885.

31. A.Facchetti. Chem. Mater. **2010**, *23*, 733-758.

32. C. Li; M. Liu; N. G. Pschirer; M. Baumgarten; K. Müllen. *Chem. Rev.* **2010**, *110*, 6817-6855.

33. J. C. Goldschmidt; S. Fischer. *Advanced. Optical. Materials.* **2015**, *3*, 510-535.

34. C. J. Lambert. *Chem. Soc. Rev.* **2015**, *44*, 875-888.

35. S. Holliday; Y. Li; C. K. Luscombe; *Progress. In. Polymer. Science.* **2017**, *70*, 34 - 51.

36. G. Li; N. Govind; M. A. Ratner; C. J. Cramer; L. Gagliardi. *J. Phys. Chem. Lett.* **2015**, *6*, 4889-4897.

37. A. Migliore. *J. Chem. Theory. Comput.* **2011**, *7*, 1712-1725.

38. T. Kawatsu; V. Coropceanu; A. Ye; J. -L. Brédas. *J. Phys. Chem. C.* **2008**, *112*, 3429-3433.

39. M. N. Paddon-Row; M. J. Shephard. *J. Am. Chem. Soc.* **1997**, *119*, 5355-5365.

40. M. V. Ivanov; V. J. Chebny; M. R. Talipov; R. Rathore. *J. Am. Chem. Soc.* **2017**, *139*, 4334-4337.

41. R. E. Larsen. *J. Phys. Chem. C.* **2016**, *120*, 9650-9660.

42. M. D. Watson; A. Fechtenkotter; K. Müllen. *Chem. Rev*. **2001**, *101*, 1267 and references therein.

43. M. Baumgarten; K. Müllen, Top. Curr. Chem. **1994**, *169*, 1 and references therein.

44. X.-Y. Cao; H. Zi; W. Zhang; H. Lu; J. Pei. *J. Org. Chem*. **2005**, *70*, 3645-3653.

45. R. Rathore; C. L. Burns. *J. Org. Chem*. **2003**, *68*, 4071-4074.

46. V.J. Chebny; J. R. Gardinier; R. Rathore. *Tetrahedron Lett*. **2008**, *49*, 4869.

47. S. H. Wadumethrige; R. Rathore. *Org. Lett*. **2008**, 10, 5139.

48. (a) R. Rathore; C. L. Burns; M. I. Deselnicu. *Org. Lett*. **2001**, *3*, 2887. (b) For a review, see: R. Rathore; J. K. Kochi. Adv. Phys. Org. Chem. 2000, 35, 193 and references therein.

49. (a) N. L. Bauld; D. J. Bellville; B. Harirchian; K. T. Lorenz; R. A. Pabon, Jr.; D. W. Reynolds; D. D. Wirth; H. S. Chiou; B. K. Marsh. *Acc. Chem. Res.* **1987**, *20*, 371. (b) G. A. Mirafzal; J. Liu; N. L. Bauld. *J. Am. Chem. Soc*. **1993**, *115*, 6072. (c) S. C. Blackstock; T. D. Selby. *J. Am. Chem. Soc.* **1998**, *120*, 12155. (d) N. G. Connelly; W. E. Geiger. *Chem. Rev*. **1996**, *96*, 877. (e) R. Rathore; J. K. Kochi. *Acta Chem. Scand.* **1998**, *52*, 114-130. (f) K. Yoshida. *Electrooxidation in Organic Chemistry. The Role of Cation Radicals as Synthetic Intermediates*; Wiley: New York, 1984.

50. R. Rathore; C. L. Burns. *J. Org. Chem.* **2003**, *68*, 4071-4074.

51. L. Zhai; R. Shukla; S. H. Wadumethrige; R. Rathore. *J. Org. Chem*. **2010**, *75*, 4748–4760.

52. L. Zhai; R. Shukla; R. Rathore. *Org. Lett.* **2009**, *11*, 3474.

53. (a) E. Clar; M. Zander. *J. Chem. Soc.* **1968**, 1861. (b) E. Clar; C. T. Ironside; M. Zander. *J. Chem. Soc.* **1959**, 142. (c) E. Clar, *The Aromatic Sextet*; Wiley: London, **1972**. (d), E. Clar. *Polycyclic Hydrocarbons*; Academic Press: New York, **1964**.

54. Reviews: (a) A. J. Berresheim; M. Mùller; K. Mùllen. *Chem. Rev.* **1999**, *99*, 1747. (b) M. D. Watson; A. Fechtenkötter; K. Mùllen. *Chem. Rev.* **2001**, *101*, 1267 and references therein.

55. C-Y. Liu; A. Fechtenkötter; M. D. Watson; K. Mùllen and A. J. Bard. *Chem. Mater.* **2003,** *15*, 124-130.

56. (a) A. J. Berresheim; M. Mùller; K. Mùllen. *Chem. Rev.* **1999**, *99*, 1747. (b) M. D. Watson; A. Fechtenkötter; K. Mùllen. *Chem. Rev.* **2001**, *101*, 1267. (c) E. Clar. *Polycyclic Hydrocarbons*; Academic Press: New York, **1964**. (d) R. G. Harvey. *Polycyclic Aromatic Hydrocarbons*; Wiley-VCH: New York, **1996**.

57. O. Hammerich; V. D. Parker. *Adv. Phys. Org. Chem*. **1984**, *20*, 55. and references therein.

58. M. Banerjee; R. Shukla; R. Rathore. *J. Am. Chem. Soc*. **2009**, *131*, 1780-1786.

59. V. J. Chebny; T. S. Navale; R. Shukla; S. V. Lindeman; R. Rathore. *Org. Lett*. **2009**, *11*, 2253.

60. T. S. Navale; L. Zhai; S. V. Lindeman; R. Rathore. *Chem. Commun*. **2009**, 2857.

61. T.S. Navale; M. V. Ivanov; M. M. Hossain; R. Rathore. *Angew. Chem. Int. Ed*. **2018**, *57*, 790-794.

62. R. Rathore; C. L. Burns; M. I. Deselnicu; S. E. Denmark; T. Bui. *Org. Synth.* **2005**, *82*, 1.

63. R. Rathore; C. L. Burns; M. I. Deselnicu. *Org. Lett*. **2001**, *3*, 2887-2890.

64. M.R. Talipov; A. Boddeda; M. M. Hossain; R. Rathore. *J. Phys. Org. Chem*. **2016**, *29* 227–233.

65. N. G. Connelly; W. E. Geiger. *Chem. Rev*. **1996**, *96*, 877–910.

66. K. T. Lorenz; N. L. Bauld. *J. Am. Chem. Soc*. **1987**, *109*, 1157–1160.

67. T. Kim; G. A. Mirafzal; J. Liu; N. L. Bauld. *J. Am. Chem. Soc*. **1993**, *115*,7653–7664.

68. A. M. Bond; R. Colton; D. A. Fiedler; J. E. Kevekordes; V. Tedesco; T. F. Mann. *Inorg. Chem*. **1994**, *33*, 5761–5766.

69. W. Yueh; N. L. Bauld. *J. Am. Chem. Soc*. **1995**, *117*, 5671–5676.

70. N. L. Bauld; J. T. Aplin; W. Yueh; H. Sarker; D. J. Bellville, *Macromolecules*. **1996**, *29*, 3661–3662.

71. K. Heinze; S. Reinhardt. *Organometallics*. **2007**, *26*, 5406–5414.

72. H. Wang; X. Wang; M. A. Winnik; I. Manners, *J. Am. Chem. Soc*. **2008**, *130*, 12921–12930.

73. C. M. Davis; K. Ohkubo; I.-T. Ho; Z. Zhang; M. Ishida; Y. Fang; V. M. Lynch; K. M. Kadish; J. L. Sessler; S. Fukuzumi. *Chem. Commun*. **2015**, *51*, 6757–6760.

74. R. Rathore; C. L. Burns. *J. Org. Chem*. **2003**, *68*, 4071– 4074.

75. T. S. Navale; L. Zhai; S. V. Lindeman; R. Rathore. *Chem. Commun*. **2009**, 2857–2859.

76. N. G. Connelly; W. E. Geiger. *Chem. Rev*. **1996**, *96*, 877–910.

77. R. Rathore; S. V. Lindeman; A. S. Kumar; J. K. Kochi. *J. Am. Chem. Soc*. **1998**, *120*, 6931–6939.

CHAPTER 1

1. F. A. Bell; A. Ledwith and D. C. Sherrington, *J. Chem. Soc. C*, **1969**, 2719–2720.

2. N. G. Connelly and W. E. Geiger, *Chem. Rev*., **1996**, *96*, 877–910.

3. K. T. Lorenz and N. L. Bauld. *J. Am. Chem. Soc.*, **1987**, *109*, 1157–1160.

4. T. Kim; G. A. Mirafzal; J. Liu and N. L. Bauld. *J. Am. Chem. Soc.*, **1993**, *115*, 7653–7664.

5. A. M. Bond; R. Colton; D. A. Fiedler; J. E. Kevekordes; V. Tedesco and T. F. Mann. *Inorg. Chem.*, **1994**, *33*, 5761–5766.

6. W. Yueh and N. L. Bauld. *J. Am. Chem. Soc.*, **1995**, *117*, 5671–5676.

7. N. L. Bauld; J. T. Aplin; W. Yueh; H. Sarker and D. J. Bellville. *Macromolecules*, **1996**, *29*, 3661–3662.

8. K. Heinze and S. Reinhardt. *Organometallics*, **2007**, *26*, 5406–5414.

9. H. Wang; X. Wang; M. A. Winnik and I. Manners. *J. Am. Chem. Soc.*, **2008**, *130*, 12921–12930.

10. C. M. Davis; K. Ohkubo; I.-T. Ho; Z. Zhang; M. Ishida; Y. Fang; V. M. Lynch; K. M. Kadish; J. L. Sessler and S. Fukuzumi. *Chem. Commun.*, **2015**, *51*, 6757–6760.

11. R. Rathore and C. L. Burns. *J. Org. Chem.*, **2003**, *68*, 4071– 4074.

12. T. S. Navale; L. Zhai; S. V. Lindeman and R. Rathore. *Chem. Commun.*, **2009**, 2857–2859.

13. L. Eberson and B. Larsson. *Acta Chem. Scand*., **1986**, *40*, 210–225.

14. R. Rathore; S. V. Lindeman; A. S. Kumar and J. K. Kochi. *J. Am. Chem. Soc.*, **1998**, *120*, 6931–6939.

15. R. Rathore and J. K. Kochi. *J. Org. Chem.*, **1995**, *60*, 4399–4411.

16. R. Rathore, C. L. Burns and M. I. Deselnicu. *Org. Synth*., **2005**, 1–9.

17. M. R. Talipov; A. Boddeda; S. V. Lindeman and R. Rathore. *J. Phys. Chem. Lett*., **2015**, *6*, 3373–3378.

18. K. Sreenath; C. V. Suneesh; V. K. R. Kumar and K. R. Gopidas. *J. Org. Chem.*, **2008**, *73*, 3245–3251.

19. M. Renz; K. Theilacker; C. Lambert and M. Kaupp, *J. Am. Chem. Soc.*, **2009**, *131*, 16292–16302.

20. M. R. Talipov; A. Boddeda; Q. K. Timerghazin and R. Rathore. *J. Phys. Chem. C*, **2014**, *118*, 21400–21408.

21. M. R. Talipov; T. S. Navale and R. Rathore, *Angew. Chem., Int. Ed.*, **2015**, *54*, 14468–14472.

22. M. R. Talipov; R. Jasti and R. Rathore. *J. Am. Chem. Soc.*, **2015**, *137*, 14999–15006.

23. A. J. Cohen; P. Mori-Sánchez and W. Yang. *Science*, **2008**, *321*, 792–794.

24. A. J. Cohen; P. Mori-Sánchez and W. Yang. *Chem. Rev.*, **2011**, *112*, 289–320.

25. W. S. E. Steckhan and W. Schmidt. *Chem. Ber.*, **1980**, *113*, 577–585.

26. H. R. Snyder; C. Weaver and C. D. Marshall. *J. Am. Chem. Soc.*, **1949**, *71*, 289–291.

27. R. Belcher; A. J. Nutten and W. I. Stephen. *J. Chem. Soc.*,**1958**, 2336–2338.

28. J. Cornforth; R. H. Cornforth and R. T. Gray. *J. Chem. Soc., Perkin. Trans. 1*, **1982**, 2289–2297.

29. H.-M. Kang; Y.-K. Lim; I.-J. Shin; H.-Y. Kim and C.-G. Cho. *Org. Lett.*, **2006**, *8*, 2047–2050.

30. N. Berton; I. Fabre-Francke; D. Bourrat; F. Chandezon and S. Sadki. *J. Phys. Chem. B*, **2009**, *113*, 14087–14093.

31. J. Vicente; J. Gil-Rubio; G. Zhou; H. J. Bolink and J. Arias-Pardilla. *J. Polym. Sci., Part A: Polym. Chem.*, **2010**, *48*, 3744–3757.

32. J. H. Cho; Y.-S. Ryu; S. H. Oh; J. K. Kwon and E. K. Yum. *Bull. Korean Chem. Soc.*, **2011**, *32*, 2461.

33. M. Wang; C. Li; A. Lv; Z. Wang; Z. Bo and F. Zhang. *Polymer*, **2012**, *53*, 324–332.

34. H.-F. Huang; S.-H. Xu; Y.-B. He; C.-C. Zhu; H.-L. Fan; X.-H. Zhou; X.-C. Gao and Y.-F. Dai. *Dyes Pig.*, **2013**, *96*, 705–713.

35. B.-Y. Lim; B.-E. Jung and C.-G. Cho. *Org. Lett*., **2014**, *16*, 4492–4495.

36. J. Safaei-Ghomi and Z. Akbarzadeh. *Ultrason. Sonochem*., **2015**, *22*, 365–370.

37. R. Rathore and J. K. Kochi. *Acta Chem. Scand*., **1998**, *52*, 114–130.

38. R. Rathore, C. L. Burns and M. I. Deselnicu. *Org. Lett.*, **2001**, *3*, 2887–2890.

39. M. Banerjee; V. S. Vyas; S. V. Lindeman and R. Rathore. *Chem. Commun.*, **2008**, 1889–1891.

40. R. Shukla; S. H. Wadumethrige; S. V. Lindeman and R. Rathore. *Org. Lett.*, **2008**, *10*, 3587–3590.

41. V. J. Chebny; T. S. Navale; R. Shukla; S. V. Lindeman and R. Rathore. *Org. Lett.*, **2009**, *11*, 2253–2256.

42. V. J. Chebny; R. Shukla; S. V. Lindeman and R. Rathore. *Org. Lett.*, **2009**, *11*, 1939–1942.

43. T. S. Navale; K. Thakur; V. S. Vyas; S. H. Wadumethrige; R. Shukla; S. V. Lindeman and R. Rathore. *Langmuir*, **2012**, *28*, 71–83.

44. F. Weinhold and C. R. Landis. Valency and bonding: a natural bond orbital donor–acceptor perspective, Cambridge University Press, Cambridge, New York, UK, **2005**.

45. R. Rathore; A. S. Kumar; S. V. Lindeman and J. K. Kochi. *J. Org. Chem*., **1998**, *63*, 5847–5856.

46. L. Zhai; R. Shukla; S. H. Wadumethrige and R. Rathore. *J. Org. Chem.*, **2010**, *75*, 4748–4760.

47. Magic blue is rather stable and does not undergo ready dimerization, and therefore it is likely that a slow decomposition of $MB^{+\bullet}$ to neutral MB catalyzes the formation of TAB. For example, see: O. Yurchenko; D. Freytag; L. zur Borg; R. Zentel; J. Heinze and S. Ludwigs. *J. Phys. Chem. B*, **2012**, *116*, 30–39. and M. Talipov and R. Rathore. Robust Aromatic Cation Radicals as Redox Tunable Oxidants, in Organic Redox Systems: Synthesis, Properties, and Applications, ed. T. Nishinaga; John Wiley & Sons, Inc, Hoboken, NJ, **2015**, pp. 131–175.

48. D. Vak; J. Jo; J. Ghim; C. Chun; B. Lim; A. J. Heeger and D.-Y. Kim. *Macromolecules*, **2006**, *39*, 6433–6439.

49. J. Vicente; J. Gil-Rubio; G. Zhou; H. J. Bolink and J. Arias-Pardilla. *J. Polym. Sci. A Polym. Chem.*, **2010**, *48*, 3744-3757.

50. H. -F. Huang; S. -H. Xu; Y. -B. He; C. -C. Zhu; H. -L. Fan; X. -H. Zhou; X. -C. Gao and Y. -F. Dai. *Dyes Pigments*, **2013**, *96*, 705-713.

51. N. Berton; I. Fabre-Francke; D. Bourrat; F. Chandezon and S. Sadki. *J. Phys. Chem. B*, **2009**, *113*, 14087-14093.

52. S. Wu; Y. Liu; G. Yu; J. Guan; C. Pan; Y. Du; X. Xiong and Z. Wang *Macromolecules*, **2014**, *47*, 2875-2882.

53. J. H. Cho; Y. -S. Ryu; S. H. Oh; J. K. Kwon and E. K. Yum. *Bull. Korean. Chem. Soc.*, **2011**, *32*, 2461.

54. J. Safaei-Ghomi and Z. Akbarzadeh. *Ultrason. Sonochem*, **2015**, *22*, 365-370.

55. L. Eberson and B. Larsson. *Acta. Chem. Scand.*, **1986**, *40*, 210-225.

56. L. Zhai; R. Shukla; S. H. Wadumethrige and R. Rathore. *J. Org. Chem.*, **2010**, *75*, 4748-4760.

57. B.-Y. Lim; B.-E. Jung and C.-G. Cho. *Org. Lett.*, **2014**, *16*, 4492-4495.

58. H.-M. Kang; Y.-K. Lim; I.-J. Shin; H.-Y. Kim and C.-G. Cho. *Org. Lett.*, **2006**, *8*, 2047-2050.

59. R. Belcher; A. J. Nutten and W. I. Stephen. *J. Chem. Soc.*, **1958**, 2336-2338.

60. B. S. Furniss, Vogel's textbook of practical organic chemistry, Pearson Education India, **1989**.

61. M. Wang; C. Li; A. Lv; Z. Wang; Z. Bo and F. Zhang. *Polymer*, **2012**, *53*, 324 - 332.

62. H. R. Snyder; C. Weaver and C. D. Marshall. *J. Am. Chem. Soc.*, **1949**, *71*, 289-291.

63. J. Cornforth; R. H. Cornforth and R. T. Gray. *J. Chem. Soc. Perk. T. 1*; **1982**, 2289-2297.

64. X. Huang and S. L. Buchwald. *Org. Lett.*, **2001**, *3*, 3417-3419.

CHAPTER 2

1. D. Vonlanthen; A. Mishchenko; M. Elbing; M. Neuburger; T. Wandlowski; M. Mayor. *Angew. Chem. Int. Ed.* **2009**, *48*, 8886.

2. A. Mishchenko; D. Vonlanthen; V. Meded; M. Burkle; C. Li; I. V. Pobelov; A. Bagrets; J. K. Viljas; F. Pauly; F. Evers. *Nano. Lett.* **2009**, *10*, 156.

3. L. Cui; B. Liu; D. Vonlanthen; M. Mayor; Y. Fu; J. -F. Li; T. Wandlowski. *J. Am. Chem. Soc.* **2011**, *133*, 7332.

4. L. Venkataraman; J. E. Klare; C. Nuckolls; M. S. Hybertsen; M. L. Steigerwald. *Nature.* **2006**, *442*, 904.

5. A. Heckmann; C. Lambert. *Angew. Chem. Int. Ed.* **2012**, *51*, 326.

6. D. Hanss; O. S. Wenger. *Eur. J. Inorg. Chem.* **2009**, *2009*, 3778.

7. K. E. Spettel; N. H. Damrauer. *J. Phys. Chem. C.* **2016**, *120*, 10815.

8. A. C. Benniston; A. Harriman. *Chem. Soc. Rev.* **2006**, *35*, 169.

9. L. Zhai; R. Shukla; S. H. Wadumethrige. R. Rathore. *J. Org. Chem.* **2010**, *75*, 4748.

10. L. Zhai; R. Shukla; R. Rathore. *Org. Lett.* **2009**, *11*, 3474.

11. R. Shukla; R. Rathore. *Synthesis.* **2008**, *2008*, 3769.

12. M. R. Talipov; A. Boddeda; S. V. Lindeman; R. Rathore. *J. Phys. Chem. Lett.* **2015**, 3373.

13. M. R. Talipov; T. S. Navale; R. Rathore. *Angew. Chem. Int. Ed.* **2015**, *54(48)*,14468-14472

14. M. R. Talipov; R. Jasti; R. Rathore. *J. Am. Chem. Soc.* **2015**, *137*, 14999.

15. M. R. Talipov; A. Boddeda; Q. K. Timerghazin; R. Rathore. *J. Phys. Chem. C.* **2014**, *118*, 21400.

16. M. R. Talipov; M. V. Ivanov; R. Rathore. *J. Phys. Chem. C.* **2016**, *120*, 6402.

17. R. B. Bates; F. A. Camou; V. Kane; P. K. Mishra; K. Suvannachut; J. J. White. *J. Org. Chem.* **1989**, *54*, 311.

18. Note that 3,4-dimethoxytoluene undergoes an irreversible electrochemical oxidation while 3,4-dimethoxy-1-*tert*-butylbenzene affords a completely reversible cyclic voltammogram, see the Supporting Information for details.

19. R. Rathore; C. L. Burns; M. I. Deselnicu. *Org. Synth.* **2005**, 1.

20. R. Rathore; J. K. Kochi. *Acta. Chemica. Scandinavica.* **1998**, *52*, 114.

21. R. Rathore; C. L. Burns; M. I. Deselnicu. *Org. Lett.* **2001**, *3*, 2887.

22. A. E. Reed; L. A. Curtiss; F. Weinhold. *Chem. Rev.* **1988**, *88*, 899.

23. F. Weinhold; C. R. Landis. in Valency and bonding: a natural bond orbital donor-acceptor perspective, Cambridge University Press, **2005**.

24. Similar results were obtained the TD-DFT calculations of the conformers of $1^{+\bullet}$-$6^{+\bullet}$ and tBu-$7^{+\bullet}$ identified in the conformational search procedure described above, see Supporting Figure 12 in original published paper.

25. B. S. Brunschwig; C. Creutz; N. Sutin. *Chem. Soc. Rev.* **2002**, *31*, 168.

26. M. R. Talipov; M. M. Hossain; A. Boddeda; K. Thakur; R. Rathore. *Org. Biomol. Chem.* **2016**, *14*, 2961.

27. R. S. Mulliken. J. Chim. Phys. Physicochim. Biol. **1949**, 46, 497.

28. G. D. Scholes; R. D. Harcourt; K. P. Ghiggino. *J. Chem. Phys.* **1995**, *102*, 9574.

29. In case of coherent tunneling charge transfer mechanism the rate of the charge transfer in biaryls is proportional to square of the coupling and, therefore, varies linearly with $\cos^2 \varphi$, see refs 2, 4, and 25.

30. A. R. Battersby; R. Binks. *J. Chem. Soc.* **1958,** 4333.

31. H. Erdtman. Justus Liebigs Ann. Chem. **1933,** 505, 195.

32. M. F. Semmelhack; P. Helquist; L. D. Jones; L. Keller; L. Mendelson; L. S. Ryono; J. Gorzynski Smith; R. D. Stauffer. *J. Am. Chem. Soc.* **1981,** *103*, 6460.

33. Ronlan, A.; V. D. Parker. *J. Org. Chem.* **1974,** *39*, 1014.

34. R. Rathore; J. K. Kochi. *J. Org. Chem.* **1996,** *61*, 627.

35. Y. Ito; T. Konoike; T. Saegusa. *J. Am. Chem. Soc.* **1975,** *97*, 649.

36. T. Biftu; N. F. Gamble; T. Doebber; S. B. Hwang; T. Y. Shen; J. Snyder; J. P. Springer; R. Stevenson. *J. Med. Chem.* **1986,** *29*, 1917.

37. R. D. Haworth; A. H. Lamberton. *J. Chem. Soc.* **1946,** 1003.

38. L. J. Fliedner Jr; M. J. Myers; J. M. Schor; I. J. Pachter. *J. Med. Chem.* **1973,** *16*, 749.

39. L. J. Fliedner Jr; M. J. Myers; J. M. Schor; I. J. Pachter. *J. Med. Chem.* **1976,** *19*, 202.

40. L. Zhai; R. Shukla; S. H. Wadumethrige; R. Rathore. *J. Org. Chem.* **2010,** *75*, 4748.

41. M. R. Talipov; A. Boddeda; M. M. Hossain; R. Rathore. *J. Phys. Org. Chem.* **2015,** *29*, 227.

42. FrischMJTrucks

43. M. R. Talipov; A. Boddeda; Timerghazin, Q. K.; Rathore, R. *J. Phys. Chem. C* **2014,** *118,* 21400.

44. M. R. Talipov; A. Boddeda; S. V. Lindeman; R. Rathore. *J. Phys. Chem. Lett.* **2015,** *6,* 3373.

45. M. R. Talipov; T. S. Navale; R. Rathore. *Angew. Chem. Int. Ed. Engl.* **2015,** *54,* 14468.

46. Talipov, M. R.; Hossain, M. M.; Boddeda, A.; Thakur, K.; Rathore, R. *Org. Biomol. Chem.* **2016,** *14,* 2961.

47. M. R. Talipov; M. V. Ivanov; R. Rathore. *J. Phys. Chem. C* **2016,** *120,* 6402.

48. C. Adamo; V. Barone. *Chem. Phys. Lett.* **1997,** *274,* 242.

49. W. J. Hehre; R. Ditchfield; J. A. Pople. *J. Chem. Phys.* **1972,** *56,* 2257.

50. S. Miertus; E. Scrocco; Tomasi. J. *Chem. Phys.* **1981,** *55,* 117.

51. M. T. Cances; V. Mennucci; J. Tomasi. *J. Chem. Phys.* **1997,** *107,* 3032.

52. M. Cossi; V. Barone; V. Mennucci; Tomasi. J. *Chem. Phys. Lett.* **1998,** *286,* 253.

53. J. Tomasi; B. Mennucci; R. Cammi. *Chem. Rev.* **2005,** *105,* 2999.

54. R. F. Ribeiro; A. V. Marenich; C. J. Cramer; D. G. Truhlar. *J. Phys. Chem. B* **2011,** *115,* 14556.

55. R. Seeger; J. A. Pople. *J. Chem. Phys.* **1977,** *66,* 3045.

56. R. Bauernschmitt; R. Ahlrichs. *J. Chem. Phys.* **1996,** *104,* 9047.

57. A. E. Reed; L. A. Curtiss; F. Weinhold. *Chem. Rev.* **1988,** *88,* 899.

58. F. Weinhold; C. R. Landis, *Valency and Bonding: a Natural Bond Orbital Donor-acceptor Perspective,* Cambridge University Press: Cambridge, UK ; New York; 2005.

59. R. E. Stratmann; G. E. Scuseria; M. J. Frisch. *J. Chem. Phys.* **1998,** *109,* 8218.

60. M. E. Casida; C. Jamorski; K. C. Casida; D. R. Salahub. *J. Chem. Phys.* **1998,** *108,* 4439.

61. R. Cammi; B. Mennucci; J. Tomasi. *J. Phys. Chem. A* **2000,** *104,* 5631.

62. M. Cossi; V. Barone. *J. Chem. Phys.* **2001,** *115,* 4708.

63. F. Furche; R. Ahlrichs. *J. Chem. Phys.* **2002,** *117,* 7433.

64. G. Scalmani; M. J. Frisch; B. Mennucci; J. Tomasi; R. Cammi; V. Barone. *J. Chem. Phys.* **2006,** *124,* 094107.

65. K. Wolinski; J. F. Hinton; P. Pulay. *J. Am. Chem. Soc.* **1990,** *112,* 8251.

66. J. Gauss. *Chem. Phys. Lett.* **1992,** 191, 614.

67. F. Jensen. *J. Chem. Theory. Comput*. **2008,** 4, 719.

68. Cxcalc (Chemaxone Calculator)

69. O. V. Ardashov; A. M. Genaev; I. V. Ilina; D. V. Korchagina; K. P. Volcho; N. F. Salakhutdinov. *Russ. J. Org. Chem.* **2010,** *46*, 1786.

70. G. B. Rocha; R. O. Freire; A. M. Simas; J. J. Stewart. *J. Comput. Chem.* **2006,** *27*, 1101.

71. Mopac Software.

CHAPTER 3

1. M. Pfaff; P. Müller; P. Bockstaller; E. Mülle; J. Subbiah; W. W. Wong; M. F. Klein; A. Kiersnowski; S. R. Puniredd; W. Pisula; A. Colsmann; D. Gerthsen; D. J. Jones. *ACS. Appl. Mater. Interfaces.* **2013**, *5*, 11554-11562.

2. J. E. Anthony. *Chem. Rev.* **2006**, *106*, 5028-5048.

3. Y. Segawa; H. Ito; K. Itami. *Nat. Rev. Mat.* **2016**, *1*, 15002.

4. X. Li; W. Cai; J. An; S. Kim; J. Nah; D. Yang; R. Piner; A. Velamakanni; I. Jung; E. Tutuc; S. K. Banerjee; L. Colombo; R. S. Ruoff. *Science.* **2009**, *324*, 1312-1314.

5. J. Wu; W. Pisula; K. Müllen. *Chem. Rev.* **2007**, *107*, 718-747.

6. R. Rathore; C. L. Burns. *J. Org. Chem.* **2003**, *68*, 4071-4074.

7. S. H. Wadumethrige; R. Rathore. *Org. Lett.* **2008**, *10*, 5139-5142.

8. S. Ito; P. T. Herwig; T. Böhme; J. P. Rabe; W. Rettig; K. Müllen. *J. Am. Chem. Soc.* **2000**, *122*, 7698-7706.

9. R. Rathore; C. L. Burns. *Org. Synth.* **2005**, 30-33.

10. R. Rathore; C. L. Burns; I. A. Guzei. *J. Org. Chem.* **2004**, *69*, 1524-1530.

11. T. Kojima; S. Hiraoka. *Org. Lett.* **2014**, *16*, 1024-1027.

12. P. N. W. Baxter. *Chemistry*. **2003**, *9*, 5011-5022.

13. R. Rathore; C. L. Burns; S. A. Abdelwahed. *Org. Lett.* **2004**, *6*, 1689-1692.

14. The oxidative cyclodehydrogenation of the isomeric **5'** (i.e., 1,2,4 isomer) produces a complex mixture of products, which could not be separated by repeated chromatographic attempts and therefore their characterization was abandoned.

15. K. L. Handoo; K. Gadru. *Current. Science.* **1986**, *55*, 920-922.

16. R. Rathore; J. K. Kochi. *Acta. Chem. Scand.* **1998**, *52*, 114-130.

17. V. J. Chebny; C. Gwengo; J. R. Gardinier; R. Rathore. *Tetrahedron. Letters.* **2008**, *49*, 4869-4872.

18. M. R. Talipov; A. Boddeda; M. M. Hossain; R. Rathore. *J. Phys. Org. Chem.* **2015**, *29*, 227-233.

19. M. R. Talipov; M. M. Hossain; A. Boddeda; K. Thakur; R. Rathore. *Org. Biomol. Chem.* **2016**, *14*, 2961-2968.

20. The bromination of ***F*HBC** produced numerous brominated regioisomers whose structures could not be resolved.

21. Z. Liu; S. P. Lau; F. Yan. *Chem. Soc. Rev.* **2015**, *44*, 5638-5679.

22. A. Facchetti. *Chem. Mater.* **2010**, *23*, 733-758.

23. P. N. W. Baxter. *Chemistry.* **2003**, *9*, 5011-5022.

24. R. Adhikari; L. Duan; L. Hou; Y. Qiu; D. Neckers; B. Shah. *Chem. Mater.* **2009**, *21*, 4638-4644.

25. R. Rathore; C. L. Burns; I. A. Guzei. *J. Org. Chem.* **2004**, *69*, 1524-1530.

26. T. Kojima; S. Hiraoka. *Org. Lett.* **2014**, *16*, 1024-1027.

27. R. Rathore; C. L. Burns. *Org. Synth.* **2005**, 30-33.

28. W. Hu; L. Liu; M. Ma; X. Zhao; A. Liu; X. Mi; B. Jiang; K. Wen. *Tetrahedron.* **2013**, *69*, 3934-3941.

29. V. J. Chebny; C. Gwengo; J. R. Gardinier; R. Rathore. *Tetrahedron. Letters.* **2008**, *49*, 4869-4872.

30. R. Rathore; C. L. Burns. *J. Org. Chem.* **2003**, *68*, 4071-4074.

31. M. R. Talipov; A. Boddeda; M. M. Hossain; R. Rathore. *J. Phys. Org. Chem.* **2015**, *29*, 227-233.

32. M. R. Talipov; M. M. Hossain; A. Boddeda; K. Thakur; R. Rathore. *Org. Biomol. Chem.* **2016**, *14*, 2961-2968.

33. D.A. Case; D.S. Cerutti; T.E. Cheatham, III; T.A. Darden; R.E. Duke; T.J. Giese; H. Gohlke; A.W. Goetz; D. Greene; N. Homeyer; S. Izadi; A. Kovalenko; T.S. Lee; S. LeGrand; P. Li; C. Lin; J. Liu; T. Luchko; R. Luo; D. Mermelstein; K.M. Merz; G. Monard; H. Nguyen; I. Omelyan; A. Onufriev; F. Pan; R. Qi; D.R. Roe; A. Roitberg; C. Sagui; C.L. Simmerling; W.M. Botello-Smith; J. Swails; R.C. Walker; J. Wang; R.M. Wolf; X. Wu; L. Xiao; D.M. York and P.A. Kollman (2017), AMBER 2017, University of California, San Francisco.

34. J. Wang; R. M. Wolf; J. W. Caldwell; P. A. Kollman; D. A. Case. *J. Comput. Chem.* **2004**, *25*, 1157-1174.

35. J. Wang; W. Wang; P. A. Kollman; D. A. Case. *J. Mol. Graph. Model.* **2006**, *25*, 247-260.

36. D. A. Case; T. E. Cheatham; T. Darden; H. Gohlke; R. Luo; K. M. Merz; A. Onufriev; C. Simmerling; B. Wang; R. J. Woods. *J. Comput. Chem.* **2005**, *26*, 1668-1688.

37. D. Hawkins; J. Cramer; G. Truhlar. *J. Phys. Chem.* **1996**, *100*, 19824-19839.

CHAPTER 4

1. A.Facchetti. Chem. Mater. **2010**, *23*, 733-758.

2. C. Li; M. Liu; N. G. Pschirer; M. Baumgarten; K.Müllen. *Chem. Rev.* **2010**, *110*, 6817-6855.

3. J. C. Goldschmidt; S. Fischer. *Advanced. Optical. Materials.* **2015**, *3*, 510-535.

4. C. J. Lambert. *Chem. Soc. Rev.* **2015**, *44*, 875-888.

5. S. Holliday; Y. Li; C. K. Luscombe. *Progress In Polymer Science.* **2017**, *70*, 34 - 51.

6. G. Li; N. Govind; M. A. Ratner; C. J. Cramer; L. Gagliardi. *J. Phys. Chem. Lett.* **2015**, *6*, 4889-4897.

7. A. Migliore. *J. Chem. Theory. Comput.* **2011**, *7*, 1712-1725.

8. T. Kawatsu; V. Coropceanu; A. Ye; J. -L. Brédas. *J. Phys. Chem. C.* **2008**, *112*, 3429-3433.

9. M. N. Paddon-Row; M. J. Shephard. *J. Am. Chem. Soc.* **1997**, *119*, 5355-5365.

10. M. V. Ivanov; M. R. Talipov; A. Boddeda; S. H. Abdelwahed; R. Rathore. *J. Phys. Chem. C.* **2017**, *121*, 1552-1561.

11. M. V. Ivanov; V. J. Chebny; M. R. Talipov; R. Rathore. *J. Am. Chem. Soc.* **2017**, *139*, 4334-4337.

12. D. Wang; M. R. Talipov; M. V. Ivanov; R. Rathore. *J. Am. Chem. Soc.* **2016**, *138*, 16337-16344.

13. R. E. Larsen. *J. Phys. Chem. C.* **2016**, *120*, 9650-9660.

14. M. V. Ivanov; D. Wang; R. Rathore. *J. Am. Chem. Soc.* **2018**, *140*, 4765-4769.

15. M. Ivanov; S. Wadumethrige; D. Wang; R. Rathore. *Chemistry.* **2017**, *23*, 8834-8838.

16. R. F. Winter. *Organometallics.* **2014**, *33*, 4517-4536.

17. W. E. Geiger; F. Barrière. *Acc. Chem. Res.* **2010**, *43*, 1030-1039.

18. C. Chi; G. Wegner. *Macromol. Rapid. Commun.* **2005**, *26*, 1532-1537.

19. M. Kaupp; M. Renz; M. Parthey; M. Stolte; F. Würthner; C. Lambert. *Phys. Chem. Chem. Phys.* **2011**, *13*, 16973-16986.

20. A. Heckmann; C. Lambert. *Angew. Chem. Int. Ed.* **2012**, *51*, 326-392.

21. S. F. Nelsen. *Chem. Eur. J.* **2000**, *6*, 581-588.

22. M. R. Talipov; A. Boddeda; M. M. Hossain; R. Rathore. *J. Phys. Org. Chem.* **2015**, *29*, 227-233.

23. M. R. Talipov; M. M. Hossain; A. Boddeda; K. Thakur; R. Rathore. *Org. Biomol. Chem.* **2016**, *14*, 2961-2968.

24. R. Rathore; C. L. Burns; M. I. Deselnicu. *Org. Synth.* **2005**, 1-9.

25. R. Rathore; C. L. Burns; M. I. Deselnicu. *Org. Lett.* **2001**, *3*, 2887-2890.

26. R. Rathore; J. K. Kochi. *Acta. Chem. Scand.* **1998**, *52*, 114-130.

27. A. J. Cohen; P. Mori-Sánchez; W. Yang. *Chem. Rev.* **2012**, *112*, 289-320.

28. D. S. Ranasinghe; J. T. Margraf; Y. Jin; R. J. Bartlett. *J. Chem. Phys.* **2017**, *146*, 034102.

29. M. Lundberg; P. E. M. Siegbahn. *J. Chem. Phys.* **2005**, *122*, 224103.

30. Y. Zhang; W. A Yang. *J. Chem. Phys.* **1998**, *109*, 2604-2608.

31. M. Félix; A. A. Voityuk. *Int. J. Quantum. Chem.* **2011**, *111*, 191-201.

32. C. Adamo; V. Barone. *Chem. Phys. Lett.* **1997**, *274*, 242-250.

33. M. R. Talipov; A. Boddeda; Q. K. Timerghazin; R. Rathore. *J. Phys. Chem. C.* **2014**, *118*, 21400-21408.

34. M. V. Ivanov; N. J. Reilly; B. Uhler; D. Kokkin; R. Rathore; S. A. Reid. *J. Phys. Chem. Lett.* **2017**, 8 (21), 5272-5276.

35. D. Kokkin; M. V. Ivanov; J. Loman; J. -Z. Cai; R. Rathore; S. A. Reid. *J. Phys. Chem. Lett.* **2018**, 2058-2061.

36. E. Cances; B. Mennucci; J. Tomasi. *J. Chem. Phys.* **1997**, *107*, 3032.

37. L. V. Ivanova; D. Wang; S. Lindeman; M. V. Ivanov; R. Rathore. *J. Phys. Chem. C.* **2018**, *122*, 9339-9345.

38. T. S. Navale; K. Thakur; V. S. Vyas; S. H. Wadumethrige; R. Shukla; S. V. Lindeman; R. Rathore. *Langmuir.* **2012**, *28*, 71-83.

39. G. Donati; D. B. Lingerfelt; A. Petrone; N. Rega; X. Li. *J. Phys. Chem. A.* **2016**, *120*, 7255-7261.

40. I. H. Nayyar; E. R. Batista; S. Tretiak; A. Saxena; D. L. Smith; R. L. Martin. *J. Chem. Theory. Comput.* **2013**, *9*, 1144-1154.

41. A. J. Neukirch; W. Nie; J. -C. Blancon; K. Appavoo; H. Tsai; M. Y. Sfeir; C. Katan; L. Pedesseau; J. Even; J. J. Crochet. *Nano. Lett.* **2016**, *16*, 3809-3816.

42. B. S. Brunschwig; C. Creutz; N. Sutin. *Chem. Soc. Rev.* **2002**, *31*, 168-184.

43. M. R. Talipov; T. S. Navale; M. M. Hossain; R. Shukla; M. V. Ivanov; R. Rathore. *Angew. Chem. Int. Ed.* **2017**, *56*, 266-269.

44. E. Hückel. *Z. Phys.* **1932**, *76*, 628-648.

45. A. A. Frost; B. Musulin. *J. Chem. Phys.* **1953**, *21*, 572-573.

46. R. Hoffmann. *Angew. Chem. Int. Ed.* **1987**, *26*, 846-878.

47. Y. Kashimoto; K. Yonezawa; M. Meissner; M. Gruenewald; T. Ueba; S. Kera; R. Forker; T. Fritz; H. Yoshida, *J. Phys. Chem. C.* **2018**, *122(22)*, 12090-12097.

48. B. Kobin; L. Grubert; S. Blumstengel; F. Henneberger; S. Hecht. *J. Mater. Chem.*, **2012**, 22, 4383–4390.

49. M. M. Elmahdy; G. Floudas; L. Oldridge; A. C. Grimsdale; K. Müllen. *ChemPhysChem*. **2006**, 7(7), 1431 – 1441.

50. W. H. Parsons; R. R. Calvo; W. Cheung; Y.K. Lee; S. Patel; J. Liu; M. A. Youngman; S. L. Dax; D. Stone; N. Qin; T. Hutchinson; M. L. Lubin; S.P. Zhang; M. Finley; Y. Liu; M. R. Brandt; C. M. Flores; M. R. Player. *J. Med. Chem*. **2015**, 58, 3859−3874.

51. S. P. Dudek; M. Pouderoijen; R. Abbel; A. P. H. J. Schenning; E. W. Meijer. *J. Am. Chem. Soc*. **2005**, 127, 11763-11768.

52. K.Onitsuka; M. Fujimoto; H. Kitajima; N. Ohshiro; F. Takei; and S. Takahashi. *Chem. Eur. J*. **2004**, 10, 6433 – 6446.

53. J.K. Jin; J.K. Choi; B.J. Kim; H.B. Kang; S.C. Yoon; H. You; H.T. Jung. *Macromolecules*, **2011**, 44 (3), 502-511.

54. J. Yang; C. Jiang; Y. Zhang; R.Yang; W.Yang; Q. Hou; Y. Cao. *Macromolecules*. **2004**, 37, 1211-1218.

55. C. Yang; F. Mehmood; T. L. Lam; S. L.F. Chan; Y. Wu; C.S. Yeung; X. Guan; K. Li; C. Y. S. Chung; C. Y. Zhou; T. Zoua; C. M. Che. *Chem. Sci.*, **2016**, 7, 3123–3136.

56. H.H. Huang; C. Prabhakar; K.C. Tang; P.T. Chou; G.J. Huang; J.S. Yang. *J. Am. Chem. Soc*. **2011**, 133 (20), 8028–8039.

57. R. Bernard; C. Barsu; P. L. Baldeck; C. Andraud; D. Cornu; J.P. Scharff and P. Miele. *Chem. Commun.*, **2008**, 3762–3764.